Department Chemie
Institut für Organische Chemie und Biochemie
Lehrstuhl für Biotechnologie

Functional Regulation of the Molecular Chaperone Hsp104 from *Saccharomyces cerevisiae*

Dipl.-Biol. (Univ.) Valerie Grimminger

Vollständiger Abdruck der von der Fakultät für Chemie der Technischen Universität München zur Erlangung des akademischen Grades eines Doktors der Naturwissenschaften genehmigten Dissertation.

Vorsitzender: Univ.-Prof. Dr. Th. Kiefhaber

Prüfer der Dissertation:

1. Univ.-Prof. Dr. J. Buchner
2. Univ.-Prof. Dr. S. Weinkauf
3. Univ.-Prof. Dr. W. Höll

Die Dissertation wurde am 27.03.2007 bei der Technischen Universität München eingereicht und durch die Fakultät für Chemie am 21.05.2007 angenommen.

I dedicate this work to

Christine Grimminger

TABLE OF CONTENTS

1. SUMMARY 1
1. ZUSAMMENFASSUNG 3
2. INTRODUCTION 7
2.1 The theory of protein folding 7
2.2 Protein folding *in vivo* 9
2.3 The aggregation of proteins 10
2.4 Molecular chaperones and folding catalysts 10
2.4.1 Protein disulfide isomerases 10
2.4.2 Peptidyl-prolyl isomerases 10
2.4.3 Molecular chaperones 11
2.5 The classes of molecular chaperones 13
2.5.1 The class of small heat shock proteins 13
2.5.2 The class of Hsp60/chaperonin proteins 13
2.5.3 The class of Hsp70 proteins 15
2.5.4 The class of Hsp90/HtpG proteins and their TPR cofactors 16
2.5.4.1 The structure and function of Hsp90/HtpG 16
2.5.4.2 The TPR domain containing proteins as chaperone cofactors 18
2.5.4.3 Cyclophilin 40 is a TPR cochaperone of Hsp90 20
2.5.5 The class of Hsp100/ClpB proteins 21
2.6 The molecular chaperone Hsp104 of yeast 23
2.6.1 The genetic regulation of Hsp104: Acquisition of stress tolerance 23
2.6.2 Disaggregation of aggregated proteins by Hsp104 25
2.6.3 Propagation of yeast prions by Hsp104 27
2.6.4 The tertiary structure of Hsp104 30
2.6.5 The domain organization of Hsp104 32
2.6.6 The structure of the nucleotide binding domains of Hsp104 34
2.6.7 Oligomerization properties of Hsp104 36
2.6.8 The ATPase function of Hsp104 37
2.6.9 The substrate binding cycle of Hsp104 39
2.7 Objectives of this study 41
3. MATERIALS AND METHODS 43
3.1 Materials 43
3.1.1 Equipment 43
3.1.2 Expendable materials 44
3.1.3 Chemicals 45
3.1.4 Antibodies, enzymes, and standards for molecular biology 46
3.1.5 Molecular chaperones and their substrates 47
3.1.6 Oligonucleotides for PCR and for sequencing 48
3.1.7 Bacterial plasmids and strains 49
3.1.8 Media and antibiotics for the propagation of *E. coli* 50
3.1.9 Yeast vectors and strains 50
3.1.10 Media and solutions for the propagation of *S. cerevisiae* 51
3.1.11 Buffers for protein chemistry 52
3.1.11.1 Buffers and solutions for the production of recombinant Hsp104 52
3.1.11.2 Buffers and solutions for the gel electrophoresis of proteins 53
3.1.11.3 Buffers and solutions for Coomassie staining 53
3.1.11.4 Buffers and solutions for silver staining 53

3.1.11.5 Buffers and solutions for western blotting 54
3.1.11.6 Buffers and solutions for co-immunoprecipitation 54
3.1.11.7 Buffers and solutions for *in vitro* experiments with Hsp104 55
3.1.11.8 Buffers and solutions for the reactivation of denatured luciferase 55
3.1.11.9 Buffers and solutions for the reactivation of denatured DHFR 56
3.1.12 Computer software and web tools 56
3.2 Molecular cloning techniques 57
3.2.1 Production, isolation and purification of DNA 57
3.2.1.1 *E. coli* plasmid DNA isolation 57
3.2.1.2 Purification of DNA fragments 57
3.2.1.3 Yeast DNA isolation 57
3.2.2 Site-directed mutagenesis of *HSP104* 57
3.2.3 Cloning of yeast vectors 58
3.3 *In vivo* analysis of *S. cerevisiae* 58
3.3.1 Yeast growth conditions 58
3.3.2 Generating gene knockouts 59
3.3.3 Plasmid shuffling in yeast 59
3.3.4 Phenotypic analysis of yeast strains 59
3.3.5 Nonsense suppression assay for the presence of [*PSI*$^+$] 60
3.3.6 Cell viability assay 60
3.3.7 Thermotolerance assay 60
3.3.8 Co-localization by fluorescence microscopy 60
3.4 Methods of protein biochemistry 61
3.4.1 Production of recombinant protein 61
3.4.1.1 Production of recombinant Cpr6 and Hsp82 61
3.4.1.2 Production of recombinant Hsp104 61
3.4.2 Labeling of Cpr6 62
3.4.3 Bradford assay 62
3.4.4 Concentration determination by UV-spectroscopy 63
3.4.5 Gel electrophoresis of proteins 63
3.4.6 Coomassie staining 64
3.4.7 Silver staining 64
3.4.8 Immunological methods 64
3.4.8.1 Western blotting 64
3.4.8.2 Co-immunoprecipitation 65
3.5 Spectroscopic methods 66
3.5.1 Fluorescence spectroscopy 66
3.5.1.1 Intrinsic fluorescence of proteins 66
3.5.1.2 ANS Fluorescence 66
3.5.1.3 Fluorescence anisotropy 67
3.5.2 Circular dichroism spectroscopy 67
3.6 Isothermal titration calorimetry 68
3.7 Static light scattering 69
3.8 Analytical ultracentrifugation 69
3.8.1 Sedimentation velocity experiments 70
3.8.2 Sedimentation equilibrium experiments 71
3.9 *In vitro* activity assays 72
3.9.1 ATPase assay 72
3.9.2 Refolding of denatured luciferase 74

3.9.3 Refolding of denatured dehydrofolate reductase 74

4. RESULTS 75
4.1 Sequence analysis and identification of the domains of Hsp104 75
4.2 Structural analysis of Hsp104 and its mutants 78
4.3 Analysis of the oligomerization state of Hsp104 and its mutants 78
4.3.1 Analysis of the oligomerization state of Hsp104 by static light scattering 79
4.3.2 Analysis of the oligomerization state of Hsp104 by analytical ultra-centrifugation 80
4.4 The ATPase function of Hsp104 is tightly regulated 81
4.4.1 Comparison of the ATP turn-over by Hsp104 to similar molecular chaperones 81
4.4.2 The Hsp104 ATPase mutants reveal an inter-domain crosstalk 82
4.4.3 The ATPase function is dependent on the quaternary structure of Hsp104 84
4.4.4 Hsp104 oligomers are stable during steady-state ATP hydrolysis 85
4.4.5 Enzymatic characterization of Hsp104 and its mutants 87
4.4.6 Affinity of Hsp104 for nucleotides 89
4.4.6.1 Fluorescence titration of Hsp104 89
4.4.6.2 ITC titration of Hsp104 91
4.5 GdmCl is a specific inhibitor of Hsp104 94
4.5.1 Low concentrations of GdmCl specifically inhibit ATP hydrolysis by Hsp104 95
4.5.2 GdmCl directly inhibits the Hsp104 ATPase 97
4.5.3 GdmCl does not affect the oligomerization of Hsp104 98
4.5.4 Binding of GdmCl to Hsp104 is nucleotide-dependent 99
4.5.5 GdmCl increases the affinity of Hsp104 for nucleotides 100
4.5.6 GdmCl stimulates the assembly of the Hsp104 hexamer 100
4.5.7 GdmCl is an uncompetitive inhibitor of Hsp104 102
4.5.8 GdmCl alters the affinity of Hsp104 for unfolded polypeptides 106
4.5.9 Luciferase refolding by Hsp104 is strongly affected by the presence of GdmCl 107
4.6 The yeast cyclophilin Cpr6 is a cochaperone of Hsp104 109
4.6.1 The quest for Hsp104 cofactors 109
4.6.2 Cpr6 is a potential cofactor of Hsp104 111
4.6.3 Cpr6 specifically modulates the ATPase activity of Hsp104 *in vitro* 112
4.6.4 Cpr6 binds to Hsp104 *in vitro* 114
4.6.4.1 Analysis of the Hsp104·Cpr6 complex by analytical ultracentrifugation 114
4.6.4.2 Analysis of the Hsp104·Cpr6 complex by fluorescence anisotropy 117
4.6.5 Cpr6 can enhance protein disaggregation by Hsp104 *in vitro* 119
4.6.5.1 Cpr6 does not affect the Hsp104-mediated refolding of luciferase 119
4.6.5.2 Cpr6 enhances Hsp104-mediated refolding of murine DHFR 120
4.6.6 Cpr6 interacts with Hsp104 *in vivo* 122
4.6.6.1 Co-immunoprecipitation of Hsp104 and Cpr6 122
4.6.6.2 Co-localization of Hsp104 and Cpr6 in living yeast cells 123

4.6.7 Deletion of *CPR6* reduces the prion propagation of yeast 125
4.6.8 Over-expression of Cpr6 restores the original [*PSI*$^+$] phenotype 127
4.6.9 The C-terminus of Hsp104 is required for the functional contribution by Cpr6 128
4.6.10 The interaction of Cpr6 and Hsp104 is required for the stress tolerance of yeast 129

5. DISCUSSION 130
5.1 The oligomerization state of Hsp104 is highly dependent on its environment 130
5.2 The ATP hydrolysis by Hsp104 is tightly regulated 131
5.2.1 Functional regulation of the nucleotide binding domains of Hsp104 131
5.2.2 Implications of the domain regulation on the ATPase cycle of Hsp104$_{WT}$ 133
5.3 GdmCl is an uncompetitive inhibitor of Hsp104 136
5.3.1 Hsp104 is the GdmCl target in yeast 136
5.3.2 Gdm$^+$ affects exclusively nucleotide-bound Hsp104 137
5.3.4 Gdm$^+$ binds to the nucleotide binding domain 1 of Hsp104 138
5.3.5 Gdm$^+$ disturbs the intrinsic regulation of Hsp104 138
5.3.6 Hsp104 inactivation by GdmCl – consequences for prion propagation in yeast 140
5.5 The cyclophilin Cpr6 is a cochaperone of Hsp104 142
5.5.1 Identification of a cofactor binding domain of Hsp104 142
5.5.2 Cpr6 interacts specifically with Hsp104 142
5.5.3 Existence of a chaperone network between Hsp70, Hsp90 and Hsp104 143
5.5.4 Implications for the mechanism of disaggregation by Hsp104 144

6. ABBREVIATIONS 146

7. REFERENCES 148

APPENDIX

A.1 Multiple sequence alignment of Hsp100/ClpB proteins
A.2 Sedimentation equilibrium experiment of Hsp104$_{WT}$ shows a 611 kDa complex
A.3 Structure of Gdm$^+$ and similar compounds
A.4 Truncation of the C-terminus of Hsp104 does not affect its hexamerization

ACKNOWLEDGEMENTS

ORIGINAL PUBLICATIONS

LIST OF FIGURES

Fig. 2.1: Energy landscape for protein folding and aggregation based on the model of an energy funnel
Fig. 2.2: The *cis* and *trans* isomers of a peptidyl-prolyl bond, C_{Xaa}-N_{Pro}
Fig. 2.3: The life cycle of a protein in *E. coli* is guided by molecular chaperones
Fig. 2.4: The crystal structure of *Methanococcus jannaschii* Hsp16.5 at 2.9 Å resolution
Fig. 2.5: The crystal structure of GroEL/ES at 3.0 Å resolution
Fig. 2.6: Simplified substrate cycle of GroEL/ES
Fig. 2.7: The ATPase cycle of HtpG and Hsp90
Fig. 2.8: Electrostatic surface representation of TPR domain-peptide complexes
Fig. 2.9: The crystal structure of bovine Cyp40 at 1.8 Å resolution
Fig. 2.10: Model of disaggregation by Hsp100/ClpB
Fig. 2.11: Overview of the domain organization of the Clp protein family
Fig. 2.12: The promoter region of *HSP104* contains several Hsf1 and Msn2/4 transcription factor binding sites
Fig. 2.13: Stress-dependent mRNA pattern of selected proteins in yeast
Fig. 2.14: The prion phenotype of [*PSI*$^+$] from yeast
Fig. 2.15: Model of the Hsp104 hexamer
Fig. 2.16: Domain structure of an Hsp100/ClpB protomer
Fig. 2.17: Structural properties of an AAA module (= NBD)
Fig. 2.18: The ATPase-coupled substrate binding cycle of Hsp104
Fig. 3.1: Particle distribution in a sedimentation equilibrium
Fig. 4.1: Hsp104 is a member of the highly conserved family of Hsp100/ClpB proteins
Fig. 4.2: Hydrophobicity plot of Hsp104 demonstrates its domain boundaries
Fig. 4.3: Far-UV CD spectra of $Hsp104_{WT}$ and $Hsp104_{TRAP}$ show a high content of α-helices
Fig. 4.4: SLS signal increases due to nucleotide induced oligomerization
Fig. 4.5: Concentration dependency of Hsp104 oligomerization monitored by SLS
Fig. 4.6: Sedimentation velocity analysis of $Hsp104_{WT}$ shows a pure species with a sedimentation coefficient of 16.5 S
Fig. 4.7: Schematic view of the point mutants in the ATPase domains of Hsp104 used in this study
Fig. 4.8: Rate constants k_{cat} of $Hsp104_{WT}$ and its ATPase mutants reveal differences in the ATP turn-over of NBD1 and NBD2
Fig. 4.9: Concentration dependency of the ATP turn-over by $Hsp104_{WT}$ and $Hsp104_{K620T}$
Fig. 4.10: $Hsp104_{WT}$·$Hsp104_{K218T}$ hetero-oligomers are stable and show an altered ATP turn-over
Fig. 4.11: ATP concentration dependency of the ATPase activities of (A) $Hsp104_{WT}$, (B) $Hsp104_{K620T}$, (C) $Hsp104_{E285Q}$, and (D) $Hsp104_{E687Q}$
Fig. 4.12: Change in ANS fluorescence upon binding to $Hsp104_{WT}$
Fig. 4.13: Titration of Hsp104 and Hsp104·ADP with ANS
Fig. 4.14: ADP titration of (A) $Hsp104_{WT}$, (B) $Hsp104_{K218T}$ and (C) $Hsp104_{K620T}$ using ANS fluorescence
Fig. 4.15: Representative ITC experiments of Hsp104
Fig. 4.16: Curing of the [*PSI*$^+$] prion phenotype by GdmCl
Fig. 4.17: GdmCl inhibits Hsp104 but not Hsp82 and GroEL
Fig. 4.18: GdmCl and NAAA – but not urea – inhibit the ATP hydrolysis activity of Hsp104
Fig. 4.19: Dependency of the degree of inhibition by GdmCl on protein concentration
Fig. 4.20: Hsp104 oligomerization monitored by static light scattering with and w/o the presence of GdmCl
Fig. 4.21: ITC titration reveals nucleotide dependency of GdmCl binding

Fig. 4.22: GdmCl increases the affinity of Hsp104 for ADP
Fig. 4.23: GdmCl can stimulate nucleotide-induced hexamerization of Hsp104
Fig. 4.24: ATP concentration dependency of the ATPase activities of $Hsp104_{WT}$ with and w/o addition of 5 mM GdmCl
Fig. 4.25: ATP concentration dependency of the ATPase activities of the Walker A mutant, $Hsp104_{K620T}$, with and w/o addition of 5 mM GdmCl
Fig. 4.26: ATP concentration dependency of the ATPase activities of the Walker B mutants, $Hsp104_{E285Q}$ and $Hsp104_{E687Q}$, with and w/o addition of 5 mM GdmCl
Fig. 4.27: Influence of RCMLa on the ATP turn-over of $Hsp104_{WT}$ with and w/o addition of GdmCl
Fig. 4.28: Luciferase refolding by the Hsp104, Hsp70, and Hsp40 chaperone system in the presence of GdmCl
Fig. 4.29: The C-terminus of eukaryotic Hsp104 and Hsp90 – but not of prokaryotic ClpB and HtpG – contains an acidic motif
Fig. 4.30: Effect of Hsp90 cofactors on the ATP turn-over of Hsp104
Fig. 4.31: An increase in the Cpr6 concentration reduces the ATP turn-over of Hsp104
Fig. 4.32: ATP dependency of Hsp104 with and w/o addition of Cpr6, (A) Michaelis-Menten plot and (B) double-reciprocal Lineweaver-Burk plot
Fig. 4.33: Sedimentation profiles of (A) Hsp104, (B) $Cpr6_{FITC}$ and (C) Hsp104·$Cpr6_{FITC}$ detected at λ_{280} and λ_{494}
Fig. 4.34: Sedimentation profiles of $Cpr6_{FITC}$ with addition of (A) $Hsp104_{K218T}$ and (B) $Hsp104_{893\Delta C}$
Fig. 4.35: Co-sedimentation analysis of Hsp104 and $Cpr6_{FITC}$
Fig. 4.36: Binding of $Cpr6_{LUY}$ to Hsp104 as monitored by fluorescence anisotropy
Fig. 4.37: Binding of $Cpr6_{LUY}$ to monomeric $Hsp104_{\Delta NM}$ monitored by fluorescence anisotropy
Fig. 4.38: Cpr6 does not affect Hsp104-mediated renaturation of luciferase
Fig. 4.39: Cpr6 promotes peptidyl-prolyl isomerization-dependent refolding of mouse DHFR
Fig. 4.40: Cpr6 enhances Hsp104-mediated renaturation of mouse DHFR
Fig. 4.41: Cpr6 and Hsp104 interact with each other *in vivo*
Fig. 4.42: Yeast cells expressing the fluorescent fusion proteins RFP-Cpr6 or Sup35NM-GFP
Fig. 4.43: Co-localization of Sup35NM-GFP with RFP-Cpr6 in $Hsp104_{TRAP}$-expressing cells
Fig. 4.44: $Hsp104_{TRAP\Delta C}$ does not mediate co-localization of RFP-Cpr6 with Sup35NM-GFP
Fig. 4.45: Model of interaction of Sup35NM-GFP and RFP-Cpr6 by associating with $Hsp104_{TRAP}$
Fig. 4.46: The disruption of the *CPR6* gene generates a weak prion phenotype [*PSI*$^+$]
Fig. 4.47: Over-expression of *CPR6* restores the strong [*PSI*$^+$] phenotype
Fig. 4.48: Deletion of the C-terminal acidic motif of Hsp104 affects its function *in vivo*
Fig. 4.49: The interaction of Hsp104 and Cpr6 is required for ethanol tolerance and for induced thermotolerance
Fig. 5.1: Different models of the ATPase cycle of hexameric AAA^+ ATPases
Fig. 5.2: Model of the ATP hydrolysis cycle by Hsp104
Fig. 5.3: Model of Gdm^+-inhibition of the ATPase cycle by Hsp104
Fig. 5.4: The molecular chaperone network of Hsp70/90/100 is based on TPR interactions
Fig. 5.5: Model of disaggregation by Hsp104 and its assisting cochaperones
Fig. 5.6: Comparison of the Hsp104·Cpr6 complex with the ribosome·triggerfactor complex

LIST OF TABLES

Tab. 2.1: List of all identified TPR domain containing proteins in yeast
Tab. 3.1: Primers for PCR amplification and mutagenesis
Tab. 3.2: Internal primers for the sequencing of *HSP104*
Tab. 3.3: Bacterial plasmids used in this work
Tab. 3.4: Bacterial strains used in this work
Tab. 3.5: Yeast vectors used in this work
Tab. 3.6: Yeast strains used in this work
Tab. 4.1: Domain organization and functional motifs of Hsp104
Tab. 4.2: Secondary structure prediction of Hsp104 based on a far-UV CD spectrum
Tab. 4.3: Sedimentation coefficients of Hsp104 and its mutants obtained by sedimentation velocity analysis
Tab. 4.4: ATP turn-over of eukaryotic heat shock proteins
Tab. 4.5: Enzymatic constants derived from the Michaelis-Menten analysis of $Hsp104_{WT}$ and its ATPase mutants
Tab. 4.6: Nucleotide affinities of $Hsp104_{WT}$ and its ATPase mutants
Tab. 4.7: Influence of the presence of 5 mM GdmCl on the enzymatic constants of $Hsp104_{WT}$ and its ATPase mutants
Tab. 4.8: Influence of the presence of Cpr6 on the enzymatic constants of $Hsp104_{WT}$

LIST OF EQUATIONS

Eq. 3.5: Calculation of the molar ellipticity
Eq. 3.6: Svedberg equation to calculate the sedimentation coefficient
Eq. 3.7: Equation to calculate the sedimentation coefficient
Eq. 3.8: Equation to describe the sedimentation equilibrium for the calculation of the molecular weight
Eq. 3.9: Calculation of the ATPase reaction slope based on NADH absorbance
Eq. 3.10: Calculation of the apparent velocity of ATP hydrolysis
Eq. 3.11: Michaelis-Menten equation
Eq. 3.12: Hill equation for cooperative enzyme catalysis

1. SUMMARY

The molecular chaperone Hsp104 of *Saccharomyces cerevisiae* represents a powerful machine for the disaggregation of proteins. It is directly involved in the renaturation of stable protein aggregates and plays a central role in prion propagation in yeast cells. Therefore, Hsp104 is crucial for protein homeostasis in yeast. Hsp104 is a hexameric AAA^+ ATPase that couples cycles of ATP hydrolysis to an unfolding of its polypeptide substrates. The current study aims to gain insight into the functional regulation of Hsp104. Such an in-depth understanding will contribute to customize Hsp104 as a tool for biotechnological and medical approaches.

Using equilibrium methods it was demonstrated that the active species of Hsp104 are hexamers. These hexamers were detected and analyzed by ultracentrifugation. Importantly, while both active hexamers and inactive monomers were shown to exist, no intermediate species such as dimers or trimers were detected. Further, it was found that Hsp104 hexamers do not disassemble during steady-state ATP hydrolysis. The extraordinary stability of the hexamer under its working conditions suggests that the hexamer maintains its oligomeric state until its “work” is done. The monomer-hexamer equilibrium might come into play in the event of stacking when substrates are too stable or too big to be processed by Hsp104. By disassembling a hexameric Hsp104 complex into monomers a blocked Hsp104 could then be recycled instead of being a subject for protein degradation.

The unfolding function of Hsp104 is fueled by ATP hydrolysis. Understanding the ATPase function of the chaperone and how it is intrinsically regulated is therefore of crucial importance to understand the functioning of the Hsp104 machinery. An Hsp104 hexamer possesses two types of nucleotide binding sites, NBD1 and NBD2. By using specifically designed mutants this study investigates the role of each nucleotide binding site and their interplay.
It was found that NBD1 is mainly responsible for the steady state ATP hydrolysis of wild-type Hsp104. In contrast, NBD2 has no apparent ATP turn-over at steady-state conditions since it is allosterically highly regulated by the ATP-bound state of NBD1. The ATPase activity by NBD2 becomes activated only when the upper NBD1-ring is fully saturated with ATP – a state that apparently does not exist under steady-state conditions of Hsp104. The *in vitro* analysis of the intrinsic regulation of the ATPase activity of Hsp104 allowed to suggest model for the regulation of ATP hydrolysis by Hsp104 comprising a non-concerted ATPase cycle in which NBD1 is active in alternating single steps of ATP binding and ATP hydrolysis while NBD2 rests in an nucleotide-bound inactive state and ensures the maintenance of oligomer stability.

In previous studies the effects of the ATPase function of Hsp104 could only be analyzed by employing specifically designed mutants. A more convenient tool for research, however, would be the availability of a specific inhibitor for the ATPase activity of Hsp104. This study identified guanidinium chloride (GdmCl) to be such a specific inhibitor of Hsp104 function *in vitro*. The mechanism of GdmCl inhibition was found to be highly specific and not linked to its denaturing properties. Trace amounts of GdmCl were found to bind to the nucleotide-bound state of NBD1 within hexameric Hsp104, exclusively. Thereby, GdmCl presumably affects the allosteric communication between the protomers. GdmCl was found to selectively inhibit the ATPase activity of Hsp104 in an uncompetitive manner and to significantly impair its chaperone function.
It is established in this respect since nearly 30 years that trace amounts of GdmCl in the growth medium abolish the prion replication in yeast cells, an effect known as prion curing. The underlying biochemical mechanism of this effect, however, remained unknown. The *in vitro* results of this study are now able to explain the observed prion curing by the uncompetitive inhibition of Hsp104 by GdmCl *in vivo*.

Above and beyond this, the current work shows for the first time a *direct* interaction of Hsp104 with a *bona fide* cofactor, the cyclophilin Cpr6. The *in vitro* analysis of the interaction of Hsp104 and Cpr6 revealed that Cpr6 act as a specific modulator of the ATPase activity and of the chaperone function of Hsp104. It was found in this study that the *in vivo* interaction of Hsp104 with Cpr6 enhances both the Hsp104-mediated prion propagation and the Hsp104-mediated thermotolerance of yeast. Cpr6 has a *cis-trans* prolyl isomerase function, which appears to be required for the proper refolding of distinct Hsp104 substrates. Thus, Cpr6 contributes to a versatile chaperone function of Hsp104. Cpr6 was originally identified as a cochaperone of Hsp90 to which it binds *via* its TPR domain. Hsp104 contains a similar acidic C-terminal Cpr6-docking motif. Accordingly, a comparable TPR interaction might take place when Cpr6 binds to both molecular chaperones. This new interaction indicates that Hsp104 is an integral part of the TPR interaction-based chaperone network in eukaryotic cells comprising chaperones such as, e.g., Hsp90 and Hsp70. The integration of Hsp104 into the Hsp90-Hsp70 chaperone network provides new perspectives for a crosstalk or substrate transfer between these chaperone classes and Hsp104.

1. ZUSAMMENFASSUNG

Das molekulare Chaperon Hsp104 aus *Saccharomyces cerevisiae* ist eine leistungsfähige Maschine für die Auflösung von Proteinaggregaten. Hsp104 ist direkt an der Resolubilisation von stabilen Proteinaggregaten beteiligt und spielt zudem bei der Prionenreplikation in Hefezellen eine zentrale Rolle. Die Aktivität von Hsp104 ist somit von entscheidender Bedeutung für die Proteinhomeostase in Hefe. Hsp104 ist eine Hexamer-bildende AAA^+ ATPase, welche die Energie aus seiner ATP Hydrolyse mechanisch an die Entfaltung von Polypeptidsubstraten koppelt. Die vorliegende Studie hat zum Ziel, ein Verständnis von der funktionalen Regulation von Hsp104 zu erlangen. Detaillierte Erkenntnisse über die Regulation der Hsp104-Maschinerie werden dazu beitragen, Hsp104 als Werkzeug für biotechnologische und medizinische Ansätze effektiv einsetzen zu können.

In dieser Studie wurde unter Verwendung von Gleichgewichtsverfahren gezeigt, daß das Hexamer die enzymatisch aktive Spezies von Hsp104 ist. Durch analytische Ultrazentrifugationsexperimente wurden Hsp104 Oligomere detektiert und analysiert. Während Hsp104 sowohl in monomerer Form als auch als Hexamer nachweisbar war, konnte die Existenz von potentiellen intermediären Spezies, wie beispielsweise Dimeren oder Trimeren, jedoch nicht gezeigt werden. Dies gibt Anlaß zu der Vermutung, daß solche intermediären Spezies entweder nicht oder nur in extrem geringer Konzentration vorliegen. Ferner konnte gezeigt werden, daß die Hexamere von Hsp104 während der *steady-state* ATP-Hydrolyse eine bemerkenswerte Stabilität aufweisen und keine Assoziationsdynamik feststellbar ist. Das erlaubt den Rückschluß, daß Hsp104 bei der Ausführung seiner Funktion als Polypeptid-enfaltende Maschine in seinem oligomeren Zustand stabil vorliegt, bis das Substrat vollständig umgesetzt ist. Das Monomer-Hexamer-Gleichgewicht könnte hingegen dann eine Rolle spielen, wenn das Substrat zu stabil oder zu groß ist, als daß es durch Hsp104 vollständig prozessiert werden könnte. Wenn in einem solchen Fall das Hsp104 Hexamer in seine monomeren Bestandteile zerfallen würde, könnte Hsp104 daraufhin erneut oligomerisieren und müßte nicht als blockiertes Hexamer der Proteindegradation zugeführt werden.

Die ATP-Hydrolyse liefert die erforderliche Energie, die Hsp104 für die Resolubilisation von stabilen Proteinaggregaten benötigt. Das Verständnis der ATPase-Funktion und ihrer intrinsischen Regulation ist somit von entscheidender Bedeutung für das Verständnis der Funktionsweise von Hsp104 als eine molekulare Maschine. Ein Hsp104-Hexamer weist zwei unterschiedliche Arten von Nukleotidbindedomainen auf, NBD1 und NBD2. Durch Verwendung von verschiedenen speziell entworfenen Mutanten wurde in dieser Studie die Funktion der einzelnen Nukleotidbindedomainen sowie deren mögliches Zusammenspiel untersucht.

Es konnte gezeigt werden, daß NBD1 in erster Linie für die messbare ATPase Aktivität des Hsp104-Hexamers unter *steady-state* Bedingungen verantwortlich ist. Im Gegensatz dazu findet an der NBD2 unter *steady-state* Bedingungen kein apparenter ATP-Umsatz statt, da die Aktivität von NBD2 durch NBD1 allosterisch reguliert wird. Die ATPase-Funktion der NBD2 scheint nur dann aktiviert zu werden, wenn der NBD1-Ring, also die Gesamtheit aller NBD1-Domänen im Hexamer, vollständig durch ATP-Bindung gesättigt ist. Ein solcher Zustand existiert in einem Hsp104 Hexamer offensichtlich kaum oder gar nicht unter *steady-state* Bedingungen. Die *in vitro*-Analyse dieser Studie erlaubt nun, ein Modell für die intrisische Regulation der ATPase-Funktion des Hsp104-Hexamers vorzuschlagen, bei dem die ATP-Hydrolyse im Rahmen eines nicht-konzertierten Zyklus stattfindet. Hierbei wird an den einzelnen Protomeren in alternierenden Einzelschritten jeweils ATP an NBD1 gebunden und hydrolysiert. Die zweite Nukleotidbindedomäne, bzw. der NBD2-ring, befindet sich im ATP-hydrolysiernden Hexamer während dessen in einem Nukleotid-gebundenen – aber inaktivem – Zustand und gewährleistet so die Stabilität des „arbeitenden" Hexamers.

Die Auswirkungen der ATPase-Aktivität von Hsp104 auf seine Chaperon-Funktion konnten bisher nur durch die Verwendung entsprechender Mutanten analysiert werden. Wenn der Forschung jedoch ein spezifischer Inhibitor der ATPase-Aktivität von Hsp104 zur Verfügung stünde, wäre dies von Vorteil. Im Rahmen dieser Arbeit wurde Guanidiniumchlorid (GdmCl) als ein spezifischer Inhibitor der ATPase-Funktion von Hsp104 *in vitro* identifiziert. Der Mechanismus der Inhibierung durch GdmCl wurde untersucht, und es hat sich herausgestellt, daß GdmCl die ATPase-Aktivität von Hsp104 selektiv inhibiert, wobei diese Wirkung mit den denaturierenden Eigenschaften von GdmCl nicht in Verbindung zu bringen ist. Vielmehr bindet GdmCl in geringen Mengen ausschließlich an die von Nukleotid besetzte NBD1 innerhalb von Hsp104-Hexameren. Hierdurch beeinflußt GdmCl vermutlich die allosterische Kommunikation zwischen den Protomeren, so daß GdmCl die ATPase-Aktivität des Hexamers auf eine unkompetetive Weise inhibiert und dessen Chaperon-Aktivität beeinträchtigt.
Seit fast 30 Jahren war in dieser Hinsicht bekannt, daß geringe Mengen an GdmCl im Nährmedium von Hefen die Prionenreplikation unterbinden. Der diesem als *Prionen-Curing* bekannten Effekt zugrunde liegende Mechanismus war jedoch unbekannt. Die *in vitro*-Daten dieser Studie erbringen den biochemischen Nachweis, daß das *in vivo* beobachtete *Prionen-Curing* auf einer von GdmCl verursachten spezifischen Inhibition von Hsp104 beruht.

Darüber hinaus ist es im Rahmen dieser Arbeit erstmalig gelungen, die direkte Interaktion von Hsp104 mit einem Chaperon-Cofaktor, dem Cyclophilin Cpr6, zu demonstrieren und zu untersuchen. Die *in vitro*-Studien ergaben, daß Cpr6 als spezifischer Modulator der ATPase-Aktivität und der Chaperon-Funktion von Hsp104 agiert. *In vivo*-Experimente haben in dieser Studie zudem gezeigt, daß die Interaktion von Hsp104 mit Cpr6 für die von Hsp104 vermittelte Thermotoleranz und Prionenreplikation in Hefe von Bedeutung ist. Cpr6 besitzt

eine *cis-trans*-Prolylisomerase-Funktion, welche für die effektive Resolubilisation von bestimmten Hsp104-Substraten erforderlich zu sein scheint. Somit spezialisiert und verbessert Cpr6 die Chaperon-Funktion von Hsp104. Ursprünglich wurde Cpr6 als Cochaperon von Hsp90 identifiziert. Die entsprechende Interaktion findet über die TPR-Domaine von Cpr6 statt. Hsp104 weist ein vorwiegend saures C-terminales Cpr6-Bindemotif auf, das dem C-terminalen TPR-Protein-Bindemotif von Hsp90 ähnelt. Dementsprechend könnte Cpr6 mit beiden molekularen Chaperonen, Hsp90 und Hsp104, auf ähnliche Weise interagieren. Diese neu identifizierte Interaktion belegt, daß Hsp104 gemeinsam mit anderen molekularen Chaperonen wie Hsp90 und Hsp70 einen integralen Bestandteil des auf TPR-Wechselwirkungen basierenden eukaryotischen Chaperon-Netzwerks darstellt. Diese Einbeziehung in das Hsp90-Hsp70 Chaperon-Netzwerk eröffnet neue Perspektiven für eine gegenseitige Wechselwirkung oder für einen Substrat-Transfer zwischen diesen Chaperon-Klassen und Hsp104.

2. INTRODUCTION

2.1 The theory of protein folding

The activity of proteins is crucial for living cells since they are involved in almost every aspect of life. The proteome, which is the protein composition at a certain state in the cell cycle, can be considered as the "executive power" of a cell. However, most proteins are only active when they exist in their specific three-dimensional structure, i.e., when they are natively folded. The ability to fold *de novo* into their functional three-dimensional structure within a short time is one of the most fundamental phenomena in nature. For more than 5 decades protein folding has been studied since Anfinsen and coworkers were the first to show, by their folding studies on ribonuclease A, that a protein can fold spontaneously and autonomously into its native conformation *in vitro*. The folding is only dependent on the amino acid sequence of the protein and on the particular set of reaction conditions (Anfinsen *et al*., 1961). The best folding yields of a protein are usually obtained at high dilutions of the protein, under physiological buffer conditions, and at low temperatures. However, most proteins, especially multi-domain proteins, do not fold correctly *in vitro* but instead tend to aggregate (Goldberg *et al*., 1991; Jaenicke and Seckler, 1997).

Theoretical models of protein folding were, and still are, developed based on *in vitro* folding experiments. The underlying fundamental question to be answered, however, remains the same: how can proteins attain their native structure within minutes – a folding problem known as the Levinthal paradox. From a mathematical view a 100-residue protein has zillions of possible conformations ($> 2^{100}$) since at least two conformations, the *cis* and the *trans* isomer of the planar peptide bond, are possible for each residue. If a timeframe of 1 picosecond is assumed for each transition between the conformational states the required time to attain the native structure byrandom search would theoretically take 10^{10} years – a time range that is not reasonable for living systems. Thus, it was postulated that a specific folding pathway exists for every protein and that the native fold is simply the end of this pathway (Levinthal, 1968).

Currently, the process of protein folding is described by thermodynamic models based on the change of free energy upon folding. Energy landscapes serve to describe the search of the unfolded protein down a funnel-like energy profile towards the native structure, which is a state of minimal free energy (see Fig. 2.1). The surface of such a folding funnel is unique for a specific polypeptide under a particular set of conditions and it is determined by both thermodynamic and kinetic properties of the folding chain reaction (Dill and Chan, 1997; Dobson and Karplus, 1999). The model also describes how partially folded states might be kinetically trapped in local energy minima. They may be prone to aggregation or they follow non-native folding pathways, which might result in protein misfolding diseases (Jahn and Radford, 2005).

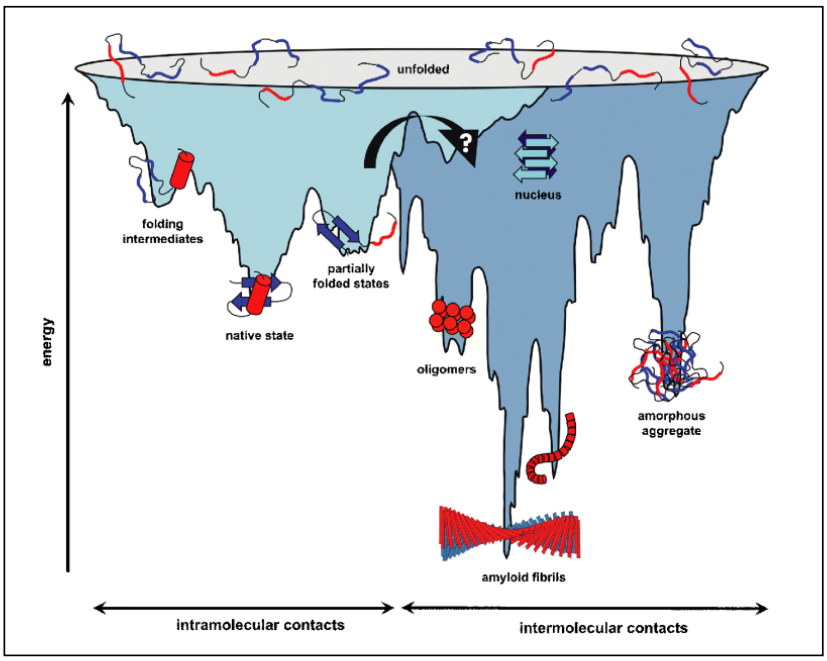

Fig. 2.1: Energy landscape for protein folding and aggregation based on the model of an energy funnel. The surface shows the multitude of conformations "funneling" towards the native state *via* intra-molecular contact formation, or towards the formation of amyloid fibrils *via* inter-molecular contacts. The species involved in converting kinetically stabilized globular structures into the amyloid fibrils is currently not defined, as indicated by the arrow. Reproduced from Jahn and Radford (Jahn *et al.*, 2005).

The driving force of folding is the gain of a maximal packing density, by the removal of water molecules out of the internal core of a protein, the so-called hydrophobic collapse (Jaenicke, 1987; Jaenicke, 1991; Dill and Shortle, 1991). However, protein folding is not a stochastic process but rather a sequential reaction with a limited number of alternative pathways. The actual folding pathway of a protein can be described as involving three steps (Creighton, 1992; Ptitsyn, 1996; Galzitskaya *et al*., 2001):

(i) The sub-millisecond stage is characterized by a partial formation of secondary structure elements (α-helix, β-sheet) and by a partial condensation resulting in the formation of so-called folding nuclei. These structures derive from short range interactions within the polypeptide chain based on hydrogen bonds, hydrophobic interactions, electrostatic interactions and van der Waals' forces.

(ii) Once the kinetic nuclei reach an energy minimum, the hydrophobic collapse takes place. The secondary structure assembles into a quasi-native tertiary structure, the so-called molten globule state. This partially folded intermediate exhibits a high content of secondary structure, a tight packing density but still many fluctuating hydrated hydrophobic amino acids. During this state some proteins pass though several intermediate states, which slightly differ in their entropy from that of the unfolded state. By this means, the molten globule exists in a sensitive equilibrium of native and misfolded conformations.

(iii) Further energy minimization by the ongoing positioning of charged residues and the formation of hydrophobic clusters promotes the generation of a stable tertiary structure with individual domains. This step is slow and *in vitro* protein folding studies revealed that the final formation of the native state can take from a fraction of a second to several minutes due to rate-limiting processes such as peptidyl-prolyl *cis-trans* isomerization, formation of disulfide bridges, and re-arrangement of non-native sub-domains (Goto and Hamaguchi, 1982; Eppens *et al*., 1997; Golbik *et al*., 1999; Schmid, 2001; Cerasoli *et al*., 2002; Singh and Appu Rao, 2002)

2.2 Protein folding *in vivo*

In vivo the situation is more complex and several additional factors influencing the process must be considered. The general protein folding within a cell must proceed within minutes or seconds, which is in contrast to some *in vitro* folding protocols requiring hours or days. Further, the initiation of protein folding already starts at the ribosomal exit site: it takes place in a vectorial manner while the N-terminal portion of the polypeptide is leaving the ribosomal tunnel whereas the C-terminal segment has not been synthesized yet (Frydman and Hartl, 1996). Nascent polypeptides emerging from the ribosome do not contain the complete information that might be necessary for successful folding. However, the rate of folding of a typical protein ($t_{½}$ < 1s) is much faster than the rate of its synthesis (4 - 20 amino acids per second, Agashe and Hartl, 2000). Thus, the folding of the N-terminus starts in the absence of a possible contribution of the C-terminus. Notably, this premature protein folding constitutes a possible problem for the attainment of a native protein structure since co-translational protein degradation exists as a form of protein quality control which destroys nascent chains that fail to fold correctly rapidly enough (Turner and Varshavsky, 2000).

Finally, the protein will be folded in a dense solution under molecular crowding conditions (~340 mg macromolecules per mL, Goodsell, 1991) comprising several different components such as proteins, DNA, lipids, sugar, metal ions, etc. This environment can favor unproductive interactions of the folding intermediates of newly synthesized proteins with other unstable proteins. Therefore, cells have developed folding helpers, which will be presented in 2.4.

A number of proteins are intrinsically unstable and their folding status is highly susceptible to changes of the cellular environment. Stress conditions, such as a sudden increase in temperature, can therefore lead to unfolding and aggregation of many proteins. The reason for this instability is the small difference in free energy of usually 4 - 60 kJ/mol between the unfolded and the folded state of a protein (Fersht and Daggett, 2002). This might be the price for the commonly observed conformational flexibility of many proteins that is essential for their function.

2.3 The aggregation of proteins

Non-specific interactions between protein folding intermediates or protein assembly intermediates increase the number of non-native folding pathways of proteins. Thereby, an increasing number of misfolded proteins accumulates and associates into big non-native oligomers, i.e., aggregates. Misfolded or aggregated proteins can harm organisms by affecting their cellular processes, as demonstrated by many examples of protein conformational disorders such as the Alzheimer's and Parkinson's disease, type II diabetes and the spongiform encephalopathies such as Creutzfeld-Jakob disease (Soto, 2001). Strikingly, many of these protein conformational disorders are caused by a formation of non-native β-sheets that are linked to each other by intra-molecular or inter-molecular hydrogen bonds resulting in a non-native amyloid formation of the affected protein (Kelly, 2000; Nelson and Eisenberg, 2006).

2.4 Molecular chaperones and folding catalysts

In order to adapt to environmental changes such as changes in temperature or oxidative stress and in order to improve the folding of susceptible proteins, cells have developed highly conserved helper proteins: folding catalysts and molecular chaperones.
Folding catalysts comprise proteins that catalyze the rate-limiting steps of protein folding, such as protein disulfide isomerization (see PDIs below, Darby *et al*., 1994) and peptidyl-prolyl isomerization (see PPIases below, Brandts *et al*., 1975). Molecular chaperones are introduced in detail below.

2.4.1 Protein disulfide isomerases

Protein disulfide isomerases (PDIs), e.g., yeast Pdi1, assist in the correct formation of disulfide bridges of proteins in the endoplasmatic reticulum (ER). They are oxidoreductases and possess a redox-active Cys-x-x-Cys motif. Further, they usually have a binding affinity for peptides, which allows efficient oxidoreductase activity. Thereby, they catalyze the formation, reduction, or isomerization of the disulfide bridges of their substrates (Frand *et al*., 2000).

2.4.2 Peptidyl-prolyl isomerases

Peptidyl-prolyl isomerases (PPIases, rotamases) are characterized by a common reaction mechanism. They catalyze the *cis-trans* isomerization of a peptide bond preceding proline residues (C_{Xaa}-N_{Pro}), i.e., of a peptidyl-prolyl bond. *Cis* peptidyl-prolyl bonds in native

proteins complicate the folding process, because the *trans* isomers predominate in unfolded or nascent polypeptides and because the *trans* → *cis* isomerizations are intrinsically slow reactions. A *cis-trans* isomerization of a peptidyl-prolyl bond has an activation enthalpy of ~80 kJ/mol, which corresponds to a rather high energy barrier (see also Fig. 2.2). Therefore, the isomerization is relatively slow and the corresponding time constants are found to be between 10 and 100 s (at 25°C, Schmid, 2001).

For the catalysis of the *cis-trans* isomerization PPIases bind to their substrates in a conformation that corresponds to the transition state of a partially rotated peptidyl-prolyl bond. Thereby, they decrease the activation energy for the rotation by 50 kJ/mol (Fischer and Aumuller, 2003). Despite the common functional mechanism many PPIases differ strongly with respect to their size, structure and substrate specificity. As a consequence of their structural differences, PPIases are divided into the classes of the cyclophilins (= cyclosporine A binding proteins such as human Cyp40), the FKBPs (FK506-binding proteins such as triggerfactor), and the parvulins (such as human Pin1). The physiological importance of these proteins is demonstrated, for example by the involvement of FKBPs and cyclophilins in immunosuppression. They form inactive complexes with their natural inhibitors rapamycin, cylosporin A and FK506 that are commonly used as immune suppressive therapeutics. Unlike FKBPs and cyclophilins, parvulins do not bind to immunosuppressive drugs. They exhibit a high substrate specificity to phosphorylated peptidyl-prolyl bonds ($C_{pSer(Thr)}$-N_{Pro}) and are involved in the regulation of the cell cycle. Thereby, they are potential targets for an anti-cancer therapy, for example, by using their natural inhibitor juglone (Wang and Etzkorn, 2006).

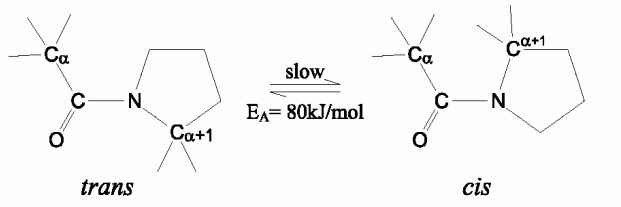

Fig. 2.2: The *cis* and *trans* isomers of a peptidyl-prolyl bond, C_{Xaa}-N_{Pro}. Reproduced from Schmid (Schmid, 2001).

2.4.3 Molecular chaperones

Molecular chaperones are proteins that have the general property to recognize non-natively folded proteins and to selectively bind to them – mostly by hydrophobic contacts. Molecular chaperones are able to prevent protein aggregation and to assist their substrates in reaching their native tertiary structure. They do not catalyze the folding reactions of proteins but rather minimize the non-native pathways of folding and protect the substrate against non-native interactions. For this reason they were called chaperones, a term that corresponds to a person protecting its ward against unwished contacts (Laskey *et al*., 1978). Molecular chaperones do

not only prevent aggregation of unfolded proteins – they also represent a major part of an interacting network of protein quality control in order to maintain cellular protein homeostasis and to even solubilize existing protein aggregates (Ben Zvi and Goloubinoff, 2001; Young *et al*., 2004; Zhao *et al*., 2005). Fig. 2.3 demonstrates in an exemplified scheme how molecular chaperones and other components of the cellular quality control system interact within the "life cycle" of a protein in *E. coli*.

Molecular chaperones were first described as proteins that are up-regulated under heat shock conditions and therefore, they were termed heat shock proteins (Pelham, 1986). However, the term heat shock protein does not only include molecular chaperones but rather all proteins induced upon heat shock. Further, many molecular chaperones are also essential under normal growth conditions. The increasing set of sequenced genomes revealed that molecular chaperones are highly conserved and found in all kingdoms of life. The following families of molecular chaperones (heat shock proteins) were classified according to their apparent size and to their function: small Hsps, Hsp60, Hsp70, Hsp90, and Hsp100. In the next chapters these main groups are briefly introduced, followed by a more detailed description of the Hsp100 proteins that are the focus of this study.

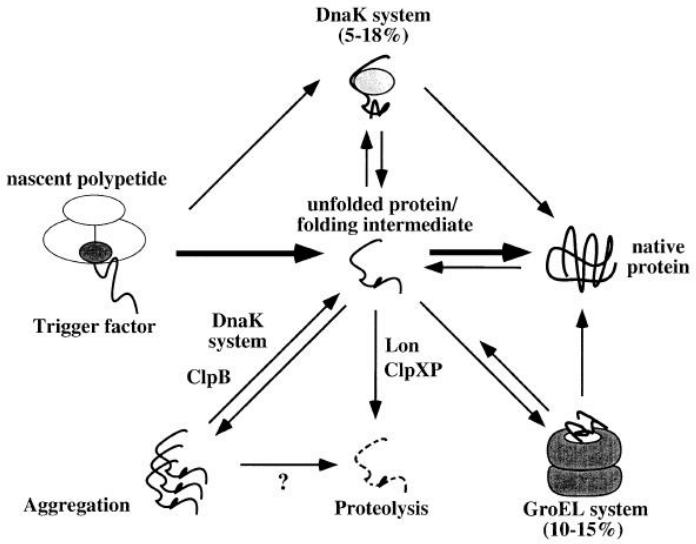

Fig. 2.3: The life cycle of a protein in *E. coli* is guided by molecular chaperones. A polypeptide is synthesized at the ribosome and folds into its native tertiary structure. Folding intermediates, which are prone to aggregation, can be protected through the association with molecular chaperones, which out-compete off-pathways of the folding process. The triggerfactor is associated with the large subunit of the ribosome and interacts with all nascent chains as they emerge from the ribosome. A fraction of newly synthesized proteins interacts with the DnaK/J/E or GroEL systems, respectively. Aggregated species that escaped the cellular protection machinery can be rescued by the ClpB/DnaK/J/E chaperone system. Non-native species, which fail to fold correctly can also be degraded by the ClpXP and Lon Protease. Reproduced from Schlieker and coworkers (Schlieker *et al*., 2002).

2.5 The classes of molecular chaperones

2.5.1 The class of small heat shock proteins

Small heat shock proteins (sHsps, e.g., human α-crystallin, yeast Hsp26, *E. coli* IbpA/B) constitute an abundant class of molecular chaperones of 15 - 40 kDa in size. This class of proteins possesses a characteristic conserved α-crystallin domain, which is rich in β-sheets (Kim *et al*., 1998; Haslbeck *et al*., 2005a).

The best characterized member of this family is α-crystallin itself, a major component of the eye lens (Horwitz, 2003). The association of many sHsps subunits into large spherical complexes in the mega Dalton range is the most notable property of sHsps (see Fig. 2.4). The complexes are hollow and possess several openings (Kim *et al.*, 1998). *In vitro*, sHsps can efficiently prevent the aggregation of heat denatured proteins (Jakob *et al*., 1993). Thereby, sHsps bind to partially folded proteins and form either soluble high molecular weight complexes with their substrate (Ehrnsperger *et al.*, 1997; Kim *et al.*, 1998; Haslbeck *et al*., 1999) or they even co-aggregate (Haslbeck *et al*., 2005b). Thus, sHsps correspond to "passively holding" chaperones, whereby they have a simple but effective buffering function by holding the substrates in a reactivation-competent state (Lee *et al*., 1997). However, the release and reactivation of aggregated proteins requires the contribution of "actively folding" chaperones, namely chaperones of the Hsp70 and Hsp100 system (Mogk *et al*., 2003b; Cashikar *et al*., 2005; Haslbeck *et al.*, 2005b).

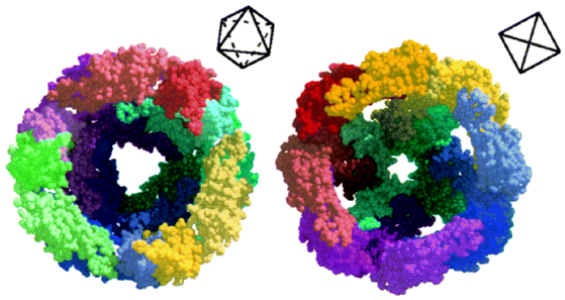

Fig. 2.4: The crystal structure of *Methanococcus jannaschii* Hsp16.5 at 2.9 Å resolution. The spherical complex with octahedral symmetry consists of 24 subunits and contains 14 openings. Reproduced from Kim and coworkers (Kim *et al.*, 1998).

2.5.2 The class of Hsp60/chaperonin proteins

Hsp60 proteins, known as chaperonins, are highly conserved essential ATPases that assist in the folding of unfolded or partially folded polypeptides. They can be divided into two families according to their functional assembly: (i) GroEL, comprising the prokaryotic and organellar members and (ii) CCT, the cytosolic members from eukaryotes, including the thermosome from archaea.

GroEL/ES from *E. coli* is the chaperone system that is currently best understood. It serves as a general model for chaperone-assisted protein folding (Sigler *et al*., 1998; Walter, 2002).

GroEL consists of 14 identical ATPase subunits of 57 kDa in size assembling into a double ring-shaped structure. Thereby, a central cavity of 45 Å in diameter is provided by each ring system (see Fig. 2.5). GroES, the essential cochaperone of GroEL, assembles into a heptameric ring structure that serves as a lid on top of the GroEL folding cavity (Xu *et al.*, 1997).

CCT, the second chaperonin family, consists of a hetero-oligomeric double ring system that is assembled of different subunits, which are structurally related to each other. In contrast to the GroEL, every ring system consists of 8 subunits (Kim *et al.*, 1994). Further, a homologue of the GroES cofactor is missing in this system since CCT contains an intrinsic helical loop functioning as a built-in lid (Meyer *et al.*, 2003).

The chaperone cycle of GroEL/ES is a tightly regulated process with a phase-delayed contribution/action of both GroEL ring systems. Initially, the protein substrate interacts with

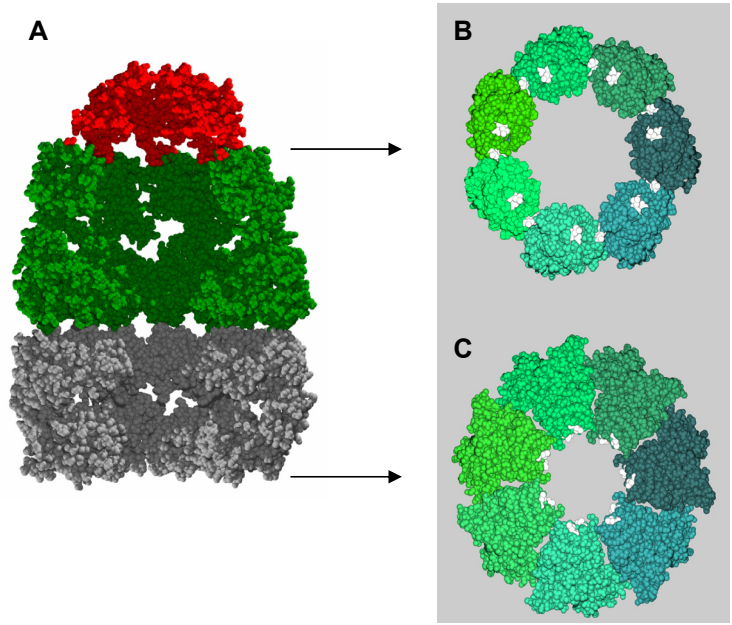

Fig. 2.5: The crystal structure of GroEL/ES at 3.0 Å resolution. The bacterial chaperonin GroEL consists of fourteen protomers assembling into two heptameric rings that form a barrel-shaped structure. (A) Cross-section of a GroEL/ES complex disclosing the central cavity of each GroEL ring. The heptameric GroES complex, which is shown in red, acts as a lid on top of one of the two GroEL rings, which are shown in green and grey, respectively. (B) Top view on the GroES-bound top ring of GroEL. The presented surface corresponds to the interface of GroEL to GroES. The hydrophobic residues in the apical domains constituting the polypeptide binding site are shown in white. Upon binding of GroES the hydrophobic residues of GroEL are rotated and become buried at this interface. The enlargement of the central cavity and the change of the inner lining provide the folding conditions for the substrate (C) Bottom view on the GroES-free bottom ring of GroEL. The hydrophobic residues in the apical domains constituting the polypeptide binding site are accessible at the inside of the central cavity in order to bind to polypeptides. Modified from Walter (Walter, 2002), which was based on data from Xu and coworkers (Xu *et al.*, 1997).

the apical domain of a substrate- and nucleotide-free GroEL ring (see Fig. 2.6). The subsequent binding of ATP and GroES to GroEL results in an enlargement of the central cavity and a displacement of the bound substrate into the cavity. The cavity serves as a protected chamber for the folding of the enclosed substrate, corresponding to an "Anfinsen cage" (Ellis, 2001). ATP hydrolysis by the substrate-bound GroEL ring and ATP binding at the opposite free ring trigger the GroES release and the substrate ejection (Walter, 2002).
In conclusion, GroEL requires ATP for the regulation of the substrate cycle together with the allosteric counter play of both ring systems. It is controversial, whether GroEL enhances substrate folding by simply providing an ATP-dependent folding compartment or whether it also uses ATP hydrolysis to actively induce conformational changes within polypeptides (Tang *et al*., 2006).

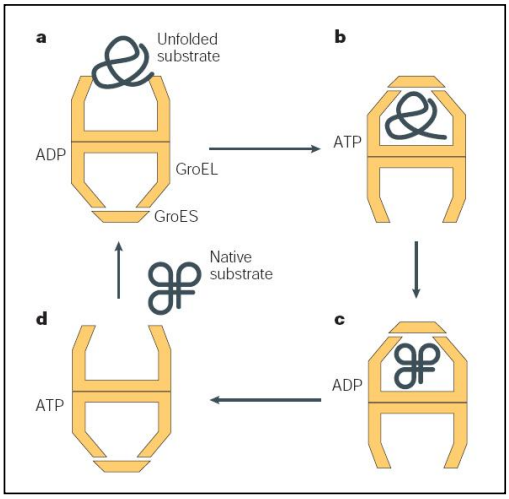

Fig. 2.6: Simplified substrate cycle of GroEL/ES. Both GroEL rings are functionally alternating within the following substrate cycle: (a) initial substrate binding to one ring of GroEL, (b) binding of ATP and the GroES-lid to the same GroEL-ring. Concurrently, the substrate is displaced into an enclosed cavity. (c) The sequestration of the substrate into the cavity allows its folding. (d) The dissociation of GroES from GroEL after ATP hydrolysis allows substrate release. Reproduced from Young and coworkers (Young *et al.*, 2004).

2.5.3 The class of Hsp70 proteins

The Hsp70 proteins are the most abundant class of molecular chaperones and are found in a rich diversity. They are involved in nearly every protein folding process and constitute a central component of the cellular chaperone network (Mayer and Bukau, 2005). Their main properties are (i) a highly regulated ATPase function, (ii) a concomitantly regulated peptide binding affinity, (iii) the interaction with cofactors, for example Hsp40 or nucleotide exchange factors, and (iv) the functional interplay with several other molecular chaperone families. Hsp70 binds selectively to hydrophobic regions of unfolded polypeptides in a nucleotide-dependent manner. In the ATP-bound state, Hsp70 exchanges polypeptide substrates rapidly. The hydrolysis of ATP converts Hsp70 to a closed state with low substrate exchange rates. This step is regulated by Hsp40 cochaperones stimulating the ATP

hydrolysis. The release of ADP that is induced by specific nucleotide exchange factors, e.g., *E. coli* GrpE, leads to an opening of the complex and transforms Hsp70 to the ATP-bound state (Bukau and Horwich, 1998). By such ATP-driven cycles of "substrate holding" and release, polypeptides can be refolded (Szabo *et al*., 1994; Buchberger *et al*., 1997). The mechanism of refolding remains to be clarified but the binding and release cycles rescue the substrate from aggregation, keep it in a soluble state and may also induce local conformational changes within the polypeptide substrate (Slepenkov *et al*., 2002).

Hsp40 proteins, such as yeast Ydj1 and *E. coli* DnaJ, are important cofactors of Hsp70 proteins containing a conserved J-domain that mediates their contact to Hsp70. They stimulate the ATP hydrolysis of Hsp70 and thereby play a crucial role in substrate binding (Liberek *et al*., 1991; Kelley, 1998; Qiu *et al*., 2007). However, Hsp40 proteins also bind to hydrophobic sequences of unfolded polypeptides and transfer them to Hsp70. Thus, Hsp40 proteins are also responsible for the targeting of Hsp70-mediated refolding (Rüdiger *et al*., 2001). The folding-active set of Hsp70 with its cofactors is called the "Hsp70 system". An example is "KJE" in *E. coli* comprising DnaK, DnaJ, and GrpE.

Hsp70 interacts with several folding pathways in the cell and the targeting of these pathways occurs *via* TPR interaction: the C-terminal EEVD motif of cytosolic eukaryotic Hsp70 mediates the interaction to tetratricopeptide repeat (TPR) domain containing proteins such as Hop/Sti1, which is also a cochaperone of Hsp90 (see below; Johnson *et al*., 1998; Scheufler *et al*., 2000).

Further, a functional interplay of the Hsp70 system exists with the Hsp100 chaperones regarding the disaggregation of protein aggregates (Glover and Lindquist, 1998), which will be presented in detail in chapter 2.6.2.

2.5.4 The class of Hsp90/HtpG proteins and their TPR cofactors

2.5.4.1 The structure and function of Hsp90/HtpG

Hsp90 is one of the most abundant cytosolic proteins in the cell (Richter and Buchner, 2001). The members of this conserved class of ATP-hydrolyzing chaperones are found in eubacteria (HtpG) as well as in eukaryotes (Hsp90).

Eucaryotic Hsp90 is responsible for the structural maturation and for the targeting of certain client proteins, such as kinases, and is thus involved in a variety of cellular processes, including development, cell cycle and steroid hormone signaling (Zhao and Houry, 2005).

Hsp90 is not a single player, its function is rather highly dependent on specific cofactors that recruit client substrates, regulate its ATPase cycle, and capture the substrate. Substrate processing by Hsp90 is considered to be a specific maturation process that depends on the

individual substrate, which is in contrast to the rather unspecific folding processes mediated by Hsp60 and Hsp70 (Pearl and Prodromou, 2006).

Hsp90/HtpG assembles to homo-dimers, a process which is mediated by the C-terminal dimerization domain. The N-terminal part of Hsp90 contains the ATPase domain and is needed for substrate interaction. Recent studies revealed that Hsp90 undergoes dramatic structural rearrangements during its ATPase cycle (Ali *et al*., 2006; Shiau *et al*., 2006; Vaughan *et al*., 2007). The domains of Hsp90 move slowly from an ATP-free "open" state to an ATP-bound "closed" state preceding ATP hydrolysis. This movement is regulated by several cofactors of Hsp90 such as Hop/Sti1. The subsequent ATP hydrolysis is controlled by p23, a cofactor that preferentially binds to the ATP-bound state of Hsp90 and slows down its ATP hydrolysis (see Fig. 2.7, Richter *et al*., 2004). Thereby, the state of Hsp90 that is required for client protein activation becomes stabilized. The employment of several cochaperones might tune the ATPase cycle of hsp90 in a client-specific manner (Pearl et al., 2006; Richter and Buchner, 2006a).

The importance of this ATPase cycle for the client protein maturation in cell signaling is demonstrated by anti-tumor agents such as geldanamycin and herbimycin A. Both are specific competitive inhibitors of Hsp90 and block the ATP binding site, which inhibits its

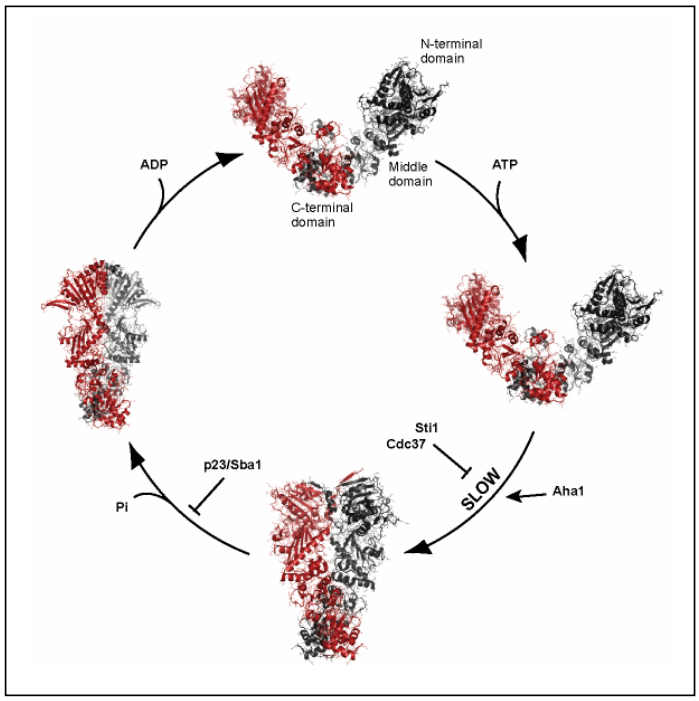

Fig. 2.7: The ATPase cycle of HtpG and Hsp90. The slow steps during the ATPase cycle are the conformational changes preceding ATP hydrolysis. They are critical for substrate maturation and are differentially regulated by several cochaperones. Modified from Richter and Buchner (Richter *et al.*, 2006a).

function in polypeptide folding (Whitesell *et al*., 1994; Lewis *et al*., 2000; Fritz and Burrows, 2006).
In contrast to the eukaryotic Hsp90, the prokaryotic HtpG lacks an extreme C-terminal segment, which provides the MEEVD motif mediating the binding to cochaperones with TPR domains. Both Hsp90 and Hsp70 contain a similar cofactor binding motif that is unique for the eukaryotic chaperone system. Hop bridges both chaperones by independent TPR domains and it is thought to promote the substrate transfer from Hsp70 to Hsp90 (Johnson *et al.*, 1998; Prodromou *et al*., 1999; Scheufler *et al.*, 2000).

2.5.4.2 The TPR domain containing proteins as chaperone cofactors

TPR domains are common tools to establish protein-protein interactions and to assemble multi protein complexes. The tetratricopeptide repeat (TPR) is a degenerated 34 amino acid sequence that is present in tandem arrays of 3-16 motifs in a wide range of proteins. Its consensus sequence is defined by a pattern of small and large hydrophobic amino acids resulting in a helix-turn-helix motif. Typically 3 tandem repeats form a super helical twist, which corresponds to a TPR domain (D'Andrea and Regan, 2003). In yeast, ~22 TPR domain containing proteins have been identified so far, see Tab. 2.1. Mostly, these TPR proteins have a modular domain structure: they consist of a domain of varying function, e.g., a phosphatase domain in Ppt1, and of one or more TPR domains mediating the contact to the protein(s) of destination. At least 10 of these yeast TPR protein members are involved in interactions with Hsp70 or Hsp90 (see Tab. 2.1). The binding of the TPR motif to these heat shock proteins is mediated by their conserved C-terminus, which is IEEVD in Hsp70 and which is MEEVD in Hsp90 (Brinker *et al*., 2002). However, the presence of a TPR domain does not automatically allow the conclusion that the factor *must* bind to an acidic C-terminus. Also other kinds of TPR interaction exist. In some cases, the heat shock proteins even share their TPR cofactors, e.g., Hop/Sti1 and Cns1 can be found in complex with both Hsp90 and Hsp70 (Wegele *et al*., 2003; Hainzl *et al*., 2004). Thus, TPR cofactors might not exclusively bind to a distinct molecular chaperone but rather serve as a cofactor assortment that is used on demand. However, a similar C-terminus sequence of the chaperone is a prerequisite for such a TPR cofactor sharing.
The specificity of a TPR domain is determined by its side chain residues that project into a central binding groove. For instance, separate TPR domains of Hop/Sti1 specifically interact with the distinct C-terminal motifs of Hsp70 (IEEVD) or Hsp90 (MEEVD). The C-terminal motifs of the molecular chaperones are forming a “carboxylate clamp” when binding in an extended conformation into the binding groove of the respective TPR domain (see Fig. 2.8). The affinity is based on electrostatic interactions although the specificity of recognition is dependent on the specific sequence upstream of the common EEVD motif of the respective molecular chaperone (Scheufler *et al.*, 2000; Brinker *et al.*, 2002).

Tab. 2.1: List of all identified TPR domain containing proteins in yeast. This list was generated based on a batabase query for TPR domain containing yeast proteins using the InterPro database of EMBL-EBI. The protein hits are in good agreement with the found set of D'Andea and Regan (D'Andrea *et al.*, 2003). The indicated binding partners interact *via* the TPR domain. Hsp90 or Hsp70 interacting proteins are shown in green. Protein localization data refer to (Huh *et al*., 2003) and molecule numbers[1] refer to (Ghaemmaghami *et al*., 2003), both provided by the protein abundance database (*yeastgfp*).

Protein	Description	Binding Partner	Localization Molecule Number	Reference
Cdc16	Part of the anaphase promoting complex, which is a ubiquitin-protein ligase, for degradation of anaphase inhibitors	Cdc23 Cdc27	Nucleus 2,753 molecules/cell	(Lamb *et al.*, 1994)
Cdc23	Part of the anaphase promoting complex, see above	Cdc16 Cdc27	Nucleus 80 molecules/cell	(Lamb *et al.*, 1994)
Cdc27	Part of the anaphase promoting complex, see above	Cdc16 Cdc23	Nucleus, cytoplasm 593 molecules/cell	(Lamb *et al.*, 1994)
Cns1	Cyclophilin seven suppressor 1, stimulates the ATPase activity of Hsp70	Hsp90 Hsp70	Cytoplasm 672 molecules/cell	(Dolinski *et al*., 1998; Hainzl *et al.*, 2004)
Cpr6	Peptidyl-prolyl *cis-trans* isomerase	Hsp90	Cytoplasm 18,600 molecules/cell	(Mayr *et al*., 2000)
Cpr7	Peptidyl-prolyl *cis-trans* isomerase	Hsp90	Cytoplasm 3,230 molecules/cell	(Mayr *et al*., 2000)
Ctr9	Component of the Paf1 complex, modulating the activity of RNA Pol II	Paf1 Cdc73	Nucleus 12,900 molecules/cell	(Koch *et al*., 1999)
Cyc8/Ssn6	Glucose repression mediator protein, transcriptional co-repressor	Tup1 Matα2	Nucleus 3,890 molecules/cell	(Tzamarias and Struhl, 1995; Smith *et al*., 1995)
Pex5	Peroxisomal membrane receptor for signal sequence (PTS1) of peroxisomal proteins, required for peroxisomal protein import	PTS1-peptides	Peroxisome 2,070 molecules/cell	(Brocard and Hartig, 2006)
Pex5C	YMR018W, putative protein, belongs to the peroxisomal targeting signal receptor family		Unknown	(Amery *et al*., 2001)
Ppt1	Serine/threonine-protein phosphatase T	Hsp90	Cytoplasm 6990 molecules/cell	(Wandinger *et al*., 2006)
Prp6	Pre-mRNA splicing factor 6, component of the snRNP complex	snRNP	Cytoplasm, nucleus 6990 molecules/cell	(Stevens and Abelson, 1999)
Sec72	Subunit of Sec63 complex, for protein import into the ER		ER membrane 5,290 molecules/cell	(Young *et al*., 2001)
Sgt2	Small glutamine-rich TPR containing protein of unknown function; similarity to human SGT, which interacts with hHsp90 and hHsp70	Hsp90 (?) Hsp70 (?)	Cytoplasm 9,424 molecules/cell	(Angeletti *et al*., 2002; Liou and Wang, 2005)
Ski3	Superkiller protein 3, associated with exosome, for translation inhibition of non-poly(A) mRNAs	Ski8	Cytoplasm 11,900 molecules/cell	(Brown *et al*., 2000)
Sti1	Heat shock protein	Hsp90 Hsp70	Cytoplasm 67,600 molecules/cell	(Richter *et al*., 2003; Wegele *et al.*, 2003)
Swa2	Clathrin uncoating factor, involved in vesicular transport	Hsp70	Cytoplasm 768 molecules/cell	(Gall *et al*., 2000)
Tah1	Hsp90 cofactor	Hsp90	Cytoplasm, nucleus 1,660 molecules/cell	(Zhao *et al.*, 2005)
Tfc4	Part of the TauA domain of TFIIIC that binds BoxA DNA promoter sites of tRNA genes	Brf1 Bdp1	Cytoplasm, nucleus 876 molecules/cell	(Liao *et al*., 2003)
Tom70	Mitochondrial import receptor, part of the TOM complex, for import of proteins	Hsp90 Hsp70	Mitochondrial membrane 45,300 molecules/cell	(Young *et al*., 2003; Wu and Sha, 2006)
Tom71	Mitochondrial outer membrane protein with similarity to Tom70	Hsp90 (?) Hsp70 (?)	Mitochondrial membrane 4,110 molecules/cell	(Schlossmann *et al*., 1996)
YNL313C	Uncharacterized protein, required for cell viability		Cytoplasm, nucleus 8,070 molecules/cell	

[1] To facilitate the interpretation of protein numbers: a given protein number of 100,000 molecules/cell refers to a minimal overall concentration of 2.4 µM since a haploid yeast cell has a cell volume of about 70 μm^3 = 7 picoliter (Sherman, 2002). Certainly, the concentration depends also on the localization of the protein, since the actual compartment of the cell where the protein is localized, the cell plasma or the nucleus, has an even smaller volume.

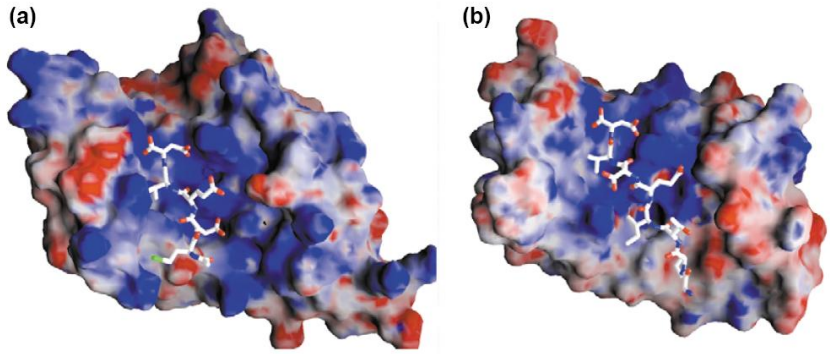

Fig. 2.8: Electrostatic surface representation of TPR domain-peptide complexes. (a) 1.9 Å resolution crystal structure of the TPR2A domain of Hop bound to the Hsp90 C-terminal peptide and (b) 1.6 Å resolution crystal structure of the TPR1 domain of Hop bound to the Hsp70 C-terminal peptide. The TPR domains of Hop are represented as solvent accessible molecular surface and are colored according to their electrostatic potential (red corresponds to a negative charge; blue corresponds to a positive charge). The peptides are represented as white lines. Reproduced from D'Andrea and Regan (D'Andrea *et al.*, 2003), which was based on data from Scheufler and coworkers (Scheufler *et al.*, 2000).

2.5.4.3 Cyclophilin 40 is a TPR cochaperone of Hsp90

The large immunophilin cyclophilin 40, for example Cyp40 in mammals or Cpr6 and Cpr7 in yeast, is a cyclosporine A binding protein with a peptidyl-prolyl *cis-trans* isomerase (PPIase) function. Therefore, it is classified as a cyclophilin (see chapter 2.4.2). It consists of an N-terminal PPIase domain and a C-terminal TPR domain (see Fig. 2.9, Taylor *et al.*, 2001). Cpr6 and Cpr7, the Cyp40 homologues from yeast, share a 40% sequence identity and are dispensable for growth, only the deletion of Cpr7 causes a slow-growing phenotype that can

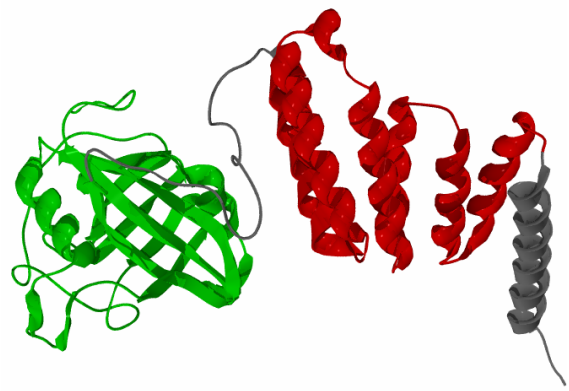

Fig. 2.9: The crystal structure of bovine Cyp40 at 1.8 Å resolution. The crystal structure shows the N-terminal PPIase domain in green and the C-terminal TPR domain in red. Bovine Cyp40 shares 45% identity to Cpr6 and 31% identity to Cpr7, thus, the Cyp40 structure serves as good model for Cpr6 and Cpr7. For the preparation of the figure, the data set of the crystal structure of $Cyp40_{B.t.}$ (PDB entry number 1IHG), Swiss PDB Viewer, and PovRay 3.5 were used.

be restored by the TPR domain alone (Duina *et al*., 1998). However, only Cpr6 is up-regulated upon heat shock (Warth *et al*., 1997; Dolinski *et al.*, 1998) indicating that it plays a role under stress conditions. Further, Cpr6 exhibits a strong PPIase activity, in contrast to the poor PPIase function of Cpr7 (Mayr *et al.*, 2000).

Cyp40 was found in Hsp90-estrogen receptor complexes and was specified as an Hsp90 cochaperone involved in steroid hormone signaling (Ratajczak *et al*., 1993; Duina *et al.*, 1998). Similarly, the yeast cyclophilins Cpr6 and Cpr7 are cochaperones of yeast Hsp90 (Mayr *et al.*, 2000). Cpr6 competes directly with Sti1/Hop for the C-terminal MEEVD-TPR-acceptor side of Hsp90 (Prodromou *et al.*, 1999). Cpr6 stimulates the ATPase activity of Hsp90 (Panaretou *et al*., 2002), and has a regulatory function as an antagonist of Sti1 (cf. Sti1 in Fig. 2.7; Richter *et al.*, 2003; Richter *et al.*, 2004). Whether or not it also functions as a PPIase in the maturation of Hsp90 substrates remains to be elucidated.

2.5.5 The class of Hsp100/ClpB proteins

Hsp100/ClpB proteins, e.g., Hsp104 in yeast and ClpB in *E. coli*, are hexameric ATPases. The main task of Hsp100/ClpB proteins is to recognize and unfold non-natively folded polypeptides. Their spectrum of substrates comprises even aggregated proteins that are precipitated. Hsp100/ClpB proteins unfold their substrate by threading it through the central pore of their hexamer (Weibezahn *et al*., 2004). This way the processed polypeptide becomes separated from the aggregate and – after being ejected from Hsp100/ClpB – has the opportunity to refold into a native protein with the support of further molecular chaperones such as the Hsp70/40 system (see Fig. 2.10 and (Glover *et al.*, 1998; Zolkiewski, 2006). This process of disaggregation by Hsp100/Clp proteins is crucial for thermotolerance of organisms since it allows the recovery of aggregated proteins after organisms are subjected toheat shock (Sanchez and Lindquist, 1990; Squires *et al*., 1991). Hsp100/ClpB proteins are found in prokaryotes, plants, fungi including their mitochondria and plastids, and in some cellular parasites, but not in animals. This incidence suggests that Hsp100/ClpB proteins are

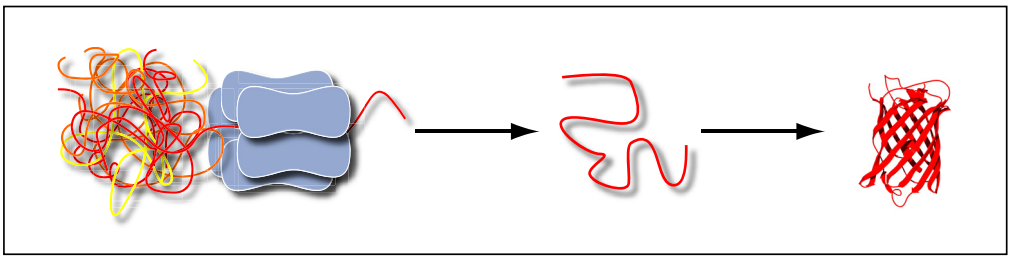

Fig. 2.10: Model of disaggregation by Hsp100/ClpB. The oligomer of Hsp100/ClpB is shown in blue. Polypeptide chains are extracted from the aggregate as single chains in order to refold correctly. The process is dependent on ATP and on the contribution of the Hsp70/40 (i.e., KJE) system. The figure was adopted from Bösl and coworkers (Bösl *et al*., 2006).

specialized disaggregation tools that are required by immobile organisms that are unable to avoid extreme stress conditions such as a sudden temperature increase.

The polypeptide extraction by Hsp100/ClpB proteins is dependent on ATP. Hsp100/ClpB proteins contain two nucleotide binding domains and they are described as ATP-fuelled molecular machines (Hanson and Whiteheart, 2005; Zolkiewski, 2006). This is in contrast to the above presented molecular chaperone families, which use ATP binding and hydrolysis rather to regulate their substrate-binding cycle than for the energy supply of an active substrate-folding process.

The unfolding machinery of Hsp100/ClpB proteins is similar to that of the related prokaryotic Clp[2] proteases. These proteases form hetero-oligomeric enzyme complexes that consist of a mostly hexameric ATPase subunit, such as ClpA, and an oligomeric protease subunit, such as ClpP (Hwang *et al*., 1988; Horwich *et al*., 1999). In the case of Clp protease complexes, the unfolded substrate is fed by the ATPase subunit to the protease subunit, which subsequently degrades it (Weber-Ban *et al*., 1999). Due to their structural similarity, Hsp100/ClpB proteins and the Clp-ATPase subunits are assigned as members of the family of Clp ATPases (Schirmer *et al*., 1996). Clp ATPases that contain one nucleotide binding domain, such as ClpX, are distinguished from those with two nucleotide binding domains per protomer, e.g., ClpA and Hsp100/ClpB proteins (see Fig. 2.11). Further structural

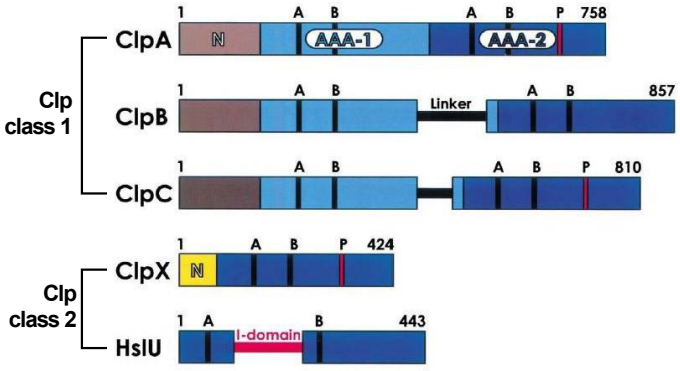

Fig. 2.11: Overview of the domain organization of the Clp protein family. Clp proteins contain structurally defined nucleotide binding domains of the AAA^+ ATPase type, the so-called AAA modules, shown in blue. Class 1 Clp proteins, such as Hsp100/ClpB, contain two AAA modules and class 2 Clp proteins contain one AAA module. An AAA module is the minimal condition for a classification as AAA^+ ATPase. Each module contains the Walker A (GxxxxGKT, x = any residue) and the Walker B (hhhhDE, h = hydrophobic residue) motif, indicated by black lines A and B. The variable N-terminal domains of Clp proteins are in most cases involved in substrate recognition. Clp ATPases, with the notable exception of Hsp100/ClpB, associate with peptidases. Some of the peptidase-associating Clp ATPases contain additionally a recognition motif for ClpP – which is the corresponding peptidase – shown by a red line. The figure was modified from Dougan and coworkers (Dougan *et al*., 2002a).

[2] Clp means caseinolytic peptidase since ClpA from *E. coli* was the first identified member of the Clp protein family. It was characterized as an ATPase subunit of the protease ClpAP, specified by its ability to hydrolyze casein *in vitro* (Hwang et al., 1987; Katayama et al., 1988).

classifications revealed that Clp proteins are a subgroup of the AAA^+ ATPase superfamily (i.e., ATPases associated with a variety of cellular activities, Neuwald *et al*., 1999; Ogura and Wilkinson, 2001). AAA^+ proteins, such as dynein, contain a conserved nucleotide binding domain, the AAA module. They are found in all kingdoms of life and they generally remodel the conformation of their substrates in an ATP-dependent manner. Similar to Clp proteins, AAA^+ ATPases are ring-shaped hexamers with a narrow central pore and nucleotide binding sites at the inter-subunit interfaces.
Hsp100/ClpB proteins do not possess any proteolytic function (Woo *et al*., 1992). They constitute the only known molecular chaperones that belong to the family of Clp proteins and to the superfamily of AAA^+ ATPases. Hsp100/ClpB proteins are presented in detail below.

2.6 The molecular chaperone Hsp104 of yeast

Hsp104 is a eukaryotic member of the Hsp100/ClpB protein family. It is found in the cytosol of yeast where it is involved in the protein homeostasis. Hsp104 dissolves stable protein aggregates, e.g., after a heat shock, and is thus required for the induced thermotolerance of yeast (Sanchez *et al.*, 1990; Sanchez *et al*., 1992). Hsp104 is expressed at a low level under normal growth conditions where it is not essential but involved in the propagation of yeast prions (Chernoff *et al*., 1995; Moryjama *et al*., 2000; Sondheimer & Lindquist, 2000; Tuite, 2000), by splitting large prion aggregates into numerous small prion seeds that are transduced to the daughter cells (Kushnirov and Ter Avanesyan, 1998; Wegrzyn *et al*., 2001).

2.6.1 The genetic regulation of Hsp104: Acquisition of stress tolerance

The heat shock response, whose hallmark is a strong increase in the expression of heat shock proteins (Hsp), is a highly conserved stress defense mechanism in all organisms. The heat shock proteins comprise the described molecular chaperones and also proteins of the cellular proteolytic system such as ubiquitin and its ligases (Hahn and Thiele, 2004; Yamamoto *et al*., 2005). Heat shock proteins of yeast have in common that their promoter sequences contain *cis*-acting heat shock elements (HSEs), which are recognized by the heat shock transcription factor Hsf1. The intensity of transcription correlates with the number of HSE elements in a promoter region of an HSP gene. The activation of the heat shock response takes place *via* the activation of trimeric Hsf1 that is – exceptional for yeast – constitutively attached to the HSE elements of specific target genes such as *HSP104* (Li *et al*., 2006). After attenuation and recovery from heat shock the transcription activation is turned off by the inactivation of Hsf1. This regulation ensures a reversible and transient response to a heat shock event (Sorger, 1990; Wu, 1995).

Apart from the Hsf1-mediated heat shock response yeast developed an additional mechanism which allows it to adapt to a wide range of stress factors. This reaction is known as general stress response and is mediated by the transcription factors Msn2 and Msn4. The activation of transcription takes place when Msn2 and Msn4 bind to the so-called stress response elements (STREs) in the promoter region of certain stress-induced genes (Martinez-Pastor *et al.*, 1996; Schmitt and McEntee, 1996). Msn2/4 activation also includes the transcription of Hsp104 (Estruch, 2000; Amoros and Estruch, 2001).

Thus, the Hsp104 transcription is controlled by both the Msn/STRE regulon and the Hsf/HSE regulon, which can act independently of each other (Grably *et al.*, 2002). The promoter region of Hsp104 contains several types of *cis*-acting elements including 5 HSE and 6 STRE elements and further transcription factor binding sites that play a role in drug and metal resistance (see Fig. 2.12). Thereby, the expression of Hsp104 is 6 - 8-fold higher in stressed cells than under non-stress conditions (Gasch *et al.*, 2000; Causton *et al.*, 2001). The multiple transcription regulation of Hsp104 ensures its expression during many forms of stress.

Hsp104 does not prevent the aggregation of proteins upon a heat shock such as Hsp26 does but rather is essential for the renaturation of aggregated cytosolic proteins. A knock-out of Hsp104 is lethal under severe stress conditions since Hsp104 actively contributes to protein homeostasis of yeast cells under stress conditions. The function of Hsp104 cannot be complemented by a similar proteolytic system such as an engineered ClpB mutant that associates with the protease subunit ClpP and that dissolves the heat induced protein aggregates by digestion (Weibezahn *et al.*, 2004). Thus, the cells essentially require the Hsp104/ClpB-mediated recovery of the enzymatic/protein functionality that is trapped in inactive protein aggregates upon exposure to a heat shock.

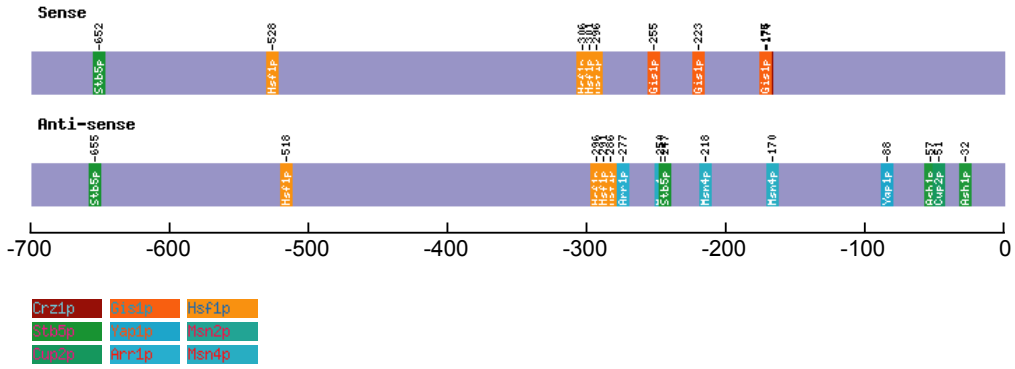

Fig. 2.12: The promoter region of *HSP104* contains several Hsf1 and Msn2/4 transcription factor binding sites. The promoter region also contains putative *cis*-acting elements for transcription factors involved in the drug and the heavy metal ion resistance of yeast (Crz1: stress response, Stb5: drug resistance, Cup2: response to elevated copper concentrations, Gis1: starvation response, Yap1: oxidative stress tolerance, and Arr1: resistance to arsenic compounds) as well as several sites for the metabolic transcription regulation, which are not shown. This figure was prepared by using the transcription factor binding site recognition tool of YEASTRACT (Teixeira *et al.*, 2006).

However, yeast survives a heat shock most efficiently when being preconditioned at a moderately elevated temperature, a phenomenon called induced thermotolerance. Only when cells are preconditioned at such a mild heat stress, they do survive a brief incubation at 48°C - 50°C relatively well, while otherwise they would die. This is mainly a result of an increased expression of Hsp104 when cells are shifted from normal growth temperature (30°C) to the mild heat shock temperature 37°C. Thus, Hsp104 plays an essential role in inducing thermotolerance of yeast (Sanchez *et al.*, 1990; Sanchez *et al.*, 1992; Lindquist and Kim, 1996).

For comparison the average mRNA levels of Hsp104, common molecular chaperones and their cofactors under stress is presented in Fig. 2.13. The figure shows the differential regulation of the indicated genes upon exposure to various forms of stress (Gasch *et al.*, 2000). It is obvious that Hsp104 is one of the most up-regulated Hsp genes upon mild heat shock, starvation, and during the stationary phase of yeast.

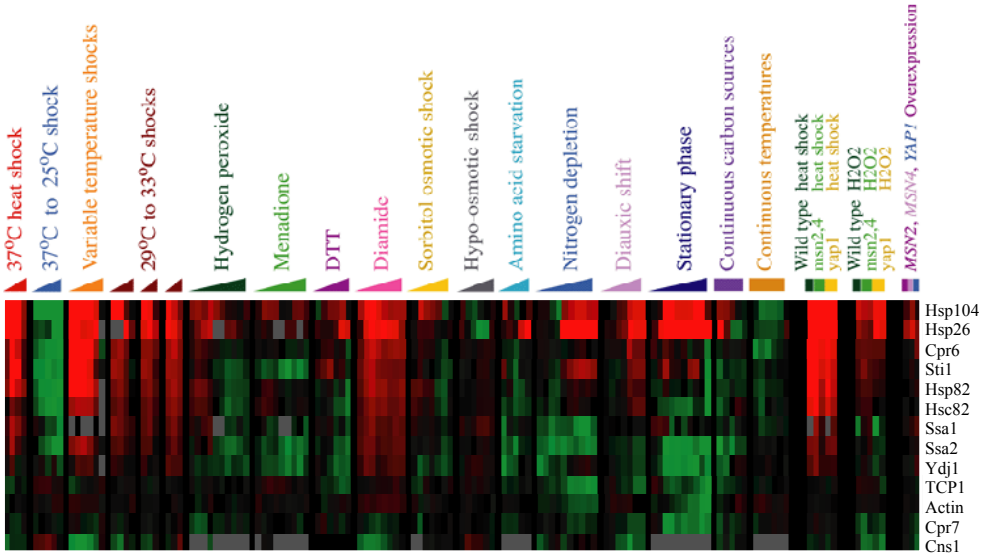

Fig. 2.13: Stress-dependent mRNA pattern of selected proteins in yeast. Red shadows indicate an up to 8-fold up-regulated and green shadows indicate an up to 8-fold down-regulated transcription in comparison to non-stress conditions. Grey shadows correspond to no determined data. The indicated yeast proteins correspond to following protein families: Hsp104 = Hsp100/ClpB; Hsp26 = sHsp; Cpr6 and Cpr7 = cyclophilin 40 cochaperones of Hsp90; Sti1 = Hop cochaperone of Hsp90 and Hsp70; Hsp82 and Hsc82 = Hsp90; Ssa1 and Ssa2 = Hsp70; Ydj1 = Hsp40; TCP1 = Hsp60 α subunit; Cns1 = cochaperone of Hsp90 and Hsp70. The figure was prepared using the transcript abundances of the indicated proteins, which were provided by http://genome-stanford.edu/cgi-bin/yeast_stress based on a DNA microarray analysis by Gasch and coworkers (Gasch *et al.*, 2000).

2.6.2 Disaggregation of aggregated proteins by Hsp104

Hsp104 plays a crucial role in conferring stress tolerance by solubilizing stable protein aggregates (Parsell *et al.*, 1994b). This function is dependent on the presence of Hsp70, since a strain with a deletion of both chaperone types, Δ*hsp104*Δ*ssa1*Δ*ssa3*Δ*ssa4*, exhibited

markedly less thermotolerance than a strain lacking only Hsp104, Δ*hsp104*, whereas the control strain Δ*ssa1*Δ*ssa3*Δ*ssa4* showed the same viability as the wild-type at heat shock conditions (Sanchez *et al*., 1993). These early *in vivo* data suggested that Hsp104 requires the Hsp70/40 chaperone system for its function. Later, it was demonstrated that Hsp104 and Hsp70/40 form a bi-chaperone network: the disaggregation function of Hsp104/ClpB was reconstituted *in vitro* and it was shown that the process critically depends on the presence of the Hsp70/40 chaperone system (Glover *et al.*, 1998; Goloubinoff *et al*., 1999; Motohashi *et al*., 1999; Zolkiewski, 1999). While the Hsp70/40 system is capable of dissolving smaller protein aggregates on its own, an efficient renaturation of polypeptides from larger aggregates requires Hsp104/ClpB (Diamant *et al*., 2000; see Fig. 2.10).

It is still controversial whether Hsp70/40 acts as a chaperone upstream, downstream, or on both sides of the polypeptide unfolding process mediated by Hsp104 and how Hsp104 generally interacts with aggregates in order to extract single polypeptide chains. Two models were proposed of how Hsp104 dissolved aggregates.

The “crowbar model” proposes that Hsp104 breaks large aggregates into smaller pieces, which can be subsequently refolded by the Hsp70 system. Thereby, the coiled-coil middle region of Hsp104/ClpB, found at the equatorial surface of the hexamer, is believed to work as a crowbar interacting with aggregates (Ben Zvi *et al.*, 2001; Glover and Tkach, 2001; Lee *et al*., 2003).

The threading model is based on the sequence homology of Hsp104 with ClpA and ClpX that commonly unfold substrates by pulling them through their central pore (Singh *et al*., 2000; see Fig. 2.10). The threading model would require a complete unfolding of polypeptide substrates since the central channel of Hsp104/ClpB is too narrow (13 Å, Lee *et al*., 2007) to allow the translocation of a folded protein unless a transient increase in the channel size occurs during the translocation process. Support for the threading model was derived from a study that combined ClpB with the ClpP peptidase subunit of ClpA (Weibezahn *et al.*, 2004). This study demonstrated the mechanistic similarity between ClpAP and “ClpBP”: it was shown that a ClpB mutant, which contained a recognition motif mediating the association with the protease subunit ClpP, could associate with ClpP and was active in the proteolytic degradation of aggregates. The proteolysis of aggregates by ClpBP was strictly dependent on the presence of the Hsp70/40 system implying that Hsp70/40 acts up-stream of the threading process. Further, a pretreatment of aggregated proteins with Hsp70/40 (DnaK/DnaJ) improves their subsequent disaggregation by ClpB (Zietkiewicz *et al*., 2004; Zietkiewicz 2006). However, current studies demonstrated that Hsp104/ClpB exhibits under certain conditions an unfolding activity that is independent of the presence of the Hsp70/40 system (Schaupp *et al*., 2007; Doyle *et al*., 2007). Thus, the threading model is in accordance with some data, however, the actual modus of function of the Hsp70/40 chaperone system remains to be conclusively determined.

Beyond the bi-chaperone network of Hsp104/ClpB and Hsp70/40 evidence is accumulating that also small heat shock proteins (sHsps), such as yeast Hsp26, contribute to the substrate

renaturation by Hsp104/ClpB. sHsps were shown to enhance the disaggregation by Hsp104/ClpB (Mogk *et al*., 2003a; Cashikar *et al.*, 2005; Haslbeck *et al.*, 2005b).
In conclusion, Hsp104 cooperates with several other cytosolic chaperones in a functional manner. The actual stability of an aggregate might require the additional contribution of chaperones such as Hsp70/40 and Hsp26 prior to the unfolding by Hsp104. However, until now, it has not been demonstrated that Hsp104 also associates with its partner chaperones and thus, the presence of a physical multi-chaperone complex such as Hsp104/70/40/26 could not be confirmed and might not exist *in vivo*.

2.6.3 Propagation of yeast prions by Hsp104

Hsp104 and ClpB have a similar function *in vivo* regarding the acquisition of thermotolerance of bacteria, fungi and plants. However, Hsp104 possesses a unique property that has not been reported for other Hsp100/ClpB proteins, yet: Hsp104 is functional in the propagation of prions in yeast.
The term prion was used by Stanley Prusiner to define the traits of the infectious self-propagating isoform of the prion protein (prion = proteinaceous infectious particle). Prions are transmissible particles that are devoid of nucleic acids and seem to be composed exclusively of a modified protein (e.g., mammalian prion protein PrP^{Sc}). For example, the normal cellular PrP (PrP^{C}) is converted into PrP^{Sc} through a posttranslational process during which it acquires high β-sheet content (S. B. Prusiner, nobel lecture 1997). Thereby, the infective pathological isoform PrP^{Sc} accumulates and causes fatal neurodegenerative diseases that are known as the transmissible spongiform encephalopathies (TSE), such as bovine spongiform encephalopathy (BSE), scrapie of sheep, and Creutzfeldt-Jakob disease (CJD) of humans. As a hallmark of these diseases, PrP^{Sc} forms large fibrillar amyloid structures called amyloid plaques that are found, e.g., in brain tissue and that are more resistant to proteases than soluble PrP^{C}. However, the most infectious units are small, non-fibrillar particles comprising 14 to 28 PrP^{Sc} molecules that function as prion seeds for the prion polymerization reaction converting PrP^{C} into PrP^{Sc} (Caughey and Lansbury, 2003; Silveira *et al*., 2005).
So far, only a few prions were described: PrP^{Sc} in mammals, [PSI^{+}], [URE3] and [PIN^{+}] in *S. cerevisiae* and [Het-s] in the filamentous fungus *Podospora anserina* generated by the proteins PrP^{C}, Sup35, Ure2, Rnq1 and HET-s, respectively (Wickner, 1994; Tuite, 1994b; Coustou *et al*., 1997; Prusiner, 1998; Derkatch *et al*., 2001). Although the primary structures of the infectious proteins in these various prion proteins are unrelated, all of them appear to form similar β-sheet-rich fibrillar aggregates commonly referred to as amyloid (Prusiner, 1998; Dobson, 1999; Chien *et al*., 2004).
Fungal prions cannot be transmitted between species (Santoso *et al*., 2000), as it is the case for certain mammalian TSE variants (Vanik *et al*., 2004). However, the transmission mechanism of fungal prions within the same species is similar to that of PrP^{Sc}: the prion

particles catalyze as seeds the conversion of the soluble natively folded protein counterpart into the prion conformation (Serio *et al*., 2000). Yeast prions, which represent non-mendelian genetic elements (Cox, 1965), are passed from one yeast cell to another by cytoplasmic mixing, either from mother to daughter cell during budding, from parent diploids to spores during meiosis or during mating of two haploid yeast cells (Wickner, 1994). Further, yeast prion particles that were generated *in vitro* are sufficient to infect yeast cells when a suitable transformation protocol is applied, which is in accordance with the protein-only mechanism of yeast-prions (Tanaka *et al*., 2004a; Brachmann *et al*., 2005; Tanaka and Weissman, 2006). Thus, yeast prions are in fact self-propagating and transmissible.

Mammalian prions cause severe diseases in contrast to yeast prions that are not necessarily a negative trait. The phenotype of yeast prions corresponds mostly to a mild loss-of-function phenotype since the insoluble prion isoform lacks the enzymatic activity of the soluble counterpart. However, in some cases the presence of prions may be of benefit to the yeast cell when exposed to certain environmental conditions (Eaglestone *et al*., 1999; True and Lindquist, 2000).

An obligatory criterion for the propagation of yeast prions is the requirement of Hsp104 for prion replication. Hsp104 breaks up large prion aggregates leading to the production of transmissible "seeds" that are transferred to daughter cells in a growing yeast culture (Paushkin *et al*., 1996; Kushnirov *et al.*, 1998; Ness *et al*., 2002; Satpute-Krishnan *et al*., 2007). A loss-of-function of Hsp104, either by deletion or by a mutation of the ATPase domains, results in the irreversible loss of all known yeast prions, [*PSI*$^+$], [URE3], and [*PIN*$^+$] (Chernoff *et al*., 1995; Moriyama *et al*., 2000; Sondheimer and Lindquist, 2000). Thereby, the inactivation of Hsp104 causes a lack of prion replication and the remaining prions are diluted out by cell division (Satpute-Krishnan *et al.*, 2007). The function of Hsp104 in prion replication might correspond to its disaggregation activity after a heat shock. It is likely that in both cases, thermotolerance and prion propagation, analogous interactions with non-soluble protein aggregates occur (Narayanan *et al*., 2003). As a side product of its disaggregase activity, Hsp104 might generate small prion particles, which might act as prion seeds. They possess large accessible surfaces serving again as a template for the subsequent prion extension, i.e., the incorporation of further soluble prion protein into the prion particles by aggregation. *In vitro*, the seeded fibrillization reaction of yeast prion proteins has been extensively studied and it was demonstrated that Hsp104 is able to generate seeds (Shorter and Lindquist, 2004). Remarkably, however, the over-expression of Hsp104 eliminates [*PSI*$^+$], but not [URE3] and [*PIN*$^+$] (Chernoff *et al.*, 1995; Derkatch *et al*., 1997; Moriyama *et al.*, 2000; Sondheimer *et al.*, 2000). One could speculate that [*PSI*$^+$] prion aggregates are physically less stable and are completely dissolved by an excess of Hsp104. In accordance with this speculation, an overproduction of Hsp104 in [*PSI*$^+$] cells results in a transfer of Sup35 from the insoluble (aggregated) into the soluble fraction (Patino *et al*., 1996; Paushkin *et al*., 1996).

Apart form Hsp104, Hsp70 and Hsp40 are also involved in prion propagation (Jones and Tuite, 2006), however, they appear not to be essential for this process and – in analogy to thermotolerance – only the deletion of Hsp104 results in a loss of the prion phenotype.

Besides the requirement of Hsp104 for prion-propagation, yeast prions share a further common property: they can be reversibly removed from cells by the presence of millimolar quantities of the agent guanidinium chloride (GdmCl; Wickner, 1994; Derkatch *et al.*, 1997; Kushnirov *et al.*, 2000; Santoso *et al.*, 2000; Sondheimer *et al.*, 2000), a phenomenon that was termed "curing" (Tuite *et al.*, 1981). The addition of 1 to 5 mM GdmCl to the growth medium inhibits the replication of yeast prions and – similar to an inactivation of Hsp104 – the remaining prions are diluted out by cell division (Eaglestone *et al.*, 2000; Ness *et al.*, 2002; Satpute-Krishnan *et al.*, 2007). The GdmCl-induced curing is a reversible trait

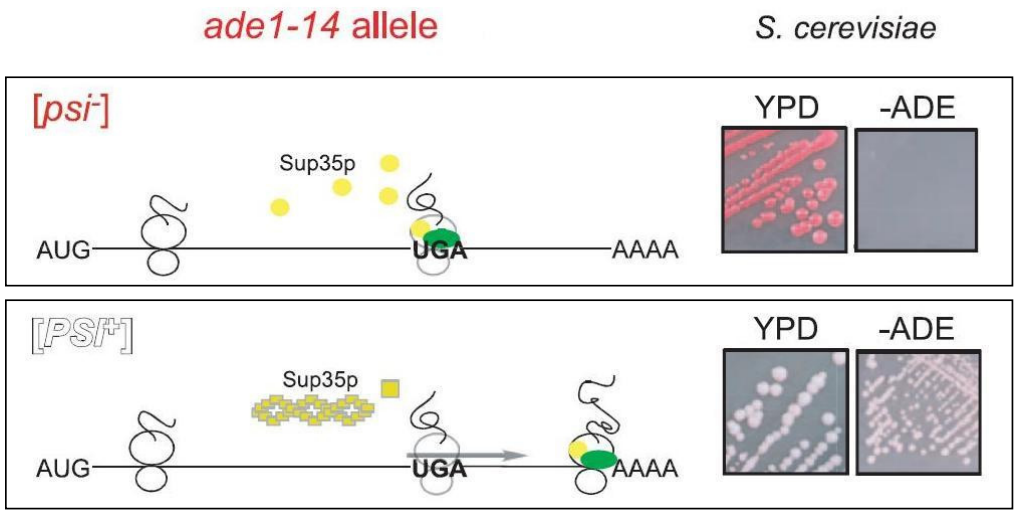

Fig. 2.14: The prion phenotype of [*PSI*$^+$] from yeast. The translation terminator Sup35 exists as a prion-free [*psi*$^-$] phenotype in a soluble and active conformation, where it is generally functional in stopping the translation of mRNA at its stop codon. In an especially engineered yeast, such as YJW532, strains, the *ade1* gene contains a nonsense mutation, *ade1-14*, which corresponds to a premature stop codon in the mRNA encoding for Ade1. The full-length protein Ade1 is part of the adenine-metabolism. Hence, the premature stop codon serves as an adenine-responsive reporter in order to monitor whether the translation termination is normal or defective.
As shown in the upper panel, translation termination is fully functional in [*psi*$^-$] yeast strains with soluble and active Sup35. Accordingly, an adenine-intermediate accumulates leading to a red colony color when cells grow on rich medium (YPD). If the growth medium lacks the amino acid adenine (-ADE), then the *ade1* gene product becomes essential. However, the strain is lacking Ade1 protein due to the premature stop codon and, therefore, yeast cells cannot grow on -ADE, i.e., they exhibit adenine auxotrophy.
The lower panel presents the opposite scenario in a prion containing [*PSI*$^+$] yeast strain. Herein, the translation terminator Sup35 mostly exists in an inactive prion aggregate and only a very small remaining soluble fraction of Sup35 is active in translation termination. Thus, translation termination is generally defective and ribosomes often fail to release polypeptides at stop codons and occasional stop codon read-through takes place. Thereby, also the premature stop codon of *ade1-14* mRNA becomes "leaky" and some full-length Ade1 is produced, a process referred to suppression of nonsense mutations or simply anti-suppression. As a consequence, the adenine biosynthesis pathway is restored. Thus, colonies appear white on YPD plates and the strain is able to grow on medium lacking adenine (-ADE), i.e., the strain exhibits adenine prototrophy. The figure was modified from Crist and Nakamura (Crist and Nakamura, 2006).

since a prion-free yeast strain can actually convert *de novo* to a prion strain with a frequency of ~10^{-6} – with the prerequisite that the gene encoding for the corresponding prion protein, has not been mutated or deleted and that active Hsp104 is present at a physiological level in the cytoplasm (Wickner, 1994; Jung and Jones, 2003).

As a representative example for a yeast prion protein serves [*PSI*$^+$] since it has been extensively studied since more than 4 decades (Cox, 1965; Cox *et al*., 1988; Tuite, 1994; Tuite and Cox, 2006). [*PSI*$^+$] is the prion form of Sup35, which is a release factor essential for translation termination and cell viability. In [*PSI*$^+$] cells, Sup35 adopts a non-soluble conformation, which leads to an increased probability of a suppression of nonsense mutations, i.e., the read-through of premature stop codons (Chernoff *et al.*, 1995; Tuite & Lindquist, 1996). Colonies of [*PSI*$^+$] strains bearing the *ade1-14* reporter gene appear white and grow on medium lacking adenine, whereas [*psi*$^-$] strains efficient in translation termination accumulate a red pigment and do not grow on medium lacking adenine (see Fig. 2.14). Thus, [*PSI*$^+$] strains can be identified on the basis of the colony color and by adenine prototrophy (Cox, 1965; Derkatch *et al*., 1996).

2.6.4 The tertiary structure of Hsp104

Hsp104 is a 102 kDa protein that assembles to a two-tiered hexameric ring structure as demonstrated by chemical cross-linking, analytical ultracentrifugation, and electron microscopy (Parsell *et al*., 1994a; Bösl *et al*., 2005). The hexamer has a diameter of approximately 160 Å with an inner pore of ~14 Å, as determined by cryo-electron microscopy (cryo-EM) analysis (Dr. P. Wendler, Birkbeck College London, UK, personal communication). A high-resolution structural analysis of Hsp104 is still missing but the crystal structure of the bacterial homologue ClpB from *Thermus thermophilus*, $ClpB_{T.t.}$, is available (Lee *et al.*, 2003) and served to generate a structural model of Hsp104 (see Fig. 2.15). When viewed from the side, the Hsp104 hexamer reveals a strong structural polarity. Each protomer comprises two different nucleotide binding domains, NBD1 and NBD2, that, mediated by a multitude of interactions, appear to be arranged within the hexamer as an NBD1 ring and an NBD2 ring, respectively. This structural polarity is a key property of the disaggregation machinery of Hsp104 since the polypeptide substrate translocation is believed to be an unidirectional process in analogy to the closely related Clp proteases (Weber-Ban *et al.*, 1999; Singh *et al.*, 2000; Kim *et al*., 2000a; Reid *et al*., 2001; Lee *et al*., 2001). The N-terminal domains of each protomer of Hsp104 are found on the “upper side” of the hexamer and are supposed to initiate the contact to the polypeptide substrates of Hsp104. The C-terminal domains are found on the “bottom side” of the hexamer and, presumably, constitute the site for substrate ejection.

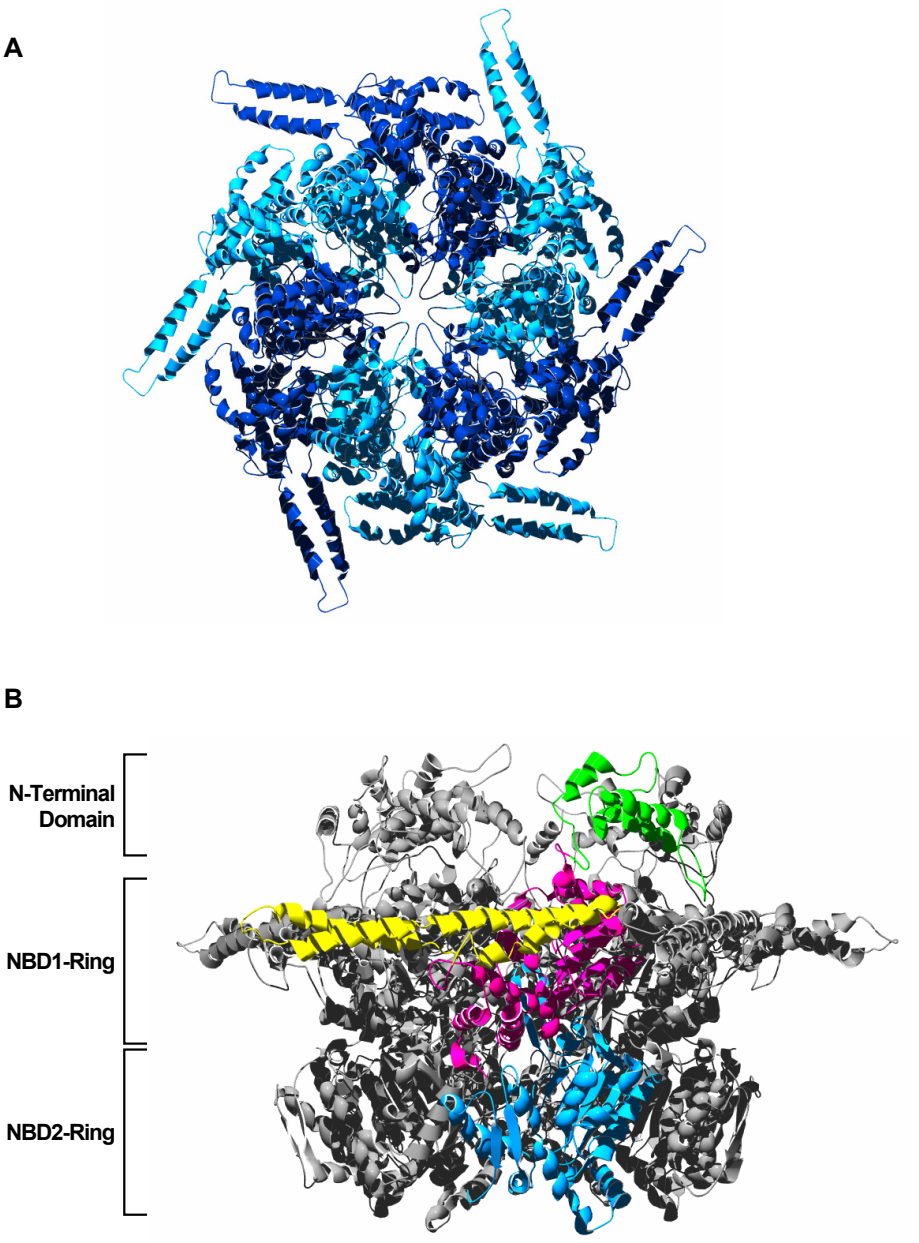

Fig. 2.15: Model of the Hsp104 hexamer. The model is based on the crystal structure of $ClpB_{T.t.}$ (Lee *et al.*, 2003), which shares 44% identity with $Hsp104_{S.c.}$. (A) Top view demonstrating the ring structure of Hsp104. (B) Side view showing the vertical polarity of Hsp104. The individual domains of one protomer within the hexamer are colored. The N-terminal domain is shown in green, NBD1 in pink, the middle domain in yellow and NBD2 in blue. The C-terminus was not solved in the $ClpB_{T.t.}$ structure and is therefore missing in the Hsp104 model. The model is based on work by Dr. S. Steinbacher (proteros biostructures GmbH, München, Germany) and the figures were prepared by Swiss PDB Viewer and PovRay 3.5.

2.6.5 The domain organization of Hsp104

Hsp104 is a multi domain protein that consists of two nucleotide binding domains of the AAA^+-ATPase type, which have a high sequence similarity to those of ClpB and ClpA, the closely related Clp ATPases in bacteria. These two so-called AAA modules comprise about 200 - 250 amino acid residues and are connected head-to-tail (see Fig. 2.16.A). The N-terminal domain and the C-terminus of Hsp104, which are flanking the NBDs, are less conserved and only Hsp100/ClpB proteins comprise additionally a middle domain inserted between the NBDs (Schirmer *et al.*, 1996; Lee *et al.*, 2003).

The ~160 residue N-terminal domain of Hsp104 is presumably α-helical, has a globular shape, and is connected by a short flexible linker to NBD1, as deducted from the crystal structure of ClpB (see Fig. 2.16.B; Lee *et al.*, 2003). The N-terminal domain mediates the initial polypeptide substrate binding, as it has been reported for ClpB from *E. coli* (Liu *et al*., 2002; Barnett *et al*., 2005; Lee *et al.*, 2007). However, a deletion of this domain does not completely abolish the disaggregation activity (Mogk *et al*., 2003c; Barnett *et al.*, 2005).

The ~120 residue middle domain, i.e., I domain, since it was originally assigned as an insertion between NBD1 and NBD2 (Schirmer *et al.*, 1996), is considered as an extension of the very C-terminal end of NBD1 (see Fig. 2.16.A, Lee *et al.*, 2003). It consists of a large coiled-coil structure and is found on the outer ring surface of both the Hsp104 hexamer model (see Fig. 2.15) and the cryo-EM structure of ClpB (Lee *et al.*, 2003). A recent cryo-EM study on ClpB demonstrated that this coiled-coil exists in different conformations depending on the nucleotide state of the subunits of Hsp104 (Lee *et al.*, 2007). Since the deletion or mutation of the middle domain results in a loss of disaggregation activity of both ClpB and Hsp104 it was suggested to play a crucial role in substrate disaggregation (Cashikar *et al*., 2002; Kedzierska *et al*., 2003; Mogk *et al.*, 2003c; Haslberger *et al*., 2007).

The ~50 residue C-terminus of Hsp104 was also proposed to be involved in substrate binding (Cashikar *et al.*, 2002). However, related Clp ATPases that are associated with protease cofactors eject the substrate at this site in order to feed it to the protease (Kim *et al*., 2000b; Lee *et al.*, 2001).

Hsp104 comprises a further acidic C-terminal extension, which is not present in ClpB and which has some similarity to the C-terminal TPR protein binding motif of eukaryotic Hsp90 and Hsp70 (Parsell *et al*., 1991; Bösl *et al.*, 2006). It is conceivable that the very C-terminus of Hsp104 comprises a TPR protein bincing motif

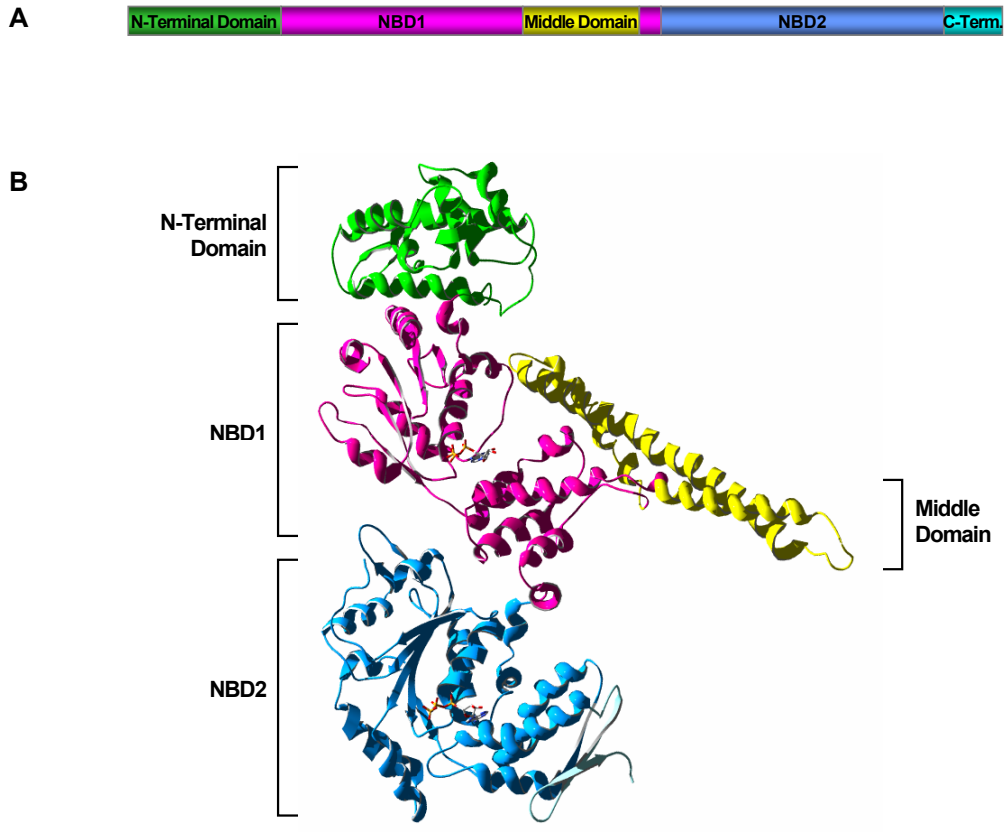

Fig. 2.16: Domain structure of an Hsp100/ClpB protomer. (A) Domain organization of Hsp104 as determined by sequence analysis (cf. Appendix A.1). (B) 3 Å resolution crystal structure of ClpB from *Thermus thermophilus* in standard orientation containing AMP-PNP. The left side of the N-terminal domain, NBD1, and NBD2 point towards the central channel of the hexamer whereas the coiled-coil middle domain points towards the outer surface of the hexamer as determined by cryo-EM analysis of oligomeric $ClpB_{T.t.}$ (Lee *et al.*, 2003). AMP-PNP, a non-hydrolysable ATP mimetic, is shown as a ball-and-stick model. The individual domains are depicted in colors. The N-terminal domain is shown in green, NBD1 in pink, the middle domain in yellow and NBD2 in blue. The C-terminus was not resolved in the $ClpB_{T.t.}$ structure and is therefore missing in figure B. Figure B was prepared using the PDB-file of the crystal structure of $ClpB_{T.t.}$ (PDB entry number 1QVR), Swiss PDB Viewer, and PovRay 3.5.

2.6.6 The structure of the nucleotide binding domains of Hsp104

A main structural property of Hsp104 are its two highly conserved nucleotide binding domains (NBDs = AAA modules) of the AAA^+ ATPase type. Both AAA modules have a similar conserved nucleotide binding fold but are not identical, as demonstrated by the X-ray diffraction analysis of several related Clp ATPases (Bochtler *et al*., 2000; Guo *et al*., 2002; Lee *et al.*, 2003). Each AAA module consists of a large sub-domain (i.e., α/β domain), which contains a 5-stranded parallel β-sheet flanked by α-helices, and a small sub-domain (i.e., α domain), which is mainly α-helical. Since the AAA module is highly conserved among Hsp104 and Clp ATPases, the structure of NBD1 from ClpA (Guo *et al.*, 2002), which is a closely related Clp ATPase, serves well to demonstrate the basic structural features of an AAA module (see Fig. 2.17). First, it is apparent that the nucleotide binds to the interface of the large and the small sub-domains of the AAA module. It is coordinated by several electrostatic interactions with both sub-domains. The most relevant residues that are responsible for nucleotide binding and hydrolysis are provided by the Walker A and the Walker B motif (Walker *et al*., 1982; Saraste *et al*., 1990).

The Walker A motif (GxxxxGKT, x = any residue) forms a flexible loop, the so-called P-loop. This loop is responsible for the binding of the nucleotide through coordination of its phosphate groups. The β- and γ-phosphate oxygens of the nucleotide form hydrogen bonds with the side-chain of the lysine residue of the Walker A motif. The lysine corresponds to the residues K218 and K620 in Hsp104. A K→T mutation in the Walker A motif leads to a complete loss of nucleotide binding (Matveeva *et al*., 1997; Babst *et al*., 1998; Watanabe *et al*., 2002; Pye *et al*., 2006).

The Walker B motif (hhhhDE, h = hydrophobic residue) is located in a β-strand and its glutamate residue is involved in the binding of a Mg^{2+} ion that coordinates the γ-phosphate of the nucleotide. Thereby, the free carboxy group of glutamate either acts as catalytic base, which is responsible for the hydrolysis of ATP, or it promotes the ATP hydrolysis by the proper positioning of a water molecule. However, an E→Q mutation in the Walker B motif results in a loss of ATP hydrolysis but not in a loss of nucleotide binding (Babst *et al.*, 1998; Watanabe *et al.*, 2002; Dalal *et al*., 2004; Pye *et al.*, 2006). In Hsp104, the Walker B glutamate corresponds to the residues E285 and E687.

Several additional conserved structural motifs such as the Sensor 1 motif (Koonin, 1993) and the Sensor 2 motif (Neuwald *et al.*, 1999) are in close proximity to the nucleotide and their mutation in Hsp104 leads to an impaired nucleotide hydrolysis and nucleotide binding, respectively (Hattendorf and Lindquist, 2002a; Hattendorf and Lindquist, 2002b).

The available monomeric crystal structures demonstrate that nucleotides can bind to a monomeric subunit of a Clp protein. However, the oligomeric crystal structures revealed that the nucleotide is bound at the interface of adjacent subunits. A combination of conserved residues from the two subunits surrounding the nucleotide creates a highly polar

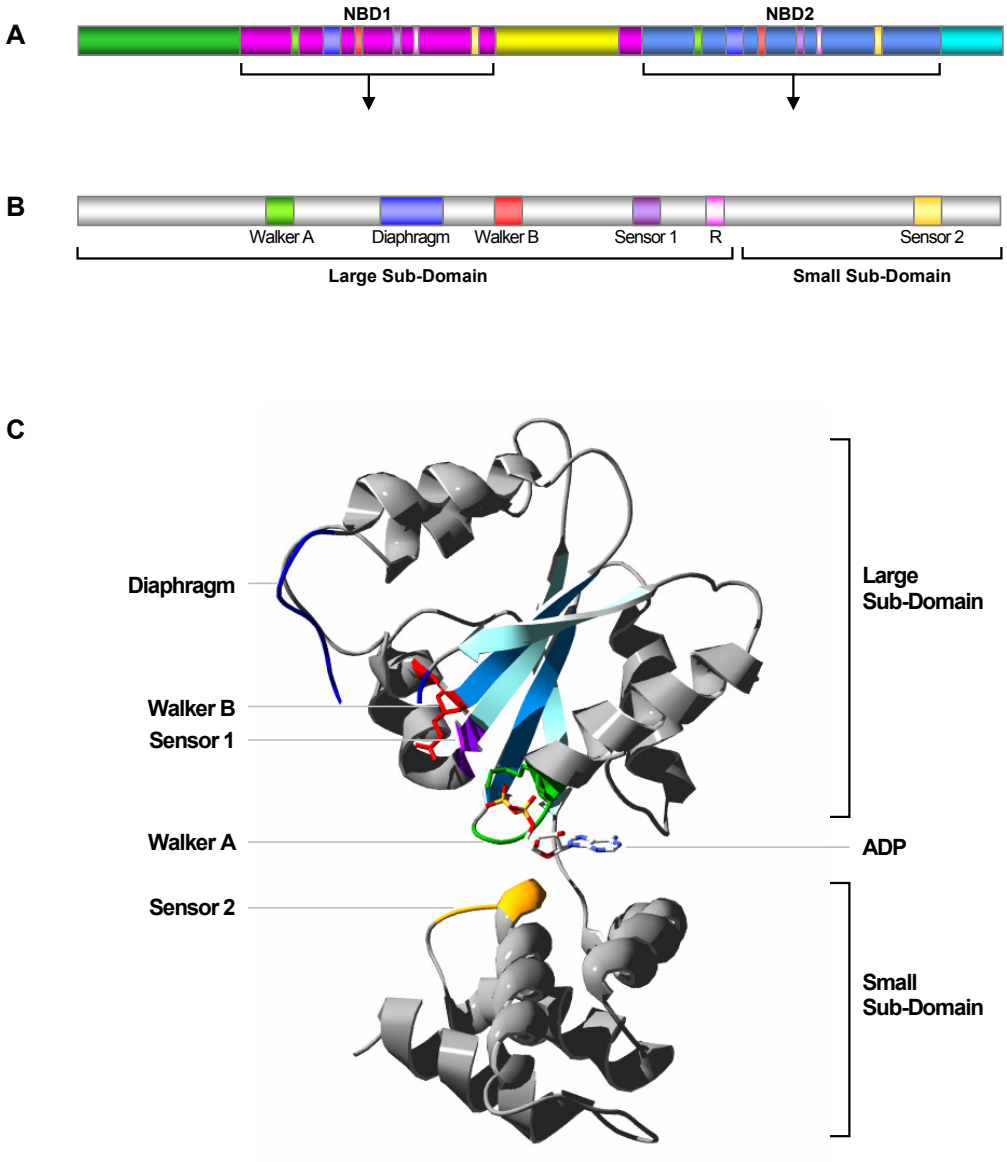

Fig. 2.17: Structural properties of an AAA module (= NBD). (A) Domain organization of Hsp104 as determined by sequence analysis (cf. Appendix A.1). (B) Schematic presentation of the sequence and the position of the most conserved motifs of an AAA module that refers to both nucleotide binding domains, NBD1 and NBD2, of Hsp104. (C) 2.6 Å resolution crystal structure of NBD1 of ClpA from *E. coli* containing ADP. Residues 180 to 411 of ClpA were selected for this presentation. Within the hexameric structures of similar Clp ATPases the right side of the AAA module points towards the center and the left site towards the outer surface. The nucleotide ADP is shown as a ball-and-stick model. The 5-stranded parallel β-sheet of the large sub-domain is presented in an alternating blue and light blue color. The Walker A motif and its lysine residue are depicted in green, whereas the Walker B motif and its glutamate residue are depicted in red. Sensor 1 and Sensor 2 are presented in violet and yellow, respectively. The Diaphragm is flexible and only partially solved in the available crystal structures from ClpA and ClpB. It is shown as an interrupted dark blue loop. The Arginine Finger is not visible on this side of the AAA module.
For the preparation of the figure the data of the crystal structure form ClpA (PDB entry number 1KSF), Swiss PDB Viewer, and PovRay 3.5 were used.

environment. Some residues of the adjacent subunits even form direct electrostatic interactions with the nucleotide. An example for such a residue is the Arginine Finger (see "R" in Fig. 2.17.B; Schmidt *et al*., 1999; Karata *et al*., 1999), which corresponds to R333/334 and R765 in Hsp104. It is not visible in Fig. 2.17.C since it is located on the opposite side of the AAA module. The Arginine Finger is not relevant for the nucleotide binding but appears to play a role in nucleotide sensing within one NBD ring. It was proposed that it coordinates the nucleotide hydrolysis and the conformational changes between the protomers and that it thereby provides the structural basis for the cooperativity of ATP hydrolysis within one NBD ring (Ogura *et al*., 2004). The mutation of the Arginine Finger leads to an impaired chaperone function, as demonstrated by mutational analysis in related Clp ATPases (Song *et al*., 2000; Weibezahn *et al*., 2003; Mogk *et al.*, 2003c).

Another important feature of the AAA module is the Diaphragm, which is a highly flexible loop that is found within two β-sheets connected by a short α-helix of the large sub-domain. It presumably extends into the central channel of the hexamer where it might interact with the other Diaphragm loops of the neighboring protomers (Guo *et al.*, 2002). It might thereby restrict the size of the central channel, and the event of ATP hydrolysis of one subunit could directly be transmitted as movements by the Diaphragm mediating the translocation of a polypeptide substrate (Lum *et al*., 2004; Schlieker *et al*., 2004; Weibezahn *et al.*, 2004; Barnett *et al.*, 2005).

In conclusion, the structure of the AAA module suggests a high level of mechanical regulation. The nucleotide is bound in a strategic position within the two domains of an AAA module and between adjacent subunits within the hexamer. Furthermore, a direct contact of core strands of the AAA module to the polypeptide substrate in the central channel might exist. This structural arrangement might allow that the energy of ATP hydrolysis can be directly translated in terms of conformational changes of the domains and in the translocation of polypeptide substrates.

2.6.7 Oligomerization properties of Hsp104

Hsp104 is considered to exist in a dynamic equilibrium of hexamers and either monomers or dimers/trimers. The hexamer, however, appears to be the active species (Schirmer *et al*., 2001; Hattendorf *et al.*, 2002b). This conclusion is based on observations that indicate that the hexamer tends to partially disassemble under non-equilibrium conditions, for instance, when techniques such as SEC-HPLC analysis are used to assess the oligomerization state (Parsell *et al.*, 1994a; Tkach and Glover, 2004; Bösl *et al.*, 2005). However, the oligomerization equilibrium – and probably also its dynamics – appear to be strongly influenced by the presence of nucleotides and ionic strength (Parsell *et al.*, 1994b; Hattendorf *et al.*, 2002b). While nucleotides stabilize the oligomeric form, salts such as KCl favor disassembly. Binding of ADP or ATP to NBD2 shifts the equilibrium towards the hexameric form and renders the hexamers more resistant to higher salt conditions. The inter-dependency

of nucleotide binding and oligomerization was first demonstrated in a study by Parsell (Parsell *et al.*, 1994a; Parsell *et al.*, 1994b), in which the effect of point mutations in the Walker A motifs on the biochemical properties of Hsp104 was analyzed. When the conserved Lys-218 in NBD1 was changed to Thr (K218T), oligomerization was barely affected. The corresponding mutation in NBD2, K620T, resulted in a decreased tendency of the protein to form hexamers. However, this defect is not very pronounced and can be overcome by increasing either the concentration of protein or nucleotide, or by decreasing the ionic strength (Bösl *et al.*, 2005, Schirmer *et al.*, 2001). Meanwhile, additional mutations in the C-terminal domain have been identified, which affect oligomerization and support the important role of NBD2 in hexamer formation (Tkach *et al.*, 2004).
The hexamer clearly appears to be the functional species of Hsp104 since mutants that are defective in oligomerization have no apparent ATP turn-over, display a decreased disaggregation activity and are unable to fully complement *hsp104* deletions in yeast (Parsell *et al.*, 1994b; Glover *et al.*, 1998; Schirmer *et al*., 1998). Whether the monomers play an active role in the disaggregation reaction or not is unknown.

2.6.8 The ATPase function of Hsp104

Similar to the oligomerization equilibrium, the ATP turn-over of Hsp104 is strongly dependent on the assay conditions such as the ionic strength and the nucleotide content (Schirmer *et al*., 1998). Since the nucleotide is bound at the interface of two adjacent subunits, the oligomerization of Hsp104 is crucial for its ATP hydrolysis. Accordingly, assay conditions that affect the oligomerization state of Hsp104, such as a high ionic strength, also affect the ATPase activity of Hsp104. Most of the ATPase studies on Hsp104 have been carried out with Walker A mutants. Both amino acid substitutions, K218T and K620T, were shown to reduce thermotolerance of yeast and to abort prion propagation (Parsell *et al.*, 1991; Schirmer *et al.*, 2001; Ness *et al.*, 2002) demonstrating the importance of both NBDs for the physiological function of Hsp104. The Walker A mutations abolish the capability of the affected domain to bind to nucleotides (Schirmer *et al.*, 1998; Watanabe *et al.*, 2002). Thus, the Hsp104 mutants, K218T and K620T, were thought to serve as an appropriate tool for unravelling the contribution of the individual NBDs to ATP hydrolysis. It was suggested that NBD2 accounts for less than 1% of the total ATPase activity (Schirmer *et al.*, 1998) although it has a high affinity for nucleotides (Hattendorf *et al.*, 2002a). Thus, it was assumed that ATP hydrolysis predominantly occurs in NBD1. This conclusion is mainly derived from experiments with the K218T mutant, in which NBD1 had been inactivated and lost the ability to bind nucleotides (Schirmer *et al.*, 1998). The corresponding mutation in NBD2 (K620T) shows a different behavior. At low protein concentration this mutant is largely unassembled (see above) and has a rather small ATPase activity. But at higher protein concentrations, the ATP turn-over reached ~25% of the wild-type level (Schirmer *et al.*, 2001). From this it was

concluded that (i) NBD2 is responsible for nucleotide-induced oligomerization and (ii) ATP hydrolysis is strongly stimulated upon hexamer formation. This dependency of the hydrolytic activity on the oligomeric state can be explained by the structure analysis of several related Clp ATPases (Bochtler *et al.*, 2000; Guo *et al.*, 2002; Lee *et al.*, 2003): the nucleotide binding pocket is located at the interface of adjacent subunits within the hexamer. Residues from two protomers are required to generate a complete ATP binding pocket, see 2.6.6. Thus, the binding of nucleotides or at least the ATP hydrolysis activity of an Hsp104 or Clp ATPase protomer is rather an inter-molecular event and presumably cannot take place in a monomer.

The specific arrangement of the NBDs within one NBD ring also implicates that nucleotide binding and/or hydrolysis of each NBD is influenced by the presence or absence of nucleotides bound in between of adjacent subunits. In other words, each ring of NBDs is subjected to an allosteric inter-protomer regulation, as revealed by the analysis of the Sensor 1 mutants of Hsp104 (Hattendorf *et al.*, 2002b). In addition, also NBD1 and NBD2 within one Hsp104 protomer communicate with each other: the nucleotide state of one domain influences the ATP activity in the other domain since mutations in either NBD1 or NBD2 changed the kinetic parameters for both sites (Hattendorf *et al.*, 2002a; Hattendorf *et al.*, 2002b). Allosteric communication between NBD1 and NBD2 was also observed for $ClpB_{E.c.}$ and $ClpB_{T.t.}$ (Schlee *et al.*, 2001; Mogk *et al.*, 2003c). The structural basis of this intra-protomer communication might be provided by the coiled-coil middle domain acting as a pin joint of NBD1 (see Fig.2X). It was found that the middle domain undergoes large motions in dependency on the nucleotide state (Lee *et al.*, 2007). These movements were previously thought to directly mediate disaggregation (Lee *et al.*, 2003) but they might also transmit the information on the nucleotide binding or hydrolysis between both NBDs. It was shown that this inter-domain communication pathway can be blocked by mutation or deletion of the middle region of Hsp104, $ClpB_{E.c.}$, and $ClpB_{T.t.}$ (Cashikar *et al.*, 2002; Mogk *et al.*, 2003c; Watanabe *et al.*, 2005).

In conclusion, cooperative ATPase activity occurs at both domains, NBD1 and NBD2, and allosteric communication occurs within and between the two nucleotide binding domains of Hsp104. However, the actual pathways of communication in Hsp104 are barely understood. Further, the assignment of the specific functions to NBD1 and NBD2 of Hsp104 are still quite preliminary since they are mostly based on studies employing the Walker A mutants, K218T and K620T, which reflect only the specific situation where no nucleotide is bound to the mutant NBD. Thus, the data obtained with Walker A mutants alone relate to an artificially constructed nucleotide-free state that might not exist for wild-type Hsp104.

It is also of great interest whether ATP hydrolysis occurs in a concerted fashion, such as in SV40 LTag helicase (Gai *et al.*, 2004), or in a sequential fashion, such as in T7 gp4 DNA helicase (Singleton *et al.*, 2000). A sequential-probabilistic model of ATP hydrolysis was proposed for the extensively studied ClpX ATPase (Martin *et al.*, 2005). However, the fashion of ATP hydrolysis by Hsp104 has not been studied yet and it is questionable whether

the model for the ClpX ATPase cycle can at all be applied to Hsp104 as well, since – different from ClpX – Hsp104 contains two NBDs (cf. Fig. 2.16), which might suggest a more advanced level of regulation.

2.6.9 The substrate binding cycle of Hsp104

The process of polypeptide substrate binding and substrate procession by Hsp104 is presently not very well understood although recent progress was made by the discovery that the ATP-bound state of NBD1 is the prerequisite for the Hsp104-substrate interaction (Bösl *et al.*, 2005). This state appears to exist only transiently in wild-type Hsp104 *in vivo* since NBD1 is the nucleotide-binding site of Hsp104 that has a very ATP high turn-over. Consequently, polypeptide binding appears to be a highly transient process. Therefore, substrate binding is very difficult to observe for the wild-type protein *in vivo* and *in vitro*. In order to populate an ATP-bound state in NBD1 either ATPγS, which is a slow hydrolyzing ATP mimetic, or a Walker B mutant (E285Q), which is impaired in ATP hydrolysis, had to be employed. Using both tools, ATPγS or a Walker B mutation, Hsp104 exhibits a high-affinity towards unfolded polypeptides such as carboxymethylated α-lactalbumin and towards stable aggregates such as Ure2 amyloid fibrils (Bösl *et al.*, 2005, and B. Bösl personal communication). A ternary complex is formed upon binding of the polypeptide substrate. This complex has a high stability and can be analyzed by non-equilibrium conditions such as SEC-HPLC. The dissociation of either ligand from the ternary substrate complex appears to be strictly coupled to the hydrolysis of ATP (or ATPγS), which gave rise to a model of an ATPase-coupled substrate cycle of Hsp104 (see Fig. 2.18). By hydrolysis Hsp104 is transferred from an ATP-bound (or ATPγS-bound) conformation displaying a high affinity towards unfolded polypeptides to a low affinity ADP-bound form, which subsequently is recharged with ATP (or ATPγS).

In the case of a Walker B double mutation (E285Q/E687Q) no ATP hydrolysis is possible at all and the ternary complex is irreversibly blocked, which is a property that signifies this mutant as a substrate trap, i.e., TRAP mutant. The ATP-dependent irreversible substrate binding by the TRAP mutant was proposed and established for related AAA^+ ATPases, too (Pak *et al*., 1999; Vale, 2000; Weibezahn *et al.*, 2003; Bolon *et al*., 2004; Burton *et al*., 2005).

Apart form the mentioned substrate binding cycle it remains to be elucidated, how the ATP hydrolysis by Hsp104 is coupled to substrate processing. For comparison, ClpX appears to possess a two-speed modus of ATP hydrolysis depending on the actual folding state and, hence, depending on the unfolding-resistance of the translocated polypeptide substrate (Kenniston *et al*., 2003). Further, ClpX exhibits a pronounced asymmetry within the homo-hexamer and different configurations of active and inactive protomers appear to support the

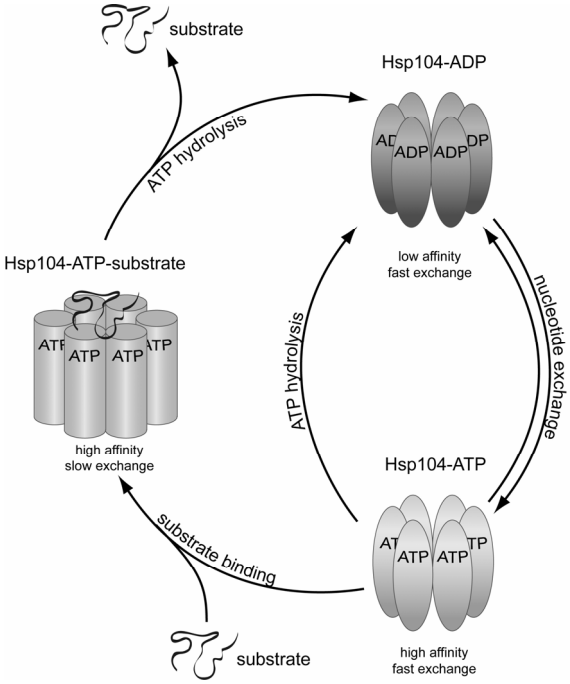

Fig. 2.18: The ATPase-coupled substrate binding cycle of Hsp104. During steady-state ATP hydrolysis the NBD1 of the molecular chaperone Hsp104 cycles between different conformational states: an ADP-bound state with a low affinity towards polypeptide substrates (top right) and an ATP-bound state with a high affinity towards polypeptides (bottom right). Substrates bind exclusively to the high affinity form of the chaperone thereby generating a ternary Hsp104·ATP·substrate complex (left). Reduced nucleotide exchange dynamics of this complex suggests that substrate binding induces a conformational change within Hsp104. As a consequence, the ternary complex is committed to hydrolysis. This lock-in mechanism ensures that the energy provided by ATP hydrolysis can be efficiently used for substrate processing. The figure was adopted from Bösl and coworkers (Bösl *et al.*, 2005).

translocation of polypeptides (Martin *et al.*, 2005; Hersch *et al*., 2005). It remains to be determined, whether substrate translocation by Hsp104 is similarly regulated or whether the presence of two NBDs and a somewhat different molecular architecture will give rise to an entirely different modus of regulation of substrate translocation by Hsp104.

2.7 Objectives of this study

The molecular chaperone Hsp104 from *Saccharomyces cerevisiae* represents a powerful machine for the disaggregation of proteins. It is directly involved in the renaturation of stable protein aggregates and plays a central role in prion propagation in yeast cells. The functional properties of Hsp104 are unique, both within the group of molecular chaperones and within the Hsp100/Clp family. An understanding of the biochemical regulation of Hsp104 might contribute to customize Hsp104 as a tool for biotechnological and medical approaches.

The main task of this work was to gain insight into the regulation of Hsp104 using biophysical, biochemical, and microbiological methods. The following key issues were addressed:

(i) Role of the oligomerization dynamics of Hsp104

Hsp104 was proposed to exist in a dynamic equilibrium of monomers, dimers/trimers, and hexamers. Do different species coexist at steady-state ATP hydrolysis under physiological conditions and – if so – can they be assigned to different functions of the molecular chaperone? To answer this question, equilibrium methods such as analytical ultracentrifugation, static light scattering, and enzymatic assays were applied since previous studies applying non-equilibrium methods such as SEC-HPLC failed to detect the exact oligomerization state of Hsp104.

(ii) Intrinsic regulation of the ATPase activity of Hsp104

The energy provided by the ATP hydrolysis is believed to drive the translocation of a polypeptide through the central channel of Hsp104. To understand the ATPase activity of the chaperone and how it is intrinsically regulated is, therefore, of crucial importance to unravel the mechanism of the Hsp104 machinery. In order to generate appropriate tools for a functional analysis, the two nucleotide binding domains of Hsp104, NBD1 and NBD2, were subjected to a series of specific point mutations. The resulting mutants allowed testing for the specific role of each NBD. In particular it was inquired how ATP binding and hydrolysis at one NBD modulate the properties of the second NBD as well as of the adjacent protomer. Identifying the allosteric pathways in Hsp104 will greatly improve our knowledge about its functional mechanism. Enzymatic assays, isothermal titration calorimetry and fluorescence spectroscopy were the selected methods for studying the intrinsic ATPase regulation of Hsp104. Thereby, a functional model for the ATPase cycle of Hsp104 was to be developed.

(iii) Inhibition of Hsp104 by guanidinium chloride

A further objective of this study was to elucidate whether or not GdmCl is a specific inhibitor of Hsp104. It is established that trace amounts of the chaotropic salt guanidinium chloride in the growth medium of yeast abolish the prion replication in yeast cells, an effect known as prion curing. However, prior to this work, it was not clear whether GdmCl acts on the prion proteins directly, or whether GdmCl influences prion formation indirectly, e.g., by affecting

Hsp104 function. In this work a detailed biochemical characterization of the influence of GdmCl on Hsp104 was to be carried out to reveal if and how the properties of Hsp104 are altered by the presence of GdmCl *in vitro*. Using a diverse set of enzymatic and biophysical methods it was examined how GdmCl interferes with Hsp104 function to draw conclusions on the ATPase cycle of Hsp104 and on the observed prion curing effect of GdmCl.

(iv) Extrinsic regulation of Hsp104: Identification and analysis of a new cofactor

Hsp104 cooperates with other molecular chaperones such as Hsp26 and Hsp70. However, these interactions are of a functional but not of a physical nature. Prior to this study, no cochaperone of Hsp104 was identified. In contrast, other molecular chaperones such as Hsp70 and Hsp90 do possess cochaperones, some of which contain TPR domains for the interaction with their chaperone counterpart. These cochaperones modulate the chaperone activity or the substrate specificity of Hsp70 and Hsp90. Thus, it was asked whether Hsp104 also possesses cochaperones. A potential interaction between Hsp104 and a cochaperone as well as the modulation of the Hsp104 function by this cochaperone was to be investigated by extensive *in vivo* and *in vitro* approaches. Further, it would be of interest if such a potential cofactor for Hsp104 can also be employed by other chaperones such as Hsp90 and Hsp70. In this case Hsp104 would constitute an integral part of the cytosolic chaperone network comprising, e.g., Hsp90 and Hsp70. To address these questions yeast prion propagation, stress tolerance and the co-localization were analyzed in addition to the biochemical and biophysical analysis including fluorescence anisotropy and the development of a new PPIase-sensitive chaperone assay for Hsp104.

3. MATERIALS AND METHODS

3.1 Materials

3.1.1 Equipment

Autoclave stem sterilizer (TRD) 601	MM (München, Germany)
Cell culture shaker Certomat S	B. Braun intl. (Melsungen, Germany)
Centrifuges	
Analytical ultracentrifuge XL-I	Beckmann (Palo Alto, USA)
Bench top centrifuge 5415 C	Eppendorf (Köln, Germany)
Centrifuge Avanti J 25	Beckmann (Palo Alto, USA)
Centrifuge J2HS	Beckmann (Palo Alto, USA)
Refrigerated centrifuge 32 R	Hettich (Tuttlingen, Germany)
Chromatographic equipment and materials	
Affi-Gel blue affinity gel	Bio-Rad (München, Germany)
Äkta Prime and Äkta FPLC	GE Healthcare (München, Germany)
HPLC with UV/ FL detector	Jasco (Groß-Umstadt, Germany)
Ni-chelating Sepharose FF	GE Healthcare (München, Germany)
Q-Sepharose FF	GE Healthcare (München, Germany)
Sephadex G25	Sigma (St. Louis, USA)
Superdex 200 Hiload 26/60	GE Healthcare (München, Germany)
Superdex 200 HR10/30	GE Healthcare (München, Germany)
Superloop, 200 mL	GE Healthcare (München, Germany)
Circular dichroism spectropolarimeter	
Jasco J-715 with PTC 343 Peltier	Jasco (Groß-Umstadt, Germany)
Film developing unit Optimax TR MS	Laboratory Equipment (Heidelberg, Germany)
Fluorescence microscope, inverse	Zeiss (Jena, Germany)
Freezer, -80°C	Sanyo (San Diego, USA)
French press Basic Z	Constant Systems (Warwick, UK)
Gel electrophoresis and blotting equipment	
Fastblot B44 apparatus	Biometra (Göttingen, Germany)
Gel electrophoresis unit Mighty Small II	GE Healthcare (München, Germany)
Haemacytometer, Neubauer Improved	Labor Optic (Friedrichsdorf, Germany)
Ice machine	Ziegra (Isernhagen, Germany)
Laboratory balances	
Sartorius analytical balance BP 121	Sartorius (Göttingen, Germany)
Sartorius universal balance	Sartorius (Göttingen, Germany)
Luminometer	
Genios Spectra Fluor plus	Tecan (Crailsheim, Germany)

Magnetic stirrer RCT basic	IKA Werke (Staufen, Germany)
Microcalorimeter VP-ITC	Microcal (Northampton, USA)
Micromanipulator MSM System	Singer (Somerset, UK)
pH-meter	WTW (Weilheim, Germany)
Power supply EPS 3500, 3501, and 1001	GE Healthcare (München, Germany)
Rocking platform shaker Polymax1040	Heidolph (Kelheim, Germany)
Spectrofluorometer	
FluoroMax 3 with autopolarizers	Jobin Yvon (Grasbrunn, Germany)
Static light scattering instrument	
miniDAWN Tristar	Wyatt Tec. (Santa Barbara, USA)
Thermo cycler Primus 25	MWG (Ebersberg, Germany)
Thermo mixer	Eppendorf (Köln, Germany)
Ultrasonic bath Sonsorex RK 100H	Bandelin (Berlin, Germany)
Ultrathurax DIAX 900	Heidolph (Kelheim, Germany)
UV/VIS spectrophotometer Cary 100	Varian (Palo Alto, USA)
Vacuum pump	Vacuumbrand (Wertheim, Germany)
Vortex MS2	IKA (Wilmington, USA)
Water bath F6 and F3	Haake (Karlsruhe, Germany)

3.1.2 Expendable materials

Cuvettes, disposable, semi-micro 1.5 mL	Brand (Wertheim, Germany)
Dialysis cassettes Slide-A-Lizer, 10 kDa	Pierce (Rockford, USA)
Dialysis membrane tubes Spectra/Por	Spectrum (Houston, USA)
Filter paper Whatman 3MM	Whatman (Brentford, UK)
Gel extraction kit QIAquick	Quiagen (Hilden, Germany)
Genomic DNA extraction kit, Geneclean	Q-BIOgene (Morgan Irvine, USA)
Micro concentrator Centriprep YM30/10	Millipore (Bedford, USA)
PCR product purification kit	Roche Diagnostics (Mannheim, Germany)
Plasmid preparation kit	Roche Diagnostics (Mannheim, Germany)
Polyethylene tubes (50 mL and 15 mL)	Greiner a Söhne (Nürtingen, Germany)
Polystyrole petri dishes	Greiner & Söhne (Nürtingen, Germany)
PVDF membrane Immobilon-P transfer	Millipore (Bedford, USA)
Sterile filters, 0.22 µm	Millipore (Bedford, USA)
Western blotting detection kit ECL Plus	GE Healthcare (München, Germany)
X-Ray film X-OMAT AR	Eastman Kodak (Rochester, USA)

3.1.3 Chemicals

N-Acetylarginine amide, acetate salt (NAAA)	Bachem (Bubendorf, Switzerland)
Acrylamide/bisacrylamide, 40% (w/v)	Roth (Karlsruhe, Germany)
Agar	Difco Laboratories (Detroit, USA)
Agarose, ultra pure	Roth (Karlsruhe, Germany)
Ampicillin	Roth (Karlsruhe, Germany)
ADP (adenosine 5'-diphosphate), disodium salt	Roche Diagnostics (Mannheim, Germany)
AMP-PNP (adenylylimido diphosphate)	Roche Diagnostics (Mannheim, Germany)
ATP (adenosine 5'-triphosphate), disodium salt	Roche Diagnostics (Mannheim, Germany)
ATPγS (adenosine-5'-O-3-thiotriphosphate)	Roche Diagnostics (Mannheim, Germany)
APS (ammonium peroxydisulfate)	Serva (Heidelberg, Germany)
Bromophenol blue S	Serva (Heidelberg, Germany)
Chloramphenicol	Roth (Karlsruhe, Germany)
Coomassie Brilliant Blue (R-250)	Serva (Heidelberg, Germany)
Coomassie protein assay reagent	Pierce (Rockford, USA)
Cyclosporin A	Sandoz (Basel, Switzerland)
Deoxynucleotides for PCR	Roth (Karlsruhe, Germany)
DTT (1,4-dithiothreitol)	Roth (Karlsruhe, Germany)
Ethanol, p. a.	Riedel de Hean AG (Seelze, Germany)
Ethidium bromide	Fluka (Sigma, St. Louis, USA)
5-FOA (5-fluoroorotic acid)	Fermentas (St. Leon-Rot, Germany)
G418-sulfate, geneticin	GibcoBRL (Karlsruhe, Germany)
GdmCl (guanidine hydrochloride)	ICN Biochemicals Inc. (Aurora, USA)
Glycerol, 99% (v/v)	ICN, Biochemicals Inc. (Aurora, USA)
HEPES (4-(2-hydroxyethyl)-1-piperazineethanesulfonic acid)	ICN, Biochemicals Inc. (Aurora, USA)
Imidazole, p. a.	Fluka (Sigma, St. Louis, USA)
IPTG (isopropyl β-D-1-thiogalactoside)	Roth (Karlsruhe, Germany)
Kanamycin	Roth (Karlsruhe, Germany)
Lucifer yellow iodoacetamide	Invitrogen (Karlsruhe, Germany)
β-Mercaptoethanol	Serva (Heidelberg, Germany)
Milk powder	Roth (Karlsruhe, Germany)
NADH (nicotinamide adenine dinucleotide)	Roche Diagnostics (Mannheim, Germany)

NADPH (nicotinamide adenine dinucleotide phosphate)	Roche Diagnostics (Mannheim,) Germany
PEP (phosphoenolpyruvate), potassium salt	Sigma (St. Louis, USA)
Peptone	Difco Laboratories (Detroit, USA)
PMSF (phenylmethylsulfonyl fluoride)	Roth (Karlsruhe, Germany)
Protease inhibitor cocktail HP and G	Serva (Heidelberg, Germany)
SDS (sodium dodecyl sulfate)	Serva (Heidelberg, Germany)
TCEP (tris(2-carboxyethyl) phosphine hydrochloride)	Pierce (Rockford, USA)
TEMED (N,N,N',N'-tetramethylenediamine)	Sigma (St. Louis, USA)
Tris (2-amino-2-(hydroxymethyl)propane-1,3-diol)	ICN, Biochemicals Inc. (Aurora, USA)
Tryptone	Difco Laboratories (Detroit, USA)
Tween 20 (polyoxyethylene(20)sorbitan monolaureate)	Calbiochem (San Diego, USA)
Urea, ultra pure	ICN, Biochemicals Inc. (Aurora, USA)
Yeast extract	Difco Laboratories (Detroit, USA)
Yeast nitrogen base	Difco Laboratories (Detroit, USA)

Additionally used chemicals were obtained from Merck (Darmstadt, Germany) and had a p.a. purity grade, if not indicated otherwise. For preparation of solutions and buffers double distilled water (ddH_2O) was used.

3.1.4 Antibodies, enzymes, and standards for molecular biology

Alkaline phosphatase (calf)	Roche Diagnostics (Mannheim, Germany)
Bovine serum albumin (BSA)	Serva (Heidelberg, Germany)
L-Lactate dehydrogenase (rabbit)	Roche Diagnostics (Mannheim, Germany)
Lysozyme	Sigma (St. Louis, USA)
Molecular weight standard for HPLC	GE Healthcare (München, Germany)
Molecular weight standard for SDS-PAGE	Bio-Rad (München, Germany)
PFU polymerase	Stratagene (La Jolla, USA)
POD anti-rabbit IgG conjugate (goat)	Sigma (St. Louis, USA)
Polyclonal anti-Cpr6 antiserum (rabbit)	Pineda Research (Berlin, Germany)
Polyclonal anti-Hsp104 antiserum (rabbit)	Pineda Research (Berlin, Germany)
Pre-stained SDS-PAGE marker Roti-Mark	Roth (Karlsruhe, Germany)

Protein A agarose beads	Roche Diagnostics (Mannheim, Germany)
PWO polymerase	Roche Diagnostics (Mannheim, Germany)
Pyruvate kinase (rabbit)	Roche Diagnostics (Mannheim, Germany)
Restriction enzymes	Roche Diagnostics (Mannheim, Germany)
RNase1 (DNase free)	Roche Diagnostics (Mannheim, Germany)
Site-directed mutagenesis kit QuikChange™	Stratagene (La Jolla, USA)
T4 DNA ligase	Promega (Madison, USA)

3.1.5 Molecular chaperones and their substrates

α-Lactalbumin (cow), reduced and carboxy-methylated (RCMLa)	Dr. B. Bösl, TU München
Cns1 (yeast)	Dr. K. Richter, TU München
Cpr6 (yeast)	this study
Cpr7 (yeast)	Dr. K. Richter, TU München
DHFR (mouse)	S. Hess, TU München
$Hsp104_{\Delta NM}$ (yeast)	A. Röthig, TU München
$Hsp104_{POINTMUTANT}$ (yeast)	this study
$Hsp104_{WT}$ (yeast)	this study
Hsp70 (human)	M. Marcinowski, TU München
Hsp82 (yeast Hsp90)	this study
Sti1 (yeast Hop)	Dr. K. Richter, TU München
Ydj1 (yeast Hsp40)	A. Schmid, TU München

All proteins listed above were purified from *E. coli* expression systems except of α-lactalbumin, which was supplied by Fluka (Buchs, Switzerland) and modified by Dr. B. Bösl.

3.1.6 Oligonucleotides for PCR and for sequencing

All oligonucleotides were obtained from MWG Biotech (Ebersberg, Germany).

Tab. 3.1: Primers for PCR amplification and mutagenesis.

Primer	Template DNA	Target Vector or Organism	Sequence 5'→ 3'
cpr6::kanMX4 forward	Euroscarf Y14165 *Δcpr6*	yeast	GAC GTG GAT GGG ACG ACC AGT AAG GAT TC
cpr6::kanMX4 reverse	Euroscarf Y14165 *Δcpr6*	yeast	GGC ACA TAT TTG GGA TAC AGT GAG GAC
CPR6 forward	yeast strain W303	pCM189/190	ATA AGG ATC CAT GAC TAG ACC TAA AAC TTT TTT TG
CPR6 reverse	yeast strain W303	pCM189/190	ATA ACT GCA GAT CAG GAG AAC ATC TTC GAA AG
RFPmars forward	pNCO-mRFPmars	pCM189/190	ATA ATA GGATCC ATG GCA TCA TCA GAA GAT GTT A
RFPmars reverse	pNCO-mRFPmars	pCM189/190	ATA ATA GGA TCC TGC ACC TGT TGA ATG
$HSP104_{WTpromoter}$ forward	yeast strain W303	pRS315	GAA AAC TGC AGT GGA TGT TCA GGA GAT CGA GTC
$HSP104_{WT}$ reverse	yeast strain W303	pRS315	GAA AAG GAT CCT ATT AAT CTA GGT CAT CAT CAA TTT CC
$HSP104_{893\Delta C}$ reverse	yeast strain W303	pRS315	GAA AAC TGC AGT GGA TGT TCA GGA GAT CGA GTC
$HSP104_{TRAP}$ forward	pQE70-$HSP104_{TRAP}$	pRS313	AAA AAG GAT CCA TGA ACG ACC AAA CGC AAT TTA CAG
$HSP104_{TRAP}$ reverse	pQE70-$HSP104_{TRAP}$	pRS313	AAA AAA GAG CTC TTA ATC TAG GTC ATC ATC AAT TTC
$HSP104_{TRAP/893\Delta C}$ reverse	pQE70-$HSP104_{TRAP}$	pRS313	AAA AAA GAG CTC TTA ACC TAA CGT GTC AGC CCC TAT AG
893ΔC forward	pQE70-$HSP104_{WT}$	pQE70-$HSP104_{WT}$	GGC TGA CAC GTT AGG TTA AGA CGA TAA TGA GGA CAG TAT G
893ΔC reverse	pQE70-$HSP104_{WT}$	pQE70-$HSP104_{WT}$	CAT ACT GTC CTC ATT ATC GTC TTA ACC TAA CGT GTC AGC C
E285Q forward	pQE70-$HSP104_{WT}$	pQE70-$HSP104_{WT}$	CTA ATT GTG TTA TTC ATT GAT CAG ATT CAC ATG TTA ATG GGT AAT G
E285Q reverse	pQE70-$HSP104_{WT}$	pQE70-$HSP104_{WT}$	CAT TAC CCA TTA ACA TGT GAA TCT GAT CAA TGA ATA ACA CAA TTA G
E687Q forward	pQE70-$HSP104_{WT}$	pQE70-$HSP104_{WT}$	CTC CGT TTT GTT ATT CGA TCA GGT AGA AAA GGC ACA TCC TGA TG
E687Q reverse	pQE70-$HSP104_{WT}$	pQE70-$HSP104_{WT}$	CAT CAG GAT GTG CCT TTT CTA CCT GAT CGA ATA ACA AAA CGG AG

The following internal primers were used for the complete sequencing of *HSP104*, which has a size of 2.27 kB.

Tab. 3.2: Internal primers for the sequencing of *HSP104*.

Primer	Sequence 5' → 3'	5' Position in *HSP104*
M1	CCA CTG TTT GTC TCA CAC TTG	1048 reverse
M2	GTT AAT GGG TAA TGG TAA GGA C	864
M3	CGA CTC CAC CAC TAA AGA TAG	1311
M4	GAA CGT GAC TTA TCA TCT GAA G	1717

3.1.7 Bacterial plasmids and strains

Tab. 3.3: Bacterial plasmids used in this work. pQE70-HSP104 constructs do not contain His-tags.

Plasmid	Description	Reference or Source
pNCO-mRFPmars	pNCO113 vector containing the synthesized gene of *mRFPmars*, coding for a monomeric red fluorescent protein, Amp^R	Prof. Dr. M. Fischer, University of Hamburg, Germany
pRSET-CPR6	coding for Cpr6 with N-terminal His-tag	(Prodromou *et al.*, 1999)
pQE70-HSP104$_{WT}$	coding for Hsp104$_{WT}$, T5 expression system, Amp^R, basis of all pQE70-HSP104$_{MUTATION}$ plasmids	Diploma thesis of V. Grimminger, TU München, Germany
pQE70-HSP104$_{K218T}$	coding for Hsp104 with Walker A point mutation causes loss of nucleotide binding to NBD1	Diploma thesis of V. Grimminger, TU München, Germany
pQE70-HSP104$_{E285Q}$	coding for Hsp104 with Walker B point mutation causes loss of ATP hydrolysis by NBD1	this study
pQE70-HSP104$_{K620T}$	coding for Hsp104 with Walker A point mutation causes loss of nucleotide binding to NBD2	Diploma thesis of V. Grimminger, TU München, Germany
pQE70-HSP104$_{K218T/\ K620T}$	coding for Hsp104 with Walker A double point mutation, causes loss of nucleotide binding to NBD1 and NBD2	Diploma thesis of V. Grimminger, TU München, Germany
pQE70-HSP104$_{E687Q}$	coding for Hsp104 with Walker B point mutation causes loss of ATP hydrolysis by NBD2	this study
pQE70-HSP104$_{E285Q/E687Q}$	coding for Hsp104 with Walker B double point mutation, causes loss of ATP hydrolysis by NBD1 and NBD2	this study
pQE70-HSP104$_{893\Delta C}$	coding for Hsp104 with nonsense mutation for truncation of C-terminus	this study

Tab. 3.4: Bacterial strains used in this work.

Strain	Genotype	Reference or Source
E. coli JM109	*recA1, supE44, endA1, hsdR17, gyrA96, relA1, thi, Δ(lac-proAB) [F', traD36 proAB$^+$ lacI^q ZΔM15]*	(Yanisch-Perron *et al*., 1985)
E. coli BL21 (DE3) pLysS	*F$^-$, dcm, ompT, hsdS, (r_B^-,m_B^-), gal,* λ(DE3) [pLysS Cam^R]	Stratagene (La Jolla, USA)
E. coli BL21 cod$^+$ RIL	*F$^-$, dcm, ompT, hsdS, (r_B^-,m_B^-), gal,* λ(DE3), *endA, Hte [argU ileY leuW Cam^R]*	Stratagene (La Jolla, USA)
E. coli BL21 cod$^+$ pUBS	*F$^-$, lon, ompT, (r_B^-,m_B^-), endA, Hte [argU ileY leuW Cam^R] pUBS [Kan^R, $lacI^q$]*	Stratagene (La Jolla, USA)

3.1.8 Media and antibiotics for the propagation of *E. coli*

LB_0 Medium:	10 g/L tryptone
(Luria-Bertani broth medium)	5 g/L yeast extract
	5 g/L NaCl
	pH 7.2 (NaOH)
Ampicillin stock solution (Amp):	100 mg/mL in ddH_2O
Chloramphenicol stock solution (Cam):	50 mg/mL in ethanol
Kanamycin stock solution (Kan):	35 mg/mL in ddH_2O

15 g Agar per one litre liquid medium were added for the preparation of agar dishes. The LB_0 medium was autoclaved in a TRD 601 autoclave stem sterilizer by a standard autoclave cycle at 121°C for 20 minutes. Antibiotic solutions were filter sterilized and stored at -20°C. They were added in a ratio of 1:1000 to the growth medium after autoclaving.

3.1.9 Yeast vectors and strains

Tab. 3.5: Yeast vectors used in this work.

Vector	Promoter	Marker	Replication	Reference or Source
pRS313	*CUP1*	*HIS3*	CEN	(Sikorski and Hieter, 1989)
pRS315	-	*LEU2*	CEN	(Sikorski *et al.*, 1989)
pCM189	$tetO_7$	*URA3*	CEN	(Gari *et al*., 1997)
pCM190	$tetO_7$	*URA3*	2µ	(Gari *et al.*, 1997)
p315_HSP104	*HSP104*	*LEU2*	CEN	this study
p315_893ΔC	*HSP104*	*LEU2*	CEN	this study
p190_CPR6	$tetO_7$	*URA3*	2µ	this study
p189_RFPCPR6	$tetO_7$	*URA3*	CEN	this study
p315_NMGFP	*GAL1-10*	*LEU2*	CEN	Dr. T. Scheibel, TU München, Germany
p313_$HSP104_{TRAP}$	*CUP1*	*HIS3*	CEN	this study
p313_$HSP104_{TRAPΔC}$	*CUP1*	*HIS3*	CEN	this study

Tab. 3.6: Yeast strains used in this work.

Strain	Genotype	Reference or source
BSC783/4a [*PSI*$^+$]	*MATα* and *MATa*, *SUQ5*, *ade2-1*$_{UAA}$, *his3-11,-15*, *leu2-3,-112*, *ura3-1*	B. S. Cox, University of Kent, UK
BSC783/4a [*psi*$^-$]	*MATα*, *SUQ5*, *ade2-1* $_{UAA}$, *his3-11,-15*, *leu2-3,-112*, *ura3-1*	B. S. Cox, University of Kent, UK
BSC783/4a *Δhsp104* [*psi*$^-$]	*MATα*, *SUQ5*, *ade2-1*$_{UAA}$, *his3-11,-15*, *leu2-3,-112*, *ura3-1*, *hsp104::LEU2*	B. S. Cox, University of Kent, UK
BSC783/4a *Δcpr6* [*PSI*$^+$]	*MATα* and *MATa*, *SUQ5*, *ade2-1*, *his3-11,-15*, *leu2-3,-112*, *ura3-1*, *cpr6::kanMX4*	this study
BSC783/4a *Δcpr6* [*psi*$^-$]	*MATα* and *MATa*, *SUQ5*, *ade2-1*, *his3-11,-15*, *leu2-3,-112*, *ura3-1*, *cpr6::kanMX4*	this study
BY4742 Y14165 *Δcpr6*	*MATα*, *his3-1*, *leu2-0*, *lys2-0*, *ura3-0*, *cpr6::kanMX4*	Euroscarf , Frankfurt, Germany
kar [*PSI*$^+$] 1152/1a or 2b	*MATa*, *ade2-1*, *kar1.1*, *lys1.1*, *can1*	B. S. Cox, University of Kent, UK
74D-694 [*PSI*$^+$]	*MATα* and *MATa*, *ade1-14*$_{UGA}$, *his3Δ-200*, *leu2-3,-112*, *trp1-289*, *ura3-52*	Y. Chernoff, Atlanta, USA
74D-694 *Δcpr6* [*PSI*$^+$]	*MATα* and *MATa*, *ade1-14*$_{UGA}$, *his3Δ-200*, *leu2-3,-112*, *trp1-289*, *ura3-52*, *cpr6::kanMX4*	this study
YJW512 [*PSI*$^+$][*PIN*$^+$]	*MATa*, *ade1-14*, *can1-100, his3-11,-15, leu2-3,-112, trp1-1, ura3-1*	L. Osherovich UCSF, USA
YJW512 *Δcpr6* [*PSI*$^+$][*PIN*$^+$]	*MATa*, *ade1-14*, *can1-100*, *his3-11,-15*, *leu2-3,-112*, *trp1-1*, *ura3-1*, *cpr6::kanMX4*	this study
YJW532 *HSP104* [*PSI*$^+$]	*MATa*, *ade1-14*, *can1-100*, *his3-11,-15*, *leu2-3,-112*, *trp1-1*, *ura3-1*, *hsp104::HIS3* [p316_HSP104]	L. Osherovich UCSF, USA
YJW532 *Δhsp104* [*psi*$^-$]	*MATa*, *ade1-14*, *can1-100*, *his3-11,-15*, *leu2-3,-112*, *trp1-1*, *ura3-1*, *hsp104::HIS3* [p315_empty]	this study
YJW532 *HSP104* [*PSI*$^+$]	*MATa*, *ade1-14*, *can1-100*, *his3-11,-15*, *leu2-3,-112*, *trp1-1*, *ura3-1*, *hsp104::HIS3* [p315_HSP104]	this study
YJW532 *893ΔC* [*PSI*$^+$]	*MATa*, *ade1-14*, *can1-100*, *his3-11,-15*, *leu2-3,-112*, *trp1-1*, *ura3-1*, *hsp104::HIS3* [p315_893ΔC]	this study
W303	*MATa*, *ade2-1, can1-100, his3-11,15, leu2-3,112*, *lys2-1*, *trp1-1*, *ura3-1*	R. Rothstein, Columbia University, NY, USA

3.1.10 Media and solutions for the propagation of *S. cerevisiae*

YEPD-Medium	10 g/L yeast extract
	10 g/L peptone
	20 g/L glucose
¼YEPD-Medium	2.5 g/L yeast extract
	10 g/L peptone
	20 g/L glucose
YNB-Medium	5.7 g/L yeast nitrogen base
	20 g/L glucose
	2 g/L amino acid drop-out mix (-LEU, -URA, -ADE, and -HIS)

YNB-Medium, copper-free, glucose-free	5.7 g/L yeast nitrogen base 30 g/L raffinose or galactose 2 g/L amino acid drop-out mix (-LEU, -URA, and -HIS)
Sporulation Medium	1 g/L yeast extract 0.5 g/L glucose 10 g/L potassium acetate

Media for special selection:

YEPD GdmCl	3 mM GdmCl in YEPD
YEPD G418 (geneticin)	200 mg/L G418 in YEPD
YNB-ADE	YNB minimal medium lacking adenine
YNB-LEU 5-FOA (5-fluorotic acid)	1 g/L 5-FOA in YNB
YEPG	glucose-free, similar to YEPD but with 4% glycerol instead of glucose

20 g Agar per one litre liquid medium were added for the preparation of agar dishes. The medium was sterilized by autoclaving for 20 minutes.

3.1.11 Buffers for protein chemistry

For preparation of solutions and buffers double distilled water (ddH_2O) was used. All solutions were titrated to the indicated pH at RT unless indicated otherwise.

3.1.11.1 Buffers and solutions for the production of recombinant Hsp104

All buffers below were degased and filtrated.

E. coli cracking buffer	50 mM Tris/HCl pH 8.1, 4°C 2 mM EDTA protease inhibitor cocktail G 20 mg/L lysozyme
Q-buffer A	50 mM Tris/HCl, pH 8.0, 4°C 1 mM EDTA 0.05% (v/v) β-mercaptoethanol
Q-buffer B	50 mM Tris/HCl, pH 8.0, 4°C 1 M NaCl 1 mM EDTA 0.05% (v/v) β-mercaptoethanol

Affi-buffer A	20 mM Tris/HCl, pH 8.0, 4°C
	0.05% (v/v) β-mercaptoethanol
Affi-buffer B	20 mM Tris/HCl, pH 8.0, 4°C
	1 M NaCl
Ni-buffer A	50 mM $Na_xH_{3-x}PO_4$, pH 7.5, 4°C
Ni-buffer B	50 mM $Na_xH_{3-x}PO_4$, pH 7.5, 4°C
	100 mM imidazole
Protein storage buffer	50 mM Tris/HCl, pH 8.0, 4°C

3.1.11.2 Buffers and solutions for the gel electrophoresis of proteins

Lämmli sample buffer (5 x)	300 mM Tris/HCl, pH 6.8
	10% (w/v) SDS
	50% (v/v) glycerol
	0.05% (w/v) bromophenol blue
	5% (v/v) β-mercaptoethanol (freshly added)
Separating gel buffer (4 x)	1.5 M Tris/HCl, pH 8.8
	0.8% (w/v) SDS
Stacking gel buffer (2 x)	250 mM Tris/HCl, pH 6.8
	0.4% (w/v) SDS
SDS running buffer (10 x)	250 mM Tris
	2 M glycine
	1% (w/v) SDS
	pH 8.8

3.1.11.3 Buffers and solutions for Coomassie staining

Coomassie staining solution	25% (v/v) isopropanol
	10% (v/v) acetic acid
	0.05% (w/v) Coomassie brilliant blue R
Coomassie destaining solution	10% (v/v) acetic acid

3.1.11.4 Buffers and solutions for silver staining

Silver fix solution I	30% (v/v) ethanol (prep. grade)
	10% (v/v) acetic acid

Silver fix solution II (freshly prepared)	30% (v/v) ethanol (prep. grade)
	0.5% (v/v) acetic acid
	0.4 M sodium acetate pH 6.0
	0.1% (w/v) sodium dithiosulfate
	2 mL glutaraldehyde (25%, v/v)
	ddH_2O to 100 mL
Silver staining solution	6 mM silver nitrate
	25 µL formaldehyde (37%, v/v, freshly added)
	ddH_2O to 100 mL
Silver developing solution (freshly prepared)	
	7.5 g sodium carbonate
	120 µL formaldehyde (37%, v/v)
	ddH_2O to 300 mL
Silver stop solution	50 mM EDTA, pH 7.5

3.1.11.5 Buffers and solutions for western blotting

WB transfer buffer	17.5 mM Tris
	150 mM glycine
	15% (v/v) methanol
PBS (10 x)	40 mM KH_2PO_4
	160 mM Na_2HPO_4
	1.15 M NaCl
	pH 7.4
PBS-T	1 x PBS
	0.1% (v/v) Tween20

3.1.11.6 Buffers and solutions for co-immunoprecipitation

IP-buffer	30 mM HEPES/KOH pH 7.5
	70 mM KCl
	5 mM $MgCl_2$
	20 mM EDTA
	0.1 mM DTT
	1% (v/v) glycerol
IP2-buffer:	IP-buffer with addition of
	1% (v/v) Tween20
	300 mM NaCl

3.1.11.7 Buffers and solutions for *in vitro* experiments with Hsp104

The buffers listed below were degased and filtrated.

Standard assay buffer	50 mM HEPES/KOH pH 7.5 150 mM KCl 10 mM $MgCl_2$
LS assay buffer (low salt)	70 mM HEPES/KOH pH 7.5 50 mM KCl 10 mM $MgCl_2$
KM assay buffer	50 mM HEPES/KOH pH 7.5 150 mM KCl 25 mM $MgCl_2$
KM-LS assay buffer	50 mM HEPES/KOH pH 7.5 25 mM $MgCl_2$
Adenine nucleotide solution	300 mM in ddH_2O, pH 7.5 (KOH), the concentration was determined spectroscopically using $\varepsilon_{259} = 15{,}400\ M^{-1}cm^{-1}$

3.1.11.8 Buffers and solutions for the reactivation of denatured luciferase

Luciferase denaturing buffer	25 mM HEPES/KOH pH 7.5 50 mM KCl 5 mM $MgCl_2$ 5 mM ATP 10 mM DTE 7 M urea
Luciferase refolding buffer	25 mM HEPES/KOH pH 7.5 50 mM KCl 15 mM $MgCl_2$ 5 mM ATP 2 mM DTE 240 µM coenzyme A 50 µg/mL BSA 10 mM PEP 0.1 mM luciferin 50 µg/mL pyruvate kinase

3.1.11.9 Buffers and solutions for the reactivation of denatured DHFR

DHFR assay buffer	70 mM HEPES/KOH pH 7.5
	50 mM KCl
	1 mM $MgCl_2$
	0.1 mM DHF
	0.1 mM NADPH
DHFR refolding buffer	70 mM HEPES/KOH pH 7.5
	50 mM KCl
	10 mM $MgCl_2$
	10 µM DHF
	10 µM NADPH
	5 mM ATP
	20 mM PEP
	50 µg/mL pyruvate kinase

3.1.12 Computer software and web tools

Adobe Creative Suite	Adobe (http://www.adobe.com)
CDNN spectra deconvolution, Vers. 2.1	University of Halle (Halle, Germany)
Chromas 2.31	Technelysium (Helensvale, Australia)
ClustalW tool for sequence alignment	EMBL-EBI (http://www.ebi.ac.uk/clustalw)
InterPro database	EMBL-EBI (http://www.ebi.ac.uk/interpro)
ISIS Draw 2.4	MDL (http://www.mdli.com)
Microsoft Office 2000	Microsoft (Redmond, USA)
mRNA pattern database (yeast)	http://genome-www.stanford.edu/yeast_stress
Origin	Origin (Northampton, USA)
Origin for ITC	Microcal and Origin (Northampton, USA)
PovRay 3.5	PovRay (http://www.povray.org)
PRIMER DESIGNER 1.02 (1990)	Scientific & Educational Software
Promoter analysis (yeast)	YEASTRACT (www.yeastract.com)
Protein abundance database (yeast)	*yeastgfp* (http://yeastgfp.ucsf.edu)
Protein structure database	RCSB (http://www.rcsb.org/pdb)
ProtParamTool	ExPasy (http://us.expasy.org)
Reference Manager	Thomson (Carlsbad, USA)
Saccharomyces genome database	SGD (http://www.yeastgenome.org)
Swiss PDB Viewer	ExPasy (http://us.expasy.org)
Ultrascan 7.2	B. Demeler (University of Texas, USA)
Vector NTI	Invitrogen (http://www.invitrogen.com)

3.2 Molecular cloning techniques

All materials and solutions used for the propagation of microorganisms and for molecular biology research were sterilized prior to use. If not indicated otherwise, all work was performed at RT. Standard protocols were used for DNA electrophoresis, restriction enzymatic digestion, ligation, bacterial growth, and transformation (Sambrook and Russell, 2001).

3.2.1 Production, isolation and purification of DNA

3.2.1.1 *E. coli* plasmid DNA isolation

The *E. coli* strains DH5α and JM109 were used for the amplification and construction of plasmids. Plasmid DNA isolation was performed using a plasmid isolation kit following the manufacturer's instructions (Roche Diagnostics, Mannheim, Germany).

3.2.1.2 Purification of DNA fragments

Fragments of DNA generated by restriction, enzymatic digestion, or by PCR (Mullis *et al*., 1986) using a thermo cycler, were purified with the PCR product purification kit. Protocols provided by the manufacturer (Roche Diagnostics, Mannheim, Germany) were followed. If required, fragments of DNA were separated by a standard DNA electrophoresis (Sambrook *et al.*, 2001). DNA bands corresponding to desired products were identified using a UV transilluminator and excised from ethidium bromide stained gels with a scalpel. Separation of DNA from the gel was achieved employing the QIAquick gel extraction kit and the protocols supplied by the manufacturer (Qiagen, Hilden, Germany).

3.2.1.3 Yeast DNA isolation

Genomic DNA from yeast was isolated using the Geneclean kit. The procedure was carried out according to the instructions of the manufacturer (Q-BIOgene, Morgan Irvine, USA).

3.2.2 Site-directed mutagenesis of *HSP104*

Site-directed mutagenesis of *HSP104* was performed using a polymerase chain reaction with the QuikChange™ site-directed mutagenesis kit. A pQE70 plasmid carrying *HSP104* was used as template for mutagenesis (see Tab. 3.3). The point mutations were generated by appropriate mutagenesis primers (see Tab. 3.1) and PFU polymerase PCR reaction according

to the protocol of the mutagenesis kit (Stratagene, La Jolla, USA). The mutations were verified by sequencing of the complete gene employing standard flanking primers. If required, additional internal primers were used for sequencing (see Tab. 3.2).

3.2.3 Cloning of yeast vectors

HSP104 and *CPR6* were cloned into yeast vectors to study their function *in vivo*. *CPR6* was amplified from genomic yeast DNA by PCR (CPR6 forward and reverse primers, see Tab. 3.1) and cloned into a pCM190 or a pCM189 vector under the control of constitutive $tetO_7$ promoter system (Gari *et al.*, 1997). Four pRS-based plasmids were constructed, p315_HSP104, p415_HSP104, p315_893ΔC and p415_893ΔC, in order to assess the *in vivo* role of the C-terminal motif of Hsp104. These *HSP104* constructs were under the control of the original *HSP104* promoter by amplifying both the *HSP104* promoter region and *HSP104* from genomic yeast DNA ($Hsp104_{WTpromoter}$ forward primer and $Hsp104_{WT}$ reverse primer or $Hsp104_{893\Delta C}$ reverse primer, respectively, see Tab. 3.1). For co-localization studies the following plasmids were constructed: pCM189_RFPCPR6, pRS313_$HSP104_{TRAP}$, and pRS313_$HSP104_{TRAP\Delta C}$. mRFPmars was amplified by PCR from the plasmid pNCO-mRFPmars and inserted into pCM189_CPR6 at the coding 5' end of *CPR6*. $HSP104_{TRAP}$ was cloned into the pRS vectors under the control of the copper promoter *CUP1*. By selection of appropriate primers $HSP104_{TRAP\Delta C}$ was generated and also cloned into pRS313. All these vectors for co-localization studies had a centromeric replication rate to ensure a homogenous copy number in every yeast cell.
The obtained plasmids were confirmed by sequencing and transformed into the particular yeast strains.

3.3 *In vivo* analysis of *S. cerevisiae*

3.3.1 Yeast growth conditions

The yeast strains used in this study are listed in Tab. 3.6. Yeast cultures were grown at 30°C in a cell culture shaker unless noted otherwise. Standard procedures for yeast cultivation, phenotypic and genetic analysis, transformation, sporulation and dissection were used (Kaiser *et al*., 1994). Cells were grown in rich media (YEPD) or glucose-based synthetic media (YNB) lacking the appropriate amino acids to guarantee plasmid maintenance. Sporulation of diploids was induced after 4 days of growth in sporulation medium (Brown and Tuite, 1998). Sporulating cultures were dissected using a micromanipulator. Cell counts were performed using a Neubauer hemacytometer (Fisher Scientific, Orlando, USA). All yeast transformations were carried out according to the lithium treatment procedure (Ito *et al*., 1983; Kaiser *et al.*, 1994). Yeast transformants were confirmed on YEPG plates in all cases

(medium containing glycerol as carbon source). Petites that are respiratory deficient do not grow on YEPG as sole carbon source and were not considered for future use.

3.3.2 Generating gene knockouts

Disruption of genomic *CPR6* was performed by a non-homologous recombination with a *cpr6::kanMX4* disruption cassette. This disruption cassette was generated by PCR on genomic DNA of the *cpr6::kanMX4* strain from Euroscarf (accession number: Y14165, primers see Tab. 3.1). The PCR product was sequenced and used for the transformation of yeast strains. Recombinant clones were selected on G418 agar plates. To prove the proper insertion of the *cpr6::kanMX4* cassette into the *CPR6* gene the clone was analyzed by PCR and confirmed by sequencing. To show that exclusively the *CPR6* gene was affected by the recombination with *cpr6::kanMX4*, the obtained strain was back-crossed with its wild-type strain. Apart form this procedure, *Δcpr6* strains were also transformed with p190_CPR6 or with p189_CPR6 in order to study the regenerated *CPR6* phenotype.

3.3.3 Plasmid shuffling in yeast

The strain YJW532 *hsp104::HIS3* [p316_HSP104], which is lacking its genomic *HSP104*, was used in plasmid shuffling experiments for complementation studies. The vector p316_HSP104 containing a *URA3* marker was exchanged against a p315_HSP104/ΔC vector containing a *LEU2* marker by streaking out the double transformants YJW532 [p316_HSP104] [p315_HSP104/ΔC] onto YNB-LEU 5-FOA agar plates. Only cells lacking *URA3* are able to grow on 5-FOA plates since the gene codes for a decarboxylase converting 5-FOA into the toxic product 5-fluorouracil. As a consequence, cells are forced to lose the *URA3* containing vector p316_HSP104. The plates were incubated for 3 days at 30°C until colonies appeared. These were selected for further studies and restreaked on YNB-URA to examine the loss of the *URA3* containing plasmid.

3.3.4 Phenotypic analysis of yeast strains

Yeast strains were grown overnight in a liquid culture at 30°C while shaking. The number of cells was counted and diluted to 2 x 10^6 cfu/mL (A_{600} = 0.1). 5 µL of each yeast suspension were then spotted onto appropriate agar plates and incubated for 2 to 7 days at 30°C

3.3.5 Nonsense suppression assay for the presence of [*PSI*$^+$]

The presence of the prion phenotype [*PSI*$^+$] was detected by its ability to suppress mutant *ade* alleles caused by premature stop codons, as described previously (Derkatch *et al.*, 1996). [*psi*$^-$] strains are not able to grow on medium lacking adenine (-ADE) and exhibit a dark red color on rich medium, while [*PSI*$^+$] strains are able to grow on -ADE and show a white or a light pink color. Weak and strong variants of [*PSI*$^+$] can be distinguished by gradually reduced growth on -ADE or by a pinker color. This [*PSI*$^+$]-mediated phenotype was assessed on ¼YEPD plates, and on YNB plates with 10 mg/L adenine, or by adenine prototrophy. Media containing 3 mM GdmCl were used to cure the prion phenotype (Tuite *et al.*, 1981).

3.3.6 Cell viability assay

The stress resistance of yeast strains was assayed by plating them onto agar plates containing ethanol or sodium chloride at various concentrations. The plates were incubated at 30°C until colonies appeared. Heat stress was tested by applying the induced thermotolerance assay, see below.

3.3.7 Thermotolerance assay

To assay the ability of yeast cells to survive at 50°C a culture was first grown in YEPD to an A_{600} of ~0.6 at 30°C. Then, the culture was transferred to 37°C for 1 h. After that a control aliquot was placed on ice and the remaining culture was harvested by centrifugation at 3000 rpm for 5 min at RT and resuspended in medium that was already pre-warmed to 50°C. The culture was maintained at 50°C for the duration of the experiment. Cell aliquots were taken every 5 min and placed on ice. Serial dilutions of both the control and the heat-shocked samples were prepared and plated onto YEPD plates to determine the number of colony forming units (CFUs).

3.3.8 Co-localization by fluorescence microscopy

For the *in vivo* co-localization assays the following vector constructs were used: (i) p189_RFPCPR6 constitutively expressing *RFPCPR6* under the control of a *tetO*$_7$ promoter, (ii) p315_NMGFP with an inducible *GAL1-10* promoter, and (iii) p313_HSP104$_{TRAP}$ or p313_HSP104$_{TRAP\Delta C}$ with an inducible copper promoter *CUP1*. The yeast cultures were pre-grown overnight in selective copper- and glucose-free YNB medium with raffinose as a carbon source. Cells were harvested by centrifugation and resuspended in a medium containing galactose. Shifting to galactose induced the expression of *NMGFP*. Additionally,

100 µM copper sulphate was added to the medium to induce $HSP104_{TRAP}$ or $HSP104_{TRAP\Delta C}$ expression. The culture was incubated for 3 to 6 h at 30°C for co-expression of the constructs. As negative controls, inducible constructs were individually expressed. Then fluorescence images were taken using live cultures. Images were scanned by an inverse fluorescence microscope equipped with a 100 x objective, with a narrow band GFP filter and a RFP filter.

3.4 Methods of protein biochemistry

3.4.1 Production of recombinant protein

3.4.1.1 Production of recombinant Cpr6 and Hsp82

Cpr6 was expressed in *E. coli* BL21-CodonPlus(DE3)-RILpLysS (see Tab. 3.4) using a pRSET vector carrying yeast *CPR6* (see Tab. 3.3) and purified, as described (Mayr *et al.*, 2000). For the production of Hsp82 a pET28 vector (see Tab. 3.3) carrying the yeast *HSP82* gene was used. Expression was carried out in *E. coli* BL21-CodonPlus(DE3)-RIL (see Tab. 3.4). Purification was performed, as described (Richter *et al*., 2001). Protein concentrations refer to monomeric protein and were determined by absorbance spectroscopy.

3.4.1.2 Production of recombinant Hsp104

The *E. coli* strain BL21cod$^+$ pUBS (Tab. 3.4) was transformed with pQE70 plasmids carrying the genes $Hsp104_{WT}$ or $Hsp104_{mutant}$ (Tab. 3.3). Transformants were selected for Amp^R, Kan^R, and Cam^R to ensure the maintenance of all plasmids. For protein production, 6 l of LB medium containing 100 mg/L ampicillin were inoculated with a 30°C overnight culture. Flasks were incubated at 30°C in a cell culture shaker until the culture had reached an A_{600} of ~0.8. Expression of *Hsp104* was induced by the addition of 0.1 mM IPTG, and cells were harvested by centrifugation after 3 - 6 h of induction.
All following procedures were carried out on ice or using pre-chilled equipment and buffers. The *E. coli* pellet was resuspended in an *E. coli* cracking buffer using an ultrathurax. The cell suspension was cracked by a french press at 2 kbar. Then the crude extract was centrifuged for 45 min at 20,000 rpm to separate the debris. The supernatant containing Hsp104 was subjected to an anion exchange chromatography using an Äcta FPLC system equipped with a Q-Sepharose FF column. The flow was set to 2 mL/min in all subsequent chromatographic steps. The protein solution was loaded on the column using a 200 mL superloop. After washing with 5 CV of Q-buffer A + 10% Q-buffer B a salt gradient from 200 to 600 mM sodium chloride was applied, and protein fractions were collected. Hsp104 typically eluted between 400 and 450 mM sodium chloride. Protein samples were analyzed by SDS-PAGE to

identify Hsp104 containing fractions. Then the fractions were pooled, diluted to a salt concentration of less than 200 mM sodium chloride and loaded onto an Affi-Gel blue column. The binding to this matrix material is dependent on the ionic strength. Therefore, a dilution or dialysis of the pooled protein before loading was essential to guarantee the quantitative binding of Hsp104. After binding the column was washed with 5 CV of Affi-buffer A and eluted by increasing the sodium chloride concentration to 1 M using Affi-buffer B. Again, fractions were collected, analyzed by SDS-PAGE and pooled. Depending on the purity the protein was either concentrated and desalted *via* a Sephadex G25 column with protein storage buffer or further purification steps were applied. Hsp104 has the ability to bind to nickel ions although the protein does not contain any His-tag. This affinity was used to attach the protein to a Ni-chelating Sepharose FF in the absence of imidazole. The sodium chloride concentration did not affect this interaction and thus, the Hsp104 pool from the Affi-Gel blue could be directly applied to a Ni-column. Since low concentrations of imidazole (30 mM) result in the elution of Hsp104 no significant purification effect was achieved. Remarkably the protein reached up to 25 mg/mL upon elution with Ni-buffer B. Size exclusion chromatography using a Superdex 200 column was used as final purification step. The running buffer was similar to the protein storage buffer. After fractionation and analysis by SDS-PAGE the protein was concentrated by a Centriprep micro concentrator to 10 mg/mL and was shock frozen in liquid nitrogen. The protein was then stored at -80°C.

3.4.2 Labeling of Cpr6

An iodoacetamide derivate of the fluorescent dye lucifer yellow was used for the labeling of Cpr6. The reaction was started by the addition of 2.4 mM lucifer yellow and 5 mM TCEP to a solution of 30 µM Cpr6 in 20 mM HEPES/KOH pH 7.0 at 25°C. After 1 h the reaction was stopped by the addition of an excess of β-mercaptoethanol. The protein was purified *via* a Sephadex G25 column equilibrated in 50 mM Tris/HCl, pH 8.0. It was concentrated by a Centriprep micro concentrator and shock frozen in liquid nitrogen. The degree of labeling was 0.7, as determined by the instructions of the manufacturer (Invitrogen, Karlsruhe, Germany).

3.4.3 Bradford assay

The Bradford assay was used to quantify the concentration of the total protein in cell lysates (Bradford, 1976). 900 µL Coomassie Protein Assay Reagent and 100 µL of the pre-diluted lysate sample were mixed in a disposable, semi-micro cuvette (d = 1cm), and incubated for 5 min at 20°C. Then the absorption at a wavelength of 595 nm (A_{595}) was determined by a Cary 100 spectrophotometer. A_{595} was used for the calculation referring to a BSA standard

curve (BSA: $A_{280,\ 0.1\%} = 0.667$). The mean of three independent samples served to calculate the protein concentration of a given cell lysate.

3.4.4 Concentration determination by UV-spectroscopy

Protein concentrations were determined under reducing conditions by absorbance spectroscopy using the Lambert-Beer law (see Eq. 3.1). The extinction coefficients ε_{276} = 31,900 $M^{-1}cm^{-1}$ for Hsp104, ε_{280} = 20,860 $M^{-1}cm^{-1}$ for Cpr6, and ε_{280} = 57,300 $M^{-1}cm^{-1}$ for Hsp82 were calculated based on the particular amino acid composition using the ProtParamTool of ExPasy (http://us.expasy.org, based on Gill and von Hippel, 1989). Molar concentrations refer to the monomeric species unless indicated otherwise.

$$c = \frac{A}{\varepsilon \cdot d}$$

Eq. 3.1: Lambert-Beer's law
c: protein concentration in molar, M
A: absorption at a given wavelength (280 nm)
d: path length of the cuvette in cm
ε: molar extinction coefficient of the sample at a given wavelength in $M^{-1}cm^{-1}$

3.4.5 Gel electrophoresis of proteins

The discontinuous sodium dodecyl sulfate polyacrylamide gel electrophoresis (SDS-PAGE) was performed to analyze protein samples according to Laemmli (Laemmli, 1970). Protein samples were mixed with Laemmli sample buffer and heated for 5 min at 95°C. The denatured samples were applied on mini SDS-gels and separated according to their size by an electric current of 25 mA per gel using a Mighty Small electrophoresis unit with 1 x SDS running buffer. The gel electrophoresis was carried out for 1 h or until the dye front reached the bottom of the gel. To estimate the size of proteins a molecular weight standard was used. The gels were stained by Coomassie staining (see 3.4.6) or by silver staining (see 3.4.7).

Following supplements were used to cast two mini-SDS gels:

Separating gel (10%)	2.5 mL 40% (w/v) acrylamide-bisacrylamide (38:2)
	2.5 mL 4 x separating gel buffer
	5 mL ddH_2O
	120 µL 10% (w/v) APS
	10 µL TEMED

Stacking gel (3%): 2.5 mL 2 x stacking gel buffer
0.375 mL 40% (w/v) acrylamide-bisacrylamide (37:1)
2.125 mL H_2O
60 µL 10% (w/v) APS
6 µL TEMED

3.4.6 Coomassie staining

The Coomassie staining procedure is a modified Fairbanks protocol (Fairbanks *et al*., 1971). The detection limit of Coomassie staining is typically 50 ng of protein.
The gel was removed from the glass plates after the electrophoresis was completed and transferred to a plastic box for staining. The gel was completely covered with Coomassie staining solution, heated in a microwave until boiling and incubated for 5 min while shaking on a rocking platform shaker. Then the gel was transferred to Coomassie destaining solution and, again, heated in the microwave until boiling. A piece of paper towel was added to remove the dye from solution. The procedure was completed by incubation in Coomassie destaining solution on the platform shaker for 1 h.

3.4.7 Silver staining

Silver staining was carried out according to a protocol of Heukeshoven (Heukeshoven and Dernick, 1988). It is a much more sensitive method than Coomassie staining to detect proteins. Typically less than 10 ng of protein can be detected with silver staining. All steps of the procedure were performed at RT on a rocking platform shaker. The SDS-gel was incubated in the silver fix solution I for 20 min. Then it was transferred to silver fix solution II and incubated over night or for a minimum of 30 min. After that the gel was washed three times with ddH_2O for 10 min and treated with silver staining solution for 30 min. Subsequently the gel was washed with ddH_2O and developed in silver developing solution containing Na_2CO_3. Upon the appearance of bands, the buffer was exchanged with silver stop solution.

3.4.8 Immunological methods

3.4.8.1 Western blotting

Protein blotting was performed using the Biometra Fastblot system. The SDS-PAGE gel was placed between two horizontal plate electrodes. The blot was assembled by placing three pieces of Whatman 3MM paper soaked in WB transfer buffer onto the bottom plate electrode

(anode). A piece of PVDF membrane, previously soaked for 30 min in WB transfer buffer was then placed on top of the paper and the protein gel was placed on the membrane. Three more pieces of pre-soaked Whatman paper were placed on top and pressed down firmly to remove air bubbles. The top plate electrode (cathode) was then arranged on top and the protein transfer was carried out by applying 72 mA per mini gel for 1 h. For estimating the size of blotted proteins the Roti-Mark prestained molecular weight standard was used. The visible bands of the standard were marked by a pen after blotting. Subsequently the membrane was blocked with 5% (w/v) milk powder in PBS-T at RT for 1 h. Then it was incubated with PBS-T with 1% milk powder containing the primary antibody (diluted 1:5,000) at RT under agitation for 1 h. After washing 3 times for 10 min with PBS-T and incubating for 1 h with the secondary anti-rabbit antibody in PBS-T (diluted 1:5,000), the membrane was washed 3 times for 10 min with PBS-T. The ECL Plus western blotting detection system was used to visualize the secondary antibody, which was a POD-anti-rabbit-IgG conjugate. Protocols provided by the manufacturer (GE Healthcare, München, Germany) were followed. The ECL-treated membrane was used for the exposure of a X-OMAT X-Ray film, which was then developed by an Optimax TR MS film developing unit.

3.4.8.2 Co-immunoprecipitation

A 1 L culture of yeast grown in an appropriate medium to an A_{600} of ~0.8 was harvested, washed and cracked in IP-buffer with 1 mM PMSF and protease inhibitor cocktail HP using a french press at 2.4 kbar. The cell extracts were centrifuged at 20,000 rpm for 20 min to remove debris. The protein concentration was determined using the Bradford assay. 5 mg of each extract were incubated at 4°C with anti-Cpr6 rabbit antibody coupled to Protein A agarose beads. Antiserum from the first day of immunization was used as a negative control. Following 2 h of incubation, the beads were washed once with IP-buffer and three times with IP2-buffer. Finally, the beads were suspended in 100 µL of Laemmli sample buffer and denatured at 95°C for 5 min. The supernatant containing released polypeptides was additionally incubated with 0.01% β-mercaptoethanol. The protein samples were analyzed by a 10% SDS-PAGE. The separated polypeptides were transferred to a PVDF membrane, and analyzed by western blotting using anti-Hsp104 antibodies.

3.5 Spectroscopic methods

3.5.1 Fluorescence spectroscopy

3.5.1.1 Intrinsic fluorescence of proteins

Delocalized π-electrons of the aromatic amino acids tryptophan, tyrosine and phenylalanine can be excited by light of a distinct wavelength and emit electromagnetic energy while returning to their ground state. This reemitted light has an increased wavelength due to energy loss by the molecule prior to emission. This phenomenon is called Stokes fluorescence change. Tryptophan shows the strongest fluorescence signal since it has the largest quantum yield and is additionally excited by the emitted light of phenylalanine and tyrosine (Cantor and Schimmel, 1980; Schmid, 1989). Thereby, the relative ratio of fluorescence emitted by tryptophan, tyrosine and phenylalanine is found to be 1100:200:8 (Schmid, 1989).
Wild-type Hsp104 contains no tryptophan. This lack of a strong chromophore can be used to estimate the purity of Hsp104, if it is assumed that contaminations contain tryptophan. However, standard fluorescence experiments such as ligand interaction studies are useless for Hsp104, since the intrinsic fluorescence signal is too weak to allow the meaningful detection of changes. Therefore, the fluorescent dye was used to detect structural changes within Hsp104, see below.

3.5.1.2 ANS Fluorescence

The fluorescent dye 8-anilino-1-naphthalene sulfonic acid (ANS) binds to hydrophobic surfaces of proteins and can be utilized to show conformational changes of a protein (Das and Surewicz, 1995). Spectra of 25 µM ANS with and without the addition of 5 µM Hsp104 were recorded at 25°C at an excitation wavelength of 380 nm. The signal difference between ANS-Hsp104 and ANS-Hsp104·ADP was used for titrations. A solution of 50 µM ANS and 1 µM Hsp104 in standard assay buffer was titrated with ADP unless indicated otherwise. The emission signal was dilution-corrected and it was plotted against the ligand concentration. The affinity of Hsp104-ligand interactions can be described by the dissociation constant K_D given in Eq. 3.2. The non-linear titration plot of the fluorescence data was fitted using Eq. 3.3 in order to calculate K_D.

$$E + L \underset{k_{off}}{\overset{k_{on}}{\rightleftharpoons}} EL \quad \text{(i)} \qquad K_D = \frac{k_{off}}{k_{on}} \quad \text{(ii)} \qquad K_D = \frac{[E][L]}{[EL]} \quad \text{(iii)}$$

Eq. 3.2: Definition of the dissociation constant K_D
K_D dissociation constant, refers to the ligand concentration at which 50% of the enzyme is present as enzyme-ligand complex [EL]
[L] concentration of the free ligand
[E] concentration of the free enzyme
[EL] concentration of the EL complex

$$y = \frac{A \cdot [L]}{[L] + K_D} + B$$

Eq. 3.3: Calculation of the dissociation constant K_D from a ligand titration to a single weak site

K_D dissociation constant, K_D was termed $K_{½}$ in the case of titrations that are based on changes of enzymatic activity upon ligand binding and that are not based on a direct physical binding signal
y: fluorescence signal or enzyme turn-over at a given ligand concentration
[L] ligand concentration (refers to the free ligand, in the case of a strong binding site this number has to be corrected dependent on the concentration of binding sites)
A amplitude of the signal change
B starting point of the non-linear regression if it does not start in the origin

3.5.1.3 Fluorescence anisotropy

Complex formation between Hsp104 and its ligands was analyzed using fluorescence anisotropy. Data were recorded at 25°C in a thermostated Fluoromax-3 fluorescence spectrometer equipped with autopolarizers. Monochromators were set to λ_{425} (excitation) and λ_{528} (emission) for lucifer yellow-labeled ligands, or to λ_{494} (excitation) and λ_{515} (emission) in the case of fluorescein-labeled ligands, respectively. Once the anisotropy signal had reached the steady-state level, binding or release of the ligand was monitored by a change in anisotropy. For control, it was experimentally verified that the unpolarized fluorescence intensity at the emission wavelength does not change upon complex formation. Titration data were fitted to a non-linear least squares fit (see Eq. 3.4).

$$r = r_f + \frac{\Delta r \cdot [L]}{[L] + K_D}$$

Eq. 3.4: Calculation of the dissociation constant K_D from a ligand titration using fluorescence anisotropy

r anisotropy signal
r_f anisotropy signal of the free labeled protein in the absence of the ligand
Δr change anisotropy upon binding of the ligand
[L] ligand concentration
K_D dissociation constant

3.5.2 Circular dichroism spectroscopy

Circular dichroism (CD) spectroscopy is a sensitive method to determine the secondary structure of proteins. It is a form of light absorption spectroscopy that measures the difference in absorbance of right and left circularly polarized light. The basis of this effect is the coupling of chromophores in an unsymmetrical conformation. The differential absorption of radiation polarized in two directions as function of frequency is called dichroism. When applied to planar polarized light, this is termed linear dichroism; for circularly polarized light, circular dichroism. It was demonstrated that far-UV CD spectra between 170 and 250 nm can be used to analyze the different secondary structures of proteins such as α-helices, β-sheets,

random coil, and others. α-helices show two strong minima at 208 nm and 222 nm, whereas β-sheets lead to a less pronounced minimum at 218 nm. In the near-UV region of 250-320 nM, chromophores of certain aromatic amino acids contribute to the signal. This signal depends on the specific environment of the aromatic amino acids and reflects more the global, three-dimensional properties of the protein. Far-UV CD spectra were recorded at 25°C in a Jasco J-715 spectropolarimeter at protein concentrations of 1 µM in degased 20 mM sodium phosphate buffer, pH 7.5, using thermostated 0.1 cm cuvettes. Spectra of each sample were accumulated up to 10 times to improve the signal-to-noise ratio. All spectra were corrected for the buffer baseline. The molar ellipticity was calculated by Eq. 3.5.

$$[\Theta]_{MW} = \frac{\Theta \cdot 100 \cdot MRW}{c \cdot d \cdot N_A}$$

Eq. 3.5: Calculation of the molar ellipticity
$[\Theta]_{MW}$ molar ellipticity referring to the molecular weight of the protein (degree cm^2 $dmol^{-1}$)
Θ: measured ellipticity (degree)
MRW: mean residue weight of the protein (g mol^{-1})
d: path length (cm)
c: protein concentration (mg/mL)
N_A: number of amino acids of the protein

3.6 Isothermal titration calorimetry

Isothermal titration calorimetry (ITC) is a method to acquire information about the interaction of a protein and its ligand by energy consumption or energy production of the binding reaction itself (Pierce *et al*., 1999). The change of heat upon the association of proteins with their ligands can be directly detected by a microcalorimeter. The instrument keeps a constant temperature and automatically compensates changes during a titration. This compensation energy that is applied by the instrument is directly monitored by titration plots that are fitted by the original ITC software. Association constant, binding enthalpy and stochiometry of a protein-ligand interaction can be determined with a single experiment.
Titration experiments were carried out using a VP-ITC microcalorimeter system. Hsp104 or its mutants were titrated at 25°C with nucleotide or GdmCl, respectively. The protein was dialyzed in Slide-A-Lizer cassettes against standard assay buffer over night prior to the experiments. Protein and ligands were additionally degased and kept at a constant temperature of 25°C. The injection volume was always 5 µL. Data analysis of the titration plots was performed with the ITC-Origin software supplied by the manufacturer (Microcal Inc. and OriginLab, Northampton) assuming a single binding site for all investigated ligands.

3.7 Static light scattering

Static light scattering (SLS) is a non-invasive equilibrium method to determine the average molecular weight of proteins or protein complexes in solution. A laser beam with a wavelength of 685 nm passes through a sample and is scattered by protein particles. This diffraction is dependent on the molecular weight of the particles and is detected at different angles with respect to the incoming laser beam (multiangle light scattering). Small detection angles give a signal that is directly proportional to the molecular weight of the protein particles but with a relatively high signal to noise ratio. Further detection angles are needed to calculate the angle dependency of the scattered light in order to determine the average molecular weight of a sample. Nevertheless, the raw data provide information about the oligomerization state of a sample when compared to a reference.
SLS experiments were performed using a miniDAWN Tristar light scattering detector equipped with a flow cell. The system was operated by an HPLC pump. SLS batch measurements of Hsp104 were carried out in standard assay buffer at 20°C. Batch samples containing 0.5-2.5 µM Hsp104, 5 mM GdmCl, and 5 mM ADP in various combinations were injected.

3.8 Analytical ultracentrifugation

Analytical ultracentrifugation (AUC) is a powerful tool to characterize the solution-state behavior of macromolecules. Theodor Svedberg, who invented the analytical ultracentrifuge in 1923, was awarded the Nobel prize in chemistry in 1926 for his research on disperse solutions using the ultracentrifuge. Three decades later the instrument served in studying the assembly of bacterial 70S ribosomes, which indeed have been specified by their sedimentation coefficient (Schachman *et al*., 1952; Tissiers and Watson, 1958). Today, the method is mainly used to determine the molecular weight and the sedimentation coefficient of proteins. By choosing the appropriate experimental setup it is also possible that one can assess the sample purity, and investigate assembly or disassembly mechanisms of macromolecular complexes.
The analytical ultracentrifuge Optima XL-I, which was used in this study, can generate an acceleration of 250,000 x g. This corresponds to 60,000 rpm and is needed to sediment a broad size range of biomolecules in solution. The sample solution was placed into aluminum cells, which was placed in a titanium rotor Ti-60. The sample cell was assembled by two quartz windows and a double sector centerpiece that contains buffer as reference and protein solution in each sector. The centrifuge was equipped with a thermostated vacuum chamber and two optical detection systems allowing that the sample was visualized in real time during sedimentation. The variable absorbance detector was typically used to measure protein concentrations at λ_{280} but it was also used to selectively monitor the concentration of a

distinct particle species containing a chromophore. The interference optics measured the sample concentration based on differences in the refractive index between sample and reference. Interference optics is a very sensitive and rapid detection system, which is most beneficial when samples contain strongly absorbing buffer components and cannot be analyzed by UV absorption.

3.8.1 Sedimentation velocity experiments

Sedimentation velocity experiments are used to determine the sedimentation coefficient, *s*, and the diffusion coefficient, *D*, of a particle in solution. An initially uniform sample is placed in the cell and centrifuged at high speed. The large centrifugal force field leads to a movement of solute molecules towards the bottom of the centrifuge cell. Thereby, a sharp boundary of particles becomes visible. The movement of this boundary is directly proportional to the sedimentation coefficient *s* and can be determined by scanning the concentration profile in defined intervals. The velocity of sedimentation is dependent on the sedimenting force F_S, which is in equilibrium with the buoyant force F_b and the frictional force F_f ($F_s + F_b + F_f = 0$, see below). The rate of sedimentation, *v*, is described by the Svedberg equation, Eq. 3.6 below.

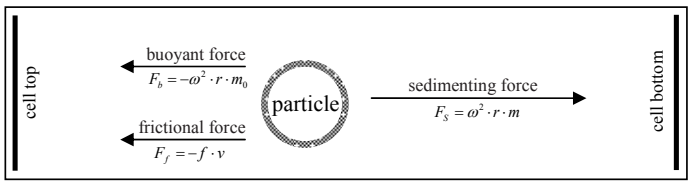

$$s = \frac{v}{r \cdot \omega^2} = \frac{M \cdot (1 - \bar{v} \cdot \rho)}{N \cdot f}$$

Eq. 3.6: Svedberg equation to calculate the sedimentation coefficient

s: sedimentation coefficient, given in Svedberg units, S = 10^{-13} sec; it is dependent on the molecular weight *M*, the density of the particle and the particle shape. Further it is dependent on the density of the solvent, the pressure, and the temperature. Therefore, sedimentation coefficients generally refer to defined conditions such as 20°C in water, which is $s_{20,W}$.

v: velocity of the molecule

$r\omega^2$: strength of the centrifugal field, ω is the angular velocity in radians/sec and r is the radial position of the particle boundary

M: molecular weight of the particle, given in g/mol

N: Avogadro's number

$\bar{v}$: partial specific volume of the solute

ρ: density of the solvent, estimated value of 1.01g/mL for the used buffer

f: frictional coefficient, which is directly related to particle shape and size, $f = RnT/D$

m: mass of a single particle, given in grams

m_o: mass of solvent displaced by the particle, $m_o = v\rho m$

Sedimentation velocity experiments of Hsp104 were performed at a rotation speed of 50,000, 55,000, or 60,000 rpm respectively. Measurements were carried out in standard assay buffer at 25°C or 30°C, respectively. In addition, the samples contained nucleotides, GdmCl or Cpr6. The distance of the sedimentation boundary from the center of the rotor, *r*, was determined for every scan, and the sedimentation coefficient *s* was calculated using Eq. 3.7 by plotting the natural logarithm of the radial position of the boundary midpoint versus time. The slope of this plot is proportional to $s \cdot \omega^2$, in which *s* represents an apparent average sedimentation coefficient.

$$\ln \frac{r}{r_0} = s \cdot \omega^2 \cdot (t - t_0)$$

Eq. 3.7: Equation to calculate the sedimentation coefficient
r: distance of the sedimentation boundary from the center of the rotor
r_0: position of the boundary at the start of the experiment, t_0
t: time of the scan
t_0: scanning start time
ω: angular velocity

Alternatively to Eq. 3.7, sedimentation coefficients were obtained by the analysis of the boundaries using the method of van Holde and Weischet (Holde and Weischet, 1978) applying the ultrascan software (B. Demeler, University of Texas Health Science Center, San Antonio, USA).

3.8.2 Sedimentation equilibrium experiments

A sedimentation equilibrium experiment is the preferred method to verify the molecular weight of macromolecules. In sedimentation equilibrium runs, a small volume of a sample solution is centrifuged at a low rotation speed for 3 to 4 days until an equilibrium state was approached. Under these equilibrium conditions the particles are distributed according to an exponential concentration gradient, which is generated when sedimentation is balanced by diffusion, see Fig. 3.1 below. The gradient is proportional to the molecular weight of the particle but independent of its shape and hydrodynamic radius (Laue and Stafford, 1999).
For a single component system, the concentration distribution is an exponential function of the buoyant mass of the particle, $M(1 - \bar{v}\rho)$, as described by Eq. 3.8. The simplest approach is to plot ln c versus r^2. According to Eq. 3.8, the slope of this line is directly proportional to M.
Equilibrium sedimentation runs were performed in order to determine the molecular weight of Hsp104 in presence of ATPγS at 20°C in standard assay buffer including a protease inhibitor. The absorbance profile in the sample cell after 70 to 85 h at 3,700 rpm was used to

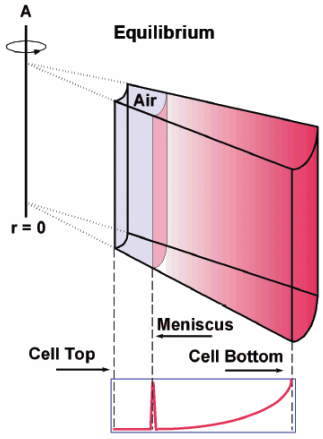

Fig. 3.1: Particle distribution in a sedimentation equilibrium.

$$c = c_0 \cdot e^{\frac{M \cdot \omega^2 \cdot (1-\bar{v}\rho)}{2 \cdot R \cdot T} \cdot (r^2 - r_0^2)}$$

Eq. 3.8: Equation to describe the sedimentation equilibrium for the calculation of the molecular weight

c:	sample concentration at radial position r
c_0:	sample concentration at the start of the experiment
r_0:	reference radial distance at the start of the experiment
R:	gas constant
T:	absolute temperature
ω:	angular velocity, given in radians/sec
M:	molecular weight of the particle, given in g/mol
v:	partial specific volume of the solute, 0.73 mL/g
ρ:	density of the solvent, 1.01g/mL

calculate the molecular weight using a radial square fit by the ultrascan software (B. Demeler, University of Texas Health Science Center, San Antonio, USA). For evaluation of the data, a buffer density of 1.0074 g/mL and a partial specific volume of 0.74 mL/g based on the amino acid composition of $Hsp104_{WT}$ were assumed.

3.9 *In vitro* activity assays

3.9.1 ATPase assay

ATP hydrolysis by Hsp104 was measured using a coupled enzymatic assay in combination with an ATP regenerating system (Norby, 1988). The ATP hydrolyzed by Hsp104 (i) is regenerated instantly by pyruvate kinase and PEP, resulting in the formation of pyruvate (ii). In a third step, pyruvate is reduced to lactate by lactate dehydrogenase and $NADH/H^+$ (iii).

$ATP + H_2O$	$\rightarrow$	$P_i + ADP$	(i)
$ADP + PEP$	$\rightarrow$	$ATP + pyruvate$	(ii)
$pyruvate + NADH/H^+$	$\rightarrow$	$lactate + NAD^+$	(iii)
$PEP + NADH/H^+$	$\rightarrow$	$lactate + NAD^+ + P_i$	

reactions catalyzed by:
(i) Hsp104
(ii) pyruvate kinase
(iii) lactate dehydrogenase

The progress of the lactate dehydrogenase reaction (iii) can be monitored spectroscopically by the decrease in absorbance at λ_{340} caused by NADH/H^+ consumption. The slope obtained by plotting NADH/H^+ concentration versus time is equivalent to the speed of ATP hydrolysis by Hsp104. Assays were carried out in thermostated 120 µL cuvettes (d = 1 cm) at 30°C using a Cary 100 spectrophotometer at λ_{340}. They were performed in standard assay buffer containing 2 mM PEP, 0.2 mM NADH, 2 U/mL pyruvate kinase, 10 U/mL lactate dehydrogenase, 5 mM ATP, and 0.5 µM Hsp104, unless indicated otherwise.

The rate of ATP hydrolysis, *v*, was calculated from Eq. 3.9. It refers to a given substrate concentration and a fixed enzyme concentration. To simplify the comparison of rates obtained for different enzyme concentrations, the apparent velocity of hydrolysis, Eq. 3.10, was always used to quantify the ATP turn-over, which is given in ATP molecules per minute and per Hsp104 molecule (min^{-1}). For each data point, three independent measurements were averaged. To evaluate the dependency of ATP hydrolysis on ATP concentration, values of *v* were fitted to the model of Michaelis-Menten in Eq. 3.11 or to the equation of Hill in Eq. 3.12 for cooperative catalysis (Segel, 1993).

$$v = \frac{1}{\varepsilon_{\mathrm{NADH}} \cdot d} \cdot \frac{dA}{dt}$$

Eq. 3.9: Calculation of the ATPase reaction slope based on NADH absorbance

v: rate of catalysis at a given enzyme and substrate concentration $v = dc/dt$, in min^{-1}
$\varepsilon_{\mathrm{NADH}}$ molar absorbance coefficient for NADH, $\varepsilon_{340} = 6{,}200\ M^{-1}cm^{-1}$
d: path length (1 cm)
dA/dt decrease in NADH absorbance at λ_{340}, given in min^{-1}

$$v_{\mathrm{app}} = \frac{v}{[\mathrm{E}]_0}$$

Eq. 3.10: Calculation of the apparent velocity of ATP hydrolysis

$[E]_{0:}$ total enzyme concentration
v_{app} apparent velocity of hydrolysis = turn-over in ATP/min per Hsp104 molecule

$$v = k_{\mathrm{cat}} \cdot [\mathrm{E}]_0 \frac{[\mathrm{ATP}]}{[\mathrm{ATP}] + K_{\mathrm{M}}}$$

Eq. 3.11: Michaelis-Menten equation

$k_{\mathrm{cat:}}$ rate constant of turn-over under substrate saturation conditions, given in min^{-1}
[ATP]: substrate concentration, given in mM
$K_{\mathrm{M:}}$ Michaelis constant, given in mM

$$v = k_{\text{cat}} \cdot [\text{E}]_0 \frac{[\text{ATP}]^h}{[\text{ATP}]^h + K_{\text{M}}{}^h}$$

Eq. 3.12: Hill equation for cooperative enzyme catalysis
h: hill constant, number of substrate binding sites per molecule of enzyme, when n = 1, the equation reduces to the Michaelis-Menten model

The ATPase assay was also used to determine the affinity of specific ligands affecting the ATP hydrolysis by Hsp104. The change in the turn-over of Hsp104 was plotted against the ligand concentration and fitted by the Eq. 3.3 in order to obtain $K_{½}$.

3.9.2 Refolding of denatured luciferase

Firefly luciferase (7 µm) was denatured for 30 min at RT in a luciferase denaturing buffer. Refolding was initiated by a 125-fold dilution in luciferase refolding buffer. As chaperones, 0.5 µM Cpr6, 0.5 µM Hsp104, 1 µM hHsp70, and 1 µM Hsp40 (Ydj1) were present, unless indicated otherwise. Refolding kinetics were recorded at 25°C for 120 min using a luminometer.

3.9.3 Refolding of denatured dehydrofolate reductase

Spontaneous refolding of 1 µM unfolded mouse dehydrofolate reductase (DHFR) was determined directly by dilution (from 500 µM in 8 M urea, 50 mM Tris/HCl, pH 8.0) into DHFR assay buffer at 25°C. The refolding of DHFR was detected by its gain of activity. DHFR catalyzes the NADPH-dependent reduction of DHF to THF. The activity of DHFR was monitored spectroscopically by the decrease in absorbance at λ_{340} using a Cary 100 spectrophotometer. The turn-over of DHFR was calculated – in accordance with Eq. 3.9 and 3.10 – from the slope dA_{340}/dt using the molar absorbance coefficient for NADPH of ε_{340} = 6,200 $M^{-1}cm^{-1}$. This assay was used to analyze the direct influence of Cpr6 on the spontaneous refolding of DHFR.
For chaperone-mediated renaturation unfolded DHFR was diluted in DHFR refolding buffer containing 1 µM Cpr6, 0.5 µM Hsp104, 1 µM Hsp70, and 1 µM Hsp40, unless indicated otherwise. The activity of DHFR in the chaperone-mediated refolding samples was determined exactly as for the samples without added chaperones to ensure an optimal comparability.

4. RESULTS

4.1 Sequence analysis and identification of the domains of Hsp104

Hsp104 is described as a 102 kDa protein consisting of 908 residues. It is known from electron microscopy and chemical crosslinking studies that it exists as hexameric arrangement (Parsell *et al.*, 1994a). Hsp104 binds to nucleotides and acts as an ATPase (Parsell *et al.*, 1991). The identification of its Walker motifs – which can be easily recognized in its sequence and which are found in many ATPases (Walker *et al.*, 1982) – allowed this functional classification. Hsp104 was also assigned to be a member of the Clp/Hsp100 protein family by means of sequence homology analysis (Walker *et al.*, 1982; Schirmer *et al.*, 1996). Later, Neuwald subjected Hsp104 to a multiple sequence alignment that allowed its further classification as an AAA^+ ATPase (Neuwald *et al.*, 1999). This alignment gave rise to the identification of further functional patterns such as the sensor motifs. However, no three dimensional structure of Hsp104 is yet available and – consequently – classical sequence analysis must still serve as the primary tool to initiate functional studies of Hsp104. Starting out from further sequence alignments and a hydrophobicity plot it was possible to obtain a deeper understanding of the classification of Hsp104, to localize the nucleotide binding domains (NBDs) including their boundaries, and to identify conserved residues of functional relevance, as described below.

The Hsp104 sequence was aligned with members of the Hsp100/ClpB family (see Appendix A.1). A phylogenetic representative mean of this family was chosen to have a consensus sequence which was valid for the whole protein family. The phylogram and the similarity table obtained by this alignment are shown in Fig. 4.1. The phylogram serves to assess the phylogenetic relationship of Hsp100/Clp proteins. Hsp104 is closely related to other fungal Hsp100 proteins whereas the mitochondrial orthologous Hsp78 from yeast gives rise to an individual family subset more related to eukaryotic Hsp100 proteins than to prokaryotic ClpB proteins. This implies that the mitochondrial Hsp78 proteins, which are found in fungi, might be derived from an eukaryotic nuclear ancestor.

The similarity table indicates the degree of conservation of this protein family. It shows two highly conserved blocks representing the nucleotide binding domains. Functional patterns such as the Walker A motif exhibit the highest conservation and are identical among this family (score value 1 in similarity table). These patterns build up the NBDs, which are highly conserved in Clp proteins. In contrast, the N-terminal domain, the middle domain and the C-terminus exhibit only low similarity.

A hydrophobicity plot of Hsp104 obtained by the method of Kyte & Doolittle was prepared (Kyte and Doolittle, 1982, Fig. 4.2). Hydrophobicity plots indicate hydrophilic patches, which might represent exposed motifs or linker regions between domains. A strong minimum is found from position 400 to 500 corresponding to the middle domain of Hsp104. It is highly

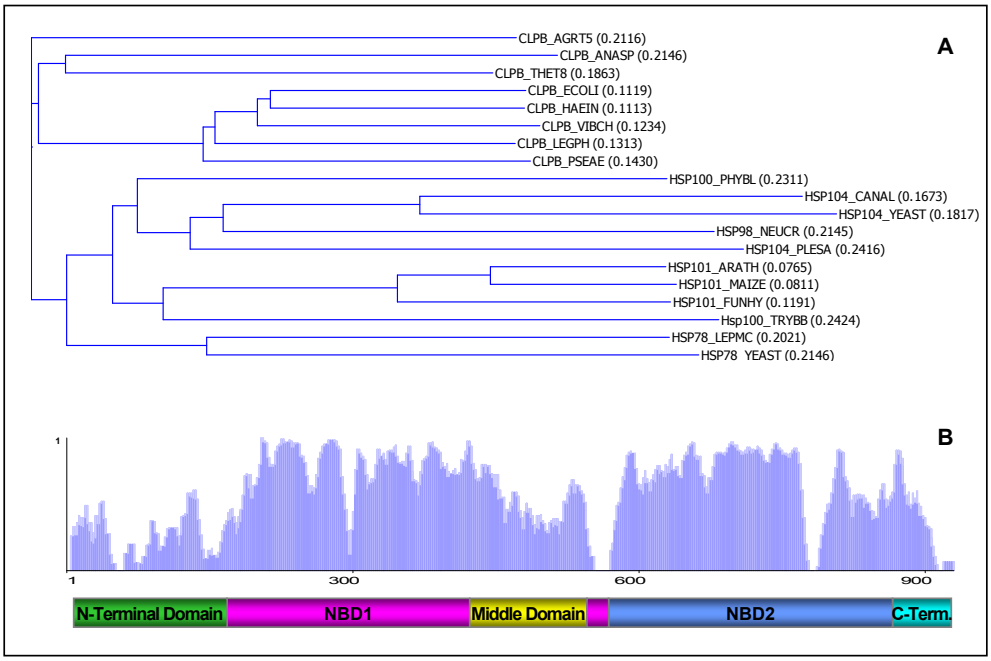

Fig. 4.1: Hsp104 is a member of the highly conserved family of Hsp100/ClpB proteins. Phylogenetic relationship and sequence conservation of members of the Hsp100/ClpB protein family. (A) Phylogram and (B) similarity table. Data are based on the multiple sequence alignment using the computational algorithms of VectorNTI, see Appendix A.1 for alignment and for species description. The plot scale corresponds to the degree of sequence identity. A similarity number of 1 indicates identical residues. The domains are assigned by a colored bar below the similarity plot.

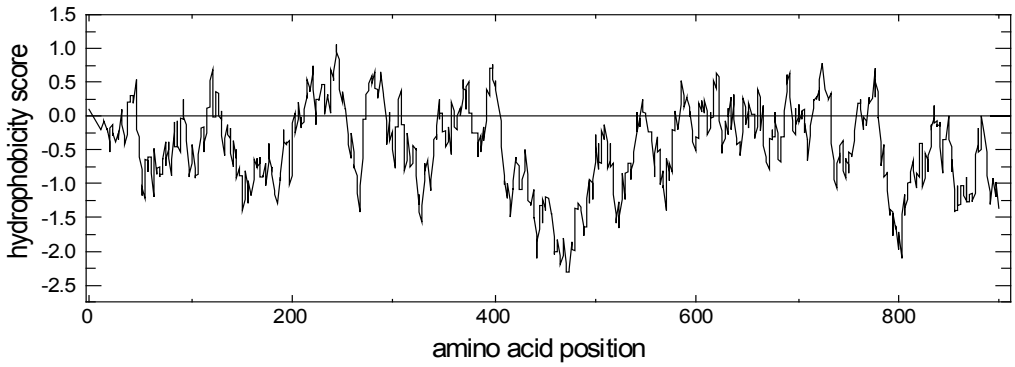

Fig. 4.2: Hydrophobicity plot of Hsp104 demonstrates its domain boundaries. The calculation of the hydrophobicity was carried out using the program ProtScale (Expasy) by the method of Kyte & Doolittle (Kyte *et al.*, 1982). The window size was 7 residues and the scale refers to the amino acid sequence of $Hsp104_{WT}$. A hydrophobicity number of -3 corresponds to a highly hydrophilic region while a +3 corresponds to a highly hydrophobic region.

charged, exclusive to the Hsp100/ClpB family and seems to represents an insertion between the two NBDs. By comparison to ClpA, which is lacking the middle domain, it becomes obvious that the middle domain insertion constitutes an interruption at the very end of the NBD1. The missing amino acids from NBD1 are found in the beginning of NBD2 as it is indicated by the colored bar below the similarity plot. Thus, the middle domain can be considered as a highly charged extension of the first NBD. Furthermore, it is important to note that the very end of the C-terminus of Hsp104 is unusually hydrophilic and thereby might be solvent exposed.

The combination of the information gained from the hydrophobicity plot and from the sequence alignment allows the prediction of the domains of Hsp104 and their boundaries (see Tab. 4.1). The sequence motifs are identified by using the analogy to the crystal structures of ClpA (Guo *et al.*, 2002) and ClpB (Lee *et al.*, 2003). Tab. 4.1 also shows a list of the point mutations that were produced and analyzed in this study.

Tab. 4.1: Domain organization and functional motifs of Hsp104. Most relevant residues are given in bold letters. Following double point mutants were also produced: K218T/K620T and E285Q/E687Q ($Hsp104_{TRAP}$).

Domain	Motif	Position	Sequence	Point Mutations
N-Terminal Domain		**0-163**		
NBD1		**164-411** **533-557**		
	NBD1 Interface	199-208	VLA**RR**IKSNP	
	NBD1 Walker A	212-219	**G**EP**G**I**GKT**	K218T
	NBD1 Diaphragm	248-264	LAALTAGA**KYKG**DFEER	
	NBD1 Walker B	280-285	**VLFIDEI**	E285Q
	NBD1 Sensor1	312-317	VIGAT**T**	
	NBD1 Arginine Finger	333-335	**RR**F	
	NBD1 Sensor 2	386-394	RRLPDSALD	
Middle Domain		**412-532**		
NBD2		**558-843**		
	NBD2 Walker A	614-621	**G**LS**G**S**GKT**	K620T
	NBD2 Diaphragm	655-665	LLGTTA**GYVG**Y	
	NBD2 Walker B	682-687	**VLLFDEV**	E687Q
	NBD2 Sensor 1	723-728	VIMTS**N**	
	NBD2 Arginine Finger	765-766	**R**I	
	NBD2 Sensor2	822-828	DM**GAR**PL	
C-Terminal Region		**844-908**		893ΔC

4.2 Structural analysis of Hsp104 and its mutants

Mutations might lead to an alteration of the structure of a protein. To demonstrate that the constructed point mutants of Hsp104 have no deficiencies in their folding far-UV CD spectra were recorded. CD spectroscopy is a very sensitive method to monitor changes in the secondary structure of a protein. Fig. 4.3 shows the representative CD spectrum of $Hsp104_{WT}$ and its double point mutant $Hsp104_{TRAP}$ (which is $Hsp104_{E285Q/E687Q}$).

The secondary structure content was predicted by using the computational algorithms of the computer program CDNN (see Tab. 4.2). It can be confirmed that the mutations did not lead to significant structural changes since the spectra of native Hsp104 and its point mutants were indistinguishable. Both spectra showed structured proteins with a high content of α-helices. The CD spectra of Hsp104 were in agreement with the work of Barnett (Barnett *et al.*, 2000) who found that ClpB, the bacterial homologue of Hsp104, has a high content of α-helical structure.

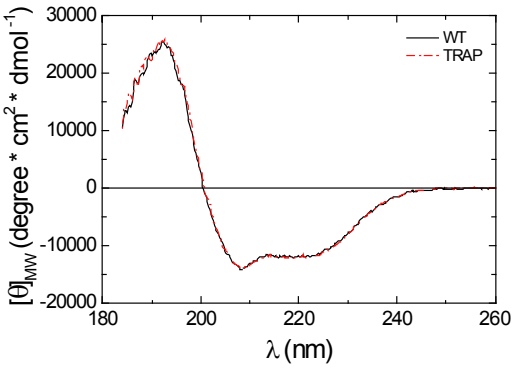

Tab. 4.2: Secondary structure prediction of Hsp104 based on a far-UV CD spectrum. The analysis was carried out by the software CDNN using a wavelength scan from 185 to 260 nm.

Structural Element	$Hsp104_{WT}$ [%]	$Hsp104_{TRAP}$ [%]
α-helix	48,5	48,3
β-sheet	8,4	8,3
β-turn	14,5	14,6
random coil	21,5	21,4
sum	92,9	92,6

Fig. 4.3: Far-UV CD spectra of $Hsp104_{WT}$ and $Hsp104_{TRAP}$ show a high content of α-helices. Spectra were recorded at 25°C using 1 µM Hsp104 in 20 mM sodium phosphate buffer, pH 7.5.

4.3 Analysis of the oligomerization state of Hsp104 and its mutants

Hsp104 was suggested to be a hexameric protein that has a ring-shaped structure as predicted by chemical crosslinking and cryo-electron microscopy studies (Parsell *et al.*, 1994a and Dr. P. Wendler, Birkbeck College London, UK, personal communication). Hsp104 hexamers possess a high content of contact surfaces between the protomers. This can be assumed based on the crystal structures of other Clp proteins (Bochtler *et al.*, 2000; Guo *et al.*, 2002; Lee *et al.*, 2003). Thus, many individual residues from each NBD contribute to the assembly rather than a distinct oligomerization spot. No particular oligomerization domain can be identified and it might be impossible to design a single point mutant that is completely incompetent for oligomerization. However, the assembly is sensitive to nucleotide binding and to the ionic strength (Parsell *et al.*, 1994a; Schirmer *et al.*, 1998). The point mutant K620T lacks

nucleotide binding to NBD2 and exhibits oligomerization defects. This argues for NBD2 to act as a nucleotide-dependent oligomerization domain. On the other hand, this mutant protein is able to overcome its defect at sufficiently high protein concentrations (Schirmer *et al.*, 2001). Hence, oligomerization is not exclusively dependent on nucleotide binding to NBD2. The oligomerization state of Hsp104 is furthermore of a dynamic nature since the protein disassembles under non-equilibrium conditions such as SEC-HPLC (Parsell *et al.*, 1994a; Tkach *et al.*, 2004; Bösl *et al.*, 2005). Seemingly, Hsp104 exists in an equilibrium of monomers and oligomers that can be shifted towards the monomers when the two species are separated by SEC. Hence, non-equilibrium tools might be not appropriate to study the oligomerization state of Hsp104. Therefore, for studying the oligomerization state of Hsp104 and its mutants the following equilibrium methods were selected: (i) static light scattering and (ii) analytical ultracentrifugation.

4.3.1 Analysis of the oligomerization state of Hsp104 by static light scattering

Static light scattering (SLS) was used to monitor changes in molecular weight at monomer concentrations from 0.5 to 2.5 µM. Fig. 4.4 shows the scattering signal change of $Hsp104_{WT}$ upon addition of nucleotides.

The scattering signal increases indicating that a nucleotide-dependent oligomerization takes place. Because the samples contained some particles with high scattering intensity, it was not possible to accurately calculate the apparent molecular weight. Nevertheless, Fig. 4.4 clearly shows that the experimental setup is suited to detect changes in the oligomeric state of Hsp104. Still it is not reasonably possible to estimate the monomer-oligomer distribution based on these data. To show the specific weight-dependent signal further experiments were carried out using a variety of different conditions. The scattering signal is directly proportional to the product of molecular weight and sample concentration. Fig. 4.5 shows the specific concentration-corrected data from light scattering experiments of $Hsp104_{WT}$ and its single point mutant $Hsp104_{K620T}$. The data signal ranges from 0.6 for the monomer to 3.6 for

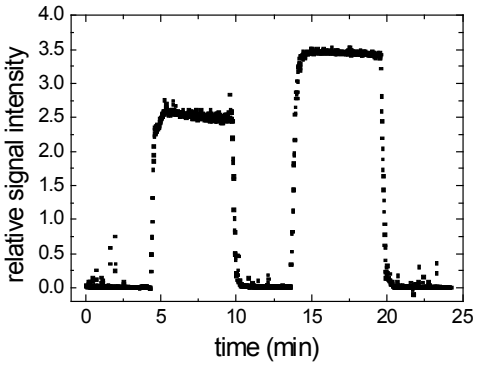

Fig. 4.4: SLS signal increases due to nucleotide induced oligomerization. Samples of 1 µM $Hsp104_{WT}$ w/o ADP (after 5 min) and with addition of 5 mM ADP (after 15 min) were applied at RT in a batch experiment on a MiniDawn light scattering detector equipped with a flow through cell. Filtered and degased standard assay buffer was used for the sample preparation and as a running buffer. An increase in signal intensity reflects an increase in the apparent molecular weight of the protein.

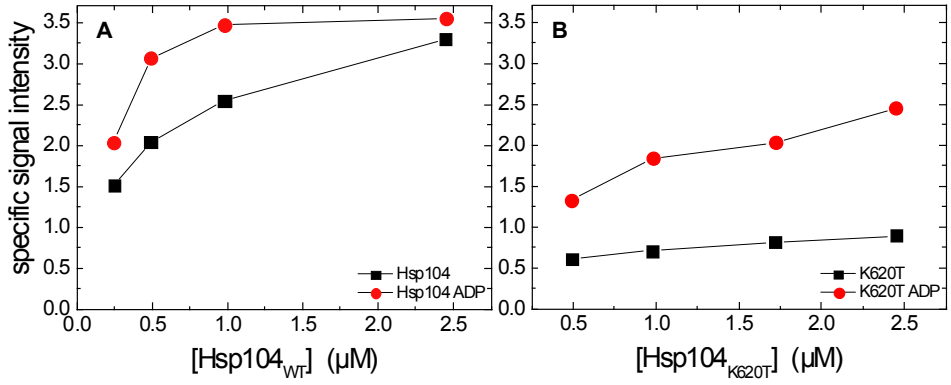

Fig. 4.5: Concentration dependency of Hsp104 oligomerization monitored by SLS. (A) $Hsp104_{WT}$ and (B) $Hsp104_{K620T}$ with and w/o addition of 5 mM ADP in standard assay buffer. The protein samples were applied on a MiniDawn light scattering detector at RT. The shown specific data are obtained by normalizing the raw signal data with respect to their concentration. The standard error was ~15%.

the hexamer, which is showing the consistency of the numbers. The data do not yield a precise molecular weight but rather show an oligomerization trend of Hsp104 that is influenced by the monomer concentration and by the presence of adenine nucleotides. Based on these data it is evident that Hsp104 exists in a dynamic oligomerization equilibrium.

4.3.2 Analysis of the oligomerization state of Hsp104 by analytical ultracentrifugation

Analytical ultracentrifugation served to determine the sedimentation coefficient and the molecular weight of Hsp104 and its mutants. All variants were analyzed by sedimentation velocity experiments to elucidate their oligomeric state. Fig. 4.6 shows a velocity experiment of $Hsp104_{WT}$ as a representative example. The data analysis by the method of van Holde-Weischet yielded a diffusion-corrected sedimentation coefficient, $s_{20,W}$, of 16.5 S in the presence of 2.5 mM ATPγS. Hsp104 generally displays sedimentation coefficients of ~16 S at 5 µM, as shown in Tab. 4.3. This is in good agreement with data from ClpB (Liu *et al.*, 2002). The molecular weight of $Hsp104_{WT}$ was additionally determined by a sedimentation equilibrium experiment yielding 611 kDa (see Appendix A.2), which correlates well with the theoretical mass of 612 kDa. Thus, the sedimentation coefficient of ~16 S refers to hexameric Hsp104.

In contrast to this data, $Hsp104_{K620T}$ without nucleotides sediments much slower with a sedimentation coefficient of 7.5 S (Tab. 4.3). It is assumed that this corresponds to the monomer. Nevertheless, the mutant K620T overcomes its oligomerization defect in the presence of adenine nucleotides under the chosen experimental conditions. The oligomerization trend monitored by static light scattering consequently leads to pure hexameric $Hsp104_{K620T}$ at higher protein concentrations in the presence of nucleotides.

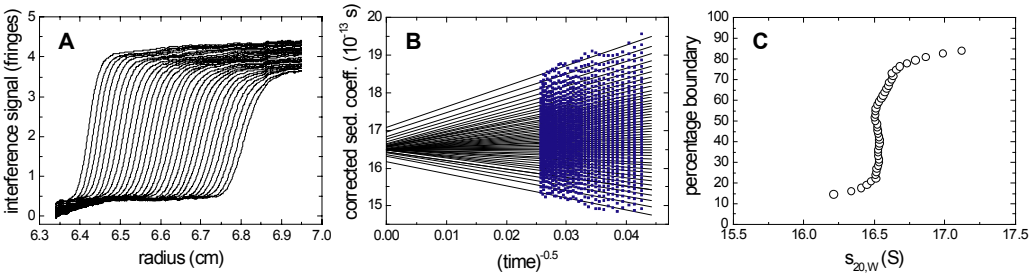

Fig. 4.6: Sedimentation velocity analysis of Hsp104$_{WT}$ shows a pure species with a sedimentation coefficient of 16.5 S. (A) Fringe displacement profiles obtained by iterative scanning throughout the experiment. (B) van Holde-Weischet extrapolation plot of the experiment shown in (A). (C) Integral distribution plot (boundary fraction versus $s_{20,w}$) from the van Holde-Weischet analysis. The sedimentation velocity was measured in an analytical ultracentrifuge at 60,000 rpm at 30°C in standard assay buffer containing 2.5 mM ATPγS and 5 µM Hsp104$_{WT}$. Data analysis was performed using the program ultrascan. The average sedimentation coefficient of Hsp104$_{WT}$/ATPγS is found to be 16.5 S.

Tab. 4.3: Sedimentation coefficients of Hsp104 and its mutants obtained by sedimentation velocity analysis. Sedimentation velocity of Hsp104 (5 µM) was measured in an analytical ultracentrifuge at 30°C in standard assay buffer. Experiments were carried out w/o nucleotide or in the presence of 1 mM ATP, 1 mM ADP, or 2.5 mM ATPγS at 60,000 rpm. Sedimentation coefficients were determined by the method of van Holde-Weischet (Holde *et al.*, 1978).

Nucleotide	Hsp104$_{WT}$	Hsp104$_{K218T}$	Hsp104$_{K620T}$	Hsp104$_{TRAP}$
ATP	n. d	n. d.	n. d.	16.3 S
ATPγS	16.5 S	15.9 S	15.5 S	16.0 S
ADP	15.5 S	16.5 S	16.0 S	16.2 S
w/o	16.1 S	16.2 S	7.5 S	15.8 S

4.4 The ATPase function of Hsp104 is tightly regulated

4.4.1 Comparison of the ATP turn-over by Hsp104 to similar molecular chaperones

A regenerative spectroscopic assay system was used to study the ATPase activity of Hsp104. In this ATPase assay, the ADP produced by the hydrolysis reaction of Hsp104 is subsequently regenerated to ATP using a PEP-dependent enzyme system (Norby, 1988, see Materials and Methods). Its advantages are that ATP has a constant concentration during the assay and that ADP is not accumulated. This setup avoids product inhibition of Hsp104 by ADP (Hattendorf *et al.*, 2002b) and allows stable physiological conditions under which ATP also shows a constant concentration level. At an ATP concentration of 5 mM – which is similar to its cytosolic concentration in yeast (Larsson *et al.*, 2000) – Hsp104 displays a turn-over number of ~38 ATP/min. In comparison to this, similar eukaryotic ATP-hydrolyzing molecular chaperones exhibit a much lower ATP turn-over (see Tab. 4.4).

Tab. 4.4: ATP turn-over of eukaryotic heat shock proteins. Turn-over numbers refer to monomeric protein unless indicated otherwise. Data were measured at ATP saturation except for Hsp104, which shows a $K_{M\ (ATP)}$ much higher than the physiological concentration of 5 mM, see also Fig. 4.11. In this table, 1 µM $Hsp104_{WT}$ was used to determine the turn-over in standard assay buffer at 30°C.

Chaperone Class	Protein	ATP/min	Comment	Reference
Hsp60	bovine CCT	2.0	refers to oligomeric CCT at 30°C, 1 mM ATP, radioactive assay (Kornberg *et al.*, 1978)	(Meyer *et al.*, 2003)
Hsp70	yeast Ssa1	0.04	refers to 37°C, 5 mM ATP, radioactive assay (Kornberg *et al.*, 1978)	(Wegele *et al.*, 2003)
Hsp90	yeast Hsp82	1.1	refers to 37°C, 1 mM ATP, regenerative ATPase assay (Norby, 1988)	(Richter *et al.*, 2006b)
Hsp100	yeast Hsp104	38.0	refers to 30°C, 5 mM ATP, regenerative ATPase assay (Norby, 1988)	this study

This remarkable difference in the ATPase activity might reflect differences in the function of the shown molecular chaperones. In the case of Hsp60, Hsp70, and Hsp90 the nucleotide binding and hydrolysis serves to induce conformational changes during their substrate cycle. These chaperones bind to their polypeptide substrate and act as a safeguard during its folding. Cycles of ATP hydrolysis are coupled to substrate binding and release cycles, which guarantees the reversibility of the substrate binding (Xu and Lindquist, 1993; Smith, 1993; Fenton and Horwich, 1997; Bukau *et al.*, 1998).

In contrast, ATP hydrolysis by Hsp100 proteins additionally promotes unfolding of the polypeptide substrate (Schaupp *et al.*, 2007). Hsp104 acts as a molecular machine and needs much energy to pull peptide chains out of stable aggregates. However, the high ATP consumption of Hsp104 might be down-regulated *in vivo* under normal growth conditions in order to avoid a waste of ATP and to enhance the efficiency of substrate disaggregation. Hsp104 is not toxic to growth of yeast even if it is over expressed to very high concentrations (Sanchez *et al.*, 1993; Lindquist *et al.*, 1996), which indicates a regulatory mechanism.

4.4.2 The Hsp104 ATPase mutants reveal an inter-domain crosstalk

To gain insight into the regulation of Hsp104, its two nucleotide binding domains, NBD1 and NBD2, were subjected to several point mutations (see Tab. 4.1 and Fig. 4.7). The point mutations were produced by site-directed mutagenesis and the constructs were expressed and purified from *E. coli*. The rate constant k_{cat} of ATP hydrolysis of wild-type Hsp104 was compared to that of the point mutants (see Fig. 4.8). Wild-type Hsp104 exhibits a k_{cat} of about 62 min^{-1}, which is in good agreement with previous studies (Schirmer *et al.*, 1998; Schirmer *et al.*, 2001).

It should be noted that the observed ATP hydrolysis of a single point mutant takes place exclusively in the remaining non-mutated NBD. The Walker A (K218T/K620T) and Walker B (E285Q/E687Q) double point mutants have no detectable ATPase activity. This serves as a control to show that both NBDs were indeed mutated in their catalytic sites.

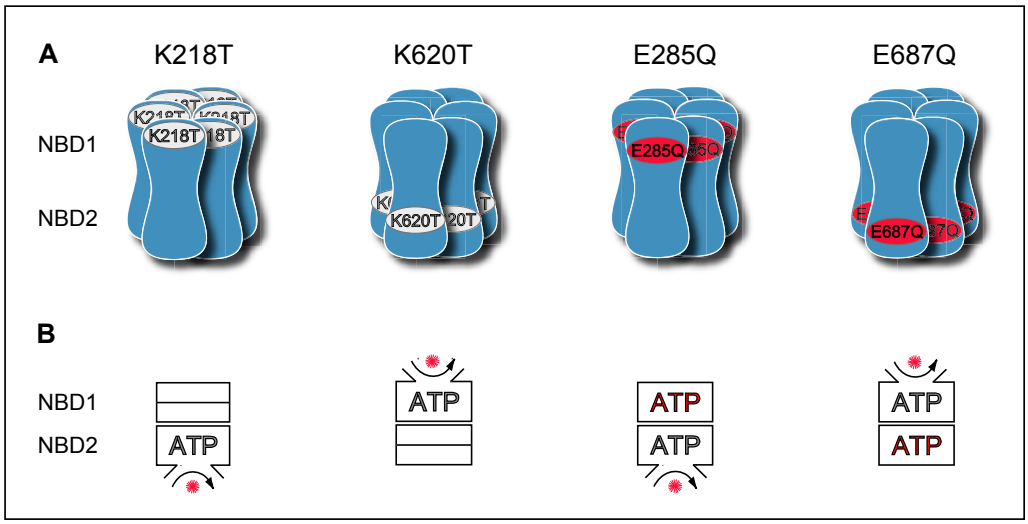

Fig. 4.7: Schematic view of the point mutants in the ATPase domains of Hsp104 used in this study. (A) Position of the mutations within the oligomeric structure. The indicated Lys→Thr mutations, shown by a grey background, target at the Walker A motif and thereby affect the nucleotide binding of the mutated NBD. The indicated Glu→Gln mutations, shown by a red background, target at the Walker B motif and affect only the ATP hydrolysis but not the nucleotide binding of the mutant NBD. (B) Schematic presentation of the theoretical nucleotide state of both NBD rings within a hexamer of each mutant. The boxes correspond to the upper or lower NBD ring of an entire oligomer; "no binding possible" at an NBD ring is indicated by an empty box, "only nucleotide binding" possible is indicated by a closed box, and a "fully functional NBD" ring is indicated by an open box with ATP hydrolysis and nucleotide exchange shown by an arrow and a red star.

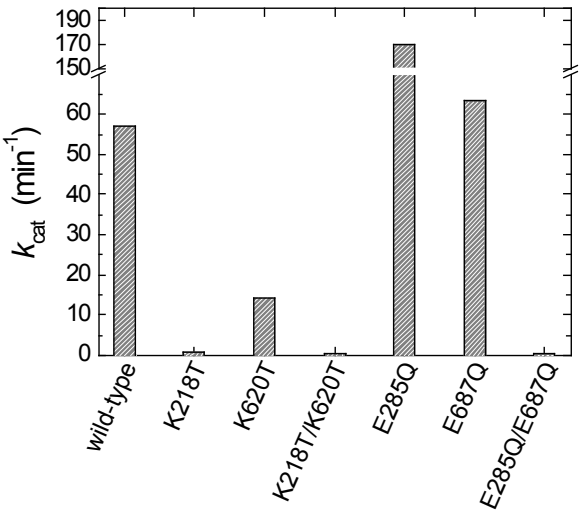

Fig. 4.8: Rate constants k_{cat} of $Hsp104_{WT}$ and its ATPase mutants reveal differences in the ATP turn-over of NBD1 and NBD2. Assays were carried out with 0.5 µM Hsp104 at 30°C using an ATP regenerating system in KM buffer. Turn-over numbers were measured at a range of ATP concentrations and data were fitted using the Hill equation, Eq. 3.12, to determine k_{cat}. The non-hydrolyzing mutants, $Hsp104_{K218T}$, $Hsp104_{K218T/K620T}$, and $Hsp104_{E285Q/E687Q}$, were measured using 5 mM ATP. An increase in the ATP concentration did not improve the ATPase activity of these mutants.

The Walker A single point mutants, K218T and K620T, which are impaired in the nucleotide binding ability in their mutated domain (Watanabe *et al.*, 2002), exhibit a significantly reduced k_{cat} or even an impaired hydrolysis, which is in agreement with previous studies (Schirmer *et al.*, 1998; Schirmer *et al.*, 2001). In the case of the mutant K620T, the activity of

NBD1 is far below the wild-type, but is still detectable, whereas in the case of the mutant K218T, the loss of activity of NBD2 is so significant that no remaining ATP hydrolysis activity could be detected. Thus, the loss of the nucleotide binding ability in either one of the NBDs leads to an impaired ATP hydrolysis ability in the remaining NBD.

The Walker B single point mutants, E285Q and E687Q, are impaired in their ATP hydrolysis function but are still able to bind nucleotides to the mutated NBD (Vale, 2000; Weibezahn *et al.*, 2003). The ATPase data reveal that the Walker B single point mutants show a similar or even higher k_{cat} than the wild-type protein. This leads to the conclusions that (i) both NBDs have the competence to hydrolyze ATP *per se*, and (ii) ATP binding to either one of the NBDs is the prerequisite for hydrolysis of the other NBD. However, the sum of the k_{cat} numbers of both mutant proteins is not equal to that of the wild-type protein, which is smaller. This implies that both of the NBDs are tightly regulated and do not actively contributing to the turn-over number of wild-type Hsp104 simultaneously or that they have a mixed negative regulation. The apparent turn-over of $Hsp104_{WT}$ might be a result of a mixed cooperativity between the NBDs.

These data demonstrate that Hsp104 has an ATPase activity that is intrinsically regulated. There appears to exist an inter-domain crosstalk between the two NBDs. In the following chapters the determination of the actual function of each NBD will be attempted.

4.4.3 The ATPase function is dependent on the quaternary structure of Hsp104

Hsp104 exists in an oligomerization equilibrium of monomers and hexamers, as shown by static light scattering (Fig. 4.5). Importantly, monomeric Hsp104 has no enzymatic activity and – consequently – mutations or assay conditions affecting the oligomerization state also reduce the ATPase activity of Hsp104 (Parsell *et al.*, 1994a). The concentration dependency of the ATPase was analyzed by reducing the overall Hsp104 content in the ATPase assay to a level that did affect the oligomerization equilibrium. Fig. 4.9 shows the dependency of the ATP turn-over on the protein concentration. $Hsp104_{WT}$ exhibits a stable ATP turn-over at protein concentrations above ~0.5 µM. The actual turn-over of ~38 min^{-1} was found to be caused by hexameric protein, as evidenced by light scattering experiments which have shown that Hsp104 exists as hexamer at this concentration in presence of nucleotides (see Fig. 4.9). Below this concentration range Hsp104 oligomers are not stable enough and the content of hexamers decreases in favor of the formation of monomers resulting in a very small apparent turn-over number below 0.05 µM. These data demonstrate how the presence of oligomers of wild-type Hsp104 is dependent on the protein concentration.

The mutant K620T has a stable turn-over of ~10 min^{-1} above 2.5 µM but does not reach the turn-over number of fully hexameric wild-type Hsp104. However, static light scattering and AUC experiments have shown that this mutant protein exists as an oligomer at concentrations between 2.5 µM and 5 µM in the presence of nucleotides. It can be assumed that a turn-over

number of ~13 min^{-1} corresponds to the hexameric $Hsp104_{K620T}$ mutant since a saturation effect was detected and no further increase in the turn-over could be reached at higher protein concentrations (data not shown). In conclusion, the K620T mutant can attain up to 25% of the wild-type ATPase activity under conditions that stabilize its oligomer.

All ATP-hydrolyzing mutants with the exception of the K620T mutant showed an oligomerization-related ATPase activity that was similar to that of wild-type Hsp104 (data not shown).

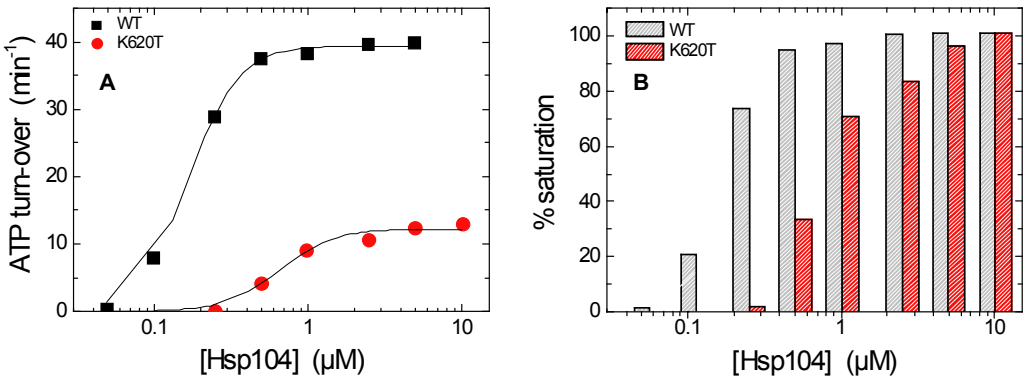

Fig. 4.9: Concentration dependency of the ATP turn-over by $Hsp104_{WT}$ and $Hsp104_{K620T}$. (A) ATP turn-over and (B) relative saturation corresponding to the maximum turn-over of $Hsp104_{WT}$ and $Hsp104_{K620T}$, respectively. Assays were carried out in standard assay buffer at 30°C using an ATP regenerating system with 5 mM ATP. The Hsp104 concentration corresponds to the monomer.

4.4.4 Hsp104 oligomers are stable during steady-state ATP hydrolysis

It was shown above that Hsp104 exists in a sensitive oligomerization equilibrium which is dependent on the protein concentration and the presence of nucleotides (see chapter 4.3). However, it is not clear whether Hsp104 oligomers maintain to be stable once they have been formed or whether they dissociate and re-associate permanently during the ATPase cycle. Hsp104 might possibly populate a complete nucleotide-free state due to the nucleotide exchange after hydrolysis. Such an associative cycle could explain the striking dynamics of oligomerization from a kinetic point of view.

The formation of hetero-oligomers between wild-type Hsp104 and its mutants served as evidence to show whether or not monomeric intermediates actually exist at some point in time during steady-state ATP hydrolysis. In theory, when another Hsp104 variant (e.g., a mutant protein) is added into a running ATPase assay of wild-type Hsp104, these intermediate monomers should re-associate and, thus, should be found again in mixed oligomers. The presence of the functionally impaired mutant protomers within the re-associated hexamer, however, would possibly block or at least impair the subsequent ATP hydrolysis. Hence, if such a dissociation and re-association occurs during the ATP hydrolysis cycle the resulting difference in activity could be used to distinguish between homo-

oligomers and mixed oligomers. The K218T mutant, which was selected for the formation of hetero-oligomers, is impaired in nucleotide binding to NBD1 and has no apparent turn-over, as shown in Fig. 4.10, and oligomerizes similar to wild-type protein (see Tab. 4.3). When the K218T mutant is added into a running ATPase assay containing $Hsp104_{WT}$, the resulting overall turn-over is similar to that obtained with pure wild-type Hsp104 previously, see column "wild-type + K218T w/o pre-incubation". Since the turn-over remained unchanged after the addition of the inactive K218T mutant, it can be concluded that either no hetero-association takes place or that the mutant protein does not affect the wild-type protein at all.
However, when both proteins are pre-incubated on ice in the absence of nucleotides and are then subjected to the same assay as above as a mixture, hetero-oligomerization can be detected (see right column). The mixed oligomers can be clearly distinguished from homo-oligomers by their significantly reduced ATPase activity. Consequently, the possibility that hetero-oligomers with the same activity as homo-oligomers might have formed during the ATP hydrolysis cycle as above can be ruled out. These data clearly show that a hetero-oligomer once formed has an ATP hydrolysis activity that is significantly impaired compared to homo-oligomeric wild-type Hsp104.
These results demonstrate that hetero-oligomers can only form before the hexameric protein is in a state of steady-state ATP hydrolysis. Moreover, the data suggest that once the ATPase cycle has started no hetero-oligomerization is possible any longer. This allows the conclusion that no oligomer association cycle exists in parallel to the ATP hydrolysis cycle. Notably, it can be excluded that the stability of these hetero-oligomers is simply an exceptional effect of the K218T mutant since hetero-oligomer formation was also found for wild-type Hsp104 in combination with all other ATPase mutants used in this study. For example, the incorporation of sub-stochiometrical amounts of $Hsp104_{E285Q}$ into wild-type oligomers also led to an irreversibly altered ATP turn-over (data not shown).
These data show that a minor amount of the K218T mutant is already able to "poison" the

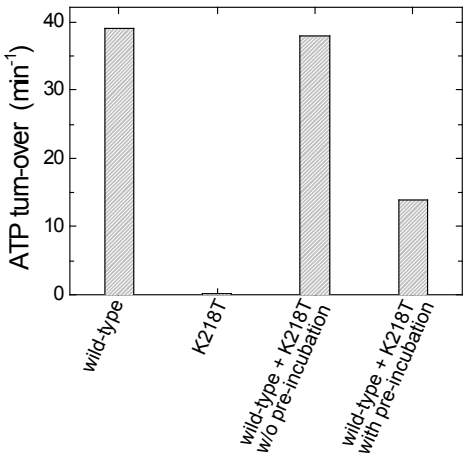

Fig. 4.10: $Hsp104_{WT}$·$Hsp104_{K218T}$ hetero-oligomers are stable and show an altered ATP turn-over. Assays were carried out in standard assay buffer at 30°C using an ATP regenerating system with 5 mM ATP. The proteins used for the ATPase assay were 0.5 µM $Hsp104_{WT,}$ 0.1 µM $Hsp104_{K218T}$ or both. $Hsp104_{WT}$ was either directly added into the thermostated assay cuvette containing ATP and all assay supplements (left columns) or Hsp104 was pre-incubated as a mixture of wild-type Hsp104 and the K218T mutant for 10 min on ice in absence of nucleotides (right column).

ATPase activity of the wild-type protein. Notably, an impaired ability of the NBD1 domain to bind to nucleotides is the only handicap of the K218T mutant.
Importantly, the ATP hydrolysis activity of the hetero-hexamer drops more than could be expected from the percentage of incorporated mutant Hsp104. Adding about 1/5 mole-% of the K218T mutant results in a loss of ATP hydrolysis activity of the resulting hetero-hexamer of about two thirds. Consequently, there is no linear relationship between the uptake of inactive mutant protein and the resulting activity loss. Hence, it can be concluded that Hsp104 exhibits an inter-subunit crosstalk: a fully active Hsp104 ATPase strongly demands for nucleotide binding to NBD1 in *all* subunits within a hexamer, and an impaired nucleotide binding to one NBD1 of the hexamer will impair the ATPase activity of the whole hexamer.

4.4.5 Enzymatic characterization of Hsp104 and its mutants

The ATP dependency of Hsp104 and its ATPase mutants were characterized by Michaelis-Menten experiments. The rate of ATP hydrolysis was measured at varying ATP concentrations in order to determine the substrate dependency of Hsp104, as shown in Fig. 4.11. Due to the obvious cooperativity of Hsp104, the Hill equation (Eq. 3.12) was selected for the fitting of the data. The obtained enzymatic constants are listed in Tab. 4.5.
The K_M constant of wild-type Hsp104, which is a measure for ATP substrate affinity, is found to correspond to physiological ATP concentrations of ~6 mM. This is in good agreement with a previous study of Schirmer (Schirmer *et al.*, 2001) who reported a K_M of 5.9 mM. This demonstrates that $Hsp104_{WT}$ has apparently a poor affinity for ATP under steady-state conditions. The rather moderate ATP affinity could lead to the conclusion that the regulation of Hsp104 activity was dependent on the cellular energy charge. Similar molecular chaperones such as Hsp90 and Hsp70 have a much lower K_M in the micromolar range and function properly at even low ATP concentrations (Hsp70: K_M = ~0.2 µM ATP, Wegele *et al.*, 2003, and Hsp90: K_M = ~400 µM ATP, Richter *et al*., 2005). However, the Hsp104 k_{cat} of 57 min^{-1} is relatively high, as already discussed (cf. chapter 4.1.1). The Michaelis-Menten analysis shows that $Hsp104_{WT}$ is an enzyme with a moderate positive cooperativity, it displays a Hill coefficient of ~1.5, again in agreement with Schirmer (Hill coefficient of 1.7, Schirmer *et al.*, 2001).
The K620T Walker A mutant shows a reduced ATPase activity (see Fig. 4.11.B). This activity derives from the remaining intact NBD1. $Hsp104_{K620T}$ exhibits a high dependency on ionic strength and loses its oligomer stability at high salt concentrations (Schirmer *et al.*, 1998; Hattendorf *et al.*, 2002a). A decrease in the salt content alters the enzymatic parameters of this mutant protein by stabilizing the oligomers. Referring to previous results on the oligomerization of this mutant protein (Parsell *et al.*, 1994a; Schirmer *et al.*, 2001) it can be assumed that it still exists as a monomer even at low ATP concentrations. The monomer is

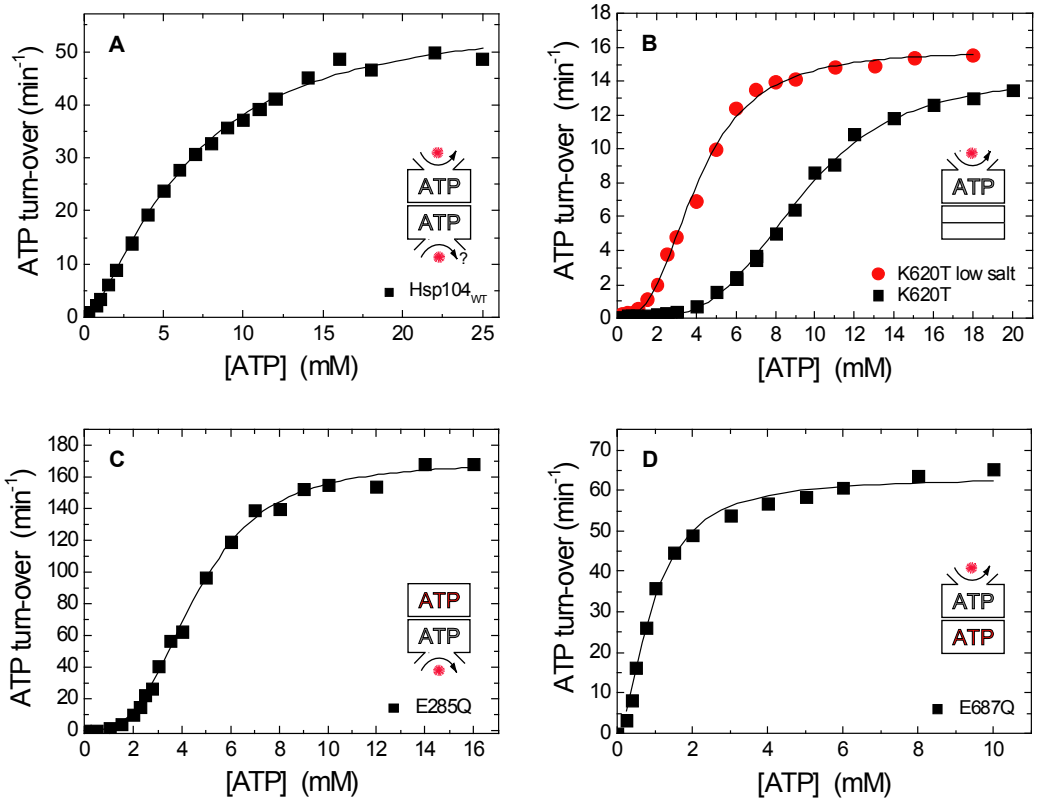

Fig. 4.11: ATP concentration dependency of the ATPase activities of (A) $Hsp104_{WT}$, (B) $Hsp104_{K620T}$, (C) $Hsp104_{E285Q}$, and (D) $Hsp104_{E687Q}$. ATP turn-over of 0.5 µM Hsp104 was determined at increasing ATP concentrations in KM assay buffer using a regenerating assay system at 30°C. The K620T mutant, which is very sensitive to ionic strength, was additionally assayed under low salt conditions in KM-LS assay buffer. Data were fitted by the Hill equation (Eq. 3.12).

Tab. 4.5: Enzymatic constants derived from the Michaelis-Menten analysis of $Hsp104_{WT}$ and its ATPase mutants. A Hill coefficient $h = 1$ means no cooperativity, $h < 1$ means negative cooperativity, and $h > 1$ means positive cooperativity.

Hsp104 Protein	$K_{M\,(ATP)}$ [mM]	k_{cat} [ATP/min]	Hill Coefficient h	Referring Figure
WT	7.3 ± 0.5	61.8 ± 2.3	1.45 ± 0.07	Fig. 4.11.A
K218T	n. d.	n. d.	n. d.	
K620T	9.2 ± 0.2	14.2 ± 0.2	3.82 ± 0.14	Fig. 4.11.B
K620T (NS)	4.0 ± 0.1	15.8 ± 0.2	2.77 ± 0.14	Fig. 4.11.B
E285Q	4.6 ± 0.1	169.3 ± 2.5	3.13 ± 0.14	Fig. 4.11.C
E687Q	0.94 ± 0.05	63.3 ± 1.3	1.77 ± 0.13	Fig. 4.11.D

inactive, which shifts the Michaelis-Menten curve of the K620T ATPase under high salt conditions to the right side, in other words the oligomerization occurs at a higher ATP concentration in comparison to low salt conditions. Hence, the Hill coefficient shows differences depending on the particular salt condition. It must be considered that the apparent high positive cooperativity is probably an oligomerization effect. The other variants of Hsp104 are not as dependent on the ionic strength and show no significantly altered enzymatic parameters in the range of 80 - 200 mM KCl (data not shown).

The Walker B mutant E285Q is inactive at low ATP concentrations and becomes strongly activated at ATP concentrations above 2 mM (see Fig. 4.11.C). The lack of activity below 2 mM ATP cannot be explained by an impaired oligomerization such as for the K620T protein. This mutant protein has no oligomerization defect (the double point mutant $Hsp104_{E285Q/E687Q}$ oligomerizes similarly to wild-type Hsp104, see Tab. 4.3). Therefore, its Hill coefficient is truly reflecting a high positive cooperativity.

The Walker B mutant E687Q has an ATPase activity comparable to the wild-type enzyme (see Fig. 4.11.D). However, its affinity for ATP is much higher: it shows a K_M of below 1 mM ATP.

In conclusion, the Michaelis-Menten analysis reveals that the apparent enzyme parameters of $Hsp104_{WT}$ are the result of a very delicate interplay of its nucleotide binding domains. There exists an intrinsic positive cooperativity along with a negative cooperativity since some mutants are more active than wild-type protein and since $Hsp104_{WT}$ displays an overall hill coefficient that is smaller than for the analyzed Hsp104 mutants.

4.4.6 Affinity of Hsp104 for nucleotides

4.4.6.1 Fluorescence titration of Hsp104

To gain further insight into the function of the two NBDs of Hsp104 the ATPase mutants were analyzed with respect to their affinity for nucleotides. Titrations were carried out using both ITC and fluorescence spectroscopy.

Fluorescence spectroscopy was employed to analyze the interaction of wild-type Hsp104 and its Walker A mutants with ADP. Hsp104 itself contains no intrinsic strong fluorophore such as tryptophan. The complex of Hsp104 and the dye ANS served to detect conformational changes of Hsp104 upon nucleotide interaction. ANS binds to hydrophobic surfaces of proteins and thereby different structural conformations can be monitored by changes in the ANS fluorescence (Das *et al.*, 1995). Fig. 4.12.A shows the fluorescence spectra of free ANS and its Hsp104-bound state. The signal intensity exhibits a strong nucleotide dependency. The complex of ANS and nucleotide-free Hsp104 shows the highest quantum yield whereas nucleotide binding to Hsp104 reduces the fluorescence signal. Hsp104 is present in its

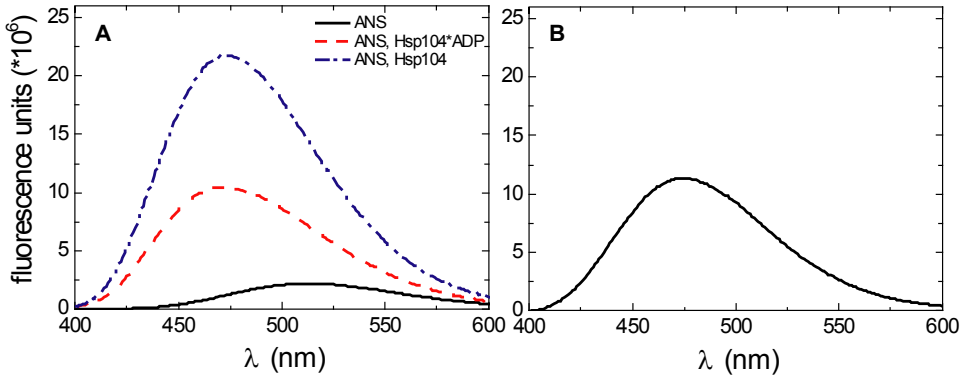

Fig. 4.12: Change in ANS fluorescence upon binding to Hsp104$_{WT}$. (A) Fluorescence spectra of ANS (black), ANS bound to Hsp104 (blue), and ANS bound to Hsp104·ADP (red), (B) difference spectrum of the Hsp104 containing samples with and w/o the presence of ADP. The concentrations used were 25 µM ANS, 5 µM Hsp104 and 1 mM ADP in standard assay buffer. Spectra were recorded at 25°C with an excitation wavelength of 380 nm. All spectra were corrected by the respective spectra lacking ANS. The fluorescence change in (B) is due to the nucleotide binding to Hsp104 and shows a difference maximum at 475 nm.

hexameric state at the concentration used, and it can be ruled out that additional oligomerization events go along with the nucleotide binding. The ANS signal change could be explained by a specific conformational change upon nucleotide binding that reduces the content of hydrophobic surfaces. However, the maximal signal change is ~50%, as shown by the difference spectrum in Fig. 4.12.B. Its maximum is located at 475 nm and it was used to analyze the protein-ligand interaction between Hsp104 and ADP.

Titrations were carried out to further characterize the binding of ANS to Hsp104. Fig. 4.13 shows an ANS titration of Hsp104 with and without the presence of nucleotides. The binding of ANS shows a $K_{D\ (ANS)}$ of 65 µM for pure Hsp104 and 72 µM for Hsp104·ADP. The affinity for both Hsp104 states is similar and – therefore – ANS can be used as a fluorescence marker for ADP titrations without affecting the binding constant for the nucleotide. ANS fluorescence served to monitor signal changes during ADP titrations of Hsp104 and its Walker A mutants. These titrations are shown in Fig. 4.14.

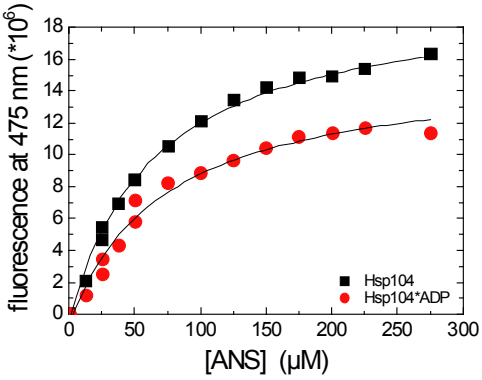

Fig. 4.13: Titration of Hsp104 and Hsp104·ADP with ANS. The concentration was 1 µM Hsp104$_{WT}$ and 500 µM ADP in standard assay buffer. Spectra were recorded at 25°C with an excitation wavelength of 380 nm. The emission signal at 475 nm was plotted against the ANS concentration and the data were fitted using Eq. 3.3.

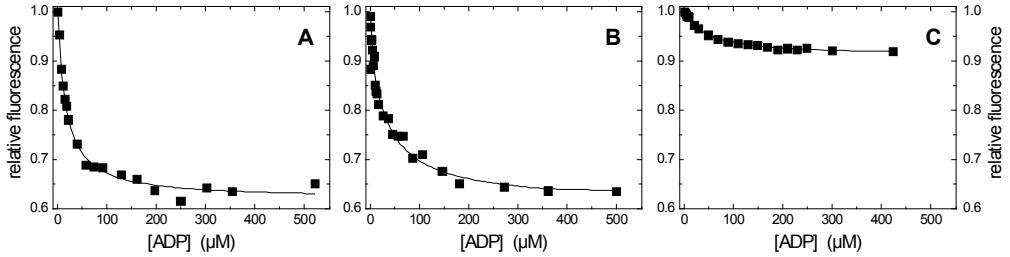

Fig. 4.14: ADP titration of (A) Hsp104$_{WT}$, (B) Hsp104$_{K218T}$ and (C) Hsp104$_{K620T}$ using ANS fluorescence. Samples of 50 µM ANS and 1 µM Hsp104$_{WT\ or\ K218T}$ in (A) and (B), and 10 µM Hsp104$_{K620T}$ in (C) were prepared using degased standard assay buffer and titrated with ADP. Spectra were recorded at 25°C with an excitation wavelength of 380 nm. The emission signal at 475 nm was normalized using the nucleotide-free starting point, and dilution-corrected. Then the relative fluorescence was plotted versus the ADP concentration and the data were fitted using Eq. 3.3.

Hsp104$_{K620T}$, the mutant which is impaired in nucleotide binding to NBD2, showed a much smaller signal amplitude than Hsp104$_{K218T}$, the corresponding NBD1 mutant (cf. Fig. 4.14.B and C). It should be noted that a 10-fold higher concentration of the K620T mutant was used to ensure that it exists in its oligomeric state at the beginning of the titration. It can be speculated that ADP binding only to NBD1 (as for the mutant K620T) induces less conformational changes than ADP binding to NBD2 (as for the mutant K218T). The wild-type Hsp104 had a signal amplitude similar to the mutant K218T. This result is surprising since it was expected that the wild-type would show a signal amplitude that reflects the sum of both NBDs since both NBDs should be binding-competent. Thus, it can be interpreted from these data that only NBD2 from wild-type Hsp104 binds to ADP or that both NBD rings become not fully saturated. However, the contribution from NBD1 to the observed signal amplitude would be rather small and care must be taken not to overestimate the sensitivity of the ANS binding. All shown variants yielded a similar $K_{D\ (ADP)}$ of ~42 µM to 27 µM and are shown in Tab. 4.6.

4.4.6.2 ITC titration of Hsp104

The affinity of Hsp104 for ADP was also analyzed by ITC for all Hsp104 ATPase variants. A representative experiment is shown in Fig. 4.15.A. The titration of the Walker B double point mutant E285Q/E687Q (Hsp104$_{TRAP}$) yielded a $K_{D\ (ADP)}$ of 16 µM. The $K_{D\ (ADP)}$ for the other proteins including wild-type Hsp104 was found to be between 50 and 26 µM (see Tab. 4.6). The affinity for ATP could not be analyzed by ITC since it is subsequently hydrolyzed. The titration with the non-hydrolyzable ATP analogue AMP-PNP was not successful since AMP-PNP does not bind to Hsp104, as shown in Fig. 4.15.B. Hsp104$_{E285Q/E687Q}$, the "TRAP" mutant, served in particular to gain insight into the affinity for ATP. This is the only mutant protein that shows a binding to ATP without subsequent hydrolysis. Tab. 4.6 lists all obtained K_D values for Hsp104 and its variants.

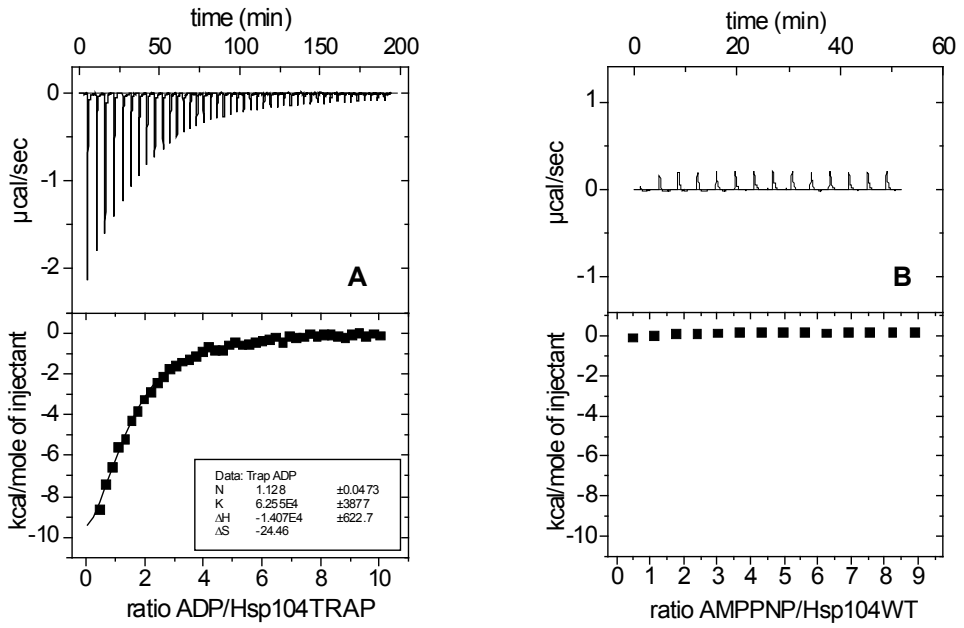

Fig. 4.15: Representative ITC experiments of Hsp104. (A) Titration of $Hsp104_{E285Q/E687Q}$, the "TRAP" mutant, with ADP and (B) titration of $Hsp104_{WT}$ with AMP-PNP. A stock solution of nucleotide (2.82 mM) was titrated to a solution of Hsp104 (25 µM) in standard assay buffer at 30°C, and the associated heat change was monitored (upper panels). After integration of the injection peaks, the resulting binding curve in A (lower panel) was analyzed by fitting of the integrated injection peaks to a single site model.

The ITC data show that the binding constants for ADP, $K_{D\ (ADP)}$, of all ATPase single point mutants are found within the same range, between 30 - 40 µM, although the Walker B double point mutant $Hsp104_{E285Q/E687Q}$ shows a higher affinity for ADP with $K_{D\ (ADP)}$ = 16 µM. One would have expected that the two Walker B single point mutants $Hsp104_{E285Q}$ and $Hsp104_{E687Q}$ have a similar affinity such as $Hsp104_{E285Q/E687Q}$ since they also possess two binding competent NBDs. Nevertheless, the differences are found within a small range.

Interestingly, the Walker B double point mutant $Hsp104_{E285Q/E687Q}$ exhibits a low binding constant to ATP, $K_{D\ (ATP)}$ = 4 µM. In other words, it has an affinity for ATP that is higher than to ADP. This result is line with previous data obtained for this mutant protein. $Hsp104_{E285Q/E687Q}$ shows an extraordinarily stable complex formation with aggregated polypeptide substrates in presence of ATP *in vitro* (Bösl *et al.*, 2005), although the applied ATP has always a small unavoidable contamination of ADP. The differences in nucleotide affinities provide an explanation for the stable complex formation.

The ATPase data reveal much higher apparent $K_{M\ (ATP)}$ values, as it was measured using the hydrolyzing Hsp104 variants (see 4.4.5). Seemingly, the enzyme has a low apparent affinity for ATP under steady-state conditions. In this context it is difficult to estimate the relevance of the ITC result above since the $Hsp104_{E285Q/E687Q}$ corresponds to an artificial all-ATP state, which simply might not exist under steady-state hydrolysis conditions.

In conclusion, the analysis of the affinities to nucleotides demonstrated that each NBD is competent for ADP binding. Further, the physical binding constant to ATP is apparently lower than to ADP. Under steady-state conditions, however, the tight allosteric regulation of the enzyme results in an apparent low affinity for ATP. One can speculate that ATP exchange is limited to only a few active sites within the wild-type oligomer, as might be the case for a sequential ATP hydrolysis.

Tab. 4.6: Nucleotide affinities of Hsp104$_{WT}$ and its ATPase mutants. K_M numbers refer to Tab. 4.5. K_D numbers were obtained by ITC experiments similar to those given in Fig. 4.15.

Hsp104 Protein	$K_{M\ (ATP)}$ [mM] ATPase Assay	$K_{D\ (ATP)}$ [µM] ITC	$K_{D\ (ADP)}$ [µM] ITC	$K_{D\ (ADP)}$ [µM] ANS Fluorescence
WT	7.3 ± 0.5	n. d.	46.0 ± 4.0	27.0 ± 2.6
K218T	n. d.	n. d.	29.0 ± 4.0	40.3 ± 4.7
K620T	9.2 ± 0.2	n. d.	37.0 ± 3.0	41.8 ± 2.3
K218T/K620T	n. d.	n. d.	0.0	n. d.
E285Q	4.6 ± 0.1	n. d.	30.0 ± 3.0	n. d.
E687Q	0.94 ± 0.05	n. d.	33.0 ± 3.0	n. d.
E285Q/E687Q	n. d.	4.0 ± 1.2	16.0 ± 1.0	n. d.

4.5 GdmCl is a specific inhibitor of Hsp104

The ATPase activity of the molecular chaperone Hsp104 can easily be affected *in vitro*. Increasing the ionic strength or lowering the ATP concentration reduces the turn-over significantly, as discussed in chapter 4.4. However, the analysis shown above focuses only on *one* functional aspect of Hsp104: the ATPase activity.

It remains to be elucidated how the energy provided by the ATPase of Hsp104 is actually used for a successful and effective disaggregation of aggregated proteins, and to what extent it is needed. Further, it is still unknown, to which extent the *in vitro* data correspond to the *in vivo* activity of the ATPase of Hsp104. Yet, an *in vivo* analysis showed that mutations interfering with the ATPase activity of Hsp104, such as the K218T mutant of Hsp104, also affect the viability of yeast under stress conditions (Parsell *et al.*, 1991). This finding supports the importance of the ATPase activity of Hsp104 to fulfill its cellular function.

Previous studies also suggest that not only induced heat shock resistance but also the prion maintenance by Hsp104 requires a fully functional Hsp104 ATPase activity (Chernoff *et al.*, 1995; Wegrzyn *et al.*, 2001). Successful prion maintenance despite a challenge with ethanol demonstrates that $Hsp104_{WT}$ is capable of also fulfilling its task under stress conditions (Eaglestone *et al.*, 1999; Ferreira *et al*., 2001). Under these demanding conditions it is likely that the ionic composition of the cytoplasm is influenced and, furthermore, the cellular energy charge might be reduced. The Hsp104 ATPase activity must be robust enough to deal with these conditions. Otherwise yeast cells would lose their prions upon exposure to stress.

In order to assess the role of ATP hydrolysis for the function of Hsp104 in more detail, it would be desirable to find a tool that allows to inhibit the ATP hydrolysis activity while affecting the remaining Hsp104 complex as little as possible. The use of a mutant within the Hsp104 hexamer appears not to be an option, because the ability to bind to ATP affects the whole complex due to an inter-domain crosstalk, as discussed above.

However, it was found in the framework of these studies that there is a compound that is able to affect Hsp104 function *in vivo* much better than heat or ethanol treatment, however, without having to depart to far from native conditions. This compound is the chaotropic salt guanidinium chloride (GdmCl). The addition of small amounts of GdmCl to the growth medium of yeast cells leads to a loss of prion propagation, a phenomenon termed *curing* (Tuite *et al.*, 1981), see Fig. 4.16. Curing by GdmCl has been observed for all yeast prions tested so far (Wickner, 1994; Derkatch *et al.*, 1997; Kushnirov *et al.*, 2000; Santoso *et al.*, 2000; Sondheimer *et al.*, 2000). For curing of yeast prions, a medium supplement of 3 - 5 mM GdmCl is sufficient, which is an amount small enough so that it will not denature any known protein. Although GdmCl seems to inhibit the replication of the prions (Eaglestone *et al.*, 2000; Ness *et al.*, 2002), several lines of evidence suggest that it does not affect the prion proteins themselves but rather Hsp104. First, GdmCl blocks the disaggregase activity of Hsp104 *in vivo* and reduces the thermotolerance of yeast (Ferreira *et al.*, 2001;

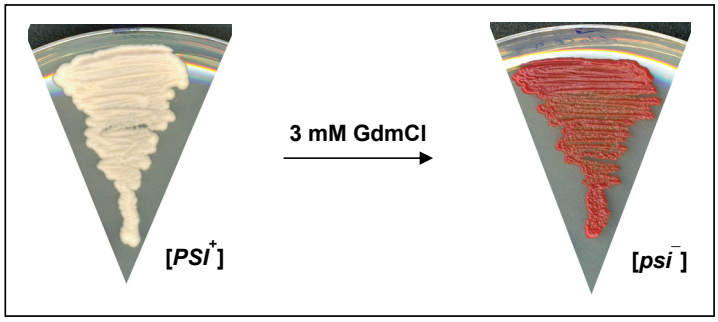

Fig. 4.16: Curing of the [*PSI*$^+$] prion phenotype by GdmCl. The yeast strain BSC783/4a [*PSI*$^+$], which contains prions, was streaked on a YEPD plate containing 3 mM GdmCl. While growing for 3 days at 30°C the cells lose their prion phenotype and convert to [*psi*$^-$], indicated by the red colony color, for details see chapter 3.3.5 or footnote in chapter 4.6.7: nonsense suppression assay for presence of [*PSI*$^+$].

Jung and Masison, 2001). Second, both GdmCl-treated and Hsp104-deficient yeast cells have similar phenotypes with respect to prion propagation (Ferreira *et al.*, 2001; Jung *et al.*, 2001). A report showed that in yeast strains with mutant Hsp104 comprising a D184S point mutation in the N-terminal nucleotide binding domain, prion phenotypes can no longer be cured by GdmCl (Jung *et al.*, 2002). Finally, Lindquist and coworkers noted that low residual concentrations of GdmCl during reactivation of chemically denatured luciferase inhibit ATP hydrolysis by Hsp104 (Glover *et al.*, 1998).
The following chapter presents the analysis of the GdmCl effects on the molecular chaperone Hsp104. This study will employ a direct *in vitro* approach to explain the curing phenomenon that is observed *in vivo*.

4.5.1 Low concentrations of GdmCl specifically inhibit ATP hydrolysis by Hsp104

Hsp104 was assayed for GdmCl sensitivity under steady-state conditions using the regenerative ATPase assay (Norby, 1988). Hsp104 exhibited a strong decrease in the ATPase activity in the presence of 5 mM GdmCl (see Fig. 4.17). To verify the specificity of inhibition, it was examined whether or not GdmCl affects other ATP-hydrolyzing oligomeric chaperones such as GroEL and Hsp82 (the yeast homologue of Hsp90). None of these enzymes exhibited sensitivity to GdmCl. Hence, it can be ruled out that GdmCl might inhibit the enzymes in the regenerative ATPase assay or might change the catalytic properties of ATPases in general.
The GdmCl sensitivity of Hsp104 was analyzed by varying the concentration of the inhibitor (see Fig. 4.18). Hsp104 already showed a significant decrease in ATPase activity in the presence of GdmCl concentrations as low as 30 µM. Remarkably, however, the ATPase activity of Hsp104 in the presence of GdmCl only drops to ~50% of the initial turn-over even at saturating concentrations of GdmCl. No further decrease in ATPase activity could be

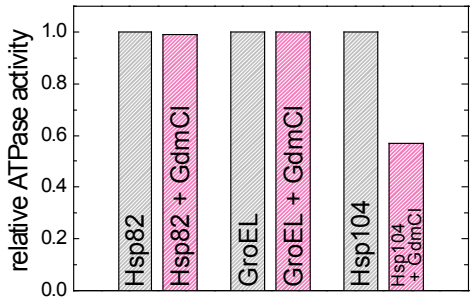

Fig. 4.17: GdmCl inhibits Hsp104 but not Hsp82 and GroEL. The ATP turn-over of 0.5 µM $Hsp104_{WT}$, Hsp82 or GroEL was assayed at 30°C in standard assay buffer using an ATP regenerating system containing 5 mM ATP with or w/o the presence of 5 mM GdmCl. The detected ATP turn-over of each protein was normalized by the corresponding turn-over number w/o GdmCl, which was Hsp82: 1.1 ATP/min, GroEL: 4.2 ATP/min, and Hsp104: 38 ATP/min.

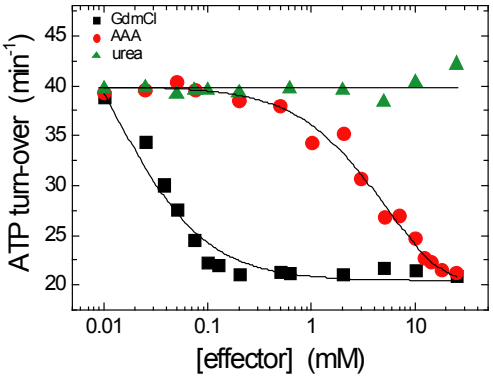

Fig. 4.18: GdmCl and NAAA – but not urea – inhibit the ATP hydrolysis activity of Hsp104. The ATP turn-over of 0.5 µM $Hsp104_{WT}$ was assayed at 30°C in standard assay buffer using an ATP regenerating system containing 5 mM ATP and various concentrations of GdmCl, urea or NAAA. The data were fitted by Eq. 3.3 and yielded a $K_{½\ (GdmCl)}$ of ~0.012 mM and a $K_{½\ (NAAA)}$ of ~4.7 mM.

detected when the GdmCl concentration was further varied from 0.2 mM to 30 mM. Thus, ATP hydrolysis by Hsp104 is not abolished completely by GdmCl. The inhibition yielded a $K_{½\ (GdmCl)}$ of 0.012 mM.

Since GdmCl might simply affect Hsp104 due to its denaturing properties, assays using urea instead of GdmCl were performed. In contrast to GdmCl, urea had no effect on ATP hydrolysis even at concentrations exceeding 10 mM. This is in agreement with findings that suggest that – unlike GdmCl – urea cannot cure yeast prion phenotypes (Cox *et al.*, 1988). It can therefore be concluded that GdmCl does not interfere with the ATPase activity by simply denaturing Hsp104.

Further, it can be ruled out that the inhibitory effect of GdmCl is a due to an increase in the ionic strength. Although the ATPase activity of Hsp104 shows sensitivity to high ionic strength (Schirmer *et al.*, 1998), the contribution of 1 mM GdmCl is too small to give a reasonable explanation for this strong inhibition. The assay contained a salt background of 150 mM KCl. Thus, exclusively guanidinium ions, Gdm^+, – and not ions *per se* – are responsible for the inhibition of Hsp104.

Compounds similar to GdmCl were analyzed, too. The amino acid arginine consists of a positively charged guanidyl group, but it had no influence on the ATPase activity of Hsp104 (data not shown). However, N-acetylarginine amide (NAAA), which comprises a similar guanidyl group, showed an inhibitory effect. It resembles the Gdm^+ ion but has

nocomparable additional charges such as free arginine (see Appendix A.3). It was found in this study that Hsp104 is not as sensitive to NAAA than to GdmCl even though the characteristics of the inhibition by NAAA show similarities to the GdmCl inhibition, in particular in view of the total amount of inhibition that can be reached and the shape of the inhibition curve. Clearly, the chemical nature of the Gdm^+ ion appears to be responsible for the observed inhibitory effect.

4.5.2 GdmCl directly inhibits the Hsp104 ATPase

The rate of ATP hydrolysis is highly dependent on the oligomeric state of Hsp104. The association into hexamers strongly increases the ATPase activity, as shown in chapter 4.3 and by Schirmer (Schirmer *et al.*, 2001). One possibility how GdmCl could indirectly reduce the apparent ATP turn-over is by stabilizing the less active monomers of Hsp104. To distinguish between direct inhibition of ATP hydrolysis and indirect effects on oligomerization, the Hsp104 concentration was varied. If GdmCl really favored Hsp104 monomer formation then one would expect that increasing the protein concentration would again favor hexamer formation and, hence, would cause an increase in ATP hydrolysis activity. A concentration change should therefore serve to detect an oligomerization dependency of the ATPase activity. Fig. 4.19 shows the ATPase activity of $Hsp104_{WT}$ with or without addition of GdmCl at different Hsp104 concentrations. When the concentration of Hsp104 is increased from 0.5 to 5 µM, the ATP turn-over increases merely slightly from ~30 min^{-1} to ~38 min^{-1} (Fig. 4.19.A , black points). Thus, the turn-over number is largely concentration independent. In the presence of 5 mM GdmCl, the activity of Hsp104 drops by about 50%, irrespective of the protein concentration used in the assay (Fig. 1.18.A, red points). This is in support of the conclusion that GdmCl does not shift the oligomerization equilibrium of the wild-type

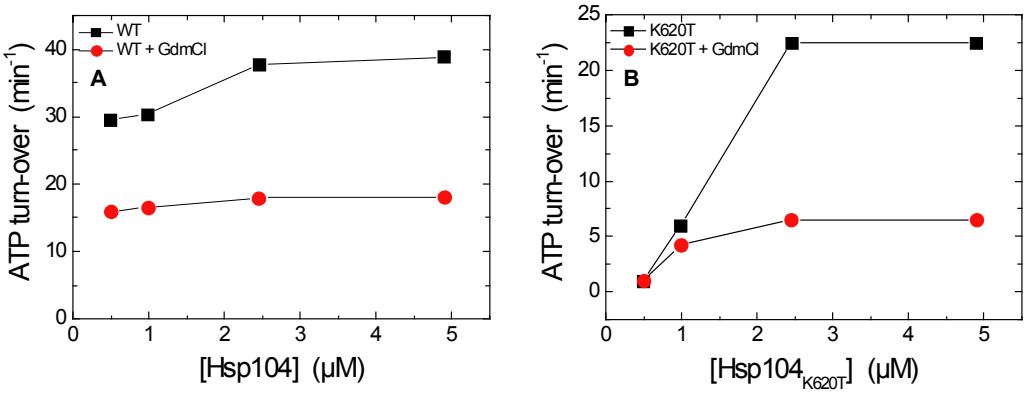

Fig. 4.19: Dependency of the degree of inhibition by GdmCl on protein concentration. The ATP turn-over of 0.5 µM (A) $Hsp104_{WT}$ and (B) $Hsp104_{K620T}$ was assayed at 30°C in standard assay buffer using an ATP regenerating system containing 5 mM ATP with or w/o addition of 5 mM GdmCl.

Hsp104 towards monomer formation. Otherwise, its inhibitory effect should be less pronounced at high protein concentrations, where the hexameric state of Hsp104 is more stable.

$Hsp104_{K620T}$ was analyzed analogous to the wild-type protein, as shown in Fig. 4.19.B. This variant is much more sensitive to assay conditions disturbing the oligomerization. $Hsp104_{K620T}$ has a defect in its oligomerization ability and easily dissociates, as shown in chapter 4.2. At low GdmCl concentrations the mutant shows no significant inhibition. It is only inhibited under conditions were it is supposed to be fully hexameric. This result confirms the presumption made for the wild-type protein: GdmCl is not an inhibitor of oligomerization – it rather directly inhibits the ATP hydrolysis of hexameric Hsp104. Since the ATPase assays provide only an indirect approach to detect changes in oligomerization static light scattering experiments were carried out additionally.

4.5.3 GdmCl does not affect the oligomerization of Hsp104

In order to provide direct evidence whether or not GdmCl changes the apparent molecular weight of Hsp104, samples containing Hsp104, GdmCl, and ADP were loaded on a sample loop of an HPLC system, and then injected into a SLS detector equipped with a flow cell. Fig. 4.20 shows the SLS signal for $Hsp104_{WT}$ and for $Hsp104_{K620T}$ at a concentration of 1 µM. Upon addition of 5 mM ADP, the scattering signal increases, indicating an increase in the apparent molecular weight due to the ADP-induced hexamerization of the chaperone. Fig. 4.20 demonstrates that GdmCl does not reduce the apparent molecular weight of $Hsp104_{WT}$. When samples containing GdmCl were injected, no significant changes in the apparent

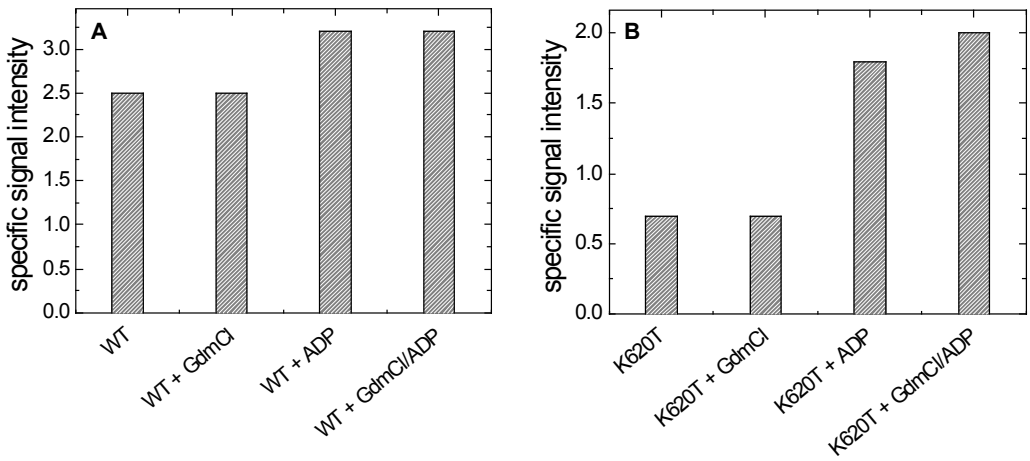

Fig. 4.20: Hsp104 oligomerization monitored by static light scattering with and w/o the presence of GdmCl, (A) $Hsp104_{WT}$ and (B) $Hsp104_{K620T}$. 1 µM protein with and w/o addition of 5 mM ADP and/or 5 mM GdmCl in standard assay buffer was applied on a MiniDawn light scattering detector at RT. The shown specific data are obtained by normalizing the raw signal data with respect to their concentration. The standard error was ~15%.

molecular weight of the wild-type protein were observed in comparison to the measurements in absence of GdmCl (Fig. 4.20.A). The K620T mutant showed no dissociation, but rather a slight increase in the apparent molecular weight, which will be explained in 4.5.6.
It can be concluded that GdmCl does not affect the oligomeric state of the chaperone, both in the presence and in the absence of ADP.

4.5.4 Binding of GdmCl to Hsp104 is nucleotide-dependent

As demonstrated above, GdmCl is not an inhibitor of oligomerization, but specifically reduces the ATP turn-over of Hsp104. To obtain a more detailed picture, the interaction between GdmCl and Hsp104 was directly studied using isothermal titration calorimetry (ITC).
When GdmCl was titrated to Hsp104 in the absence of ADP, no binding signal could be monitored (Fig. 4.21.A). Thus, GdmCl does not bind to nucleotide-free Hsp104. However, when the titration was carried out with 5 mM ADP, present in both injection syringe and sample, binding of GdmCl to Hsp104 was observed (Fig. 4.21.B). Using a model with one binding site per monomer, the analysis of the ITC data yielded an apparent $K_{D\,(GdmCl)}$ of

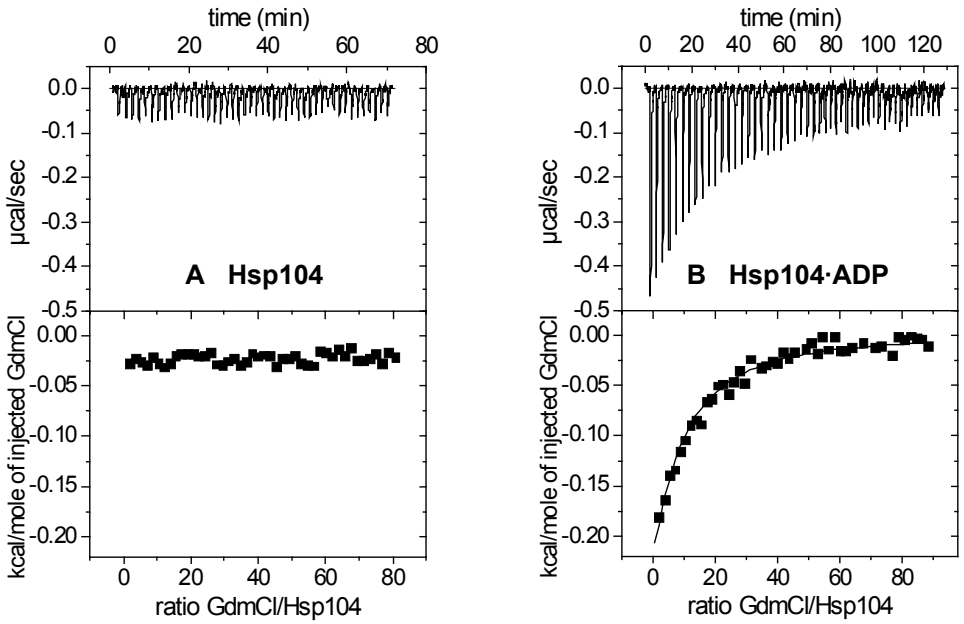

Fig. 4.21: ITC titration reveals nucleotide dependency of GdmCl binding. GdmCl was titrated to $Hsp104_{WT}$ (A) in the absence of nucleotides and (B) in the presence of 2 mM ADP. A stock solution of GdmCl (14.1 mM) was used for the titration to a solution of 30 µM $Hsp104_{WT}$ in standard assay buffer at 30°C. The associated heat change was monitored (upper panels) and used for a data integration resulting in binding curves (lower panels), which were analyzed assuming one binding site per Hsp104 monomer.

600 µM. In the absence of Hsp104 no signal could be observed (data not shown). It can therefore be ruled out that the signal reflects the formation of a complex between GdmCl and ADP. Further experiments showed that GdmCl binds to Hsp104·ATPγS with similar affinity (data not shown). In summary, the results suggest that GdmCl interacts only with nucleotide-bound Hsp104, while the type of adenine nucleotide appears to be less important.

4.5.5 GdmCl increases the affinity of Hsp104 for nucleotides

Since GdmCl only binds to Hsp104 in the presence of nucleotides, thermodynamics predicts that GdmCl in turn should promote nucleotide binding. Thus, a series of ITC experiments in which Hsp104 was titrated with an ADP stock solution was carried out in the presence of increasing concentrations of GdmCl. The corresponding K_D for ADP was calculated from the binding curves. It is apparent that increasing concentrations of GdmCl enhance the binding of ADP to Hsp104 (see Fig. 4.22). In the absence of GdmCl, ADP binds with an apparent K_D of ~50 µM. In the presence of 10 mM GdmCl, this value decreases to about 20 µM. The increased affinity for ADP is mainly due to an increase in binding enthalpy, ΔH, in the presence of GdmCl (data not shown). At saturating concentrations of GdmCl, binding of ADP is 2.5-fold tighter than in the absence of GdmCl.

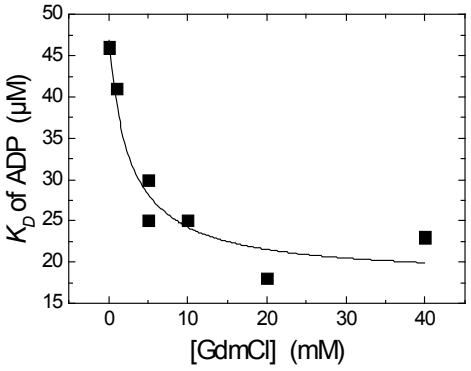

Fig. 4.22: GdmCl increases the affinity of Hsp104 for ADP. ADP was titrated to a solution of 25 µM $Hsp104_{WT}$ in standard assay buffer at 30°C. Each data point refers to an ITC experiment with a defined GdmCl concentration in both the syringe and the sample cell solution. The binding constant, K_D, was obtained by fitting the ITC data to a single site model.

4.5.6 GdmCl stimulates the assembly of the Hsp104 hexamer

The ITC measurements showed that the affinity of Hsp104 for nucleotides is increased in the presence of GdmCl. Since nucleotide binding induces the hexamerization of Hsp104, it was asked next whether or not GdmCl could also *promote* the nucleotide-dependent hexamerization of Hsp104. The SLS traces recorded in the presence of ADP seem to indicate that this is not the case for wild-type Hsp104. However, these measurements were carried out under conditions where $Hsp104_{WT}$ was largely hexameric, and there was a danger that a

stimulatory effect of GdmCl might have remained unnoticed. Notably, the oligomerization defective mutant, $Hsp104_{K620T}$, exhibited a slight increase in its scattering signal, which could be due to an improved oligomerization (see Fig. 4.20).

Analytical ultracentrifugation was employed to search for conditions under which $Hsp104_{WT}$ is dissociated even in the presence of ADP. The screen showed that at 800 mM KCl, the sedimentation coefficient of Hsp104 hardly increases upon addition of 30 µM ADP (8.7 S versus 8.0 S), indicating that the protein can no longer associate under these conditions (compare Fig. 4.23). This is in agreement with a study reporting that at high salt concentration, the hexameric state of Hsp104 is destabilized (Hattendorf *et al.*, 2002b). The sedimentation profile of a protein sample containing 800 mM KCl and 30 µM ADP is shown in Fig. 4.23.A. The lines represent absorbance scans recorded at increasing times of sedimentation. Upon addition of 10 mM GdmCl to the buffer (Fig. 4.23.B), the sedimentation of the protein is significantly faster (s = 13.3 S) suggesting that the hexameric species becomes more populated. This stimulatory effect of GdmCl on Hsp104 assembly is even more evident when the migration of the sedimentation boundary is plotted as a function of time (Fig. 4.23.C). The slope of this graph is a measure for the sedimentation velocity of the protein. Clearly, sedimentation is faster in the presence of GdmCl, indicating that Hsp104 increases in size. Importantly, this effect of GdmCl was not observed when nucleotides were missing in the sample (data not shown). These results demonstrate that GdmCl indeed can stimulate the association of $Hsp104_{WT}$ to hexamers under conditions where nucleotide-dependent hexamerization is energetically less favorable.

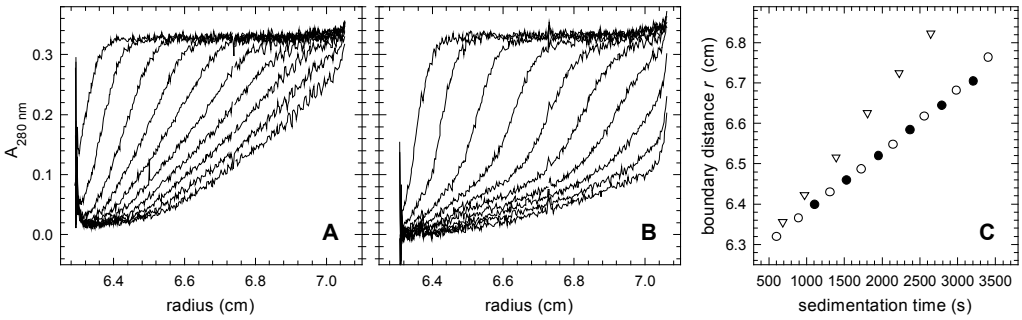

Fig. 4.23: GdmCl can stimulate nucleotide-induced hexamerization of Hsp104. The sedimentation velocity of $Hsp104_{WT}$ (10 µM) was measured in an analytical ultracentrifuge at 25°C in 50 mM HEPES/KOH, pH 7.5, 800 mM KCl, 10 mM $MgCl_2$. (A) Sedimentation profile for Hsp104 in the presence of 30 µM ADP. The lines represent absorbance scans at increasing times of sedimentation. (B) Sedimentation profile for Hsp104 in the presence of 30 µM ADP and 10 mM GdmCl. (C) The distance of the sedimentation boundary from the rotor center, r, is plotted vs. the time t for Hsp104 alone (•), Hsp104/ADP (○), and Hsp104/ADP/GdmCl (▽). The slope dr/dt reflects the sedimentation velocity.

4.5.7 GdmCl is an uncompetitive inhibitor of Hsp104

To further characterize the inhibitory effect of GdmCl on ATP hydrolysis, the dependency of the turn-over number on ATP concentration was examined, both in the presence and in the absence of GdmCl.

In the absence of GdmCl, a plot of ATP turn-over versus ATP concentration shows a Michaelis-Menten-like profile with an apparent K_M of ~7 mM (see Fig. 4.24.A and Tab. 4.7). The data were fitted by the Hill equation (Eq. 3.12) since Hsp104 exhibited cooperativity. In the presence of 5 mM GdmCl, the kinetics of the hydrolysis follow again a Michaelis-Menten-like behavior, but the respective parameters K_M and k_{cat} are changed. The Hill coefficient, h, is also slightly decreased. At high ATP concentrations, the turn-over number is found to be 24 min^{-1}, only 39% of the value determined in the absence of GdmCl. At the same time, the K_M for ATP is decreased to 3 mM, indicating that ATP binds more tightly in the presence of GdmCl. This finding is consistent with the effect of GdmCl on ADP binding that was observed using ITC (cf. Fig. 4.22). The effect of GdmCl is best described by the model of uncompetitive inhibition, in which the inhibitor reversibly binds to the enzyme-substrate complex (here: Hsp104·ATP) and renders it less active (Segel, 1993). Because the turn-over of the enzyme-substrate complex is slowed down, k_{cat} will be decreased in the presence of the inhibitor. At the same time, the inhibitor stabilizes the enzyme-substrate complex resulting in a decrease in K_M. This type of inhibition can be easily identified: it gives rise to a series of parallel lines in a Lineweaver-Burk plot, because K_M and k_{cat} are reduced to the same extent. This is exactly what was observed for GdmCl (see Fig. 4.24.B). In the presence of 5 mM GdmCl, both K_M and k_{cat} decrease about 2.5-fold.

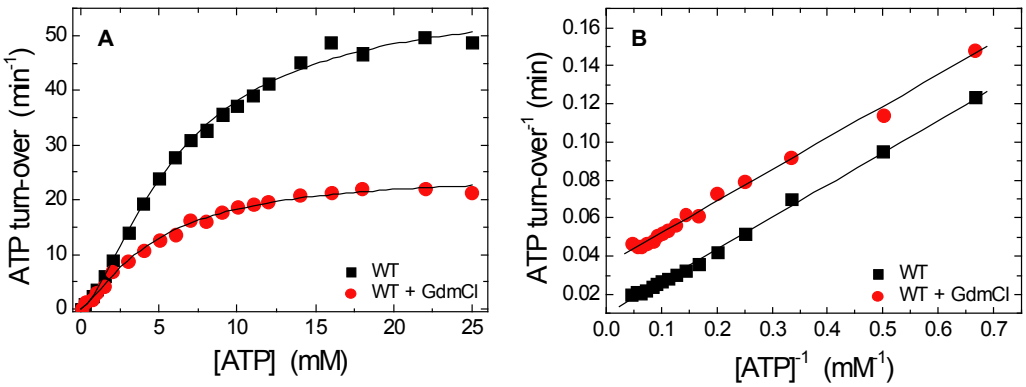

Fig. 4.24: ATP concentration dependency of the ATPase activities of $Hsp104_{WT}$ with and w/o addition of 5 mM GdmCl. (A) Michaelis-Menten plot and (B) double-reciprocal Lineweaver-Burk plot. The ATP turn-over of 0.5 µM Hsp104 was determined at increasing ATP concentrations in KM buffer using a regenerating assay system at 30°C. Data were fitted by the Hill equation (Eq. 3.12). The lines in (B) represent least-square-fits of the data of (A). The data showed a GdmCl-dependent change of k_{cat} and K_M of a factor of 2.5. The fitting by the Michaelis-Menten equation (Eq. 3.11) yielded the same factor (Grimminger *et al.*, 2004).

Hsp104$_{K620T}$ was analyzed in comparison to the wild-type protein, as shown in Fig. 4.25 and Tab. 4.7. According to its oligomerization defect, this mutant was analyzed both under physiological salt conditions (see Fig. 4.25.A and B) and under low salt conditions (see Fig. 4.25.C and D). The difference in ionic strength was chosen in order to assess a possible oligomerization dependency of the GdmCl inhibition. Low salt conditions are supposed to stabilize the oligomers of Hsp104$_{K620T}$ (Hattendorf *et al.*, 2002a). Thus, oligomerization events depending on the presence of ATP should be less pronounced under low salt conditions.

Surprisingly, the mutant shows at low ATP concentrations an increase in the ATP turn-over in the presence of GdmCl both at physiological and under low salt conditions. The expected inhibition could only be detected at higher ATP concentrations. However, the calculated k_{cat}

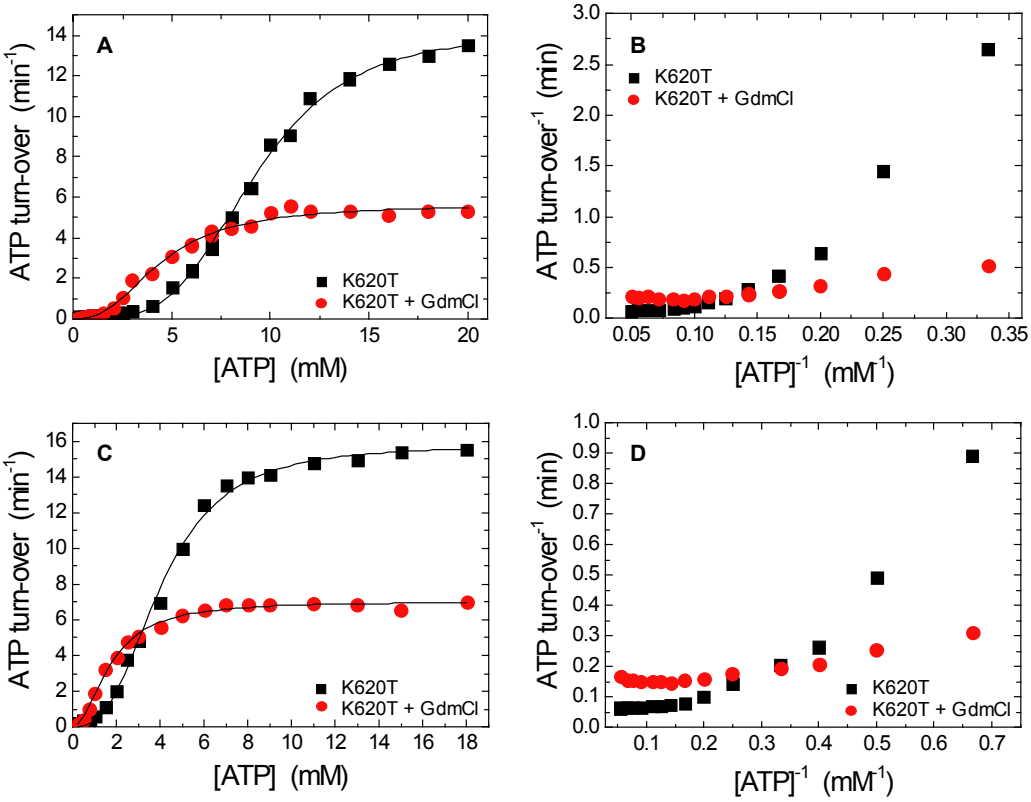

Fig. 4.25: ATP concentration dependency of the ATPase activities of the Walker A mutant, Hsp104$_{K620T}$, with and w/o addition of 5 mM GdmCl. (A) Michaelis-Menten plot and (B) Lineweaver-Burk plot under physiological salt conditions. (C) Michaelis-Menten plot and (D) Lineweaver-Burk plot under low salt conditions. The ATP turn-over of 0.5 µM Hsp104$_{K620T}$ was determined at increasing ATP concentrations in KM buffer or KM-LS buffer using a regenerating assay system at 30°C. Data were fitted by the Hill equation (Eq. 3.12). It should be noted that the salt background of the KM assays does not correspond to a normal ATPase assay: it contains more magnesium and KCl. Therefore, the data of Hsp104$_{K620T}$ are not identical to those shown before (cf. Fig. 4.19).

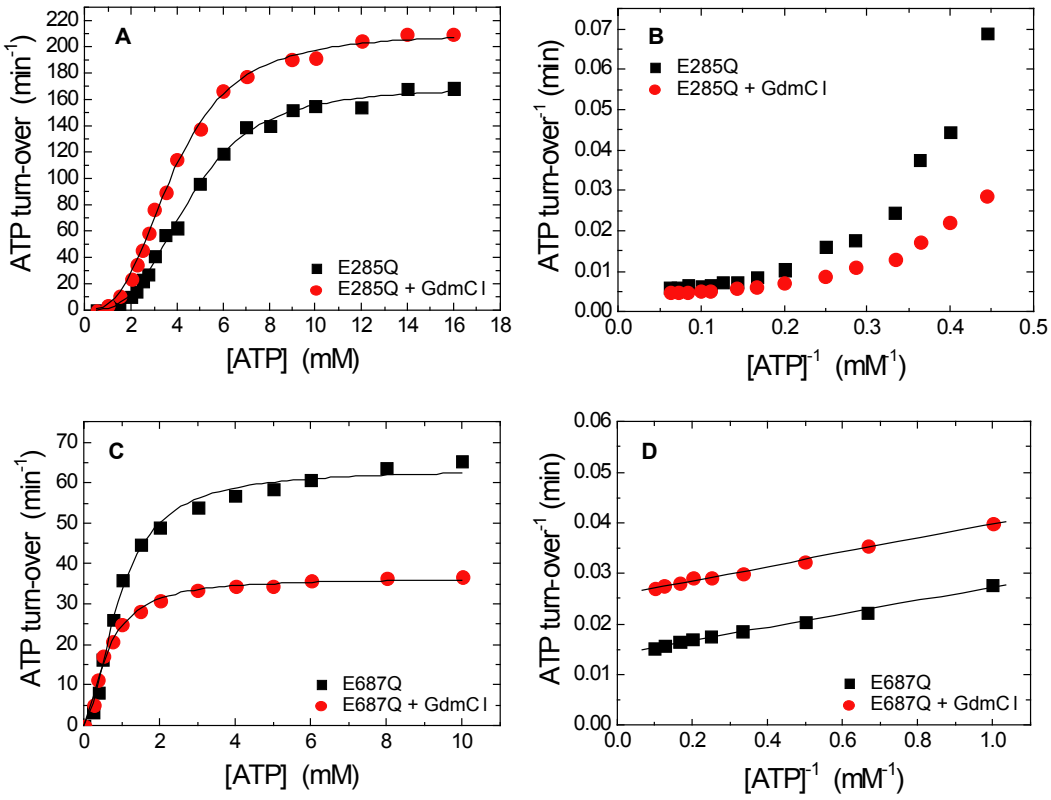

Fig. 4.26: ATP concentration dependency of the ATPase activities of the Walker B mutants, Hsp104$_{E285Q}$ and Hsp104$_{E687Q}$, with and w/o addition of 5 mM GdmCl. (A) Michaelis-Menten plot and (B) Lineweaver-Burk plot of Hsp104$_{E285Q}$. (C) Michaelis-Menten plot and (D) Lineweaver-Burk plot of Hsp104$_{E687Q}$. The ATP turn-over of 0.5 µM Hsp104 $_{E687Q}$ or 0.2 µM Hsp104$_{E285Q}$ was determined at increasing ATP concentrations in KM buffer using a regenerating assay system at 30°C. Data were fitted by the Hill equation (Eq. 3.12).

number is reduced by the presence of GdmCl by a factor of 2.5, which is similar to the inhibition of wild-type Hsp104. The ATP dependency of the inhibition kinetics of Hsp104$_{K620T}$ results in crossing data sets in the Lineweaver-Burk presentation (cf. Fig. 4.25.B and D). The inhibition and the acceleration of the ATPase activity by GdmCl compensate each other at 7 mM ATP under physiological salt conditions and at 3 mM ATP under low salt conditions. The salt dependency of this phenomenon strongly suggests that an oligomerization event is responsible for the activation.

Hsp104$_{K620T}$ exhibits a substrate-dependent ATPase activity with an apparent Hill coefficient of ~3.8, as already shown in chapter 4.4.5. This high apparent cooperativity is related to the oligomerization defect of Hsp104$_{K620T}$: at low ATP concentrations is this mutant mainly monomeric – and therefore inactive; an increase in the ATP content stabilizes the hexameric species resulting in a higher apparent hydrolytic activity. GdmCl enhances the affinity for nucleotides and thereby promotes the nucleotide-dependent oligomerization of Hsp104 under conditions were Hsp104 is mainly monomeric (cf. Fig. 4.20.B and Fig. 4.23). Thus, the

presence of GdmCl compensates in part for the oligomerization defect of this mutant. The GdmCl-induced hexamers are potentially hydrolytically active but at the same time inhibited by GdmCl. This inhibition is, however, not complete so that its remaining activity appears at low ATP concentrations as "activation" relative to GdmCl-free monomeric $Hsp104_{K620T}$. Once the ATP concentration is high enough to sufficiently stabilize GdmCl-free oligomeric $Hsp104_{K620T}$ it becomes possible to make a comparison of equivalent oligomeric species in order to investigate the GdmCl inhibition.

It can be concluded that the ATP dependency of $Hsp104_{K620T}$ is a result of two effects: (i) increase in the oligomer content and (ii) inhibition of the ATP turn-over of hexameric protein. Thus, $Hsp104_{K620T}$ exhibits a pseudo mixed inhibition.

The ATP dependency of the turn-over number of the Walker B mutants, $Hsp104_{E285Q}$ and $Hsp104_{E687Q}$, was also analyzed in the presence of GdmCl. Fig. 4.26 presents the Michaelis-Menten plot and Lineweaver-Burk plot of these mutants. The kinetic parameters are shown in Tab. 4.7.

The E285Q mutant is activated by GdmCl. It shows no inhibition by GdmCl under all tested conditions. Its K_M is only slightly reduced by GdmCl but the k_{cat} is increased from ~170 to ~210 min^{-1}. This protein has no oligomerization defect, as shown in chapter 3.3, but it should be noted that this mutant is disabled in ATP hydrolysis of NBD1. It stably binds ATP to NBD1 and it possesses only one active ATPase domain: NBD2. As discussed in chapter 4.4, NBD2 is allosterically regulated; the permanent ATP-state of NBD1 accelerates the active ATPase domain NBD2. This allosteric regulation might explain the activation by GdmCl. As shown by $Hsp104_{K620T}$, GdmCl promotes the ATP binding to NBD1. Thus, it stabilizes the most active state of the E285Q mutant. The NBD2 itself seems not to be inhibited by GdmCl

Tab. 4.7: Influence of the presence of 5 mM GdmCl on the enzymatic constants of $Hsp104_{WT}$ and its ATPase mutants.

Hsp104 Protein	$K_{M\,(ATP)}$ [mM]	k_{cat} [ATP/min]	Hill Coefficient *h*	Referring Figure
WT	7.3 ± 0.5	61.8 ± 2.3	1.45 ± 0.07	Fig. 4.24
WT + GdmCl	3.0 ± 0.1	23.9 ± 0.5	1.33 ± 0.07	
K620T	9.2 ± 0.2	14.2 ± 0.2	3.82 ± 0.14	Fig. 4.25.A/B
K620T + GdmCl	4.5 ± 0.1	5.6 ± 0.1	2.45 ± 0.17	
K620T (LS)	4.0 ± 0.1	15.8 ± 0.2	2.77 ± 0.14	Fig. 4.25.C/D
K620T + GdmCl (LS)	1.73 ± 0.05	7.0 ± 0.1	1.97 ± 0.11	
E285Q	4.6 ± 0.1	169.3 ± 2.5	3.13 ± 0.14	Fig. 4.26.A/B
E285Q + GdmCl	3.9 ± 0.1	210.6 ± 2.5	2.86 ± 0.11	
E687Q	0.94 ± 0.05	63.3 ± 1.3	1.77 ± 0.13	Fig. 4.26.C/D
E687Q + GdmCl	0.62 ± 0.03	36.4 ± 0.6	1.56 ± 0.11	

and its activation can be considered as a consequence of GdmCl effect on NBD1.
The E687Q mutant of Hsp104 is inhibited by GdmCl and exhibits inhibition kinetics with a striking similarity to the uncompetitive inhibition of wild-type protein. Again, K_M and k_{cat} are reduced in about the same extent giving rinse to parallel lines in the Lineweaver-Burk plot. However, the factor of inhibition is found to be ~1.6, which is smaller than the observed factor of $Hsp104_{WT}$ (2.5). It has to be considered that this mutant has only one ATP-hydrolyzing domain: NBD1. The data clearly demonstrate that NBD1 is the targeted domain of the GdmCl inhibition. The similarity to the inhibition of wild-type protein provides further evidence that NBD1 constitutes the active ATPase domain during steady-state of $Hsp104_{WT}$, an assumption made in chapter 4.4.

4.5.8 GdmCl alters the affinity of Hsp104 for unfolded polypeptides

The ATPase analysis above showed that GdmCl strongly influences the ATPase of Hsp104 under steady-state conditions. However, the information gained on the ATPase alone has only a limited relevance with respect to the key function of Hsp104 function – the refolding of denatured proteins. In order to study the ATPase activity of Hsp104 under refolding conditions a permanently unfolded protein was added to the ATPase assay. Bovine α-lactalbumin that had been reduced and carboxymethylated (RCMLa) is a permanently unfolded protein (Ewbank and Creighton, 1993). Here it served as a substrate for Hsp104. RCMLa binds exclusively to Hsp104·ATP, a species that transiently exists under steady-state conditions (Bösl *et al.*, 2005). Especially NBD1 has to be present in its ATP-bound state for substrate binding (Schaupp *et al.*, 2007). Fig. 4.27 shows that RCMLa stimulates the ATP turn-over of $Hsp104_{WT}$, which is in good agreement with previous results indicating that RCMLa stimulates the ATPase activity of Hsp104 about 2- to 3-fold (Cashikar *et al.*, 2002). The stimulation shows a $K_{½\,(RCMLa)}$ of ~25 µM. The addition of GdmCl inhibits the ATP turn-over of the complex Hsp104·RCMLa and eliminates the activation by RCMLa: the relative extent of inhibition increases with the increasing RCMLa concentration. Concurrently, $K_{½\,(RCMLa)}$ is reduced to 14 µM. The higher affinity for the protein substrate might be explained as follows: if more subunits of NBD1 are occupied by ATP it is more likely that a substrate molecule can bind to Hsp104 (Schaupp *et al.*, 2007). GdmCl reduces the turn-over of the ATPase but also increases the affinity of NBD1 for nucleotides. Thus, the state that is competent for binding to unfolded proteins, Hsp104·ATP, becomes more populated; this effect of GdmCl on NBD1 increases the apparent affinity for unfolded proteins. Interestingly, the acceleration of the ATPase activity by RCMLa is lost in the presence of GdmCl, indicating that the substrate interaction became non-functional.

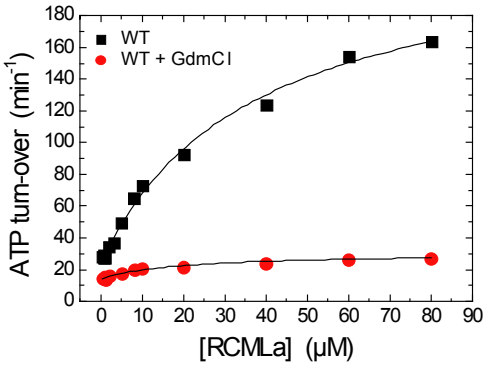

Fig. 4.27: Influence of RCMLa on the ATP turn-over of $Hsp104_{WT}$ with and w/o addition of GdmCl. ATP turn-over of 0.5 µM Hsp104 was determined at increasing RCMLa concentrations in standard assay buffer using a regenerating assay system at 30°C. Data were fitted by Eq. 3.3. and yielded $K_{½\,(RCMLa)}$ of ~25 µM for pure Hsp104 and $K_{½\,(RCMLa)}$ of ~14 µM for Hsp104+GdmCl.

It can thus be concluded that GdmCl is no inhibitor of the substrate interaction, but rather increases the number of bound ATP molecules while at the same time inhibiting the ATPase function so that ATP will remain bound to Hsp104 without being hydrolyzed. The result is a less functional ATPase of Hsp104 and possibly a non-functional chaperone.

4.5.9 Luciferase refolding by Hsp104 is strongly affected by the presence of GdmCl

In 1998 Glover and Lindquist demonstrated the refolding activity of a chaperone system consisting of Hsp104, Hsp70, and Hsp40 (Glover *et al.*, 1998). This milestone publication suggested a disaggregation function of Hsp104 *in vitro*. In the refolding assay, denatured firefly luciferase was incubated with the molecular chaperones in the presence of 5 mM ATP and an ATP regenerating system. Interestingly, Glover noticed the inhibition of the ATPase activity of Hsp104 by a low residual concentration of GdmCl present in refolding reactions following the addition of the unfolded substrate. He recommended using urea instead of GdmCl to unfold luciferase prior to the refolding by Hsp104. Indeed, urea was also used in this study to obtain unfolded luciferase as a refolding substrate for Hsp104; the luciferase refolding assay was used to assess the refolding activity of Hsp104 with the addition of different GdmCl concentrations, as shown in Fig. 4.28. The presence of 5 mM GdmCl in the luciferase assay strongly reduces the refolding velocity, which is the observed slope, but also the total yield of reactivated luciferase (see Fig. 4.28). The presence of 10 mM GdmCl completely abolishes the Hsp104-dependent refolding. In contrast, however, GdmCl does not affect the poor refolding by the Hsp70/40 system on its own (data not shown). Lu and Cyr showed that GdmCl-denatured luciferase could be renatured by Ydj1/Hsp40 and Ssa1/Hsp70 (Lu and Cyr, 1998) and studies on the analogous bacterial ClpB/KJE system never reported of a GdmCl sensitivity. Further, GdmCl is used for the unfolding of ClpB/KJE substrates (Schlee and Reinstein, 2002; Zietkiewicz *et al.*, 2004; Tanaka *et al.*, 2004b) and activity problems caused by GdmCl were never reported. Thus, the reduced refolding of luciferase by GdmCl must be a consequence of the specific inhibition of Hsp104 ATPase activity.

Luciferase refolding shows a maximum plateau that is reached when PEP is exhausted and ATP depletion starts. This form of the kinetics is based on the ATPase activity of Hsp104 and – in turn – it also affects the refolding function Hsp104. The other chaperone Hsp70 exhibits a significantly smaller K_M and is not as sensitive to energy depletion as Hsp104 (Hsp104: K_M = ~7 mM ATP (this work) and Hsp70: K_M = ~0.2 µM ATP (Wegele *et al.*, 2003). In the presence of 5 mM GdmCl the refolding plateau is reduced by a factor of 1/3 and it is observed later in the refolding assay. This shape of the refolding kinetics is due to the reduced ATP turn-over of Hsp104 in the presence of GdmCl. ATP consumption by Hsp104 is significantly reduced and the energy reservoir lasts longer. However, the overall refolding yield of free Hsp104 is not reached and higher GdmCl concentrations even completely abolish the refolding although the ATPase data confirm that a residual ATPase activity remains. These results show that GdmCl not only reduces the ATP turn-over and thereby the efficiency of refolding but also disturbs Hsp104 beyond its ATPase activity. Rather, GdmCl is a potent inhibitor of the refolding *per se*. One might argue that the binding of GdmCl to Hsp104 leaves the enzyme to be an intact hexamer, which exhibits a non-functional ATPase activity and which is furthermore allosterically hindered so that it can fulfill its refolding function merely partially. It is also possible that luciferase might become irreversibly trapped by the complex Hsp104·ATP·GdmCl, which exhibits both a higher ATP affinity and a higher substrate affinity (see above).

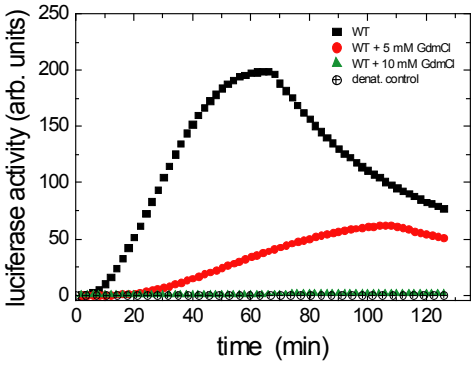

Fig. 4.28: Luciferase refolding by the Hsp104, Hsp70, and Hsp40 chaperone system in the presence of GdmCl. 2.5 µM of each chaperone, $Hsp104_{WT}$, Hsp70, and Hsp40, were used to refold urea-denatured luciferase using an ATP regenerating system with 5 mM ATP and 10 mM PEP at 25°C. These samples contained additionally the indicated GdmCl amounts or no GdmCl. Denatured luciferase w/o addition of chaperones or GdmCl served as a negative control.

4.6 The yeast cyclophilin Cpr6 is a cochaperone of Hsp104

4.6.1 The quest for Hsp104 cofactors

The disaggregation function of Hsp104 strongly relies on the assistance of the Hsp70/40 chaperone system (Glover *et al.*, 1998). The combination of these molecular chaperones is the *sine qua non*, the absolute condition, for effective disaggregation of denatured polypeptides. However, the so-called cochaperones persist in a functional interplay; none of them was found to be associated with Hsp104. Generally, no directly interacting cofactor of Hsp104 has been identified so far, although it is possible that Hsp104 might be associated with some regulatory cofactors *in vivo*.

For example, several related Clp ATPases form complexes with specific adaptor proteins, e.g., the stringent starvation protein B, SspB, binds to the ATPase ClpX (Levchenko *et al*., 2000; Flynn *et al*., 2001), the adaptor protein ClpS binds to the ATPase ClpA (Dougan *et al*., 2002b), and the adaptor protein MecA binds to the ATPase ClpC (Turgay *et al*., 1997). These adaptor proteins modulate the substrate specificity or the chaperone activity of the bound Clp ATPases. Hence, activity modulation by specific cofactors is a common feature of the Clp protein family whereas the solo attempt by Hsp104 and ClpB represents an exception (Dougan *et al.*, 2002a).

Furthermore, Hsp104 displays an unaccountable high ATPase activity *in vitro* (see chapter 4.4.1). Therefore, it can be assumed that Hsp104 might need a down-regulation *in vivo* in order to ensure an energetically efficient disaggregation. A potential cofactor might simply have the function of reducing an unnecessary ATP consumption by avoiding that the Hsp104 apparatus runs idle without substrate. Also, the analysis of the substrate interaction of Hsp104 revealed that the ATP-state of NBD1 is crucial for initial substrate contact (Bösl *et al.*, 2005). This nucleotide binding domain has a very high ATP turn-over *in vitro*, and a factor down-regulating the ATP turn-over *in vivo* might improve the efficiency of substrate binding by populating the NBD1-ATP state.

In 2001, the group of Picard showed by co-immunoprecipitations that some cofactors of Hsp90 are associated with Hsp104. Sti1, Cpr7, and Cns1 form complexes with Hsp104 *in vivo* under respiratory growth conditions (Abbas-Terki *et al*., 2001). These proteins utilize tetratricopeptide repeat (TPR) domains to interact with the acidic C-terminus of Hsp90.

Remarkably, Hsp104 contains a C-terminal acidic sequence, IDDDLD, which is similar to the TPR protein binding motif of Hsp90, MEEVD (D'Andrea *et al.*, 2003). Fig. 4.29 presents a multiple sequence alignment of Hsp100/Clp proteins and Hsp90/HtpG proteins. Both eukaryotic protein families, Hsp100 and Hsp90, contain a C-terminal acidic extension, which is missing in the corresponding prokaryotic members. This striking similarity had already been noticed when Hsp104 was introduced by Parsell and coworkers (Parsell *et al.*, 1991). It is established that the MEEVD sequence serves as TPR protein interaction motif of eukaryotic Hsp90 proteins, which is missing in the prokaryotic members of HtpG

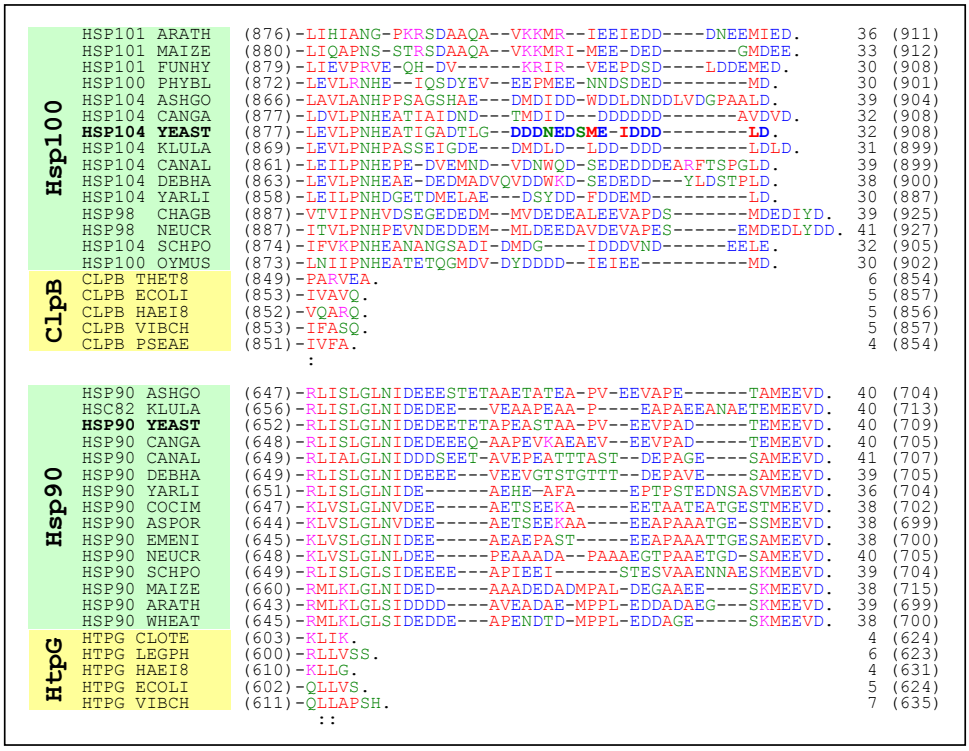

Fig. 4.29: The C-terminus of eukaryotic Hsp104 and Hsp90 – but not of prokaryotic ClpB and HtpG – contains an acidic motif. Multiple sequence alignment of the C-terminal region of Hsp100/ClpB proteins and Hsp90/HtpG proteins. The alignment was carried out by the ClustalW tool, provided by EMBL-EBI, independently for both the set of C-termini of Hsp104/ClpB proteins, and for the set of C-termini Hsp90/HtpG proteins. The amino acids are depicted in different colors dependent on their chemical nature: basic in pink, acidic in blue, polar and non-charged in green, and hydrophobic in red. Eukaryotic and prokaryotic sequences can be clearly distinguished by the differing lengths of the C-termini. Eukaryotic members of both heat shock protein families carry a negatively charged C-terminal extension. A truncation mutant of Hsp104, $Hsp104_{893\Delta C}$, was constructed based on this alignment. It is lacking the very C-terminal amino acids depicted in bold letters within the Hsp104 sequence, see the following chapter.
The following Hsp100/ClpB proteins were selected for the alignment: HSP101 ARATH: P42730 - *Arabidopsis thaliana*, HSP101 MAIZE: Q6RYQ7 - *Zea mays*, HSP101 FUNHY: Q2VDS9 - *Funaria hygrometrica*, HSP100 PHYBL: Q96TW3 - *Phycomyces blakesleeanus*, HSP104 ASHGO: Q750I7 AGL036Cp - *Ashbya gossypii*, HSP104 CANGA: Q6FTB3 - *Candida glabrata*, HSP104 YEAST: P31539 - *Saccharomyces cerevisiae*, HSP104 KLULA: Q6CJJ3 - *Kluyveromyces lactis*, HSP104 CANAL: Q96W69 - *Candida albicans*, HSP104 DEBHA: Q6BQM2 - *Debaryomyces hansenii*, HSP104 YARLI: Q6C4C2 - *Yarrowia lipolytica*, HSP98 CHAGB: Q2H8W3 - *Chaetomium globosum*, HSP98 NEUCR: P31540 - *Neurospora crassa*, HSP104 SCHPO: O94641 - *Schizosaccharomyces pombe*, HSP100 OYMUS: Q9UVM4 - *Pleurotus sajor-caju*, CLPB THET8: Q9RA63 - *Thermus thermophilus*, CLPB ECOLI: P63284 - *Escherichia coli*, CLPB HAEI8: Q4QM42 - *Haemophilus influenza*, CLPB VIBCH: Q9KU18 - *Vibrio cholerae*, CLPB PSEAE: Q9HVN5 - *Pseudomonas aeruginosa*.
The following Hsp90/HtpG proteins were selected for the alignment: HSP90 ASHGO:, Q8J2M3 - *Ashbya gossypii*, HSC82 KLULA: Q6CQZ9 - *Kluyveromyces lactis*, HSP90 YEAST: P02829 - *Saccharomyces cerevisiae*, HSP90 CANGA: Q6FLU9 - *Candida glabrata*, HSP90 CANAL: P46598 - *Candida albicans*, HSP90 DEBHA: Q6BSA2 - *Debaryomyces hansenii*, HSP90 YARLI: Q6CCN4 - *Yarrowia lipolytica*, HSP90 COCIM: Q1DY84 - *Coccidioides immitis*, HSP90 ASPOR: Q2U9Y1 - *Aspergillus oryzae*, HSP90 EMENI: Q5ATW1 - *Emericella nidulans*, HSP90 NEUCR: Q9C2E7 - *Neurospora crassa*, HSP90 SCHPO: P41887 - *Schizosaccharomyces pombe*, HSP90 MAIZE: Q08277- *Zea mays*, HSP90 WHEAT: Q9XGF1- *Triticum aestivum*, HSP90 ARATH: P55737- *Arabidopsis thaliana*, HTPG CLOTE: Q894P6 - *Clostridium tetani*, HTPG LEGPH: Q5ZVS1 - *Legionella pneumophila*, HTPG HAEI8: Q4QP81 - *Haemophilus influenzae*, HTPG ECOLI: P0A6Z3 - *Escherichia coli*, HTPG VIBCH: P22359 - *Vibrio colerae*.

(Pearl *et al.*, 2006). For Hsp100 proteins no function has yet been defined for the C-terminal tail but its phylogenetic occurrence is similar to that of Hsp90. Although it seems to be less conserved, it might also serve as a TPR protein docking motif. For this reason, it is very likely that the co-immunoprecipitations of Hsp90 cofactors and Hsp104, which was performed by Picard and coworkers, are mediated by a TPR interaction (Abbas-Terki *et al.*, 2001). This potential TPR protein interaction offers a new perspective: Hsp104 might recruit its cofactors from the Hsp90 cofactor pool in yeast.

4.6.2 Cpr6 is a potential cofactor of Hsp104

Some TPR cofactors interfere with the ATPase activity of Hsp90 and the binding can be indirectly monitored by a change in ATP turn-over. For example, Sti1 reduces the ATPase activity of Hsp90 (Richter *et al.*, 2003). It is conceivable that a possible interaction of these factors with Hsp104 might also lead to an altered turn-over of the ATPase. In order to analyze such a possibility, ATPase assays were carried out in the presence of several TPR proteins that are known as Hsp90 cochaperones: Sti1/Hop, Cns1, Sgt2, Cpr6, and Cpr7. Since these cofactors have no intrinsic ATPase activity (data not shown), the observed ATP hydrolysis can be completely accounted to Hsp104. Fig. 4.30 shows the influence of Hsp90 cochaperones on the ATP turn-over of Hsp104. Of the five tested cochaperones, only Cpr6 displayed a marked effect on the ATP hydrolysis. It decreases the ATP turn-over of Hsp104 by ~70%, from 38 min^{-1} to 13 min^{-1}. Cpr6, the cyclophilin 6, consists of an N-terminal peptidyl-prolyl isomerase (PPIase) domain and a TPR domain (Duina *et al.*, 1996a). It was not reported by Picard and coworkers that Cpr6 associates with Hsp104, however, they did not include Cpr6 in their Co-IP analysis (Abbas-Terki *et al.*, 2001).

The inhibitory effect of Cpr6 persisted in the presence of cyclosporine A, a cyclophilin-specific inhibitor affecting the PPIase function of Cpr6 (data not shown), indicating that Hsp104 is not recognized as a Cpr6 substrate for peptidyl-prolyl isomerization. Therefore, it can be assumed that Cpr6 specifically interacts with Hsp104 and does not act as PPIase on it.

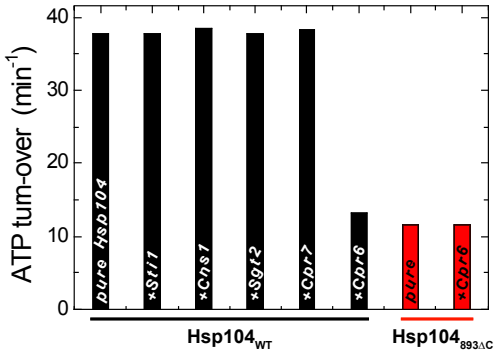

Fig. 4.30: Effect of Hsp90 cofactors on the ATP turn-over of Hsp104. 0.5 µM $Hsp104_{WT}$ was incubated with 5 µM of the indicated cofactors and the ATP turn-over was measured in the presence of 5 mM ATP using the regenerating ATPase assay. Sti1, Cns1, Sgt2, Cpr7, and Cpr6 contain at least one TPR domain. As a control, the mutant $Hsp104_{893\Delta C}$, depicted in red, which is lacking the putative cofactor interaction domain at its C-terminus, was additionally analyzed similar to wild-type with and w/o the presence of 5 µM Cpr6. All measurements were carried out at 30°C in LS assay buffer.

However, it is still not possible to tell from this data alone whether or not Cpr6 is a specific Hsp104 cofactor. Moreover, the observation that only Cpr6 affects the ATPase activity of Hsp104 does not exclude that the other tested TPR cofactors might exhibit a *silent* interaction with Hsp104.

In order to further investigate whether or not Cpr6 is a specific cofactor of Hsp104, a C-terminally truncated mutant of Hsp104, $Hsp104_{893\Delta C}$, was prepared. This mutant lacks the very last C-terminal residues, DDDNEDSMEIDDDLD, which are containing the putative TPR cofactor binding site. Interestingly, $Hsp104_{893\Delta C}$ exhibits a reduced intrinsic ATPase activity in comparison to $Hsp104_{WT}$. The truncation is quite small and is located in the less conserved C-terminal region outside of any nucleotide binding domain. The truncation does not affect the oligomerization state, as determined by AUC (see Appendix A.4). In contrast to full length Hsp104, $Hsp104_{893\Delta C}$ was not affected by Cpr6. The low ATP turn-over by $Hsp104_{893\Delta C}$ remains unexpected, but the data demonstrate that the C-terminus of Hsp104 is required for the Cpr6 effect.

4.6.3 Cpr6 specifically modulates the ATPase activity of Hsp104 *in vitro*

The influence of Cpr6 on the ATPase activity of Hsp104 was analyzed by varying the concentration of the cofactor, and by examining the dependency of the turn-over number on the presence of Cpr6 (see Fig. 4.31). Hsp104 exhibits a detectable decrease in the ATPase activity in the presence of Cpr6 concentrations as low as 0.5 µM. However, it only drops to ~9 min^{-1}, which is ~22% of the initial turn-over, even at saturating concentrations of Cpr6. Thus, Cpr6 does not completely abolish the ATP hydrolysis of Hsp104. The inhibition yielded a $K_{½\,(Cpr6)}$ of 2.0 µM.

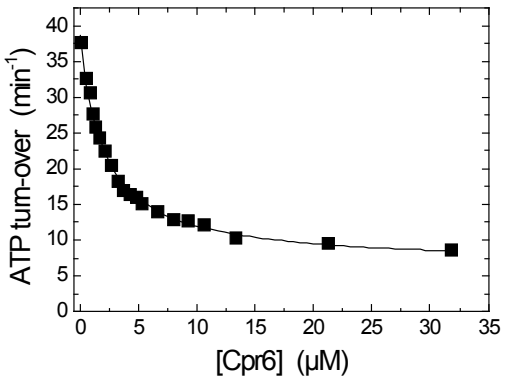

Fig. 4.31: An increase in the Cpr6 concentration reduces the ATP turn-over of Hsp104. 0.5 µM $Hsp104_{WT}$ were incubated with increasing concentrations of Cpr6 and the ATP turn-over was measured in the presence of 5 mM ATP. The data were fitted by Eq. 3.3 and yielded a $K_{½\,(Cpr6)}$ of ~2 µM. The measurements were carried out using the LS assay buffer.

The analysis of the ATP dependency at a constant Cpr6 concentration of 10 µM reveals a Michaelis-Menten-like profile with a decreased k_{cat}, and an increased apparent K_M of ~5 mM; both changed by a factor of 2 in comparison to free Hsp104 (see Fig. 4.32 and Tab. 4.8). Thus, Cpr6 acts as a non-competitive inhibitor of the ATPase activity of Hsp104, as also demonstrated by the Lineweaver-Burk presentation in which the linear fits cross at y = 0 min. Cpr6 specifically alters the enzymatic properties of Hsp104 resulting in a decreased Hill coefficient *h*, which refers to a reduced cooperativity. Cpr6 may affect ATP hydrolysis by stabilizing a less active conformation of Hsp104 and/or by reducing domain mobility in the Hsp104 hexamer.

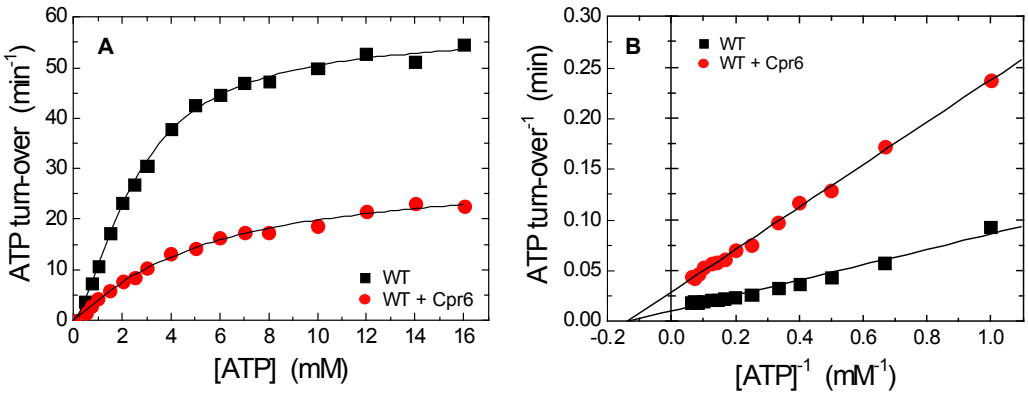

Fig. 4.32: ATP dependency of Hsp104 with and w/o addition of Cpr6, (A) Michaelis-Menten plot and (B) double-reciprocal Lineweaver-Burk plot. ATP turn-over of 0.5 µM Hsp104 was determined at increasing ATP concentrations with and w/o the presence of 10 µM Cpr6 in KM-LS buffer using a regenerating assay system at 30°C. Data were fitted by the Hill equation (Eq. 3.12). The lines in (B) represent least-square-fits of the data of (A). The data showed a Cpr6-dependent change of k_{cat} and K_M by a factor of 2.

Tab. 4.8: Influence of the presence of Cpr6 on enzymatic constants of $Hsp104_{WT}$.

Protein	$K_{M\,(ATP)}$ [mM]	k_{cat} [ATP/min]	Hill Coefficient *h*
WT	2.6 ± 0.1	56.7 ± 0.8	1.54 ± 0.06
WT + Cpr6	5.2 ± 0.7	29.4 ± 1.9	1.12 ± 0.08

4.6.4 Cpr6 binds to Hsp104 *in vitro*

As demonstrated above, Cpr6 interacts functionally with Hsp104. It specifically reduces its ATPase activity. To obtain a more detailed picture of this relationship, the interaction of Cpr6 and Hsp104 was directly studied using biophysical techniques. ITC titrations were not possible due to a lack of a sufficient binding signal (data not shown). Apparently, the binding of Cpr6 to Hsp104 causes only very small changes in enthalpy. A SEC-HPLC analysis was also not satisfying: only a very small, non significant amount of Cpr6 was found to co-elute with Hsp104 (data not shown) indicating that the complex Hsp104·Cpr6 either has a low stability or exists only transiently during a specific enzymatic state of Hsp104. Nevertheless, the equilibrium methods analytical ultracentrifugation (AUC) and fluorescence anisotropy were successfully employed to detect and to study Hsp104·Cpr6 complex formation.

4.6.4.1 Analysis of the Hsp104·Cpr6 complex by analytical ultracentrifugation

AUC was applied to monitor the binding of fluorescein-labeled Cpr6 to Hsp104 under equilibrium conditions. Fig. 4.33 shows the results of sedimentation velocity experiments of both proteins with detection at two different wavelengths. Hexameric Hsp104 with ~600 kDa quickly moves towards the bottom of the sample cell. It thereby exhibits a sedimentation profile at λ_{280} corresponding to its high sedimentation coefficient of 16 S, which corresponds to the hexamer (see Fig. 4.33.A). However, at λ_{494} it remains invisible (see the blue data set). In contrast, monomeric $Cpr6_{FITC}$ with ~40 kDa moves much slower to the bottom of the cell and exhibits a smaller sedimentation coefficient of 3 S, as determined by both the sedimentation profile at λ_{280} and at λ_{494} (see Fig. 4.33.B). The huge size difference between Hsp104 and $Cpr6_{FITC}$ is of advantage in a co-sedimentation experiment, see Fig. 4.33.C: the mixture of both proteins reveals a combined sedimentation profile at λ_{280}, as it can be expected from a two-component mixture. In contrast, the profile at λ_{494} reveals that a small fraction of $Cpr6_{FITC}$ sediments as it would be expected from high molecular weight species of ~16 S (shown by a red arrow) although Cpr6 has a molecular weight of only ~40 kDa. This demonstrates that $Cpr6_{FITC}$ interacts physically with Hsp104. The relative amount of Hsp104-bound $Cpr6_{FITC}$ is relatively small in comparison to the total $Cpr6_{FITC}$ signal, indicating that only a minor fraction of $Cpr6_{FITC}$ actually binds to Hsp104 under these conditions. Free $Cpr6_{FITC}$ and Hsp104·$Cpr6_{FITC}$ can be distinguished easily by their significant difference in molecular weight to analyze the complex formation.

The co-sedimentation experiments were performed in the presence of 0.5 mM ATPγS to ensure 100% of the Hsp104 exists in a hexameric form. It is known that ATPγS also induces substrate binding of Hsp104 (Bösl *et al.*, 2005). In order to strictly exclude that the complex formation takes place *via* a substrate interaction, $Hsp104_{K218T}$ was used for a co-

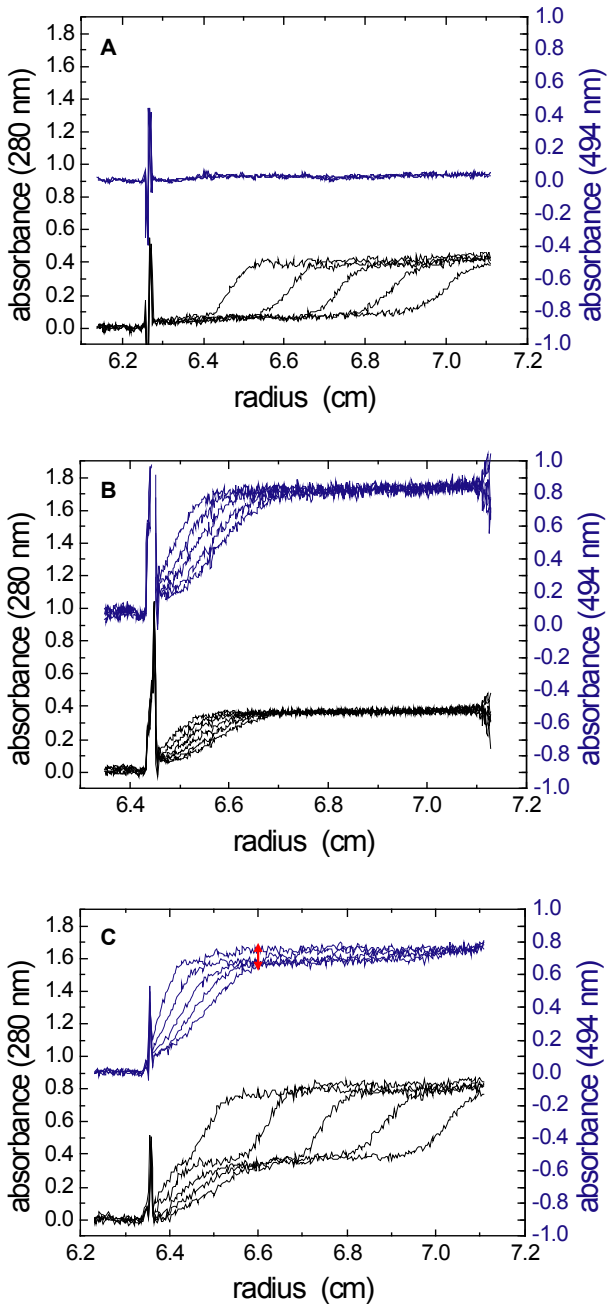

Fig. 4.33: Sedimentation profiles of (A) Hsp104, (B) Cpr6$_{FITC}$ and (C) Hsp104 + Cpr6$_{FITC}$ detected at λ_{280} and λ_{494}. The detection at λ_{494}, shown in blue, selectively monitors the sedimentation profile of Cpr6$_{FITC}$, whereas the detection at λ_{280}, shown in black, monitors the sedimentation profile of both proteins. 10 µM Hsp104$_{WT}$ and/or 30 µM Cpr6$_{FITC}$ were spun in an analytical ultracentrifuge at 40,000 rpm in LS assay buffer with 0.5 mM ATPγS at 25°C. Scans were recorded at both wavelengths with a time interval of 5 min.

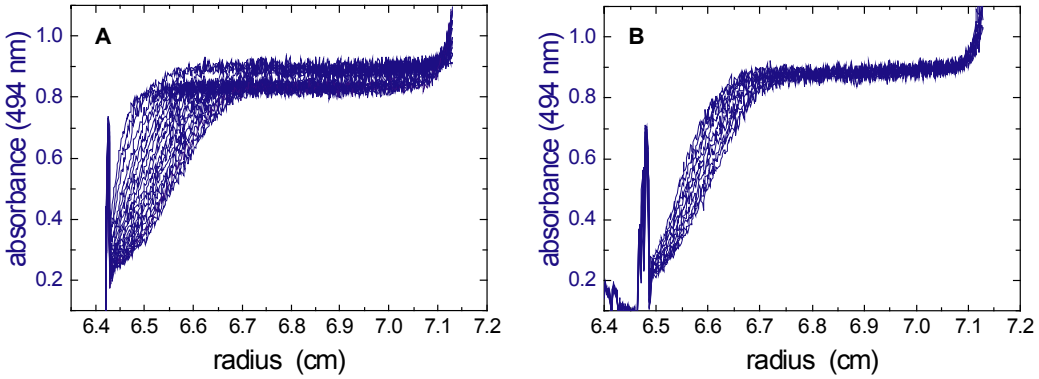

Fig. 4.34: Sedimentation profiles of $Cpr6_{FITC}$ with addition of (A) $Hsp104_{K218T}$ and (B) $Hsp104_{893\Delta C}$. The absorption was detected at λ_{494}, selectively monitoring the sedimentation profile of $Cpr6_{FITC}$. 30 µM $Cpr6_{FITC}$, 10 µM $Hsp104_{K218T}$ or 10 µM $Hsp104_{893\Delta C}$, and 5 mM ATPγS for (A) or 0.5 mM ATPγS for (B) were spun in an analytical ultracentrifuge at 40,000 rpm in LS assay buffer at 25°C. Scans were recorded with a time interval of 150 s. The sedimentation profile of $Cpr6_{FITC}$ appears to be slightly different from those of the previous figure, which is due to different scanning intervals.

sedimentation experiment in the presence of 5 mM ATPγS. This mutant is not able to interact with polypeptide substrates since it is incompetent for nucleotide binding to NBD1, a crucial prerequisite for substrate binding (Bösl *et al.*, 2005). $Hsp104_{K218T}$ co-sedimented with $Cpr6_{FITC}$ similar to $Hsp104_{WT}$ indicating that no substrate interaction is responsible for the complex formation (see Fig. 4.34.A). In an additional control experiment $Hsp104_{893\Delta C}$, the mutant which is lacking the putative Cpr6 binding site was analyzed. $Hsp104_{893\Delta C}$ showed no co-sedimentation with $Cpr6_{FITC}$, as demonstrated in Fig. 4.34.B. Clearly, the complex formation between Cpr6 and Hsp104 is not due to substrate interactions and is dependent on the C-terminus of Hsp104.

A series of co-sedimentation experiments of $Hsp104_{WT}$ and $Cpr6_{FITC}$ revealed that an increase in the concentration of $Cpr6_{FITC}$ at a constant Hsp104 level increases the relative yield of the high molecular weight species, the Hsp104-bound $Cpr6_{FITC}$. The amount of the high molecular weight complex $Hsp104{\cdot}Cpr6_{FITC}$ was quantified and plotted against the total $Cpr6_{FITC}$ concentration, as shown in Fig. 4.35. Assuming one Cpr6 binding site per Hsp104 monomer, the yield of Hsp104-bound Cpr6 converges but does not reach a full saturation under the experimental conditions. The complex amount remains to be below the applied Hsp104 concentration of 10 µM. Even at extremely high Cpr6 concentrations of more than 60 µM, which is no longer a physiological condition, no saturation of all Hsp104 molecules can be detected. In contrast, $K_{½\ (Cpr6)}$, detected enzymatically, was found to be ~2.0 µM (see Fig. 4.31). It can be assumed that a sub-stochiometrical ratio of Cpr6, e.g., $(Hsp104)_6{\cdot}(Cpr6)_1$, is sufficient to alter the enzymatic properties of Hsp104 in the ATPase assay. However, such a primary complex will not be distinguishable from more saturated complexes, such as $(Hsp104)_6{\cdot}(Cpr6)_{1+x}$, by using AUC. The accuracy and specificity of this

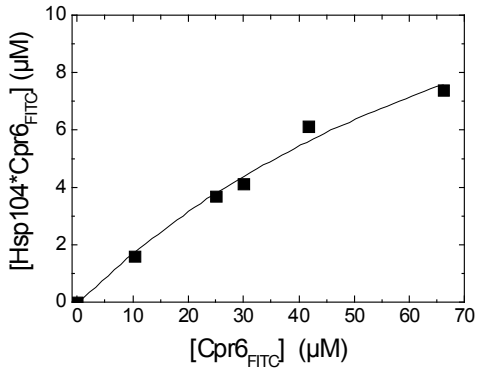

Fig. 4.35: Co-sedimentation analysis of Hsp104 and $Cpr6_{FITC}$. The complex quantity of $Hsp104{\cdot}Cpr6_{FITC}$ was determined using 10 µM $Hsp104_{WT}$ in the presence of increasing $Cpr6_{FITC}$ concentrations. The protein mixtures were analyzed by sedimentation velocity experiments at a detection wavelength of λ_{494} at 40,000 rpm in LS assay buffer with 0.5 mM ATPγS at 25°C. Scans were recorded with a time interval of 150 s. The Hsp104-bound $Cpr6_{FITC}$, which can be clearly distinguished from free $Cpr6_{FITC}$, was determined from the sedimentation profile and plotted against the total $Cpr6_{FITC}$ concentration.

experiment is too low to monitor the population of the different complex species, $(Hsp104)_6{\cdot}(Cpr6)_{1+x}$.

However, the fact that a full saturation in the AUC analysis could not be achieved even by using very high and non-physiological Cpr6 concentrations demonstrates that a full saturation is hardly possible and that an Hsp104 hexamer will probably not bind to 6 Cpr6 molecules at a physiological concentration of the cofactor. The physiological concentration of both proteins is unknown but the total molecule numbers of a lag-phase growing yeast cell are available, as follows: ~19,000 molecules Cpr6 per cell correspond to an minimal overall concentration 0.5 µM Cpr6 and ~33,000 molecules Hsp104 per cell correspond to an minimal overall concentration of 0.8 µM Hsp104 (Ghaemmaghami *et al.*, 2003) if the cytosol volume were equal to the total cell volume (cf. Tab.2.1 and footnote 2 on page 19). However, the real cytosol volume is only a fraction of the total cell volume. Estimating the cytosol to be 1/5 of the total cell volume, the estimated basal concentrations of Hsp104 and Cpr6 must be 5-fold higher. Moreover, both Cpr6 and Hsp104 are 6 - 8-fold up-regulated at stress conditions (Gasch *et al.*, 2000). Thus, both proteins might be present at cytosolic concentrations between 15 and 40 µM under stress conditions, which is still not enough to generate a $(Hsp104)_6{\cdot}(Cpr6)_6$ complex.

4.6.4.2 Analysis of the Hsp104·Cpr6 complex by fluorescence anisotropy

Fluorescence anisotropy is a more sensitive equilibrium method to detect complex formation than the co-sedimentation experiments shown above. The detection of fluorescence anisotropy also depends on a fluorescent chromophore and, hence, only labeled proteins can be studied. An increased anisotropy signal of the analyzed protein corresponds to an increase in the hydrodynamic radius of the particle. Lucifer yellow-labeled Cpr6, $Cpr6_{LUY}$, showed a change in its anisotropy signal from 0.14 to 0.17 when $Hsp104_{WT}$ hexamers were added to the cuvette, see arrow in Fig. 4.36. It can be assumed that complex formation is responsible

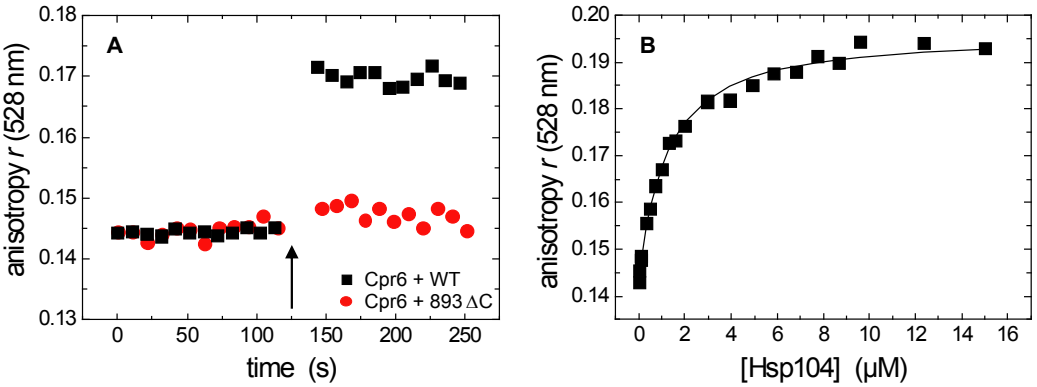

Fig. 4.36: Binding of $Cpr6_{LUY}$ to Hsp104 as monitored by fluorescence anisotropy. (A) Lucifer yellow-labeled Cpr6 (0.5 µM) was incubated in a fluorescence spectrometer equipped with polarizers. After recording the anisotropy of free $Cpr6_{LUY}$, 1 µM $Hsp104_{WT}$ or $Hsp104_{893\Delta C}$ were added at the time point indicated by the arrow. (B) 0.5 µM $Cpr6_{LUY}$ was titrated with $Hsp104_{WT}$ and binding was monitored by the increase in fluorescence anisotropy at 528 nm. The line represents a non-linear least squares fit in accordance with Eq. 3.4. All experiments were carried out in LS assay buffer at 25°C. It should be noted that the Hsp104 concentration is always given as a monomer concentration. Each Hsp104 protomer contains an acidic C-terminal motif, which is the putative Cpr6 binding site. However, is it not known how many Cpr6 binding sites are accessible in an Hsp104 hexamer. Thus, the addition of a certain amount of Hsp104 molecules might not correspond to the same amount of binding sites in this titration.

for the signal change since the rotational mobility of $Cpr6_{LUY}$ is reduced due to its sequestration in the $(Hsp104)_6{\cdot}(Cpr6_{LUY})$ complex. The addition of ATP, ADP, and ATPγS had no influence on the resulting signal of the complex of $Cpr6_{LUY}$ and $Hsp104_{WT}$ (data not shown). When the $Hsp104_{893\Delta C}$ mutant was used instead, the anisotropy signal remained unchanged demonstrating that no binding occurs. This result verifies the specificity of the anisotropy data and confirms that the C-terminus of Hsp104 is required for the interaction with Cpr6. Further, the experimental setup was used to quantify the complex formation between $Cpr6_{LUY}$ and $Hsp104_{WT}$ (see Fig. 4.36.B).

It has to be considered that no formation of an $(Hsp104)_6{\cdot}(Cpr6)_6$ complex is possible under physiological conditions, as revealed by the AUC analysis. Therefore, it can be assumed that the titration curve does not reflect the binding of 6 molecules of Cpr6 per Hsp104 hexamer, $(Hsp104)_6{\cdot}(Cpr6)_6$, but rather to a sub-stochiometrical complex such as $(Hsp104)_6{\cdot}(Cpr6)_1$. A non-linear least squares fit yielded a dissociation constant of $K_{D\ (Hsp104)}$ = 1.0 µM, with the presumption that every added Hsp104 hexamer offers 6 similar binding sites, $(Hsp104)_6{\cdot}(Cpr6)_6$. However, the previous results have shown that this model does not reflect the situation *in vivo*, since 6 Cpr6 molecules do not simultaneously bind to an Hsp104 hexamer. Consequently, this calculation of K_D is based on a borderline case. Using the other extreme case assuming one Cpr6 binding site per Hsp104 hexamer, in $(Hsp104)_6{\cdot}(Cpr6)_1$, a dissociation constant of $K_{D\ ((Hsp104)_6)}$ = 76 nM was obtained. Both fits converge the data and hence, it remains unclear whether or not the binding signal also comprises other stochiometric complexes such as $(Hsp104)_6{\cdot}(Cpr6)_{1+x}$, wherein x = 1 - 4.

In order to find out whether or not the incomplete binding of Cpr6 to Hsp104 hexamers is possibly due to a negative cooperativity of Cpr6 binding, a monomeric mutant of Hsp104, $Hsp104_{\Delta NM}$, was used in a similar titration. The 45 kDa protein is lacking the complete N-terminal half of the enzyme; it compromises only NBD2 and the C-terminus (Anne Röthig, master thesis). However, the construct still contains the potential Cpr6 binding domain and is suitable for a titration of Cpr6. Since this mutant is incompetent for hexamer formation, binding to one Cpr6 binding site will not be restricted by neighboring Cpr6 molecules. Fig. 4.37 presents the titration of Cpr6 with $Hsp104_{\Delta NM}$. The binding signal reaches only a signal of ~0.154 due to the small size difference of both proteins. A non-linear least squares fit yielded a dissociation constant of $K_{D\ (Hsp104_{\Delta NM})}$ of ~40 nM. Thus, the binding affinity of Cpr6 for monomeric Hsp104 is in the same range as the affinity for a single binding site in a wild-type hexamer, $K_{D\ ((Hsp104)_6)}$ = 76 nM (referring to $(Hsp104)_6 \cdot (Cpr6)_1$, see above).

It can therefore be assumed that Cpr6 has a high affinity for wild-type Hsp104 but once a Cpr6 molecule is bound to the Hsp104 hexamer, an addition of further Cpr6 molecules to the same hexamer is hindered and only occurs at Cpr6 concentrations higher than 10 µM (cf. AUC data). The reason for this might be a structural asymmetry of $(Hsp104)_6$. For example, only one protomer might present an accessible C-terminus. Another possible explanation would be sterical hindrance if the Cpr6-binding sites are located in a very close proximity to each other.

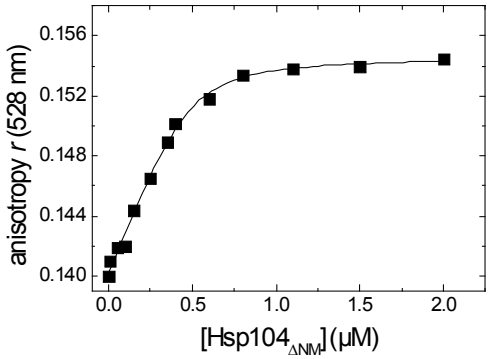

Fig. 4.37: Binding of $Cpr6_{LUY}$ to monomeric $Hsp104_{\Delta NM}$ monitored by fluorescence anisotropy. 0.5 µM $Cpr6_{LUY}$ were titrated with $Hsp104_{NM}$ and binding was monitored by the increase in fluorescence anisotropy at 528 nm. The line represents a non-linear least squares fit, cf. Eq. 3.4, yielding a dissociation constant of K_D = 40 nM. The experiment was carried out in LS assay buffer at 25°C.

4.6.5 Cpr6 can enhance protein disaggregation by Hsp104 *in vitro*

4.6.5.1 Cpr6 does not affect the Hsp104-mediated refolding of luciferase

So far, the results show that Cpr6 is a specific ligand of Hsp104 that reduces its ATP turn-over. Since ATP hydrolysis is essential for protein disaggregation (Glover *et al.*, 1998), an obvious question to ask was whether or not Cpr6 would also inhibit Hsp104-mediated disaggregation processes such as the reactivation of urea-denatured luciferase (Glover *et al.*,

1998). Surprisingly, Cpr6 had, even in 20-fold excess over Hsp104, no adverse effect on the recovery of active luciferase. Refolding rates and yields were indistinguishable from a reaction carried out in the absence of Cpr6 (see Fig. 4.38). Thus, it appears that Cpr6 is able to reduce the ATP consumption of Hsp104 by ~70% (cf. Fig. 4.31) without detrimental effects on the disaggregation activity of Hsp104. To demonstrate that the inhibition of Hsp104 can have a pronounced influence on luciferase reactivation, a refolding experiment in the presence of 10 mM guanidinium chloride, a specific inhibitor of Hsp104 that was shown to cause a ~2.5-fold reduction in ATP hydrolysis (see chapter 4.5), was performed. Indeed, there was barely any active luciferase detectable under these conditions.

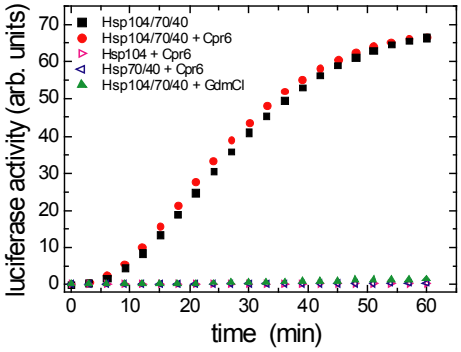

Fig. 4.38.: Cpr6 does not affect Hsp104-mediated renaturation of luciferase. Reactivation of urea-denatured firefly luciferase (55 nM) was measured at 25°C in the presence of chaperones, 5 mM ATP, and an ATP regenerating system. 0.5 µM Hsp104, 2.5 µM Hsp70, 2.5 µM Hsp40, and 10 µM Cpr6 were present in the indicated combinations. A control sample also contained 10 mM GdmCl.

4.6.5.2 Cpr6 enhances Hsp104-mediated refolding of murine DHFR

Cyclophilins such as Cpr6 have been implicated in the proper folding and maturation of some proteins of the secretory pathway (Stamnes *et al*., 1991), and are also involved in the activation of steroid hormone receptors by Hsp90 (Prodromou *et al.*, 1999). *In vitro*, Cpr6 exhibits peptidyl-prolyl *cis-trans* isomerase activity (Fischer *et al*., 1989; Mayr *et al.*, 2000). As demonstrated above, Cpr6 had no influence on the refolding of luciferase. Therefore, it was searched for another substrate for which Cpr6 could exhibit its beneficial effect on the Hsp104-mediated recovery. Murine dihydrofolate reductase (DHFR), an enzyme whose folding rate is known to be limited by peptidyl-prolyl isomerization (von Ahsen *et al*., 2000) was chosen as a substrate for a novel Hsp104 renaturation assay. Prior to the development of an Hsp104 assay it was established that Cpr6 actually improves spontaneous refolding of DHFR. Urea-denatured DHFR shows spontaneous refolding when diluting it into a thermostated cuvette with DHFR assay buffer. Within 4 minutes, the enzyme shows maximal gain of activity but it aggregates subsequently and – consequently – the activity gain decreases fast and irreversibly. The maximal gain of DHFR activity in presence of Cpr6 is shown in Fig. 4.39. Cpr6 improves the spontaneous refolding yield by ~50% but still the DHFR aggregates again. Thus, Cpr6 can only act on unfolded DHFR but not on aggregates.

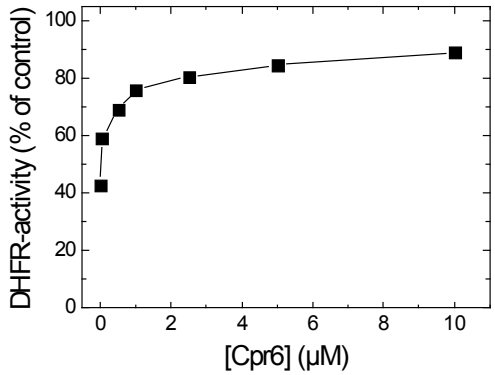

Fig. 4.39: Cpr6 promotes peptidyl-prolyl isomerization-dependent refolding of mouse DHFR. Spontaneous refolding of 1 µM unfolded mouse DHFR was determined directly by dilution from urea into DHFR assay buffer with and w/o presence of Cpr6 at 25°C. The refolding of DHFR was detected by its maximum gain of activity after 4 min refolding in DHFR assay buffer. The activity of 1 µM native DHFR was used for the normalization.

Stable renaturation requires the presence of the Hsp104/70/40 chaperone system, as shown in the assay in Fig. 4.40. Unfolded DHFR was diluted from 8 M urea into refolding buffer containing various combinations of chaperones. The refolding yield was detected by removing aliquots from the renaturation sample and measuring it for DHFR activity as above. As shown in Fig. 4.40.A, the PPIase Cpr6 alone slightly enhanced refolding in comparison to the spontaneous reaction. However, the overall yield remained low because most of the DHFR molecules aggregated. When the yeast disaggregation system consisting of Hsp104/70/40 was present during refolding, a strong increase in the recovery of DHFR was observed. But only a combination of disaggregase activity and catalysis of peptidyl-prolyl isomerization by Cpr6 provided optimal refolding conditions indicating that the complex Hsp104·Cpr6 is functional in the refolding of denatured DHFR.

Upon addition of cyclosporine A (CsA), a specific inhibitor of the PPIase activity, the beneficial influence of Cpr6 on DHFR reactivation was no longer observed (Fig. 4.40.B).

The $Hsp104_{893\Delta C}$ deletion mutant exhibited a similar refolding yield in comparison to wild-type Hsp104 although the ATP turn-over of this protein was reduced by the deletion of the C-terminus. Thus, the reduction of ATPase activity (see 4.6.2) does not result in a concomitant loss of the chaperone function of the $Hsp104_{893\Delta C}$ mutant. However, in contrast to the wild-type protein, the $Hsp104_{893\Delta C}$ mutant did not show a synergistic effect with Cpr6 demonstrating that the PPIase must be associated with the disaggregating chaperone. Thus, the lack of the Hsp104-Cpr6 interaction almost abolishes the beneficial effect of Cpr6 on the long-term refolding of DHFR.

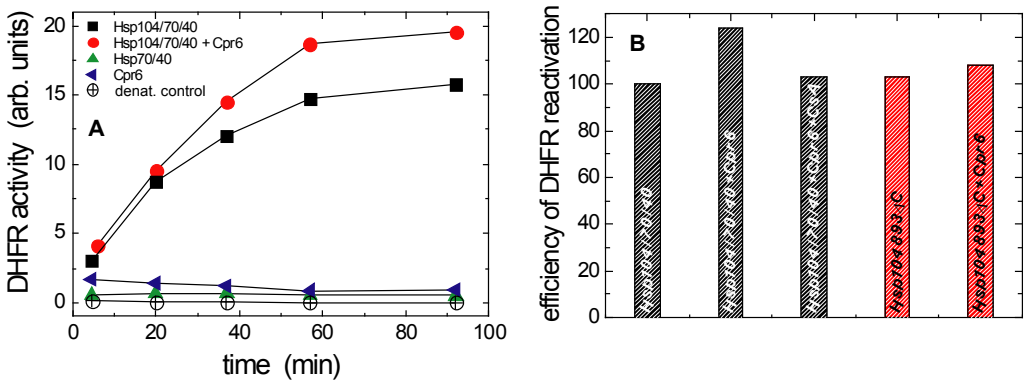

Fig. 4.40: Cpr6 enhances Hsp104-mediated renaturation of mouse DHFR. (A) Reactivation of denatured mouse DHFR (2 µM) was measured at 25°C in the presence of chaperones, 5 mM ATP, and an ATP regenerating system. 0.5 µM $Hsp104_{WT}$ or $Hsp104_{893\Delta C}$, 1 µM Hsp70, 1 µM Hsp40, and 1 µM Cpr6 were added to the indicated refolding samples. A control sample also contained 10 mM GdmCl. (B) Reactivation of DHFR was carried out as shown in the figure on the left using 1 µM Hsp70, 1 µM Hsp40, and the chaperones that are indicated in figure B. For control, 5 µM CsA were added to one sample. The yield of active DHFR after 1 h was normalized with respect to the sample containing only $Hsp104_{WT}$/Hsp70/40. The standard error was ~5%.

4.6.6 Cpr6 interacts with Hsp104 *in vivo*

4.6.6.1 Co-immunoprecipitation of Hsp104 and Cpr6

As shown above, Cpr6 interacts functionally and physically with Hsp104 *in vitro*. Both proteins form an oligomeric complex with a binding constant in the nM range. However, a biochemical analysis *in vitro* cannot address the question whether or not the Hsp104·Cpr6 complex is of functional importance *in vivo*. In Picard's screen for Hsp104 cofactors, Cpr6 had not been reported as an Hsp104 associated protein (Abbas-Terki *et al.*, 2001). Thus, it had to be analyzed that Cpr6 interacts with Hsp104 in yeast cells. For this a co-immunoprecipitation assay was established. When lysate of the yeast strain BSC783/4a expressing both Hsp104 and Cpr6 was incubated with an antibody against Cpr6, Hsp104 was co-precipitated with Cpr6 (see Fig. 4.41). In contrast, no band corresponding to Hsp104 was detected when a lysate from a BSC783/4a *Δhsp104* deletion strain was used, confirming that the band, which was detected in the wild-type lysate, indeed represents Hsp104. In BSC783/4a cells lacking Cpr6, BSC783/4a *Δcpr6*, no Hsp104 was detected proving that Hsp104 itself is not recognized by the anti-Cpr6 antibody.

To investigate whether or not complex formation *in vivo* also depends on the MEEVD-like motif of Hsp104, cells expressing only the truncated version $Hsp104_{893\Delta C}$ instead of the full-length protein were used (compare YJW532 *893ΔC* to YJW532 *HSP104*). $Hsp104_{893\Delta C}$ was not precipitated along with Cpr6 confirming that the MEEVD-like motif is critical for complex formation. Moreover, an altered binding of Cpr6 to Hsp104 under fermentative growth conditions was not observed (data not shown), as had been reported by Picard and coworkers for other Hsp104-associated TPR proteins (Abbas-Terki *et al.*, 2001).

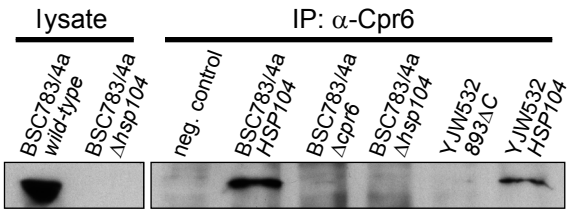

Fig. 4.41: Cpr6 and Hsp104 interact with each other *in vivo*. Left panel: the yeast lysate was analyzed in a western blot decorated with anti-Hsp104 antibodies, no band is visible in the lysate from the *Δhsp104* strain. Right panel: co-immunoprecipitation was carried out on extracts prepared from the indicated yeast strains using an anti-Cpr6 antibody. For negative control, extract from wild-type BSC783/4a was incubated with pre-immune serum in order to perform a similar Co-IP. The antibody-antigen complex was bound to protein A agarose. After washing and elution the protein samples were analyzed by SDS-PAGE and blotted on a membrane. Again, the western blot was decorated with anti-Hsp104 antibodies.

4.6.6.2 Co-localization of Hsp104 and Cpr6 in living yeast cells

To verify the actual existence of the Hsp104·Cpr6 complex *in vivo* a co-localization study was performed. It was asked whether or not Cpr6 is co-localized with substrate processing Hsp104 in living cells. Sup35NM-GFP was used as bait for Hsp104. This fusion protein contains the NM part of the Sup35 prion protein and forms green fluorescent prion-like particles when expressed in [*PSI*$^+$] cells (Patino *et al*., 1996). Since Hsp104 interacts only transiently with its substrates, the TRAP mutant of Hsp104, Hsp104$_{E285Q/E687Q}$, was

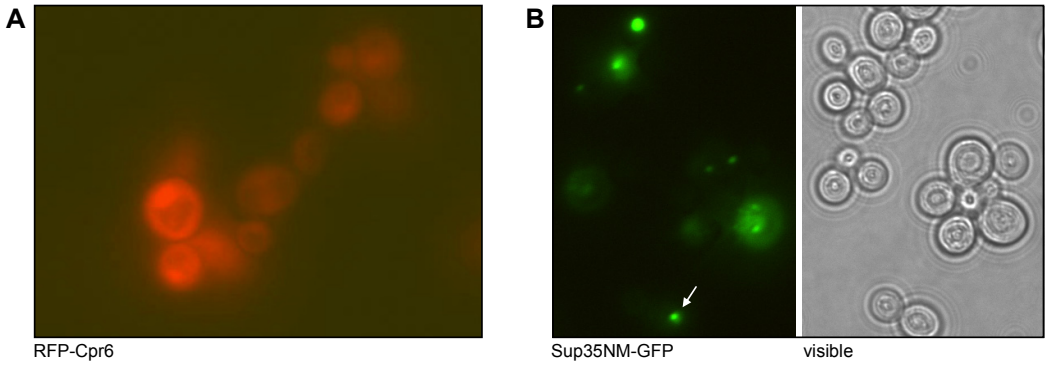

Fig. 4.42: Yeast cells expressing the fluorescent fusion proteins RFP-Cpr6 or Sup35NM-GFP. (A) Cells of YJW512 with a *Δcpr6* background constitutively expressing RFP-Cpr6 from the plasmid p189_RFPCPR6 under the control of a *tetO*$_7$ promoter. The culture was analyzed by fluorescence microscopy. RFP-Cpr6 was diffusely dispersed in the cytoplasm. 100% of the cells showed RFP expression although the fluorescence intensity varied depending on the age of the culture. The expression of RFP-Cpr6 was also verified by western blot analysis with anti-cpr6 antibodies. (B) Fluorescent foci of yeast cells after induction of Sup35NM-GFP. Sup35NM-GFP was expressed from the galactose inducible plasmid p315_NMGFP in the strain YJW512 harboring the [*PSI*$^+$] prion. After 6 h of expression green fluorescent foci (see arrow) became visible, as monitored by fluorescence microscopy. After 6 h of expression the majority of the cells displayed at least one fluorescent foci. The foci size depended on the duration of the NMGFP expression.

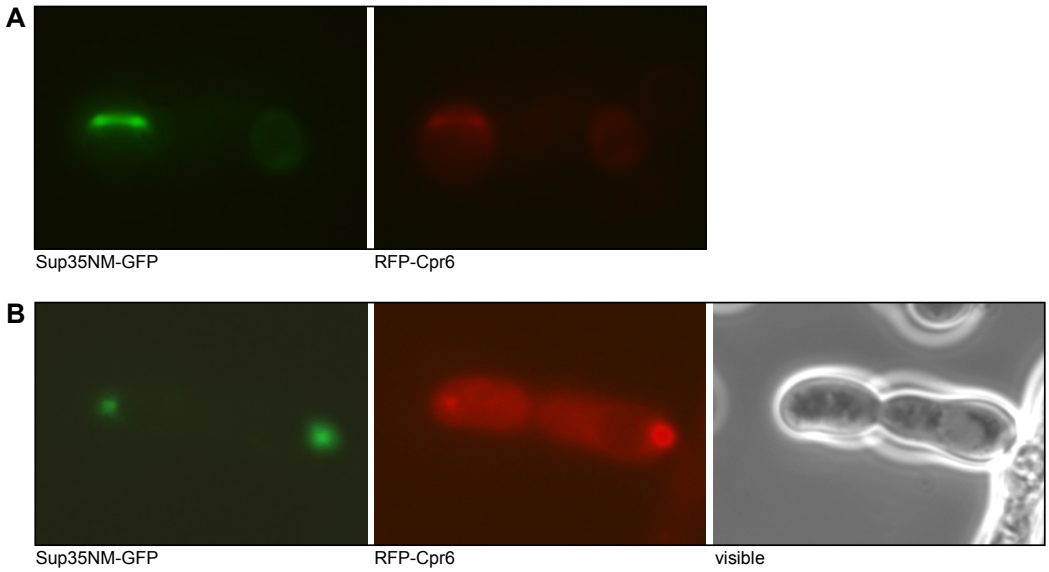

Fig. 4.43: Co-localization of Sup35NM-GFP with RFP-Cpr6 in Hsp104$_{TRAP}$-expressing cells. (A) and (B) refer to different co-localization examples. A culture of YJW512, harboring the [*PSI*$^{+}$] prion constitutively expressed RFP-Cpr6. To test for co-localization Sup35NM-GFP was expressed from a galactose inducible plasmid for 6 h, and Hsp104$_{TRAP}$ was expressed from a copper inducible plasmid for 3 h. After expression of both fluorescent fusion proteins, green fluorescent foci of Sup35NM, which were co-localized with RFP-Cpr6 became visible. The induction of Hsp104$_{TRAP}$ from the copper inducible plasmid was verified by western blot analysis using an isogenic strain, which was lacking the chromosomal *HSP104* copy.

additionally expressed in the analyzed yeast cells. The TRAP mutant is unable to hydrolyze ATP and thus. forms stable complexes with polypeptides in the presence of ATP (Bösl *et al.*, 2005). For the co-localization experiments, yeast strains carrying a combination of plasmids coding for the following proteins were constructed: (i) constitutively expressed RFP-Cpr6, (ii) galactose inducible Sup35NM-GFP, and (iii) copper inducible Hsp104$_{TRAP}$. A similar strain expressing Hsp104$_{TRAP\Delta C}$ instead of Hsp104$_{TRAP}$ served as a control.

Cells exclusively expressing RFP-Cpr6 displayed a diffuse red color under the fluorescence microscope indicating that Cpr6 is located throughout the cytosol (Fig. 4.42.A). In an analogous experiment cells harboring only the galactose inducible Sup35NM-GFP plasmid were analyzed. After a protein expression for 3 - 6 h they displayed green fluorescent foci of aggregated Sup35NM-GFP (Fig. 4.42.B). The fluorescent foci correspond to prion aggregates (Patino *et al.*, 1996).

The co-expression experiment was initiated by the induction of Sup35NM-GFP expression in cells that constitutively expressed RFP-Cpr6. After 3 - 6 h the cells started to show green fluorescent foci of aggregated Sup35NM-GFP protein (Fig. 4.42.A). However, the RFP-Cpr6 distribution remained disperse, indicating that Cpr6 alone is unable to associate with aggregated Sup35NM-GFP. Only after the additional expression of Hsp104$_{TRAP}$ a co-

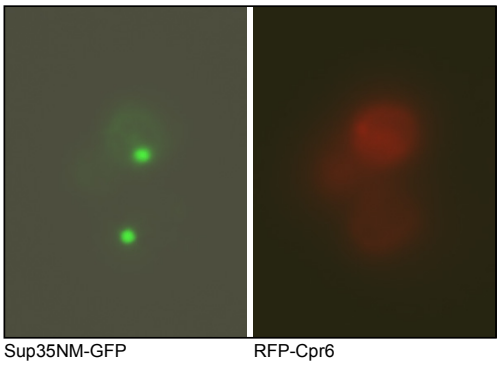

Fig. 4.44: $Hsp104_{TRAP\Delta C}$ does not mediate co-localization of RFP-Cpr6 with Sup35NM-GFP. A culture of YJW512, harboring the [*PSI*$^+$] prion, is shown. It constitutively expressed RFP-Cpr6. Similar to Fig. 4.43, Sup35NM-GFP was expressed for 6 h, and $Hsp104_{TRAP\Delta C}$ for 3 h. Green fluorescent foci of Sup35NM-GFP were not found to co-localize with RFP-Cpr6.

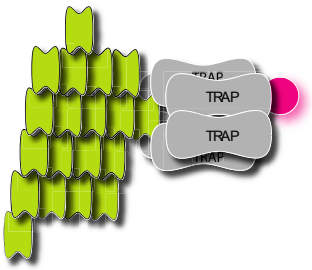

Fig. 4.45: Model of interaction of Sup35NM-GFP and RFP-Cpr6 by associating with $Hsp104_{TRAP}$. The Sup35NM-GFP aggregate is shown in green, the oligomer of $Hsp104_{TRAP}$ in grey, and RFP-Cpr6 in red. $Hsp104_{TRAP}$, which is escorted by Cpr6, is able to form stable complexes with its substrate (Bösl *et al.*, 2005). This complex should persist as long as the cellular energy charge provides an excess of ATP (ATP/ADP > 1).

localization of Cpr6 with the Sup35NM particles was observed (see Fig. 4.43.A and B). This demonstrates that Cpr6 can bind to the C-terminus of Hsp104 when it is engaged with a physiological substrate *in vivo*, see model in Fig. 4.45. A similar experiment with cells expressing $Hsp104_{TRAP\Delta C}$ did not show any co-localization of Sup35NM-GFP and RFP-Cpr6 confirmin once more that the C-terminus of Hsp104 is required for the Cpr6 interaction (see Fig. 4.44).

4.6.7 Deletion of *CPR6* reduces the prion propagation of yeast

The current results strongly suggest that the cyclophilin Cpr6 is a cochaperone of Hsp104. Both *CPR6* and *HSP104* are up-regulated upon heat shock (Gasch *et al.*, 2001) and are present in similar concentrations in the cell under normal growth conditions (Ghaemmaghami *et al.*, 2003). However, *CPR6* is not essential in yeast, the null mutant is viable and shows no unusual phenotype with respect to growth rate under normal laboratory conditions (Duina *et al*., 1996b; Dolinski *et al*., 1997). Cpr6 does not seem to be essential for Hsp104 function but improves its performance in certain cases. It can be assumed that the efficiency of some Hsp104-dependent processes is reduced in yeast cells lacking *CPR6*, resulting in a mild Δ*hsp104* phenotype. To test this hypothesis and to gain insights into the Cpr6 dependency of

Hsp104 *in vivo*, suitable *Δcpr6* strains were constructed for the analysis of the yeast [*PSI*$^+$] prion phenotype.

The [*PSI*$^+$] strain BSC783/4a was selected in order to generate a suitable Δ*cpr6* strain for the analysis of the *HSP104*-related phenotype. *CPR6* was disrupted from the yeast strain by a *cpr6::kanMX4* disruption cassette. The resulting strain did not express any Cpr6, as confirmed by sequencing and by western blot analysis. It displayed pink colonies referring to a weak [*PSI*$^+$] phenotype in comparison to the original wild-type [*PSI*$^+$] strain[3]. To find out whether the weak phenotype of Δ*cpr6* was due to the lack of Cpr6 or due to the *kanMX4* disruption protocol itself the strain was crossed back with a corresponding wild-type prion-free [*psi*$^-$] BSC783/4a strain. The resulting diploids were entirely [*PSI*$^+$] and the subsequent analysis of the tetrads revealed a 2:2 segregation pattern of a weak and a strong [*PSI*$^+$] phenotype (see Fig. 4.46.A). Upon further analysis it became evident that the weak [*PSI*$^+$ spores correspond to Δ*cpr6* growth on G418, cf. Fig. 4.47.B. This result demonstrates that]

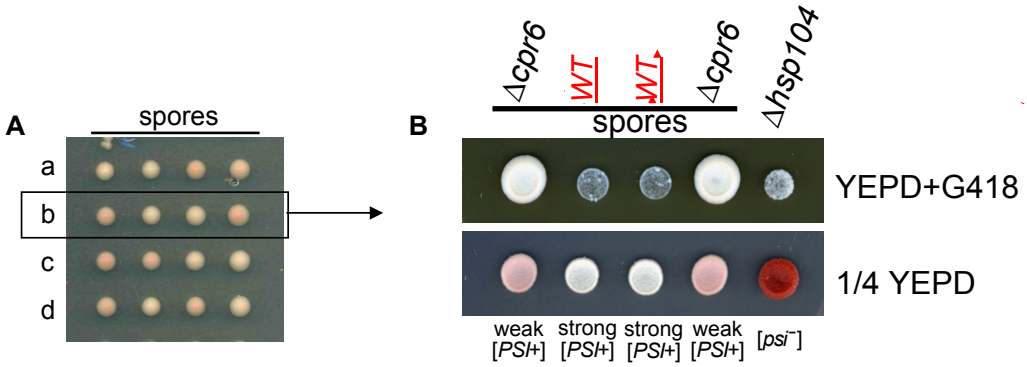

Fig. 4.46: The disruption of the *CPR6* gene generates a weak prion phenotype [*PSI*$^+$]. (A) A selection of tetrads derived from the cross BSC783/4a *Δcpr6* [*PSI*$^+$] × BSC783/4 [*psi*$^-$] reveals a 2:2 segregation pattern of the white/strong and pink/weak prion phenotype [*PSI*$^+$]. The tetrads were grown on ¼YEPD. (B) Phenotypic analysis of the tetrad b, comprising BSC783/4a *Δcpr6* and wild-type, and the isogenic *Δhsp104* strain. First panel: the growth on plates containing the antibiotic geneticin G418 signifies the spores containing the *cpr6::kanMX4* disruption cassette. Second panel: the propagation of the [*PSI*$^+$] prion in the strains, as determined by colony color. The pink color of the *CPR6* deletion strain indicates that prion propagation is affected but not lost, compared to [*psi*$^-$] phenotype of *Δhsp104*.

[3] The colony color of this strain is dependent on the amount of soluble Sup35. The [*PSI*$^+$] prion is caused by the aggregation of the translation termination factor Sup35. The levels of soluble Sup35 are low in [*PSI*$^+$] cells, leading to an increased read-through of stop codons, which is a suppression of nonsense mutations. The presence of the prion phenotype [*PSI*$^+$] can be detected by its ability to suppress mutant *ade* alleles caused by premature stop codons, as described previously. Therefore, [*psi*$^-$] strains are not able to grow on medium lacking adenine (-ADE) and exhibit a dark red color on rich medium, while [*PSI*$^+$] strains are able to grow on -ADE and show a white or a light-pink color. Weak and strong variants of [*PSI*$^+$] can be distinguished by gradually reduced growth on -ADE or by a more pink color (Derkatch *et al.*, 1996; Tuite and Cox, 2003).

Formatted: Font: (Default) Arial, 13 pt, Italic, French (Switzerland)

Formatted: Font: (Default) Arial, 13 pt, Italic, French (Switzerland)

the *cpr6::kanMX4* disruption cassette was inherited as a monogenic trait, a good control that no additional genes were disrupted by accident. It also demonstrates that Δ*cpr6* indeed causes a weak prion phenotype that, however, is sufficient for prion cytoduction upon mating. Present in a wild-type background the prions derived from the *Δcpr6* parent strain exhibited a restored strong [*PSI*$^+$] phenotype indicating that only the number but not the conformation of the prions had been affected in the Δ*cpr6* parent strain (different prion *conformations* result in weaker or stronger [*PSI*$^+$] phenotypes and would have been inherited, Derkatch *et al.*, 1996; Tuite *et al.*, 2003; Tanaka *et al.*, 2004b; Tanaka *et al.*, 2006). The obtained spores of one tetrad (tetrad b, cf. Fig. 4.46.A) were selected for further analysis of the capability of propagating the [*PSI*$^+$] prion and of the establishment of stress tolerance (cf. below, Fig. 4.49), two processes known to be dependent on Hsp104 function. As shown in Fig. 4.46.B, cells lacking *CPR6* displayed a pink colony color, corresponding to a weak [*PSI*$^+$] phenotype. In contrast, the isogenic Δ*hsp104* strain displayed a red colony color, which refers to [*psi*$^-$].

4.6.8 Over-expression of Cpr6 restores the original [*PSI*$^+$] phenotype

The tetrad analysis indicated that the weak [*PSI*$^+$] phenotype of *Δcpr6* can be reverted to a strong phenotype when transducing the prions into a wild-type strain. In a comparable analysis *CPR6* was reintroduced into BSC783/4a *Δcpr6* by transformation with a high copy plasmid encoding *CPR6*. As shown in Fig. 4.47, the strong white [*PSI*$^+$] phenotype was restored when cells expressed Cpr6 from a plasmid (see *Δcpr6+CPR6*) although the genomic *CPR6* copy was still disrupted (cf. growth on G418). All variants expressing Cpr6 also showed a similar adenine prototrophy, which is commonly used to assess the [*PSI*$^+$]

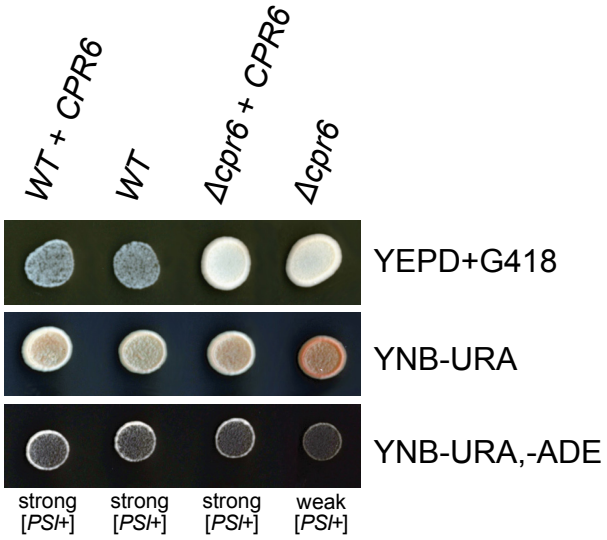

Fig. 4.47: Over-expression of *CPR6* restores the strong [*PSI*$^+$] phenotype. BSC783/4a *Δcpr6* and the wild-type strain were transformed either with the *CPR6* over expressing high copy vector p190_*CPR6* or with an empty p190 vector carrying an *URA3* marker, and spotted on the indicated media. Expression of Cpr6 in the deletion strain restores the white color and adenine prototrophy indicating that [*PSI*$^+$] propagation is normal again.

phenotype by the growth on plates lacking adenine (-ADE). For comparison, cells with a weak [*PSI*$^+$] phenotype hardly grew on -ADE plates (see *Δcpr6*). The [*PSI*$^+$] phenotype of cells over expressing Cpr6 is indistinguishable from that of wild-type cells. Seemingly, the Hsp104-dependent [*PSI*$^+$] phenotype cannot be further improved by an excess of Cpr6.

4.6.9 The C-terminus of Hsp104 is required for the functional contribution by Cpr6

Since *CPR6* is needed for the strong [*PSI*$^+$] prion state of wild-type yeast, it was next examined whether or not the beneficial effect of Cpr6 depends on its physical interaction with Hsp104. In order to test the physical interaction $Hsp104_{WT}$ had to be exchanged against $Hsp104_{893\Delta C}$, which is lacking the Cpr6 binding motif. However, *HSP104* is essential for prion maintenance. Therefore, the strain YJW532 *hsp104::HIS3* [*PSI*$^+$] [p316_HSP104], in which the chromosomal copy of *HSP104* is replaced by a plasmid-based *HSP104* gene, was used in the following plasmid shuffling experiments (Zenthon *et al*., 2006). The *HSP104* encoding plasmid was exchanged with a second plasmid carrying either *HSP104*, the truncated $HSP104_{893\Delta C}$ mutant, or no *HSP104* at all. The obtained strains were analyzed with respect to the consequences of the C-terminal Hsp104 truncation for [*PSI*$^+$] maintenance. As expected, colonies expressing $Hsp104_{WT}$ showed the strongest prion phenotype, while colonies containing the empty vector turned red, demonstrating that [*PSI*$^+$] was lost due to the lack of *HSP104* (Fig. 4.48). Colonies expressing the mutant $Hsp104_{893\Delta C}$ were almost as red as the strain lacking *HSP104* altogether, suggesting that prion propagation is severely affected by the deletion of the MEEVD-like motif in Hsp104. However, the weak prion phenotype still corresponded to [*PSI*$^+$] since GdmCl curing was possible; only [*psi*$^-$] leads to a loss of adenine autotrophy. Clearly, this implies that binding to the C-terminal domain of Hsp104 is necessary for the prion enhancing effect of Cpr6.

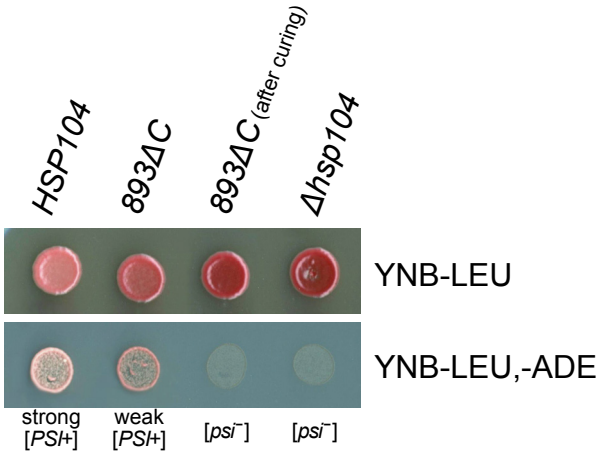

Fig. 4.48: Deletion of the C-terminal acidic motif of Hsp104 affects its function *in vivo*. The strain YJW532 *hsp104::HIS3* [*PSI*$^+$] [p316_HSP104] was used for plasmid shuffling with p315_HSP104, p315_893ΔC or empty vector carrying a *LEU2* marker. The system allows the non-invasive exchange of the Hsp104 variant without affecting the prion phenotype by the procedure. After verifying that the obtained strains were free of p316_HSP104, they were spotted on the indicated media. It should be noted that owing to the different strain background [*PSI*$^+$] colonies appear more pink than BSC783/4a.

4.6.10 The interaction of Cpr6 and Hsp104 is required for the stress tolerance of yeast

So far, the above experiments demonstrated that the interaction of Cpr6 and Hsp104 is relevant for the prion phenotype of yeast. In order to assess further Hsp104-dependent processes, stress tolerance was studied. It is established that Hsp104 is of critical importance for ethanol tolerance (Sanchez *et al.*, 1992) and induced thermotolerance of yeast (Parsell *et al.*, 1991).

As shown in Fig. 4.49.A, the *Δcpr6* spores exhibited a reduced growth on plates containing 15% ethanol compared to the wild-type spores. The *CPR6* deletion strain also showed a decreased recovery from thermal stress (see Fig. 4.49.B) indicating that *CPR6* is indeed involved in stress tolerance. From Fig. 4.49 it is apparent that the phenotype of a *CPR6* deletion is qualitatively similar, but less pronounced compared to an *HSP104* deletion strain. Thus, the *Δcpr6*-phenotype is related to the *Δhsp104*-phenotype, suggesting a functional interaction of the gene products, Cpr6 and Hsp104. This interaction clearly depends on the C-terminal Cpr6 binding motif of Hsp104: the truncated variant, $HSP104_{893\Delta C}$, exhibits a reduced thermotolerance similar to *Δcpr6*.

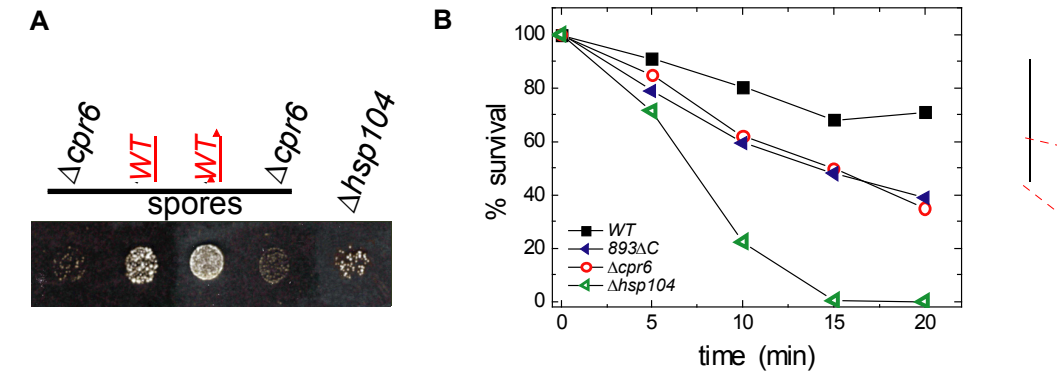

Fig. 4.49: The interaction of Hsp104 and Cpr6 is required for ethanol tolerance and for induced thermotolerance. (A) The tetrad b from strain BSC783/4a, comprising *Δcpr6* and wild-type, and additionally the isogenic *Δhsp104* strain were assessed by their growth on YEPD plates containing 15% ethanol. (B) Thermotolerance assay of the strains YJW512 wild-type (= *WT*), YJW512 *cpr6::kanMX4* (= *Δcpr6*), YJW532 *hsp104::HIS3* (= *Δhsp104*), YJW532 *hsp104::HIS3* [p315_893ΔC] (= *893ΔC*). All used YJW strains have a similar genetic background based on W303.

Formatted: Font: (Default) Arial, 13 pt, Italic, French (Switzerland)

Formatted: Font: (Default) Arial, 13 pt, Italic, French (Switzerland)

5. DISCUSSION

5.1 The oligomerization state of Hsp104 is highly dependent on its environment

This work shows that Hsp104 forms hexameric particles of ~600 kDa with an average sedimentation coefficient of 16.5 S, as analyzed by the sedimentation velocity and by sedimentation equilibrium experiments. It was previously suggested that Hsp104 existed in a dynamic equilibrium between the active, hexameric form and inactive monomers or dimers/trimers (Schirmer *et al.*, 2001; Hattendorf *et al.*, 2002b) since the hexamer tends to partially disassemble under non-equilibrium conditions, for instance when techniques such as SEC-HPLC analysis are used to assess the oligomerization state (Tkach *et al.*, 2004; Bösl *et al.*, 2005). This study demonstrates that Hsp104 exists to almost 100% as hexameric species at equilibrium in the presence of nucleotides and at a protein concentration of 5 µM while – importantly – no intermediate dimeric or trimeric species are detectable.
Moreover, this study shows that under equilibrium conditions a significant amount of monomeric Hsp104 is only found in the absence of nucleotides and in combination with a low protein concentration (< 0.2 µM). Further, the postulated dynamics of the oligomerization state are not observed during ATP hydrolysis. Importantly, Hsp104 forms non-dissociating oligomers under steady-state conditions, as shown in 4.4.4 and Fig. 5.2. The incorporation of a sub-stochiometrical amount of an inactive mutant into wild-type Hsp104 oligomers results in a significantly reduced of ATP turn-over. It can be assumed that these hetero-oligomers are non-functional and that they also can be formed *in vivo*. For example, the co-expression of wild-type Hsp104 and the Walker A mutants $Hsp104_{K218T}$, $Hsp104_{K620T}$ or $Hsp104_{K218T/K620T}$ results in an elimination of the prion phenotype [PSI^{+}], i.e., the mutants have a dominant negative effect on the Hsp104-mediated prion-propagation (Chernoff *et al.*, 1995; Satpute-Krishnan *et al.*, 2007). From these data, Yury Chernoff assumed that mutant monomers inactivate the whole hexameric unit of Hsp104 – an assumption that is in good agreement with the enzymatic data obtained in this study.

Regarding the function of the NBDs it was found that NBD2 has the predominant role in nucleotide-induced oligomerization, since the K620T mutant with an impaired NBD2 displayed an oligomerization defect (see Tab. 4.3), which is in good agreement with previous studies (Parsell *et al.*, 1994a; Schirmer *et al.*, 1998; Schirmer *et al.*, 2001). However, the oligomerization state does not appears to be exclusively dependent on nucleotide binding to NBD2 since the mutant overcomes its oligomerization defect at sufficiently high ATP and protein concentrations, see K_M analysis 4.4.5. The nucleotide-induced oligomerization of the K620T protein can only be caused by ATP binding to NBD1. Thus, both nucleotide binding domains contribute to the stability of the oligomerization state if they are bound to nucleotides, even though NBD1 appears to have a rather minor function in nucleotide-induced oligomerization *in vitro* in comparison to NBD2.

In conclusion, Hsp104 forms hexamers with a stability that is highly dependent on the molecular environment. It is important to note in this respect that Hsp104 exists as a stable oligomer under its "working conditions", in other words: Hsp104 oligomers are stable when they hydrolyze ATP at a physiological ATP concentration and at a physiological salt condition of 150 - 200 mM. The cytosolic Hsp104 concentration *in vivo* remains to be determined but can be roughly estimated to be about 0.8 µM, assuming that a haploid yeast cell with 70 μm^3 cell volume (Sherman, 2002) contains ~33,000 Hsp104 molecules (Ghaemmaghami *et al.*, 2003, cf. also page 117). This corresponds to a level of Hsp104 where its oligomerization is found to be rather concentration-independent. However, this could be a further parameter to regulate the Hsp104 activity *in vivo*, namely by adapting the Hsp104 concentration to a level that favor or favor not the generation of hexamers. In accordance with these assumptions there are findings showing that upon a heat shock the Hsp104 expression is increased about 6 - 8-fold compared to stress-free conditions (Gasch *et al.*, 2000). Thus, the oligomer formation is certainly enhanced under conditions were the survival of the yeast cell highly depends on a fully functional Hsp104.

One might speculate that, once monomers are found together, oligomerize, and are busy processing a polypeptide substrate in the cell, they maintain their oligomeric state until the "work" is done. But even more, the monomer-hexamer equilibrium might come into play during the event of "frustration" when substrates are too stable or too big to be processed by Hsp104. By disassembling a hexameric form into monomers a blocked Hsp104 could then be recycled instead of being subjected to protein degradation.

5.2 The ATP hydrolysis by Hsp104 is tightly regulated

5.2.1 Functional regulation of the nucleotide binding domains of Hsp104

This study demonstrates that Hsp104 is an ATPase that is subjected to a tight allosteric regulation. Its active nucleotide-bound form is a hexamer. The protomers within a hexamer communicate with each other since the nucleotide-bound or -unbound state in one subunit affects the activity of the whole oligomer (see 4.4.4). Also within one protomer there exists a crosstalk: mutations in one NBD affect the activity of the other NBD (see 4.4.2). Both NBD1 and NBD2 of one protomer within a hexamer are fully functional: they are in principle capable of nucleotide binding (see 4.4.6) and hydrolysis (see 4.4.2) although they perform differently with respect to turn-over and the promotion of the oligomerization. It was previously suggested that NBD1 mainly contributes to the steady-state ATP hydrolysis of wild-type Hsp104, whereas NBD2 is considered to have only a stabilizing function (Schirmer *et al.*, 1998; Schirmer *et al.*, 2001). This assumption was based on data obtained with Walker A mutants.

The Walker B mutations, which were analyzed in this study, allow a much deeper understanding of the cooperativity within the Hsp104 oligomer and allow deriving a much more detailed model of the ATP hydrolysis by Hsp104.

The regulation of NBD1

NBD1 appears to be allosterically rather independent of NBD2: the K620T mutant, corresponding to a nucleotide-free state of NBD2, can hydrolyze ATP with ~30% activity in comparison to wild-type Hsp104 at sufficiently high ATP concentrations – although no nucleotide is bound to NBD2. The E687Q mutant can bind to ATP but is incompetent for ATP hydrolysis. Although this mutant corresponds to a permanent ATP-bound state in NBD2, it shows enzymatic properties with respect to ATP hydrolysis that are more or less identical to wild-type Hsp104. This supports the conclusion that NBD1 mainly contributes to the steady-state ATP hydrolysis of wild-type Hsp104. Even though NBD1 is allosterically independent of NBD2 it still requires its contribution so that oligomer stability can be ensured. Otherwise NBD2 would require higher ATP concentrations in order to support a stable oligomer formation, which is a prerequisite for active hydrolysis (cf. K620T mutant). The very low K_M of the E687Q mutant demonstrates that NBD1 has a high intrinsic affinity for ATP if the oligomer is perfectly stabilized by a non-hydrolyzing NBD2 in an ATP state. Further, an optimal ATP hydrolysis of NBD1 requires nucleotide binding to *all* nucleotide pockets of NBD1 within a hexamer since one empty NBD1 subunit spoils the hydrolysis of the whole NBD1 ring (see 4.4.4). Thus, there appears to exist an intrinsic nucleotide dependency within the NBD1 ring.

The regulation of NBD2

NBD2 is allosterically highly regulated by the nucleotide state of NBD1: the K218T mutant, corresponding to a nucleotide-free state in NBD1, is virtually inactive, whereas the E285Q mutant, corresponding to a state where ATP is permanently bound to NBD1, is extremely active and shows a very high Hill coefficient (see 4.4.5). However, the only difference between the mutants K218T and E285Q is the ATP-bound or ATP-free state of NBD1. Presumably, NBD1 in the E285Q mutant exclusively exists in an ATP-bound state under the regenerating assay conditions, since no ADP accumulates during steady-state hydrolysis (Norby, 1988). Thus, these findings are in support of the significant dependency of the activity of NBD2 on the all-ATP state of NBD1, i.e., the all-ATP state of NBD1 is the prerequisite for the very fast ATP hydrolysis in NBD2.

5.2.2 Implications of the domain regulation on the ATPase cycle of $Hsp104_{WT}$

It was shown above that NBD1 has a high affinity for ATP and that it could therefore argued that NBD1 in principle can exist in an all-ATP-bound state, which is the prerequisite for the ATP hydrolysis at NBD2. However, this assumption is somewhat contradicted by the data that were obtained in this study: the ATP turn-over observed for wild-type Hsp104 is not similar to the ATP turn-over of the Hsp104 mutant E285Q, which is defective in ATP hydrolysis in NBD1 and will therefore reach a state where all nucleotide binding sites in NBD1 are occupied by ATP. The ATP turn-over observed for wild-type Hsp104 corresponds rather to that of the E687Q mutant that is defective in ATP hydrolysis in the NBD2 domain.
If the all-ATP-NBD1 state was present with a significant population in nature it would be expected that Hsp104 – at least at high ATP concentrations – was able to reach the same ATP turn-over as the E285Q mutant. However, a similarly high ATP turn-over as for the E285Q protein was never observed for wild-type Hsp104. Thus, the E285Q mutant corresponds to a state, which might have an extremely short life-time, or which might rarely occur, or even possibly not exist during steady-state ATP hydrolysis of wild-type protein.

Taken together, (i) only NBD1 appears to contribute to the ATP turn-over of wild-type Hsp104, (ii) hydrolysis in NBD1 and NBD2 requires nucleotide binding to *all* nucleotide pockets of NBD1 within a hexamer, and (iii) the all-ATP state of NBD1 is apparently not populated.
These conditions fit to a model of non-concerted (which could be sequential or probabilistic) ATP hydrolysis: the different NBD1 domains are bound to ATP *and* to ADP instead of to ATP only (see Fig. 5.1). This binding mode is found in the case of the non-concerted ATP hydrolysis that is reported for the Hsp104 homologue ClpX (Martin *et al.*, 2005). Such a mixed ADP/ATP-bound state in NBD1 would guarantee the basal ATPase function of NBD1 contributing to the apparent ATP turn-over of wild-type Hsp104 and would inhibit ATP hydrolysis in NBD2 at the same time. The function of such a negative allostery could be to avoid a nucleotide exchange after hydrolysis in NBD2 in order to maintain oligomer stability. However, it remains to be elucidated whether or not NBD2 might have a further function in addition to its contribution to the nucleotide-dependent oligomer stabilization – otherwise it would be sufficient if NBD2 only bound to nucleotides without hydrolysis, acting as a degenerated nucleotide sensor NBD. An example of such a non-functional NBD can be found in dynein but also in the distantly related F1 ATPase, where catalytically inactive subunits connect the hexamer (Boyer, 1997; Kon *et al*., 2004).
Conclusively, the ATPase cycle of Hsp104 seems to be driven by a non-concerted ATP hydrolysis of NBD1 (see Fig. 5.1 and Fig. 5.2). The details of this reaction remain to be determined but active ATP hydrolysis requires the nucleotide-bound state of all NBDs, a state that can be maintained when ADP is step by step exchanged for new ATP. The

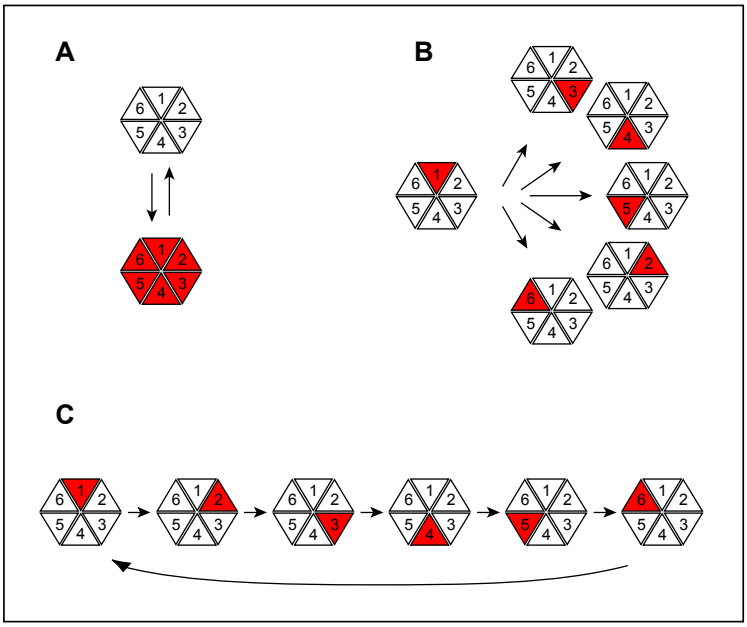

Fig. 5.1: Different models of the ATPase cycle of hexameric AAA$^+$ ATPases. (A) Concerted, (B) probabilistic, and (C) sequential ATP hydrolysis cycle. ClpX was found to have a non-concerted probabilistic ATPase cycle (Martin *et al.*, 2005). Concerted ATP hydrolysis was found for SV40 LTag helicase (Gai *et al.*, 2004) and non-concerted sequential ATP hydrolysis was found for T7 gp4 DNA helicase (Singleton *et al.*, 2000).

exchange of ADP at one NBD1 might be the pace maker of ATP hydrolysis of an adjacent ATP-NBD1.

This mechanism is still speculative, but would be in accordance with the data obtained in this study and would furthermore also be in line with the published data from other groups. Clearly, no intermediate state appears to exist where neither NBD1 nor NBD2 are completely nucleotide-free. Otherwise steady-state oligomers would also exist in an oligomerization equilibrium – which is not the case. Rather, NBD2 exists in a non-hydrolyzing all-nucleotide-bound state stabilizing the oligomer.

It should be noted that the described putative ATPase-cycle is likely to interfere with the substrate refolding cycle of Hsp104. The ATPase properties of one NBD or even of one protomer might be altered during the refolding of a polypeptide substrate. The addition of RCMLa, a permanently unfolded polypeptide substrate of Hsp104, leads to a strong increase in ATP turn-over (see 4.5.8). One can speculate that this striking increase in ATP turn-over can be attributed to NBD2 that becomes activated upon binding or procession of polypeptide substrates.

Based on this study it became clear that the system of ATP hydrolysis by Hsp104 is a much more complex process than was originally suggested (Hattendorf *et al.*, 2002b). It is likely

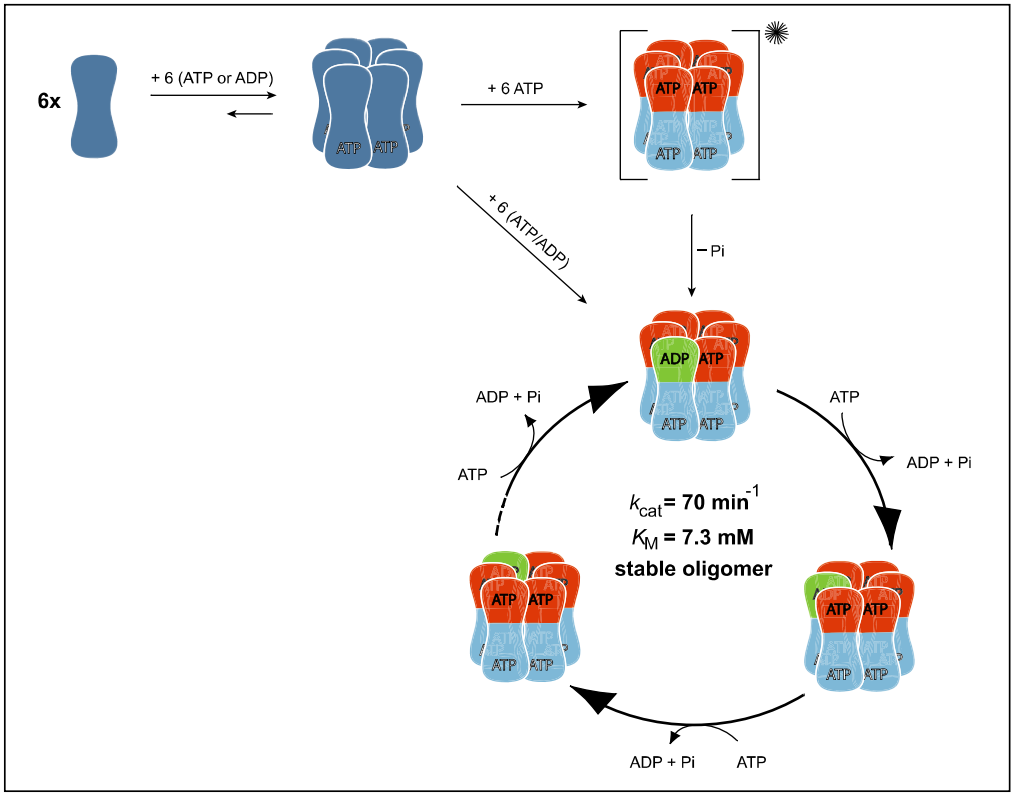

Fig. 5.2: Model of the ATP hydrolysis cycle by Hsp104. The inactive species are depicted in dark blue. Individual domains with the principle capability to hydrolyze ATP are shown in red. Domains in the ADP state are indicated in green and inactive nucleotide-bound domains in light blue. The monomer and an intermediate oligomer that has only nucleotide bound to NBD2 exist in an oligomerization equilibrium which can be shifted by the nucleotide concentration. Full nucleotide binding to NBD1 triggers the ATP hydrolysis. Either there exists an extremely short living transient complex of 6-ATP-NBD1, indicated by brackets and star, which subsequently hydrolyzes at least one ATP molecule, or the nucleotide binds as a mixture of ATP and ADP to NBD1 directly from the beginning of ATP hydrolysis. During ATP hydrolysis of the NBD1 ring the NBD2 ring remains to be inactive – presumably – in its ATP state since it lacks the activating signal of fully saturated ATP-bound NBD1.

that the ATPase is indeed sequentially hydrolyzing ATP but that it additionally alters its ATP hydrolysis when it is engaged with a polypeptide substrate or when regulating cofactors bind to it. Further, a sequential type of ATP hydrolysis implies that the ATPase system is sensitive towards the ratio of ATP and ADP present in the assay. It would be worth to use physiological ATP/ADP ratios in order to provide a most “natural” environment for proceeding the studies on the allostery of Hsp104. Consequently, to gain further insight into the function of Hsp104 it is suggested as a next step to employ specific intrinsic probes such as tryptophan mutants that are not deficient in the ATP hydrolysis, to study the actual state of an NBD ring or of one NBD binding site. This can be done during steady-state or under substrate refolding conditions to also take the influence of substrate interactions into account when analyzing the ATPase activity.

5.3 GdmCl is an uncompetitive inhibitor of Hsp104

5.3.1 Hsp104 is the GdmCl target in yeast

The phenomenon of GdmCl induced prion curing in yeast was observed a long time before the epigenetic elements [*PSI*$^+$] and [URE] were recognized as yeast prions (Tuite *et al.*, 1981; Wickner, 1994). For more than two decades scientists used to add 1-5 mM GdmCl to the growth medium in order to stabilize the [*psi*$^-$] phenotype of yeast (Brown *et al.*, 1998), without any further understanding of the underlying biology. Currently, Hsp104 was identified as a target of GdmCl inhibition causing the prion curing, i.e., the disappearance of prion protein aggregates in yeast cultures *in vivo*, since without Hsp104 prion particles can no longer be inherited by daughter cells.

In vitro, the results of this study show that low concentrations of GdmCl change the enzymatic properties of Hsp104, thereby providing a strong link between curing and Hsp104 inactivation *in vivo*. The data also demonstrate that the observed Hsp104 inactivation *in vitro* is not related to the denaturing properties of GdmCl since even 100-fold higher amounts of urea have no effect on ATP hydrolysis. This is in perfect agreement with *in vivo* experiments showing that urea lacks the curing potency of GdmCl (Cox *et al.*, 1988).

GdmCl was found to exclusively inhibit Hsp104. No other ATP-hydrolyzing molecular chaperone was affected by GdmCl, neither in the ATPase assays, nor in the refolding assays of this study. In addition, homologous proteins of other organisms are also not affected by GdmCl. ClpB from *Thermus thermophilus* is not sensitive to GdmCl (J. Reinstein, MPI for Medical Research in Heidelberg, Germany, personal communication). Hsp104 from *Candida albicans*, Hsp104$_{C.a.}$, which shares 64% sequence identity with Hsp104 from *S. cerevisiae* (Hsp104$_{S.c.}$), is sufficient to complement the function of Hsp104$_{S.c.}$ after plasmid shuffling, but the transgenic yeast cells cannot be cured from [*PSI*$^+$] by the addition of GdmCl to the growth medium indicating GdmCl insensitivity of Hsp104$_{C.a.}$ (Zenthon *et al.*, 2006). Apparently, the GdmCl inhibition is unique to Hsp104$_{S.c.}$ among Hsp100 proteins and molecular chaperones from yeast.

A specific sensitivity towards GdmCl was only reported for some distantly related ATPases. First, millimolar concentrations of guanidine ions compete with free Ca^{2+} for the binding to a glutamate residue at the cytoplasmatic site of the Na,K-ATPase PCMA from dog kidney (plasma membrane calcium pump, Gatto *et al*., 2006). Second, millimolar concentrations of GdmCl inhibit the replication of the poliovirus by binding to the nucleotide binding region of the protein2C ATPase (Murray and Nibert, 2007). The mentioned ATPases might be affected differently than Hsp104 but these examples demonstrate that GdmCl is able to form specific interactions with functional residues of enzymes.

The specific properties of the yeast phenotype that results after GdmCl treatment also appear to be exclusively linked to a modification of the Hsp104 function, which would suggest that Hsp104 is the exclusive target of GdmCl in yeast.

5.3.2 Gdm^+ affects exclusively nucleotide-bound Hsp104

This study demonstrates that the interaction of Hsp104 and GdmCl is highly specific: it depends on the nucleotide state of Hsp104. The ITC experiments show that no binding of GdmCl was observed in the absence of ADP. Thus, either the nucleotide directly contacts GdmCl, or the binding of GdmCl to Hsp104 requires a conformational change in Hsp104 that is induced by nucleotide binding. The first alternative, a direct interaction of GdmCl with the nucleotide, can, however, be ruled out since free ADP did not form a complex with GdmCl.
Interestingly, NAAA (N-acetylarginine amide) had also a slight inhibitory effect on the ATPase activity of Hsp104, supporting the assumption that the positively charged guanidyl group *per se* might be the inhibitory element of GdmCl (for comparison of the structures, see Appendix A.3). Hsp104 has a lower affinity for NAAA, which might be due to its larger dimensions. Presumably, Gdm^+ has the right size to interact with the nucleotide binding pocket and the bound nucleotide, thereto interfering with the nucleotide hydrolysis of Hsp104. Gdm^+ is able to form hydrogen bonds and has a positively charged nitrogen located at its surface. Thus, Gdm^+ can build up strong electrostatic interactions with the negatively charged amino acid residues of the nucleotide binding pocket and/or with the negatively charged phosphate groups of the bound nucleotide. One can deduce from its structure that Gdm^+ might resemble an additional or misplaced arginine in the nucleotide binding pocket. This could slow down ATP hydrolysis, for instance by masking the γ-phosphate group of the catalytic residues or by avoiding that an incoming water molecule can make contact with the ATP.
The analysis of the ATP dependency of Gdm^+ binding revealed that Gdm^+ upon binding to the Hsp104·ATP complex even increases the affinity of the Hsp104 for ATP. The factor of inhibition and the factor of increased affinity is found to be 2.5 for $Hsp104_{WT}$, which is consistent with the findings for the affinity for ADP using ITC. This type of inhibition is adequately described by the model of uncompetitive inhibition, which requires that (i) Gdm^+ binds to the enzyme-substrate complex, Hsp104·ATP, but not to the free enzyme and (ii) both K_M and k_{cat} are reduced to the same extent. The inhibition by Gdm^+ is only partial, i.e., the ternary enzyme-substrate-inhibitor complex, Hsp104·ATP·Gdm^+, can still be active in ATP hydrolysis, although more slowly than Hsp104·ATP. In agreement with the experimental findings, the model also predicts that the inhibitory effect becomes more pronounced at a high ATP concentration (compare Fig. 4.23). Higher ATP concentrations will have the consequence that the species Hsp104·ATP is more populated. This – of course – is the species that the inhibitor Gdm^+ binds to.

5.3.4 Gdm^+ binds to the nucleotide binding domain 1 of Hsp104

Several ATPase mutants of Hsp104 were used to identify NBD1 as target domain for the Gdm^+ inhibition. Only Hsp104 variants equipped with an active hydrolyzing NBD1 exhibited an inhibition in the presence of Gdm^+. This finding is in agreement with Jung and coworkers who found that D184, a residue of NBD1, is responsible for the GdmCl sensitivity *in vivo* (Jung *et al.*, 2002). Lindquist and coworkers have shown that under steady-state conditions, NBD1 accounts for most of the ATPase activity displayed by Hsp104 (Hattendorf *et al.*, 2002b). Thus, Gdm^+ attacks the most vulnerable spot of Hsp104 under steady-state conditions.

NBD2 is not directly affected by Gdm^+ but shows an altered turn-over in the presence of Gdm^+ due to the allosteric stimulation by NBD1, which exists as NBD1·ATP·Gdm^+ complex in $Hsp104_{E285Q}$. The altered turn-over of $Hsp104_{E285Q}$ can be explained by a higher affinity of NBD1 for nucleotides in the presence of Gdm^+. The increased affinity of NBD1 for nucleotides can also serve to explain the increased affinity of Hsp104·ATP·Gdm^+ for unfolded proteins such as RCMLa, since the ATP-bound state of NBD1 is a prerequisite for binding of the substrate proteins to the N-terminus of Hsp104 (Bösl *et al.*, 2005; Schaupp *et al.*, 2007). The enhancement of the nucleotide-dependent oligomerization, as observed by AUC and SLS, appears to be also a consequence of the increased nucleotide affinity of NBD1.

The current results of the Gdm^+ effect on the ATPase cycle of Hsp104 are summarized in a model of the ATPase cycle in Fig. 5.3.

5.3.5 Gdm^+ disturbs the intrinsic regulation of Hsp104

Interestingly, ATP hydrolysis of Hsp104 is not completely abolished in the presence of Gdm^+, but only reduced to about 35% of its normal level. *In vivo* data on the other hand suggest that the Hsp104 function is lost entirely when yeast grows in a medium containing GdmCl, because the phenotype of the resulting yeast colonies resembles that of an *hsp104* knockout. A closer look at the time dependency of the prion curing *in vivo* may provide an explanation for this apparent contradiction. Wegrzyn and coworkers report that although growing [PSI^+] cells in medium containing GdmCl causes curing of the prion phenotype. This process is significantly slower than curing by removal or inactivation of Hsp104 (Wegrzyn *et al.*, 2001). While in the first case, [psi^-] cells only appear after at least 3 - 5 generations, curing in the second case already starts after two generations. The authors interpret these differences in curing kinetics by suggesting that either the mechanism of curing by GdmCl is independent of Hsp104, or GdmCl does not completely inactivate Hsp104. The results oft his study are in agreement with the latter possibility: Gdm^+ only

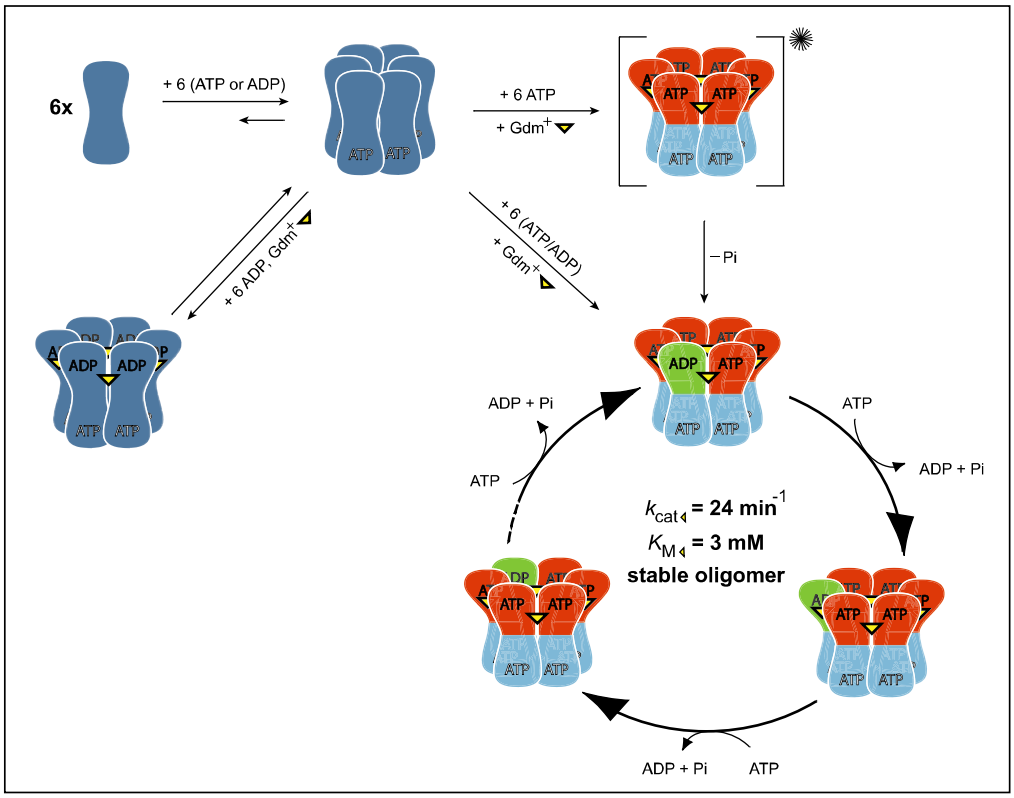

Fig. 5.3: Model of Gdm^+-inhibition of the ATPase cycle by Hsp104. The model corresponds to Fig. 5.2. The guanidinium ion is symbolized by a yellow triangle, presumably binding in the groove of two adjacent protomers. The inactive species are given in dark blue. Individual domains with the principle capability to hydrolyze ATP are given in red. Domains of the active hexamer that are present in the ADP state are given in green and inactive nucleotide-bound domains are given in light blue. Gdm^+ exclusively binds to the NBD1 of oligomeric Hsp104. The binding is dependent on the presence of ATP or ADP in NBD1. Thereby, the oligomerization equilibrium is shifted toward the oligomeric state. The active ATPase species is inhibited by Gdm^+ in an uncompetitive manner: Gdm^+ reduces k_{cat} and K_M to the same extent.

partially inhibits the ATPase activity of Hsp104. Additional support comes from experiments in which the cellular level of Hsp104 was reduced. For prion curing to occur, it was sufficient to decrease the expression of the chaperone to ~25% of the normal level (Wegrzyn *et al.*, 2001). Nevertheless, the experimental data of this study suggest that Gdm^+ does not only change the rate of hydrolysis, but also the molecular context of this reaction. The cooperativity of ATP hydrolysis and the stimulation by an unfolded protein substrate, RCMLa, were strongly affected or even abolished by Gdm^+. These features of Hsp104 require an intrinsic signal and energy transmission within the hexamer. Their loss indicates that Gdm^+ does not only reduce the ATPase activity of Hsp104. One could envision that Gdm^+ blocks the transmission of the energy provided by ATP hydrolysis to the site of Hsp104 where the "work" is actually done, whatever this work may be exactly on a molecular level.

Already small amounts of Gdm^+ impair the enzyme since the apparent $K_{½\ (GdmCl)}$ was found to be ~12 µM by means of an ATPase assay. In contrast, the physical binding constant, $K_{D\ (GdmCl)}$, was found to be much higher at 500 µM, as determined by ITC. Thus, a full Gdm^+ saturation of Hsp104 does not result in a stronger inhibition of the ATPase function but rather in a complete loss of chaperone activity, as determined by the refolding assay at higher Gdm^+ concentrations. It was not possible to determine the exact stochiometry of the GdmCl interaction in this study but one might speculate that only one Gdm^+ ion bound to an Hsp104 hexamer affects the ATPase signal transmission and reduces it to 40% activity, whereas a fully Gdm^+ saturated hexamer still retains an ATPase activity of 40% but completely loses its refolding function.

5.3.6 Hsp104 inactivation by GdmCl – consequences for prion propagation in yeast

Over the past years, a wealth of data has been accumulated both *in vivo* and *in vitro* showing convincingly that destroying the capability of Hsp104 to hydrolyze ATP results in a loss of its function (Patino *et al.*, 1996; Schirmer *et al.*, 1998). Most of these studies were carried out with mutants, in which conserved lysine residues in NBD1 (K218T) and/or NBD2 (K620T) were replaced by threonine. These mutations strongly reduce the capability of the affected domain ether to bind to nucleotides or to hydrolyze them (Schirmer *et al.*, 1998). Both mutations reduce the thermotolerance (Parsell *et al.*, 1991) of yeast and can cause curing of the [*PSI*$^+$] phenotype *in vivo* (Schirmer *et al.*, 2001; Ness *et al.*, 2002).

The results of this study provide evidence that, more specifically, the rate and the cooperativity of hydrolysis of ATP is important for the biological activity of Hsp104. In the presence of Gdm^+ nucleotide binding to Hsp104 and its affinity for unfolded proteins is enhanced. The increased substrate affinity might even increase the stochiometry of the substrate interaction; if a hexamer of Hsp104 interacts only with one substrate polypeptide under normal conditions its refolding or prion remodeling function would be strongly disturbed by the simultaneous binding of several polypeptide chains in presence of Gdm^+. However, the stochiometry of a *productive* Hsp104-substrate interaction remains to be determined and such a type of inhibition is still somewhat speculative. Regardless of the number of bound substrate molecules per Hsp104 hexamer Gdm^+ binding was found to increase the affinity of Hsp104 for its substrate. The inhibitor Gdm^+ might slow down the prion replication or the growth of the seeds by causing a decoration of aggregates, i.e., the prion seeds, with inactive Hsp104·ATP·Gdm^+ complexes. Such an inactive Hsp104 coat would block the aggregates: it would prevent them from proteolysis but it would also prohibit the addition of further soluble proteins to the complex as long as Gdm^+ is present in the cytoplasm. If GdmCl was removed from the culture, the complex of Hsp104·ATP·Gdm^+ would dissociate due to its poor binding constant, Hsp104 would retain its activity, and the persisting prions would exist in their normal form again.

Several features of GdmCl induced prion curing are in accordance with this hypothesis. First, GdmCl curing is a consequence of the inhibition of prion seed replication and of the dilution of the preexisting prion seeds upon cell division. Notably, curing does not occur by proteolytic degradation of prion seeds (Eaglestone *et al.*, 2000; Ness *et al.*, 2002). Second, GdmCl reduces the ability of newly synthesized Sup35 to enter prion aggregates (Ness *et al.*, 2002; Satpute-Krishnan *et al.*, 2007). Third, the [*PSI*$^{+}$] phenotype can be restored, once GdmCl is removed from the culture. This is depending on the duration of GdmCl treatment. Thus, curing is reversible if prion seeds are not yet diluted out. The seeds that persist after GdmCl treatment are rapidly remodeled to efficient prion templates upon Hsp104 reactivation (Eaglestone *et al.*, 2000; Satpute-Krishnan *et al.*, 2007).

Thus, it would be interesting to find out whether or not the presence of GdmCl also increases the affinity of Hsp104 for protein aggregates or prion seeds *in vivo*. GdmCl induced curing should differ from that caused by the introduction of the Walker A double point mutant (K218T/K620T), which cannot interact with substrates, but it should have some similarities to that caused by the introduction of the Walker B double point mutant (E285Q/E287Q), which also exhibits a higher substrate affinity.

5.5 The cyclophilin Cpr6 is a cochaperone of Hsp104

5.5.1 Identification of a cofactor binding domain of Hsp104

The C-terminus of Hsp104 comprises a negatively charged motif, which is similar to that of Hsp70 and Hsp90 (yHsp70: VEEVD, yHsp90: MEEVD, yHsp100: IDDDLD, see also the sequence alignment in Fig. 4.29). This striking similarity had already been noticed when Hsp104 was introduced by Parsell and coworkers. They found that the eukaryotic Hsp70, Hsp90, and Hsp100 proteins share an acidic C-terminal sequence, which is absent in their prokayotic and organellar homologues (Parsell *et al.*, 1991). In the meantime it had been established that the acidic motif of Hsp70 (Liu *et al*., 1999) and Hsp90 (Carrello *et al*., 1999) serves as a TPR protein interaction motif, which is restricted to the eukaryotic chaperone system. In contrast, no function has yet been defined for the C-terminal tail of eukaryotic Hsp100 proteins but its phylogenetic occurrence is similar to that of Hsp70 and Hsp90.
The current study now provides evidence that the C-terminus of Hsp104 is in fact involved in the interaction with a TPR domain containing protein, the cyclophilin Cpr6. The crystal structure analysis of C-terminal peptides of Hsp70 and Hsp90 with distinct TPR domains in Hop has shown that the acidic C-terminal motif is anchored by a network of electrostatic interactions, the carboxylate clamp, with specific residues in the binding groove of the TPR domain (see Fig. 2.8). Especially contacts to the hydrophobic residues upstream of the EEVD motif appear to play a critical role in selective recognition of chaperones (Scheufler *et al.*, 2000; Brinker *et al.*, 2002). Hsp104 presents a similar but different binding motif, IDDDLD, which is recognized by Cpr6. Thus, Hsp104 might provide a new type binding motif for TPR proteins.

5.5.2 Cpr6 interacts specifically with Hsp104

Cpr6 is a yeast cyclophilin homologue to human Cyp40 consisting of an N-terminal peptidyl-prolyl *cis-trans* isomerase (PPIase) domain and a tetratricopeptide repeat (TPR) domain (Duina *et al.*, 1996b). It was originally identified as a cochaperone of Hsp82, the yeast homologue of Hsp90 (Duina *et al.*, 1996a).
This study presents several lines of evidence that strongly suggest that Cpr6 also acts as a cochaperone of Hsp104:
(i) Cpr6 binds specifically to Hsp104 both *in vitro* and *in vivo*. The physical binding constant of Cpr6 was found to be ~40 nM Hsp104, which is similar to that determined for Hsp90 (41 nM, K. Richter, TU München, Germany, PhD. thesis). Although Hsp90 is more abundant in yeast cells (~450,000 molecules per cell) than Hsp104 (~33,000 molecules Hsp104 per cell and ~19,000 molecules Cpr6 per cell), it is engaged with many other cofactors (see Fig. 5.4) and, therefore, most likely only a small fraction of Hsp90 actually interacts with Cpr6. Moreover, already one Cpr6 molecule per Hsp104 hexamer is necessary and sufficient to

modulate its function (cf. chapter 4.6.3 and 4.6.4). Thus, the existing Cpr6 pool would be sufficient for more than one chaperone and a parallel interaction of Cpr6 with both chaperones, Hsp90 and Hsp104 is very likely. In accordance with this, the co-immunoprecipitation and the co-localization analysis of Cpr6 and Hsp104 revealed that both proteins are associated under normal growth conditions (i.e., with Hsp90 present). Thus, both Hsp90 and Hsp104 interact with Cpr6 *in vivo*.

(ii) Cpr6 is a modulator of Hsp104, it reduces ATP turn-over of Hsp104 but at the same time enhances the reactivation of aggregated proteins such as mouse DHFR. Cpr6 reduces the ATP turn-over of Hsp104, a property that does not require the PPIase function of Cpr6. Interestingly, the reduction of the ATP turn-over does not lead to a concurrent reduction of the refolding activity (cf. 4.6.2 to 4.6.5). The refolding of aggregated polypeptide substrates is rather enhanced since the energy efficiency of this process increases with Cpr6 binding to Hsp104. Furthermore, it was demonstrated that Cpr6 especially enhances the refolding yield of substrates with an extraordinarily slow peptidyl-prolyl *cis-trans* isomerization. This is a property that is mediated on the PPIase function of Cpr6.

(iii) The phenotype of yeast cells lacking *CPR6* qualitatively resembles that of yeast cells lacking *HSP104*. *Δcpr6* yeast strains show a significantly weaker prion phenotype and a reduced stress tolerance, phenotypic traits that are directly Hsp104-related. The co-localization analysis revealed that Cpr6 is associated with Sup35NM-GFP-bound $Hsp104_{TRAP}$. Thus, Cpr6 is directly involved in Hsp104-dependent processes.

5.5.3 Existence of a chaperone network between Hsp70, Hsp90 and Hsp104

This study demonstrates that Cpr6 is a joint cofactor of Hsp104 and Hsp90. Additional TPR domain containing cofactors of Hsp90, namely Cpr7, Cns1, and Sti1, were also found to be associated with Hsp104 under respiratory growth conditions (Abbas-Terki *et al.*, 2001). Further, it is established that Hsp90 and Hsp70 share some TPR cofactors, e.g., Sti1 and Cns1 (Wegele *et al.*, 2003; Hainzl *et al.*, 2004). Thus, TPR cofactors do not exclusively bind to a distinct molecular chaperone but rather serve as a cofactor assortment that is used on demand. Mostly, these TPR proteins have a modular domain composition: they consist of a domain of varying function, e.g., a phosphatase domain in Ppt1 (Wandinger *et al.*, 2006), and of at least one TPR domain mediating the contact to the chaperone(s) of destination. The advantages of such a system are obvious: the core chaperone can gain additional functions by simply recruiting the appropriate TPR proteins to the MEEVD binding site, and a single set of cochaperones, on the other hand, can assist various core chaperones involved in the folding of polypeptide chains. The current data show that Hsp104 cooperates with the established chaperone network of Hsp70 and Hsp90 of yeast cells (see Fig. 5.4). TPR proteins build the connections within this network. For instance, substrates can be transferred

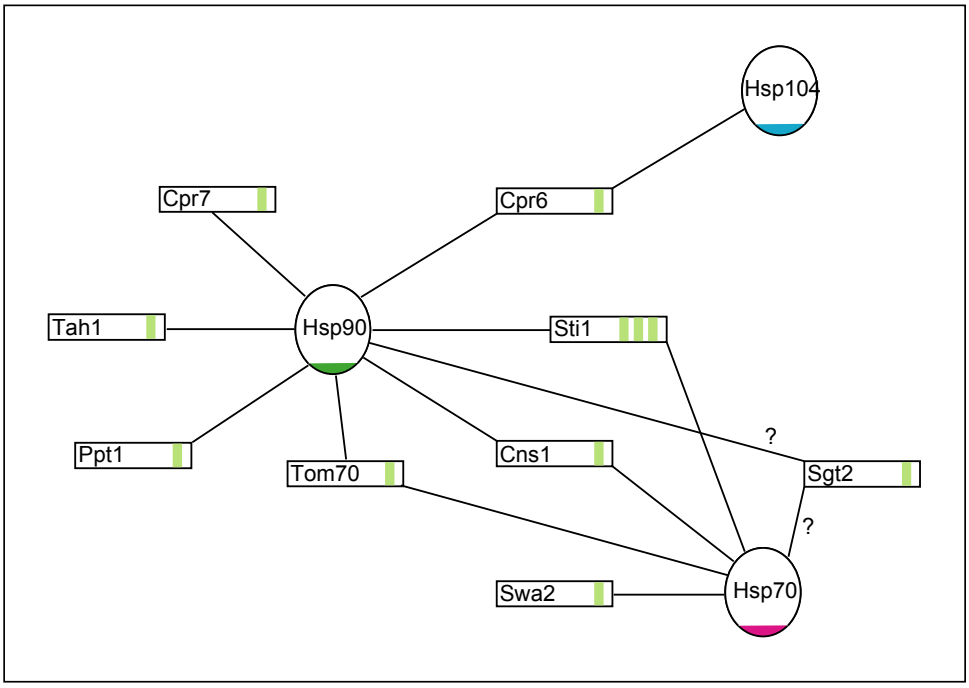

Fig. 5.4: The molecular chaperone network of Hsp70/90/100 is based on TPR interactions. The indicated interactions in yeast refer to the current knowledge based on this study and on established TPR interactions listed in Tab. 2.1.

from the Hsp70 to Hsp90 with the help of Sti1, a protein consisting of two TPR domains that creates a physical link between both chaperones (Wegele *et al.*, 2003). A similar cofactor comprising two TPR domains could link Hsp104 in the same way to Hsp70, an interaction that would be beneficial for the Hsp104-mediated protein disaggregation since Hsp104 functionally depends on Hsp70 in order to efficiently solubilize protein aggregates(Glover *et al.*, 1998).

5.5.4 Implications for the mechanism of disaggregation by Hsp104

According to current models, Hsp104 dissolves protein aggregates by mechanically extracting individual polypeptide chains from the aggregate (see Fig. 5.5). Although the details of this ATP-dependent reaction are presently still not fully understood, it appears to involve the translocation of the extracted polypeptide through the central pore of the chaperone, presumably from the N-terminal to the C-terminal NBD of Hsp104 (Weibezahn *et al.*, 2004; Schaupp *et al.*, 2007). Thus, the C-terminal polypeptide exit site of the Hsp104 hexamer can be considered as resembling the exit site of a prokaryotic ribosome (see Fig. 5.6). In both cases the polypeptide emerges in an unfolded state which is, depending on its folding properties, a delicate moment for the substrate protein. The substrate would be at risk

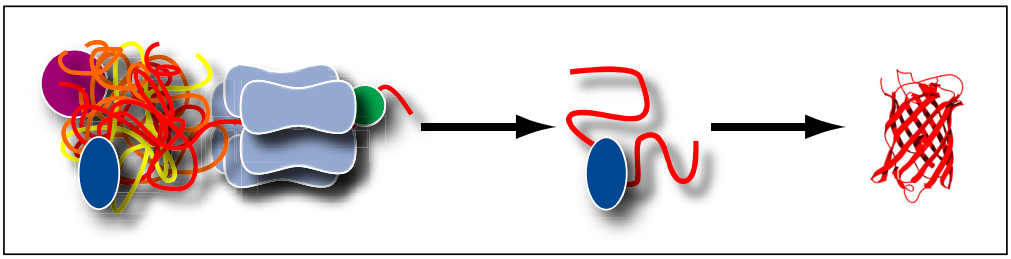

Fig. 5.5: Model of disaggregation by Hsp104 and its assisting cochaperones. The oligomer of Hsp104 is shown in light blue, Cpr6 in green, and further assisting molecular chaperones in magenta and blue. Polypeptide chains are extracted from the aggregate as single chains in order to refold correctly. The subsequent refolding reaction of the substrate requires protection and/or catalysis of slow folding steps by assisting cochaperones such as Cpr6.

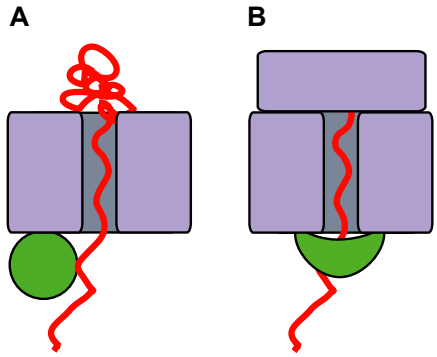

Fig. 5.6: Comparison of the Hsp104·Cpr6 complex with the ribosome·triggerfactor complex. (A) Hsp104, in blue, extracts single polypeptide chains from stable aggregates. Thereby, the polypeptide emerges from the C-terminal exit site of Hsp104 in an extended conformation. Similarly, the newly synthesized polypeptide emerges from the ribosome in an extended unfolded conformation. In both cases triggerfactor and Cpr6 (both in green) protect the unfolded peptide and can act as peptidyl-prolyl isomerases in order to catalyze slow peptidyl-prolyl-depended folding steps.

to be proteolytically degraded or to aggregate, e.g., subsequent aggregation was observed for the disaggregation by Hsp104 *in vitro* in the absence of the other cochaperones (Schaupp *et al.*, 2007). Thus, an emerging unfolded polypeptide chain strongly demands either protection or an immediate subsequent catalyzed folding reaction in order to achieve its native state. The ribosome recruits the PPIase triggerfactor to associate with nascent polypeptide chains (Ferbitz *et al*., 2004). Similarly, Cpr6 would be located at the exit site of Hsp104 and might be involved in the inter-conversion of different *cis*/*trans* isomers of Hsp104 substrates whose folding is slowed down by peptidyl-prolyl isomerization. One might speculate that even more TPR cofactors with different functions bind to the remaining free C-termini of Hsp104. A large set of TPR domain cofactors provides the Hsp70/90 system with additional functions (see Tab. 2.1). It would be interesting to learn to what extent Hsp104 is able to use further TPR domain proteins to adapt its function to be optimal for the specific substrate that is presently refolded.

6. ABBREVIATIONS

Å	Angstrom (0.1 nm)
A	Ampère
aa	amino acid
NAAA	N-acetylarginine amide
AAA^+	ATPases associated with diverse cellular activities
ADP	adenosine 5'-diphosphate
Amp	ampicillin
AMP-PNP	adenylylimido diphosphate
Amp^R	ampicillin resistance marker, gene coding for β-lactamase
ANS	8-anilino-1-naphthalene sulfonic acid
APS	ammonium peroxydisulfate
ATP	adenosine 5'-triphosphate
ATPase	adenosine 5'-triphosphatase
ATPγS	adenosine 5'-O-3-thiotriphosphate
AUC	analytical ultracentrifugation
A_x	absorbance at wavelength x, path length 1 cm
bp	base pair
BSA	bovine serum albumin
c	concentration
CD	circular dichroism
CFU	colony forming units
Clp	caseinolytic protease, contains an AAA^+ ATPase subunit
$ClpB_{E.c.}$	Hsp100/ClpB homologue from *Escherichia coli*
$ClpB_{T.t.}$	Hsp100/ClpB homologue from *Thermus termophilus*
Cm	chloramphenicol
Co-IP	co-immunoprecipitation
Cpr	cyclosporin-sensitve proline rotamase
$Cpr6_{FITC}$	fluorescein-labeled Cpr6
$Cpr6_{LUY}$	lucifer yellow-labeled Cpr6
cryo-EM	cryo-electron microscopy
CsA	cyclosporine A, a specific inhibitor of the PPIase function of cyclophilins
C-terminal	carboxy terminal
C-terminus	carboxy terminus
CV	column volume
ddH_2O	double distilled water
Da	Dalton (1 Da = 1 g/mol)
DHF	dihydrofolate
DHFR	dihydrofolate reductase
DNA	desoxyribonucleic acid
DTT	1,4-dithiothreitol
ε	molar extinction coefficient (M^{-1} cm^{-1})
E. coli	*Escherichia coli*
ECL	enhanced chemiluminescence
EDTA	ethylene diamine tetraacidicacid
Eq.	equation
Fig.	figure
FL	fluorescence
5-FOA	5-fluoroorotic acid
FPLC	fast protein liquid chromatography
g	gram
G418	geneticin sulfate
GdmCl	guanidine hydrochloride
GFP	green fluorescent protein
h	hour
HEPES	4-(2-hydroxyethyl)-1-piperazineethanesulfonic acid
HPLC	high pressure liquid chromatography
HSE	heat shock element
HSF	heat shock factor
Hsp	heat shock protein

$Hsp104_{C.a.}$	Hsp100/ClpB homologue from *Candida albicans*
$Hsp104_{S.c.}$	Hsp100/ClpB homologue from *S. cerevisiae*
$Hsp104_{TRAP}$	synonym of the double Walker B mutant $Hsp104_{E285Q/E687Q}$
IPTG	isopropyl β-D-thiogalactoside
ITC	isothermal titration calorimetry
$K_{½}$	analogous to dissociation constant, to describe apparent affinity of a specific ligand, derived from activity change of the enzyme
Kan	kanamycin
kB	kilo base pairs
K_D	dissociation constant
kDa	kilo Dalton
K_M	Michaelis constant
λ	wavelength
L	liter
LB	Luria Bertani
LS	low salt
µ	micro (10^{-6})
m	milli (10^{-3}) *or* meter
M	molar (mol/L)
MCS	multiple cloning site
min	minute
mRNA	messenger RNA
MW	molecular weight
n	nano (10^{-9})
n. d.	not determined
NADH	nicotinamide adenine dinucleotide
NADHP	nicotinamide adenine dinucleotide phosphate
NBD	nucleotide binding domain, refers to an AAA module in Hsp100/ClpB
N-terminal	amino terminal
N-terminus	amino terminus
p. a.	*pro analysis*
PBS	phosphate buffered saline
PCR	polymerase chain reaction
PEP	phosphoenol pyruvate
pH	*potentia hydrogenii*
PMSF	phenylmethylsulfonyl fluoride
PPIase	peptidyl-prolyl *cis-trans* isomerase
PVDF	polyvinylidene difluoride
RCMLa	reduced and carboxymethylated α-lactalbumin
RFP	red fluorescent protein
RNA	ribonucleic acid
rpm	rotations per minute
RT	room temperature, 20°C
s	second
S. cerevisiae	*Saccharomyces cerevisiae*
SDS	sodium dodecyl sulfate
SDS-PAGE	sodium dodecyl sulfate polyacrylamide gel electrophoresis
SEC	size exclusion chromatography
SLS	static light scattering
Tab.	table
TCEP	tris (2-carboxyethyl) phosphine hydrochloride
TEMED	N, N, N', N'-tetramethylethylendiamine
Tris	2-amino-2-(hydroxymethyl) propane-1,3-diol
tRNA	transfer RNA
U	units
UV	ultra violet
V	Volt
v/v	volume per volume
VIS	visible
w/v	weight per volume
WT	wild-type

7. REFERENCES

1. Abbas-Terki,T., Donze,O., Briand,P.A., and Picard,D. (2001). Hsp104 interacts with Hsp90 cochaperones in respiring yeast. *Mol. Cell Biol.,* **21,** 7569-7575.
2. Agashe,V.R. and Hartl,F.U. (2000). Roles of molecular chaperones in cytoplasmic protein folding. *Semin. Cell Dev. Biol.,* **11,** 15-25.
3. Ali,M.M., Roe,S.M., Vaughan,C.K., Meyer,P., Panaretou,B., Piper,P.W., Prodromou,C., and Pearl,L.H. (2006). Crystal structure of an Hsp90-nucleotide-p23/Sba1 closed chaperone complex. *Nature,* **440,** 1013-1017.
4. Amery,L., Sano,H., Mannaerts,G.P., Snider,J., Van Looy,J., Fransen,M., and Van Veldhoven,P.P. (2001). Identification of PEX5p-related novel peroxisome-targeting signal 1 (PTS1)-binding proteins in mammals. *Biochem. J.,* **357,** 635-646.
5. Amoros,M. and Estruch,F. (2001). Hsf1p and Msn2/4p cooperate in the expression of *Saccharomyces cerevisiae* genes HSP26 and HSP104 in a gene- and stress type-dependent manner. *Mol. Microbiol.,* **39,** 1523-1532.
6. Anfinsen,C.B., Haber,E., Sela,M., and White,F.H. (1961). The kinetics of formation of native ribonuclease during oxidation of the reduced polypeptide chain. *Proc. Natl. Acad. Sci. U. S. A,* **47,** 1309-1314.
7. Angeletti,P.C., Walker,D., and Panganiban,A.T. (2002). Small glutamine-rich protein/viral protein U-binding protein is a novel cochaperone that affects heat shock protein 70 activity. *Cell Stress Chaperones.,* **7,** 258-268.
8. Babst,M., Wendland,B., Estepa,E.J., and Emr,S.D. (1998). The Vps4p AAA ATPase regulates membrane association of a Vps protein complex required for normal endosome function. *EMBO J.,* **17,** 2982-2993.
9. Barnett,M.E., Nagy,M., Kedzierska,S., and Zolkiewski,M. (2005). The amino-terminal domain of ClpB supports binding to strongly aggregated proteins. *J. Biol. Chem.,* **280,** 34940-34945.
10. Barnett,M.E., Zolkiewska,A., and Zolkiewski,M. (2000). Structure and activity of ClpB from *Escherichia coli*. Role of the amino-and -carboxyl-terminal domains. *J. Biol. Chem.,* **275,** 37565-37571.
11. Ben Zvi,A.P. and Goloubinoff,P. (2001). Mechanisms of disaggregation and refolding of stable protein aggregates by molecular chaperones. *J. Struct. Biol.,* **135,** 84-93.
12. Bochtler,M., Hartmann,C., Song,H.K., Bourenkov,G.P., Bartunik,H.D., and Huber,R. (2000). The structures of HslU and the ATP-dependent protease HslU-HslV. *Nature,* **403,** 800-805.
13. Bolon,D.N., Grant,R.A., Baker,T.A., and Sauer,R.T. (2004). Nucleotide-dependent substrate handoff from the SspB adaptor to the AAA+ ClpXP protease. *Mol. Cell,* **16,** 343-350.
14. Bösl,B., Grimminger,V., and Walter,S. (2005). Substrate binding to the molecular chaperone Hsp104 and its regulation by nucleotides. *J. Biol. Chem.,* **280,** 38170-38176.
15. Bösl,B., Grimminger,V., and Walter,S. (2006). The molecular chaperone Hsp104-A molecular machine for protein disaggregation. *J. Struct. Biol.*.
16. Boyer,P.D. (1997). The ATP synthase--a splendid molecular machine. *Annu. Rev. Biochem.,* **66,** 717-749.
17. Brachmann,A., Baxa,U., and Wickner,R.B. (2005). Prion generation in vitro: Amyloid of Ure2p is infectious. *EMBO J.,* **15,** 3127-3134.
18. Bradford,M. (1976). A rapid and sensitive method for the quantitation of microgram quantities of protein utilizing the principle of protein-dye binding. *Anal. Biochem,* **72,** 248-254.
19. Brandts,J.F., Halvorson,H.R., and Brennan,M. (1975). Consideration of the Possibility that the slow step in protein denaturation reactions is due to cis-trans isomerism of proline residues. *Biochemistry,* **14,** 4953-4963.
20. Brinker,A., Scheufler,C., von der Mule,F., Fleckenstein,B., Herrmann,C., Jung,G., Moarefi,I., and Hartl,F.U. (2002). Ligand discrimination by TPR domains. *J. Biol. Chem.,* **277,** 19265-19275.

21. Brocard,C. and Hartig,A. (2006). Peroxisome targeting signal 1: is it really a simple tripeptide? *Biochim. Biophys. Acta,* **1763,** 1565-1573.

22. Brown, A. J. P. and Tuite, M. F. Yeast Gene Analysis. Methods in Microbiology. 26. 1998. New York, Acad. Press.

23. Brown,J.T., Bai,X., and Johnson,A.W. (2000). The yeast antiviral proteins Ski2p, Ski3p, and Ski8p exist as a complex in vivo. *RNA,* **6,** 449-457.

24. Buchberger,A., Schröder,H., Hesterkamp,T., Schönfeld,H.J., and Bukau,B. (1997). Substrate shuttling between the DnaK and GroEL systems indicates a chaperone network promoting protein folding. *J. Mol. Biol.,* **261,** 328-333.

25. Bukau,B. and Horwich,A.L. (1998). The Hsp70 and Hsp60 chaperone machines. *Cell,* **92,** 351-366.

26. Burton,R.E., Baker,T.A., and Sauer,R.T. (2005). Nucleotide-dependent substrate recognition by the AAA+ HslUV protease. *Nat. Struct. Mol. Biol.,* **12,** 245-251.

27. Cantor, C. R. and Schimmel, P. R. Biophysical Chemistry. Techniques for the study of biological structure and function. 1980. W.H. Freeman & Co.

28. Carrello,A., Ingley,E., Minchin,R.F., Tsai,S., and Ratajczak,T. (1999). The common tetratricopeptide repeat acceptor site for steroid receptor-associated immunophilins and hop is located in the dimerization domain of Hsp90. *J. Biol. Chem.,* **274,** 2682-2689.

29. Cashikar,A.G., Duennwald,M., and Lindquist,S.L. (2005). A chaperone pathway in protein disaggregation. Hsp26 alters the nature of protein aggregates to facilitate reactivation by Hsp104. *J. Biol. Chem.,* **280,** 23869-23875.

30. Cashikar,A.G., Schirmer,E.C., Hattendorf,D.A., Glover,J.R., Ramakrishnan,M.S., Ware,D.M., and Lindquist,S.L. (2002). Defining a pathway of communication from the C-terminal peptide binding domain to the N-terminal ATPase domain in a AAA protein. *Mol. Cell,* **9,** 751-760.

31. Caughey,B. and Lansbury,P.T. (2003). Protofibrils, pores, fibrils, and neurodegeneration: separating the responsible protein aggregates from the innocent bystanders. *Annu. Rev. Neurosci.,* **26,** 267-298.

32. Causton,H.C., Ren,B., Koh,S.S., Harbison,C.T., Kanin,E., Jennings,E.G., Lee,T.I., True,H.L., Lander,E.S., and Young,R.A. (2001). Remodeling of yeast genome expression in response to environmental changes. *Mol. Biol. Cell,* **12,** 323-337.

33. Cerasoli,E., Kelly,S.M., Coggins,J.R., Boam,D.J., Clarke,D.T., and Price,N.C. (2002). The refolding of type II shikimate kinase from Erwinia chrysanthemi after denaturation in urea. *Eur. J. Biochem.,* **269,** 2124-2132.

34. Chernoff,Y.O., Lindquist,S.L., Ono,B., Inge-Vechtomov,S.G., and Liebman,S.W. (1995). Role of the chaperone protein Hsp104 in propagation of the yeast prion-like factor [*psi*+]. *Science,* **268,** 880-884.

35. Chien,P., Weissman,J.S., and DePace,A.H. (2004). Emerging principles of conformation-based prion inheritance. *Annu. Rev. Biochem.,* **73,** 617-656.

36. Coustou,V., Deleu,C., Saupe,S., and Begueret,J. (1997). The protein product of the het-s heterokaryon incompatibility gene of the fungus Podospora anserina behaves as a prion analog. *Proc. Natl. Acad. Sci. U. S. A,* **94,** 9773-9778.

37. Cox,B.S. (1965). [*PSI*], a cytoplaasmic suppressor of supersuppressors in yeast. *Heredity,* **20,** 505-521.

38. Cox,B.S., Tuite,M.F., and McLaughlin,C.S. (1988). The psi factor of yeast: a problem in inheritance. *Yeast,* **4,** 159-178.

39. Creighton,T.E. (1992). Protein folding pathways determined using disulphide bonds. *Bioessays,* **14,** 195-199.

40. Crist,C.G. and Nakamura,Y. (2006). Cross-Talk between RNA and Prions. *J. Biochem.,* **140,** 167-173.

41. D'Andrea,L.D. and Regan,L. (2003). TPR proteins: the versatile helix. *Trends Biochem. Sci.,* **28,** 655-662.

42. Dalal,S., Rosser,M.F., Cyr,D.M., and Hanson,P.I. (2004). Distinct roles for the AAA ATPases NSF and p97 in the secretory pathway. *Mol. Biol. Cell,* **15,** 637-648.

43. Darby,N.J., Freedman,R.B., and Creighton,T.E. (1994). Dissecting the mechanism of protein disulfide isomerase: catalysis of disulfide bond formation in a model peptide. *Biochemistry,* **33,** 7937-7947.

44. Das,K.P. and Surewicz,W.K. (1995). Temperature-induced exposure of hydrophobic surfaces and its effect on the chaperone activity of α-crystallin. *FEBS Lett.,* **369,** 321-325.

45. Derkatch,I.L., Bradley,M.E., Hong,J.Y., and Liebman,S.W. (2001). Prions affect the appearance of other prions: the story of [PIN(+)]. *Cell,* **106,** 171-182.

46. Derkatch,I.L., Bradley,M.E., Zhou,P., Chernoff,Y.O., and Liebman,S.W. (1997). Genetic and environmental factors affecting the de novo appearance of the [*PSI*+] prion in *Saccharomyces cerevisiae*. *Genetics,* **147,** 507-519.

47. Derkatch,I.L., Chernoff,Y.O., Kushnirov,V.V., Inge-Vechtomov,S.G., and Liebman,S.W. (1996). Genesis and variability of [*PSI*] prion factors in *Saccharomyces cerevisiae*. *Genetics,* **144,** 1375-1386.

48. Diamant,S., Ben Zvi,A.P., Bukau,B., and Goloubinoff,P. (2000). Size-dependent disaggregation of stable protein aggregates by the DnaK chaperone machinery. *J. Biol. Chem.,* **275,** 21107-21113.

49. Dill,K.A. and Chan,H.S. (1997). From Levinthal to pathways to funnels. *Nat. Struct. Biol.,* **4,** 10-19.

50. Dill,K.A. and Shortle,D. (1991). Denatured states of proteins. *Annu. Rev. Biochem.,* **60,** 795-825.

51. Dobson,C.M. (1999). Protein misfolding, evolution and disease. *Trends Biochem. Sci.,* **24,** 329-332.

52. Dobson,C.M. and Karplus,M. (1999). The fundamentals of protein folding: bringing together theory and experiment. *Curr. Opin. Struct. Biol.,* **9,** 92-101.

53. Dolinski,K., Muir,S., Cardenas,M., and Heitman,J. (1997). All cyclophilins and FK506 binding proteins are, individually and collectively, dispensable for viability in *Saccharomyces cerevisiae*. *Proc. Natl. Acad. Sci. U. S. A,* **94,** 13093-13098.

54. Dolinski,K.J., Cardenas,M.E., and Heitman,J. (1998). CNS1 encodes an essential p60/Sti1 homolog in *Saccharomyces cerevisiae* that suppresses cyclophilin 40 mutations and interacts with Hsp90. *Mol. Cell Biol.,* **18,** 7344-7352.

55. Dougan,D.A., Mogk,A., Zeth,K., Turgay,K., and Bukau,B. (2002a). AAA+ proteins and substrate recognition, it all depends on their partner in crime. *FEBS Lett.,* **529,** 6-10.

56. Dougan,D.A., Reid,B.G., Horwich,A.L., and Bukau,B. (2002b). ClpS, a substrate modulator of the ClpAP machine. *Mol. Cell,* **9,** 673-683.

57. Doyle,S.M., Shorter,J., Zolkiewski,M., Hoskins,J.R., Lindquist,S., and Wickner,S. (2007). Asymmetric deceleration of ClpB or Hsp104 ATPase activity unleashes protein-remodeling activity. *Nat. Struct. Mol. Biol.,* **14,** 114-122.

58. Duina,A.A., Chang,H.C., Marsh,J.A., Lindquist,S., and Gaber,R.F. (1996a). A cyclophilin function in Hsp90-dependent signal transduction. *Science,* **274,** 1713-1715.

59. Duina,A.A., Marsh,J.A., and Gaber,R.F. (1996b). Identification of two CyP-40-like cyclophilins in *Saccharomyces cerevisiae*, one of which is required for normal growth. *Yeast,* **12,** 943-952.

60. Duina,A.A., Marsh,J.A., Kurtz,R.B., Chang,H.C., Lindquist,S., and Gaber,R.F. (1998). The peptidyl-prolyl isomerase domain of the CyP-40 cyclophilin homolog Cpr7 is not required to support growth or glucocorticoid receptor activity in *Saccharomyces cerevisiae*. *J. Biol. Chem.,* **273,** 10819-10822.

61. Eaglestone,S.S., Cox,B.S., and Tuite,M.F. (1999). Translation termination efficiency can be regulated in *Saccharomyces cerevisiae* by environmental stress through a prion-mediated mechanism. *EMBO J.,* **18,** 1974-1981.

62. Eaglestone,S.S., Ruddock,L.W., Cox,B.S., and Tuite,M.F. (2000). Guanidine hydrochloride blocks a critical step in the propagation of the prion-like determinant [*PSI*(+)] of *Saccharomyces cerevisiae*. *Proc. Natl. Acad. Sci. U. S. A,* **97,** 240-244.

63. Ehrnsperger,M., Graber,S., Gaestel,M., and Buchner,J. (1997). Binding of non-native protein to Hsp25 during heat shock creates a reservoir of folding intermediates for reactivation. *EMBO J.,* **16,** 221-229.

64. Ellis,R.J. (2001). Macromolecular crowding: obvious but underappreciated. *Trends Biochem. Sci.,* **26,** 597-604.

65. Eppens,E.F., Nouwen,N., and Tommassen,J. (1997). Folding of a bacterial outer membrane protein during passage through the periplasm. *EMBO J.,* **16,** 4295-4301.

66. Estruch,F. (2000). Stress-controlled transcription factors, stress-induced genes and stress tolerance in budding yeast. *FEMS Microbiol. Rev.,* **24,** 469-486.

67. Ewbank,J.J. and Creighton,T.E. (1993). Structural characterization of the disulfide folding intermediates of bovine alpha-lactalbumin. *Biochemistry,* **32,** 3694-3707.

68. Fairbanks,G., Steck,T.L., and Wallach,D.F.H. (1971). Electrophoretic Analysis of Major Polypeptides of Human Erythrocyte Membrane. *Biochemistry,* **10,** 2606-&.

69. Fenton,W.A. and Horwich,A.L. (1997). GroEL-mediated protein folding. *Protein Sci.,* **6,** 743-760.

70. Ferbitz,L., Maier,T., Patzelt,H., Bukau,B., Deuerling,E., and Ban,N. (2004). Trigger factor in complex with the ribosome forms a molecular cradle for nascent proteins. *Nature,* **431,** 590-596.

71. Ferreira,P.C., Ness,F., Edwards,S.R., Cox,B.S., and Tuite,M.F. (2001). The elimination of the yeast [*PSI*+] prion by guanidine hydrochloride is the result of Hsp104 inactivation. *Mol. Microbiol.,* **40,** 1357-1369.

72. Fersht,A.R. and Daggett,V. (2002). Protein folding and unfolding at atomic resolution. *Cell,* **108,** 573-582.

73. Fischer,G. and Aumuller,T. (2003). Regulation of peptide bond cis/trans isomerization by enzyme catalysis and its implication in physiological processes. *Rev. Physiol Biochem. Pharmacol.,* **148,** 105-150.

74. Fischer,G., Wittmann-Liebold,B., Lang,K., Kiefhaber,T., and Schmid,F.X. (1989). Cyclophilin and peptidyl-prolyl cis-trans isomerase are probably identical proteins. *Nature,* **337,** 476-478.

75. Flynn,J.M., Levchenko,I., Seidel,M., Wickner,S.H., Sauer,R.T., and Baker,T.A. (2001). Overlapping recognition determinants within the ssrA degradation tag allow modulation of proteolysis. *Proc. Natl. Acad. Sci. U. S. A,* **98,** 10584-10589.

76. Frand,A.R., Cuozzo,J.W., and Kaiser,C.A. (2000). Pathways for protein disulphide bond formation. *Trends Cell Biol.,* **10,** 203-210.

77. Fritz, L. and Burrows, F. Methods for treating genetically-defined proliferative disorders with Hsp90 inhibitors. 469469[United States Application 20060079493469469]. 2006.

78. Frydman,J. and Hartl,F.U. (1996). Principles of chaperone-assisted protein folding: differences between in vitro and in vivo mechanisms. *Science,* **272,** 1497-1502.

79. Gai,D., Zhao,R., Li,D., Finkielstein,C.V., and Chen,X.S. (2004). Mechanisms of conformational change for a replicative hexameric helicase of SV40 large tumor antigen. *Cell,* **119,** 47-60.

80. Gall,W.E., Higginbotham,M.A., Chen,C., Ingram,M.F., Cyr,D.M., and Graham,T.R. (2000). The auxilin-like phosphoprotein Swa2p is required for clathrin function in yeast. *Curr. Biol.,* **10,** 1349-1358.

81. Galzitskaya,O.V., Ivankov,D.N., and Finkelstein,A.V. (2001). Folding nuclei in proteins. *FEBS Lett.,* **489,** 113-118.

82. Gari,E., Piedrafita,L., Aldea,M., and Herrero,E. (1997). A set of vectors with a tetracycline-regulatable promoter system for modulated gene expression in *Saccharomyces cerevisiae*. *Yeast,* **13,** 837-848.

83. Gasch,A.P., Spellman,P.T., Kao,C.M., Carmel-Harel,O., Eisen,M.B., Storz,G., Botstein,D., and Brown,P.O. (2000). Genomic expression programs in the response of yeast cells to environmental changes. *Mol. Biol. Cell,* **11,** 4241-4257.

84. Gatto,C., Helms,J.B., Prasse,M.C., Huang,S.Y., Zou,X., Arnett,K.L., and Milanick,M.A. (2006). Similarities and differences between organic cation inhibition of the Na,K-ATPase and PMCA. *Biochemistry,* **45,** 13331-13345.

85. Ghaemmaghami,S., Huh,W.K., Bower,K., Howson,R.W., Belle,A., Dephoure,N., O'Shea,E.K., and Weissman,J.S. (2003). Global analysis of protein expression in yeast. *Nature,* **425,** 737-741.

86. Gill,S.C. and von Hippel,P.H. (1989). Calculation of protein extinction coefficients from amino acid sequence data. *Anal. Biochem.,* **182,** 319-326.

87. Glover,J.R. and Lindquist,S. (1998). Hsp104, Hsp70, and Hsp40: a novel chaperone system that rescues previously aggregated proteins. *Cell,* **94,** 73-82.

88. Glover,J.R. and Tkach,J.M. (2001). Crowbars and ratchets: Hsp100 chaperones as tools in reversing protein aggregation. *Biochem. Cell Biol.,* **79,** 557-568.

89. Golbik,R., Fischer,G., and Fersht,A.R. (1999). Folding of barstar C40A/C82A/P27A and catalysis of the peptidyl-prolyl cis/trans isomerization by human cytosolic cyclophilin (Cyp18). *Protein Sci.,* **8,** 1505-1514.

90. Goldberg,M.E., Rudolph,R., and Jaenicke,R. (1991). A kinetic study of the competition between renaturation and aggregation during the refolding of denatured-reduced egg white lysozyme. *Biochemistry,* **30,** 2790-2797.

91. Goloubinoff,P., Mogk,A., Zvi,A.P., Tomoyasu,T., and Bukau,B. (1999). Sequential mechanism of solubilization and refolding of stable protein aggregates by a bichaperone network. *Proc. Natl. Acad. Sci. U. S. A,* **96,** 13732-13737.

92. Goodsell,D.S. (1991). Inside a living cell. *Trends Biochem. Sci.,* **16,** 203-206.

93. Goto,Y. and Hamaguchi,K. (1982). Unfolding and refolding of the constant fragment of the immunoglobulin light chain. *J. Mol. Biol.,* **156,** 891-910.

94. Grably,M.R., Stanhill,A., Tell,O., and Engelberg,D. (2002). HSF and Msn2/4p can exclusively or cooperatively activate the yeast HSP104 gene. *Mol. Microbiol.,* **44,** 21-35.

95. Grimminger,V., Richter,K., Imhof,A., Buchner,J., and Walter,S. (2004). The prion curing agent guanidinium chloride specifically inhibits ATP hydrolysis by Hsp104. *J. Biol. Chem.,* **279,** 7378-7383.

96. Guo,F., Maurizi,M.R., Esser,L., and Xia,D. (2002). Crystal structure of ClpA, an Hsp100 chaperone and regulator of ClpAP protease. *J. Biol. Chem.,* **277,** 46743-46752.

97. Hahn,J.S. and Thiele,D.J. (2004). Activation of the *Saccharomyces cerevisiae* heat shock transcription factor under glucose starvation conditions by Snf1 protein kinase. *J. Biol. Chem.,* **279,** 5169-5176.

98. Hainzl,O., Wegele,H., Richter,K., and Buchner,J. (2004). Cns1 is an activator of the Ssa1 ATPase activity. *J. Biol. Chem.,* **279,** 23267-23273.

99. Hanson,P.I. and Whiteheart,S.W. (2005). AAA+ proteins: have engine, will work. *Nat. Rev. Mol. Cell Biol.,* **6,** 519-529.

100. Haslbeck,M., Franzmann,T., Weinfurtner,D., and Buchner,J. (2005a). Some like it hot: the structure and function of small heat-shock proteins. *Nat. Struct. Mol. Biol.,* **12,** 842-846.

101. Haslbeck,M., Miess,A., Stromer,T., Walter,S., and Buchner,J. (2005b). Disassembling protein aggregates in the yeast cytosol. The cooperation of Hsp26 with Ssa1 and Hsp104. *J. Biol. Chem.,* **280,** 23861-23868.

102. Haslbeck,M., Walke,S., Stromer,T., Ehrnsperger,M., White,H.E., Chen,S., Saibil,H.R., and Buchner,J. (1999). Hsp26: a temperature-regulated chaperone. *EMBO J.,* **18,** 6744-6751.

103. Haslberger,T., Weibezahn,J., Zahn,R., Lee,S., Tsai,F.T., Bukau,B., and Mogk,A. (2007). M domains couple the ClpB threading motor with the DnaK chaperone activity. *Mol. Cell,* **25,** 247-260.

104. Hattendorf,D.A. and Lindquist,S.L. (2002a). Analysis of the AAA sensor-2 motif in the C-terminal ATPase domain of Hsp104 with a site-specific fluorescent probe of nucleotide binding. *Proc. Natl. Acad. Sci. U. S. A,* **99,** 2732-2737.

105. Hattendorf,D.A. and Lindquist,S.L. (2002b). Cooperative kinetics of both Hsp104 ATPase domains and interdomain communication revealed by AAA sensor-1 mutants. *EMBO J.,* **21,** 12-21.

106. Hersch,G.L., Burton,R.E., Bolon,D.N., Baker,T.A., and Sauer,R.T. (2005). Asymmetric interactions of ATP with the AAA+ ClpX6 unfoldase: allosteric control of a protein machine. *Cell,* **121,** 1017-1027.

107. Heukeshoven,J. and Dernick,R. (1988). Improved Silver Staining Procedure for Fast Staining in Phastsystem Development Unit .1. Staining of Sodium Dodecyl-Sulfate Gels. *Electrophoresis,* **9,** 28-32.

108. Holde,v.K.E. and Weischet,W.O. (1978). Boundary Analysis of Sedimentation-Velocity Experiments with Monodisperse and Paucidisperse Solutes. *Biopolymers,* **17,** 1387-1403.

109. Horwich,A.L., Weber-Ban,E.U., and Finley,D. (1999). Chaperone rings in protein folding and degradation. *Proc. Natl. Acad. Sci. U. S. A,* **96,** 11033-11040.

110. Horwitz,J. (2003). Alpha-crystallin. *Exp. Eye Res.,* **76,** 145-153.

111. Huh,W.K., Falvo,J.V., Gerke,L.C., Carroll,A.S., Howson,R.W., Weissman,J.S., and O'Shea,E.K. (2003). Global analysis of protein localization in budding yeast. *Nature,* **425,** 686-691.

112. Hwang,B.J., Park,W.J., Chung,C.H., and Goldberg,A.L. (1987). *Escherichia coli* contains a soluble ATP-dependent protease (Ti) distinct from protease La. *Proc. Natl. Acad. Sci. U. S. A,* **84,** 5550-5554.

113. Hwang,B.J., Woo,K.M., Goldberg,A.L., and Chung,C.H. (1988). Protease Ti, a new ATP-dependent protease in *Escherichia coli*, contains protein-activated ATPase and proteolytic functions in distinct subunits. *J. Biol. Chem.,* **263,** 8727-8734.

114. Ito,H., Fukuda,Y., Murata,K., and Kimura,A. (1983). Transformation of Intact Yeast-Cells Treated with Alkali Cations. *J. Bact.,* **153,** 163-168.

115. Jaenicke,R. (1987). Folding and association of proteins. *Prog. Biophys. Mol. Biol.,* **49,** 117-237.

116. Jaenicke,R. (1991). Protein folding: local structures, domains, subunits, and assemblies. *Biochemistry,* **30,** 3147-3161.

117. Jaenicke,R. and Seckler,R. (1997). Protein misassembly in vitro. *Adv. Protein Chem.,* **50,** 1-59.

118. Jahn,T.R. and Radford,S.E. (2005). The Yin and Yang of protein folding. *FEBS J.,* **272,** 5962-5970.

119. Jakob,U., Gaestel,M., Engel,K., and Buchner,J. (1993). Small heat shock proteins are molecular chaperones. *J. Biol. Chem.,* **268,** 1517-1520.

120. Johnson,B.D., Schumacher,R.J., Ross,E.D., and Toft,D.O. (1998). Hop modulates Hsp70/Hsp90 interactions in protein folding. *J. Biol. Chem.,* **273,** 3679-3686.

121. Jones,G.W. and Tuite,M.F. (2006). Chaperoning prions: the cellular machinery for propagating an infectious protein? *Bioessays,* **27,** 823-832.

122. Jung,G. and Jones,G. (2003). Yeast Prions. *J. Biol. Macromol.,* **3,** 41-46.

123. Jung,G., Jones,G., and Masison,D.C. (2002). Amino acid residue 184 of yeast Hsp104 chaperone is critical for prion-curing by guanidine, prion propagation, and thermotolerance. *Proc. Natl. Acad. Sci. U. S. A,* **99,** 9936-9941.

124. Jung,G. and Masison,D.C. (2001). Guanidine hydrochloride inhibits Hsp104 activity in vivo: a possible explanation for its effect in curing yeast prions. *Curr. Microbiol.,* **43,** 7-10.

125. Kaiser,C., Michaelis,S., and Mitchell,A. (1994). *Methods in Yeast Genetics.* Cold Spring Harbor Laboratory Press, Cold Spring Harbor, NY.

126. Karata,K., Inagawa,T., Wilkinson,A.J., and Tatsuta,T. (1999). Dissecting the role of a conserved motif (the second region of homology) in the AAA family of ATPases. *J. Biol. Chem.,* **274,** 26225-26232.

127. Katayama,Y., Gottesman,S., Pumphrey,J., Rudikoff,S., Clark,W.P., and Maurizi,M.R. (1988). The two-component, ATP-dependent Clp protease of *Escherichia coli*. Purification, cloning, and mutational analysis of the ATP-binding component. *J. Biol. Chem.,* **263,** 15226-15236.

128. Kedzierska,S., Akoev,V., Barnett,M.E., and Zolkiewski,M. (2003). Structure and function of the middle domain of ClpB from *Escherichia coli*. *Biochemistry,* **42,** 14242-14248.

129. Kelley,W.L. (1998). The J-domain family and the recruitment of chaperone power. *Trends Biochem. Sci.,* **23,** 222-227.

130. Kelly,J.W. (2000). Mechanisms of amyloidogenesis. *Nat. Struct. Biol.,* **7,** 824-826.

131. Kenniston,J.A., Baker,T.A., Fernandez,J.M., and Sauer,R.T. (2003). Linkage between ATP consumption and mechanical unfolding during the protein processing reactions of an AAA+ degradation machine. *Cell,* **114,** 511-520.

132. Kim,K.I., Cheong,G.W., Park,S.C., Ha,J.S., Woo,K.M., Choi,S.J., and Chung,C.H. (2000a). Heptameric ring structure of the heat-shock protein ClpB, a protein-activated ATPase in *Escherichia coli*. *J. Mol. Biol.,* **303,** 655-666.

133. Kim,K.K., Kim,R., and Kim,S.H. (1998). Crystal structure of a small heat-shock protein. *Nature,* **394,** 595-599.

134. Kim,S., Willison,K.R., and Horwich,A.L. (1994). Cytosolic chaperonin subunits have a conserved ATPase domain but diverged polypeptide-binding domains. *Trends Biochem. Sci.,* **19,** 543-548.

135. Kim,Y.I., Burton,R.E., Burton,B.M., Sauer,R.T., and Baker,T.A. (2000b). Dynamics of substrate denaturation and translocation by the ClpXP degradation machine. *Mol. Cell,* **5,** 639-648.

136. Koch,C., Wollmann,P., Dahl,M., and Lottspeich,F. (1999). A role for Ctr9p and Paf1p in the regulation G1 cyclin expression in yeast. *Nucleic Acids Res.,* **27,** 2126-2134.

137. Kon,T., Nishiura,M., Ohkura,R., Toyoshima,Y.Y., and Sutoh,K. (2004). Distinct functions of nucleotide-binding/hydrolysis sites in the four AAA modules of cytoplasmic dynein. *Biochemistry,* **43,** 11266-11274.

138. Koonin,E.V. (1993). A common set of conserved motifs in a vast variety of putative nucleic acid-dependent ATPases including MCM proteins involved in the initiation of eukaryotic DNA replication. *Nucleic Acids Res.,* **21,** 2541-2547.

139. Kornberg,A., Scott,J.F., and Bertsch,L.L. (1978). Atp Utilization by Rep Protein in Catalytic Separation of Dna Strands at A Replicating Fork. *J. Biol. Chem.,* **253,** 3298-3304.

140. Kushnirov,V.V., Kryndushkin,D.S., Boguta,M., Smirnov,V.N., and Ter Avanesyan,M.D. (2000). Chaperones that cure yeast artificial [*PSI+*] and their prion-specific effects. *Curr. Biol.,* **10,** 1443-1446.

141. Kushnirov,V.V. and Ter Avanesyan,M.D. (1998). Structure and replication of yeast prions. *Cell,* **94,** 13-16.

142. Kyte,J. and Doolittle,R.F. (1982). A simple method for displaying the hydropathic character of a protein. *J. Mol. Biol.,* **157,** 105-132.

143. Laemmli,U.K. (1970). Cleavage of Structural Proteins During Assembly of Head of Bacteriophage-T4. *Nature,* **227,** 680-&.

144. Lamb,J.R., Michaud,W.A., Sikorski,R.S., and Hieter,P.A. (1994). Cdc16p, Cdc23p and Cdc27p form a complex essential for mitosis. *EMBO J.,* **13,** 4321-4328.

145. Larsson,C., Pahlman,I.L., and Gustafsson,L. (2000). The importance of ATP as a regulator of glycolytic flux in *Saccharomyces cerevisiae*. *Yeast,* **16,** 797-809.

146. Laskey,R.A., Honda,B.M., Mills,A.D., and Finch,J.T. (1978). Nucleosomes are assembled by an acidic protein which binds histones and transfers them to DNA. *Nature,* **275,** 416-420.

147. Laue,T.M. and Stafford,W.F. (1999). Modern applications of analytical ultracentrifugation. *Annu. Rev. Biophys. Biomol. Struct.,* **28,** 75-100.

148. Lee,C., Schwartz,M.P., Prakash,S., Iwakura,M., and Matouschek,A. (2001). ATP-dependent proteases degrade their substrates by processively unraveling them from the degradation signal. *Mol. Cell,* **7,** 627-637.

149. Lee,G.J., Roseman,A.M., Saibil,H.R., and Vierling,E. (1997). A small heat shock protein stably binds heat-denatured model substrates and can maintain a substrate in a folding-competent state. *EMBO J.,* **16,** 659-671.

150. Lee,S., Choi,J.M., and Tsai,F.T. (2007). Visualizing the ATPase cycle in a protein disaggregation maschine: structural basis for substrate binding by ClpB. *Mol. Cell,* **25,** 261-271.

151. Lee,S., Sowa,M.E., Watanabe,Y.H., Sigler,P.B., Chiu,W., Yoshida,M., and Tsai,F.T. (2003). The structure of ClpB: a molecular chaperone that rescues proteins from an aggregated state. *Cell,* **115,** 229-240.

152. Levchenko,I., Seidel,M., Sauer,R.T., and Baker,T.A. (2000). A specificity-enhancing factor for the ClpXP degradation machine. *Science,* **289,** 2354-2356.

153. Levinthal,C. (1968). Are there pathways for protein folding? *J. Chim. Phys.,* **65,** 44-45.

154. Lewis,J., Devin,A., Miller,A., Lin,Y., Rodriguez,Y., Neckers,L., and Liu,Z.G. (2000). Disruption of hsp90 function results in degradation of the death domain kinase, receptor-interacting protein (RIP), and blockage of tumor necrosis factor-induced nuclear factor-kappaB activation. *J. Biol. Chem.,* **275,** 10519-10526.

155. Li,N., Zhang,L.M., Zhang,K.Q., Deng,J.S., Prandl,R., and Schoffl,F. (2006). Effects of heat stress on yeast heat shock factor-promoter binding in vivo. *Acta Biochim. Biophys. Sin. (Shanghai),* **38,** 356-362.

156. Liao,Y., Willis,I.M., and Moir,R.D. (2003). The Brf1 and Bdp1 subunits of transcription factor TFIIIB bind to overlapping sites in the tetratricopeptide repeats of Tfc4. *J. Biol. Chem.,* **278,** 44467-44474.

157. Liberek,K., Marszalek,J., Ang,D., Georgopoulos,C., and Zylicz,M. (1991). *Escherichia coli* DnaJ and GrpE heat shock proteins jointly stimulate ATPase activity of DnaK. *Proc. Natl. Acad. Sci. U. S. A,* **88,** 2874-2878.

158. Lindquist,S. and Kim,G. (1996). Heat-shock protein 104 expression is sufficient for thermotolerance in yeast. *Proc. Natl. Acad. Sci. U. S. A,* **93,** 5301-5306.

159. Liou,S.T. and Wang,C. (2005). Small glutamine-rich tetratricopeptide repeat-containing protein is composed of three structural units with distinct functions. *Arch. Biochem. Biophys.,* **435,** 253-263.

160. Liu,F.H., Wu,S.J., Hu,S.M., Hsiao,C.D., and Wang,C. (1999). Specific interaction of the 70-kDa heat shock cognate protein with the tetratricopeptide repeats. *J. Biol. Chem.,* **274,** 34425-34432.

161. Liu,Z., Tek,V., Akoev,V., and Zolkiewski,M. (2002). Conserved amino acid residues within the amino-terminal domain of ClpB are essential for the chaperone activity. *J. Mol. Biol.,* **321,** 111-120.

162. Lu,Z. and Cyr,D.M. (1998). Protein folding activity of Hsp70 is modified differentially by the hsp40 co-chaperones Sis1 and Ydj1. *J. Biol. Chem.,* **273,** 27824-27830.

163. Lum,R., Tkach,J.M., Vierling,E., and Glover,J.R. (2004). Evidence for an unfolding/threading mechanism for protein disaggregation by *Saccharomyces cerevisiae* Hsp104. *J. Biol. Chem.,* **279,** 29139-29146.

164. Martin,A., Baker,T.A., and Sauer,R.T. (2005). Rebuilt AAA + motors reveal operating principles for ATP-fuelled machines. *Nature,* **437,** 1115-1120.

165. Martinez-Pastor,M.T., Marchler,G., Schuller,C., Marchler-Bauer,A., Ruis,H., and Estruch,F. (1996). The *Saccharomyces cerevisiae* zinc finger proteins Msn2p and Msn4p are required for transcriptional induction through the stress response element (STRE). *EMBO J.,* **15,** 2227-2235.

166. Matveeva,E.A., He,P., and Whiteheart,S.W. (1997). *N*-ethylmaleimide-sensitive fusion protein contains high and low affinity ATP-binding sites that are functionally distinct. *J. Biol. Chem.,* **272,** 26413-26418.

167. Mayer,M.P. and Bukau,B. (2005). Regulation of Hsp70 Chaperones by Co-chaperones. In Buchner,J. and Kiefhaber,T. (Eds.), *Protein Folding Handbook*, . Wiley-VCH, Weinheim, pp. 516-562.

168. Mayr,C., Richter,K., Lilie,H., and Buchner,J. (2000). Cpr6 and Cpr7, two closely related Hsp90-associated immunophilins from *Saccharomyces cerevisiae*, differ in their functional properties. *J. Biol. Chem.,* **275,** 34140-34146.

169. Meyer,A.S., Gillespie,J.R., Walther,D., Millet,I.S., Doniach,S., and Frydman,J. (2003). Closing the folding chamber of the eukaryotic chaperonin requires the transition state of ATP hydrolysis. *Cell,* **113,** 369-381.

170. Mogk,A., Deuerling,E., Vorderwulbecke,S., Vierling,E., and Bukau,B. (2003a). Small heat shock proteins, ClpB and the DnaK system form a functional triade in reversing protein aggregation. *Mol. Microbiol.,* **50,** 585-595.

171. Mogk,A., Schlieker,C., Friedrich,K.L., Schonfeld,H.J., Vierling,E., and Bukau,B. (2003b). Refolding of Substrates Bound to Small Hsps Relies on a Disaggregation Reaction Mediated Most Efficiently by ClpB/DnaK. *J. Biol. Chem.,* **278,** 31033-31042.

172. Mogk,A., Schlieker,C., Strub,C., Rist,W., Weibezahn,J., and Bukau,B. (2003c). Roles of individual domains and conserved motifs of the AAA+ chaperone ClpB in oligomerization, ATP hydrolysis, and chaperone activity. *J. Biol. Chem.,* **278,** 17615-17624.

173. Moriyama,H., Edskes,H.K., and Wickner,R.B. (2000). [URE3] prion propagation in *Saccharomyces cerevisiae*: requirement for chaperone Hsp104 and curing by overexpressed chaperone Ydj1p. *Mol. Cell Biol.,* **20,** 8916-8922.

174. Motohashi,K., Watanabe,Y., Yohda,M., and Yoshida,M. (1999). Heat-inactivated proteins are rescued by the DnaK.J-GrpE set and ClpB chaperones. *Proc. Natl. Acad. Sci. U. S. A,* **96,** 7184-7189.

175. Mullis,K., Faloona,F., Scharf,S., Saiki,R., Horn,G., and Erlich,H. (1986). Specific Enzymatic Amplification of Dna Invitro - the Polymerase Chain-Reaction. *Cold Spring Harbor Symposia on Quantitative Biology,* **51,** 263-273.

176. Murray,K.E. and Nibert,M.L. (2007). Guanidine Hydrochloride Inhibits Mammalian Orthoreovirus Growth by Reversibly Blocking the Synthesis of Double-Stranded RNA. *J. Virol.*.

177. Narayanan,S., Bosl,B., Walter,S., and Reif,B. (2003). Importance of low-oligomeric-weight species for prion propagation in the yeast prion system Sup35/Hsp104. *Proc. Natl. Acad. Sci. U. S. A,* **100,** 9286-9291.

178. Nelson,R. and Eisenberg,D. (2006). Structural models of amyloid-like fibrils. *Adv. Protein Chem.,* **73,** 235-282.

179. Ness,F., Ferreira,P., Cox,B.S., and Tuite,M.F. (2002). Guanidine hydrochloride inhibits the generation of prion "seeds" but not prion protein aggregation in yeast. *Mol. Cell Biol.,* **22,** 5593-5605.

180. Neuwald,A.F., Aravind,L., Spouge,J.L., and Koonin,E.V. (1999). AAA+: A class of chaperone-like ATPases associated with the assembly, operation, and disassembly of protein complexes. *Genome Res.,* **9,** 27-43.

181. Norby,J.G. (1988). Coupled assay of Na+,K+-ATPase activity. *Methods Enzymol.,* **156,** 116-119.

182. Ogura,T., Whiteheart,S.W., and Wilkinson,A.J. (2004). Conserved arginine residues implicated in ATP hydrolysis, nucleotide-sensing, and inter-subunit interactions in AAA and AAA+ ATPases. *J. Struct. Biol.,* **146,** 106-112.

183. Ogura,T. and Wilkinson,A.J. (2001). AAA+ superfamily ATPases: common structure--diverse function. *Genes Cells,* **6,** 575-597.

184. Pak,M., Hoskins,J.R., Singh,S.K., Maurizi,M.R., and Wickner,S. (1999). Concurrent chaperone and protease activities of ClpAP and the requirement for the N-terminal ClpA ATP binding site for chaperone activity. *J. Biol. Chem.,* **274,** 19316-19322.

185. Panaretou,B., Siligardi,G., Meyer,P., Maloney,A., Sullivan,J.K., Singh,S., Millson,S.H., Clarke,P.A., Naaby-Hansen,S., Stein,R., Cramer,R., Mollapour,M., Workman,P., Piper,P.W., Pearl,L.H., and Prodromou,C. (2002). Activation of the ATPase activity of hsp90 by the stress-regulated cochaperone aha1. *Mol. Cell,* **10,** 1307-1318.

186. Parsell,D.A., Kowal,A.S., and Lindquist,S. (1994a). Saccharomyces cerevisiae Hsp104 protein. Purification and characterization of ATP-induced structural changes. *J. Biol. Chem.,* **269,** 4480-4487.

187. Parsell,D.A., Kowal,A.S., Singer,M.A., and Lindquist,S. (1994b). Protein disaggregation mediated by heat-shock protein Hsp104. *Nature,* **372,** 475-478.

188. Parsell,D.A., Sanchez,Y., Stitzel,J.D., and Lindquist,S. (1991). Hsp104 is a highly conserved protein with two essential nucleotide-binding sites. *Nature,* **353,** 270-273.

189. Patino,M.M., Liu,J.J., Glover,J.R., and Lindquist,S. (1996). Support for the prion hypothesis for inheritance of a phenotypic trait in yeast. *Science,* **273,** 622-626.

190. Paushkin,S.V., Kushnirov,V.V., Smirnov,V.N., and Ter Avanesyan,M.D. (1996). Propagation of the yeast prion-like [*psi*+] determinant is mediated by oligomerization of the SUP35-encoded polypeptide chain release factor. *EMBO J.,* **15,** 3127-3134.

191. Pearl,L.H. and Prodromou,C. (2006). Structure and mechanism of the Hsp90 molecular chaperone machinery. *Annu. Rev. Biochem.,* **75,** 271-294.

192. Pelham,H.R. (1986). Speculations on the functions of the major heat shock and glucose-regulated proteins. *Cell,* **46,** 959-961.

193. Pierce,M.M., Raman,C.S., and Nall,B.T. (1999). Isothermal titration calorimetry of protein-protein interactions. *Methods-A Companion to Methods in Enzymology,* **19,** 213-221.

194. Prodromou,C., Siligardi,G., O'Brien,R., Woolfson,D.N., Regan,L., Panaretou,B., Ladbury,J.E., Piper,P.W., and Pearl,L.H. (1999). Regulation of Hsp90 ATPase activity by tetratricopeptide repeat (TPR)-domain co-chaperones. *EMBO J.,* **18,** 754-762.

195. Prusiner,S.B. (1998). Prions. *Proc. Natl. Acad. Sci. U. S. A,* **95,** 13363-13383.

196. Ptitsyn,O.B. (1996). A determinable but unresolved problem. *FASEB J.,* **10,** 3-4.

197. Pye,V.E., Dreveny,I., Briggs,L.C., Sands,C., Beuron,F., Zhang,X., and Freemont,P.S. (2006). Going through the motions: The ATPase cycle of p97. *J. Struct. Biol.,* **156,** 12-28.

198. Qiu,X.-B., Shao,Y.-M., Miao,S., and Wang,L. (2007). The diversity of the DnaJ/Hsp40 family, the crucial partners for Hsp70 chaperones. *Cell Mol. Life Sci.,* **63,** 2560-2570.

199. Ratajczak,T., Carrello,A., Mark,P.J., Warner,B.J., Simpson,R.J., Moritz,R.L., and House,A.K. (1993). The cyclophilin component of the unactivated estrogen-receptor contains a tetratricopeptide repeat domain and shares identity with p59. *J. Biol. Chem.,* **268,** 13187-13192.

200. Reid,B.G., Fenton,W.A., Horwich,A.L., and Weber-Ban,E.U. (2001). ClpA mediates directional translocation of substrate proteins into the ClpP protease. *Proc. Natl. Acad. Sci. U. S. A,* **98,** 3768-3772.

201. Richter,K. and Buchner,J. (2001). Hsp90: chaperoning signal transduction. *J. Cell Physiol,* **188,** 281-290.

202. Richter,K. and Buchner,J. (2006a). hsp90: twist and fold. *Cell,* **127,** 251-253.

203. Richter,K., Meinlschmidt,B., and Buchner,J. (2005). Hsp90: From Dispensable Heat SHock Protein to Global Player. In Buchner,J. and Kiefhaber,T. (Eds.), *Protein Folding Handbook*, . Wiley-VCH, Weilheim, pp. 768-829.

204. Richter,K., Moser,S., Hagn,F., Friedrich,R., Hainzl,O., Heller,M., Schlee,S., Kessler,H., Reinstein,J., and Buchner,J. (2006b). Intrinsic inhibition of the Hsp90 ATPase activity. *J. Biol. Chem.,* **281,** 11301-11311.

205. Richter,K., Muschler,P., Hainzl,O., and Buchner,J. (2001). Coordinated ATP hydrolysis by the Hsp90 dimer. *J. Biol. Chem.,* **276,** 33689-33696.

206. Richter,K., Muschler,P., Hainzl,O., Reinstein,J., and Buchner,J. (2003). Sti1 is a non-competitive inhibitor of the Hsp90 ATPase. Binding prevents the N-terminal dimerization reaction during the atpase cycle. *J. Biol. Chem.,* **278,** 10328-10333.

207. Richter,K., Walter,S., and Buchner,J. (2004). The Co-chaperone Sba1 connects the ATPase reaction of Hsp90 to the progression of the chaperone cycle. *J. Mol. Biol.,* **342,** 1403-1413.

208. Rüdiger,S., Schneider-Mergener,J., and Bukau,B. (2001). Its substrate specificity characterizes the DnaJ chaperone as scanning factor for the DnaK chaperone. *EMBO J.,* **20,** 1-9.

209. Sambrook,J. and Russell,D.W. (2001). *Molecular Cloning: A Laboratory Manual*. Cold Spring Harbor Laboratory Press, Cold Spring Harbor, New York.

210. Sanchez,Y. and Lindquist,S.L. (1990). HSP104 required for induced thermotolerance. *Science,* **248,** 1112-1115.

211. Sanchez,Y., Parsell,D.A., Taulien,J., Vogel,J.L., Craig,E.A., and Lindquist,S. (1993). Genetic evidence for a functional relationship between Hsp104 and Hsp70. *J. Bacteriol.,* **175,** 6484-6491.

212. Sanchez,Y., Taulien,J., Borkovich,K.A., and Lindquist,S. (1992). Hsp104 is required for tolerance to many forms of stress. *EMBO J.,* **11,** 2357-2364.

213. Santoso,A., Chien,P., Osherovich,L.Z., and Weissman,J.S. (2000). Molecular basis of a yeast prion species barrier. *Cell,* **100,** 277-288.

214. Saraste,M., Sibbald,P.R., and Wittinghofer,A. (1990). The P-loop - a common motif in ATP- and GTP-binding proteins. *Trends Biochem. Sci.,* **15,** 430-434.

215. Satpute-Krishnan,P., Langseth,S.X., and Serio,T.R. (2007). Hsp104-dependent remodeling of prion complexes mediates protein-only inheritance. *PLoS Biol.,* **5,** e24.

216. Schachman,H.K., Pardee,A.B., and Stanier,R.Y. (1952). Studies on the Macromolecular Organization of Microbial Cells. *Archives of Biochemistry and Biophysics,* **38,** 245-260.

217. Schaupp,A., Marcinowski,M., Grimminger,V., Bösl,B., and Walter,S. (2007). Processing of proteins by the molecular chaperone Hsp104. *J. Biol. Chem.*.

218. Scheufler,C., Brinker,A., Bourenkov,G., Pegoraro,S., Moroder,L., Bartunik,H., Hartl,F.U., and Moarefi,I. (2000). Structure of TPR domain-peptide complexes: critical elements in the assembly of the Hsp70-Hsp90 multichaperone machine. *Cell,* **101,** 199-210.

219. Schirmer,E.C., Glover,J.R., Singer,M.A., and Lindquist,S. (1996). HSP100/Clp proteins: a common mechanism explains diverse functions. *Trends Biochem. Sci.,* **21,** 289-296.

220. Schirmer,E.C., Queitsch,C., Kowal,A.S., Parsell,D.A., and Lindquist,S. (1998). The ATPase activity of Hsp104, effects of environmental conditions and mutations. *J. Biol. Chem.,* **273,** 15546-15552.

221. Schirmer,E.C., Ware,D.M., Queitsch,C., Kowal,A.S., and Lindquist,S.L. (2001). Subunit interactions influence the biochemical and biological properties of Hsp104. *Proc. Natl. Acad. Sci. U. S. A,* **98,** 914-919.

222. Schlee,S., Groemping,Y., Herde,P., Seidel,R., and Reinstein,J. (2001). The chaperone function of ClpB from *Thermus thermophilus* depends on allosteric interactions of its two ATP-binding sites. *J. Mol. Biol.,* **306,** 889-899.

223. Schlee,S. and Reinstein,J. (2002). The DnaK/ClpB chaperone system from *Thermus thermophilus*. *Cell Mol. Life Sci.,* **59,** 1598-1606.

224. Schlieker,C., Bukau,B., and Mogk,A. (2002). Prevention and reversion of protein aggregation by molecular chaperones in the *E. coli* cytosol: implications for their applicability in biotechnology. *J. Biotechnol.,* **96,** 13-21.

225. Schlieker,C., Weibezahn,J., Patzelt,H., Tessarz,P., Strub,C., Zeth,K., Erbse,A., Schneider-Mergener,J., Chin,J.W., Schultz,P.G., Bukau,B., and Mogk,A. (2004). Substrate recognition by the AAA+ chaperone ClpB. *Nat. Struct. Mol. Biol.,* **11,** 607-615.

226. Schlossmann,J., Lill,R., Neupert,W., and Court DA (1996). Tom71, a novel homologue of the mitochondrial preprotein receptor Tom70. *J. Biol. Chem.,* **271,** 17890-17895.

227. Schmid,F.X. (1989). *Protein structure: A practical approach.* IRL Press, Oxford.

228. Schmid,F.X. (2001). Prolyl isomerases. *Adv. Protein Chem.,* **59,** 243-282.

229. Schmidt,M., Lupas,A.N., and Finley,D. (1999). Structure and mechanism of ATP-dependent proteases. *Curr. Opin. Struct. Biol.,* **3,** 584-591.

230. Schmitt,A.P. and McEntee,K. (1996). Msn2p, a zinc finger DNA-binding protein, is the transcriptional activator of the multistress response in Saccharomyces cerevisiae. *Proc. Natl. Acad. Sci. U. S. A,* **93,** 5777-5782.

231. Segel,I.H. (1993). *Enzyme Kinetics.* Wiley & Sons, New York.

232. Serio,T.R., Cashikar,A.G., Kowal,A.S., Sawicki,G.J., Moslehi,J.J., Serpell,L., Arnsdorf,M.F., and Lindquist,S.L. (2000). Nucleated conformational conversion and the replication of conformational information by a prion determinant. *Science,* **289,** 1317-1321.

233. Sherman,F. (2002). Getting started with yeast. *Methods Enzymol.,* **350,** 3-41.

234. Shiau,A.K., Harris,S.F., Southworth,D.R., and Agard,D.A. (2006). Structural Analysis of *E. coli* hsp90 reveals dramatic nucleotide-dependent conformational rearrangements. *Cell,* **127,** 329-340.

235. Shorter,J. and Lindquist,S. (2004). Hsp104 catalyzes formation and elimination of self-replicating Sup35 prion conformers. *Science,* **304,** 1793-1797.

236. Sigler,P.B., Xu,Z., Rye,H.S., Burston,S.G., Fenton,W.A., and Horwich,A.L. (1998). Structure and function in GroEL-mediated protein folding. *Annu. Rev. Biochem.,* **67,** 581-608.

237. Sikorski,R.S. and Hieter,P. (1989). A system of shuttle vectors and yeast host strains designed for efficient manipulation of DNA in Saccharomyces cerevisiae. *Genetics,* **122,** 19-27.

238. Silveira,J.R., Raymond,G.J., Hughson,A.G., Race,R.E., Sim,V.L., Hayes,S.F., and Caughey,B. (2005). The most infectious prion protein particles. *Nature,* **437,** 257-261.

239. Singh,R.R. and Appu Rao,A.G. (2002). Reductive unfolding and oxidative refolding of a Bowman-Birk inhibitor from horsegram seeds (Dolichos biflorus): evidence for "hyperreactive" disulfide bonds and rate-limiting nature of disulfide isomerization in folding. *Biochim. Biophys. Acta,* **1597,** 280-291.

240. Singh,S.K., Grimaud,R., Hoskins,J.R., Wickner,S., and Maurizi,M.R. (2000). Unfolding and internalization of proteins by the ATP-dependent proteases ClpXP and ClpAP. *Proc. Natl. Acad. Sci. U. S. A,* **97,** 8898-8903.

241. Singleton,M.R., Sawaya,M.R., Ellenberger,T., and Wigley,D.B. (2000). Crystal structure of T7 gene 4 ring helicase indicates a mechanism for sequential hydrolysis of nucleotides. *Cell,* **101,** 589-600.

242. Slepenkov,S.V., Witt,S.N., and Bukau,B. (2002). The unfolding story of the *Escherichia coli* Hsp70 DnaK: is DnaK a holdase or an unfoldase? *Mol. Microbiol.,* **45,** 1197-1206.

243. Smith,D.F. (1993). Dynamics of heat shock protein 90-progesterone receptor binding and the disactivation loop model for steroid receptor complexes. *Mol. Endocrinol.,* **7,** 1418-1429.

244. Smith,R.L., Redd,M.J., and Johnson,A.D. (1995). The tetratricopeptide repeats of Ssn6 interact with the homeo domain of alpha 2. *Genes Dev.,* **9,** 2903-2910.

245. Sondheimer,N. and Lindquist,S. (2000). Rnq1: an epigenetic modifier of protein function in yeast. *Mol. Cell,* **5,** 163-172.

246. Song,H.K., Hartmann,C., Ramachandran,R., Bochtler,M., Behrendt,R., Moroder,L., and Huber,R. (2000). Mutational studies on HslU and its docking mode with HslV. *Proc. Natl. Acad. Sci. U. S. A,* **97,** 14103-14108.

247. Sorger,P.K. (1990). Yeast heat shock factor contains separable transient and sustained response transcriptional activators. *Cell,* **62,** 793-805.

248. Soto,C. (2001). Protein misfolding and disease; protein refolding and therapy. *FEBS Lett.,* **498,** 204-207.

249. Squires,C.L., Pedersen,S., Ross,B.M., and Squires,C. (1991). ClpB is the *Escherichia coli* heat shock protein F84.1. *J. Bacteriol.,* **173,** 4254-4262.

250. Stamnes,M.A., Shieh,B.H., Chuman,L., Harris,G.L., and Zuker,C.S. (1991). The cyclophilin homolog ninaA is a tissue-specific integral membrane protein required for the proper synthesis of a subset of Drosophila rhodopsins. *Cell,* **65,** 219-227.

251. Stevens,S.W. and Abelson,J. (1999). Purification of the yeast U4/U6.U5 small nuclear ribonucleoprotein particle and identification of its proteins. *Proc. Natl. Acad. Sci. U. S. A,* **96,** 7226-7231.

252. Szabo,A., Langer,T., Schröder,H., Flanagan,J., Bukau,B., and Hartl,F.U. (1994). The ATP hydrolysis-dependent reaction cycle of the *Escherichia coli* Hsp70 system-DnaK, DnaJ and GrpE. *Proc. Natl. Acad. Sci. U. S. A,* **91,** 10345-10349.

253. Tanaka,M., Chien,P., Naber,N., Cooke,R., and Weissman,J.S. (2004a). Conformational variations in an infectious protein determine prion strain differences. *Nature,* **428,** 323-328.

254. Tanaka,M. and Weissman,J.S. (2006). An efficient protein transformation protocol for introducing prions into yeast. *Methods Enzymol.,* **412,** 185-200.

255. Tanaka,N., Collins,S.R., Toyama,B.H., and Weissman,J.S. (2006). The physical basis of how prion conformations detemine strain phenotypes. *Nature,* **442,** 585-589.

256. Tanaka,N., Tani,Y., Hattori,H., Tada,T., and Kunugi,S. (2004b). Interaction of the N-terminal domain of *Escherichia coli* heat-shock protein ClpB and protein aggregates during chaperone activity. *Protein Sci.,* **13,** 3214-3221.

257. Tang,Y.C., Chang,H.C., Roeben,A., Wischnewski,D., Wischnewski,N., Kerner,M.J., Hartl,F.U., and Hayer-Hartl,M. (2006). Structural features of the GroEL-GroES nano-cage required for rapid folding of encapsulated protein. *Cell,* **125,** 903-914.

258. Taylor,P., Dornan,J., Carrello,A., Minchin,R.F., Ratajczak,T., and Walkinshaw,M.D. (2001). Two structures of cyclophilin 40: folding and fidelity in the TPR domains. *Structure. (Camb.),* **9,** 431-438.

259. Teixeira,M.C., Monteiro,P., Jain,P., Tenreiro,S., Fernandes,A.R., Mira,N.P., Alenquer,M., Freitas,A.T., Oliveira,A.L., and Sa-Correia,I. (2006). The YEASTRACT database: a tool for the analysis of transcription regulatory associations in *Saccharomyces cerevisiae*. *Nucleic Acids Res.,* **34,** D446-D451.

260. Tissiers,A. and Watson,J.D. (1958). Ribonucleoprotein Particles from *Escherichia coli* . *Nature,* **182,** 778-780.

261. Tkach,J.M. and Glover,J.R. (2004). Amino acid substitutions in the C-terminal AAA+ module of Hsp104 prevent substrate recognition by disrupting oligomerization and cause high temperature inactivation. *J. Biol. Chem.,* **279,** 35692-35701.

262. True,H.L. and Lindquist,S. (2000). A yeast prion provides a mechanism for genetic variation and phenotypic diversity. *Nature,* **407,** 477-483.

263. Tuite,M.F. (1994). Genetics. Psi no more for yeast prions. *Nature,* **370,** 327-328.

264. Tuite,M.F. (2000). Yeast prions and their prion-forming domain. *Cell,* **100,** 289-292.

265. Tuite,M.F. and Cox,B.S. (2003). Propagation of yeast prions. *Nat. Rev. Mol. Cell Biol.,* **4,** 878-890.

266. Tuite,M.F. and Cox,B.S. (2006). The [*PSI*+] prion of yeast: a problem of inheritance. *Methods,* **39,** 9-22.

267. Tuite,M.F., Mundy,C.R., and Cox,B.S. (1981). Agents that cause a high frequency of genetic change from [*psi+*] to [*psi-*] in *Saccharomyces cerevisiae*. *Genetics,* **98,** 691-711.

266. Turgay,K., Hamoen,L.W., Venema,G., and Dubnau,D. (1997). Biochemical characterization of a molecular switch involving the heat shock protein ClpC, which controls the activity of ComK, the competence transcription factor of Bacillus subtilis. *Genes Dev.,* **11,** 119-128.

269. Turner,G.C. and Varshavsky,A. (2000). Detecting and measuring cotranslational protein degradation in vivo. *Science,* **289,** 2117-2120.

270. Tzamarias,D. and Struhl,K. (1995). Distinct TPR motifs of Cyc8 are involved in recruiting the Cyc8-Tup1 corepressor complex to differentially regulated promoters. *Genes Dev.,* **9,** 821-831.

271. Vale,R.D. (2000). AAA proteins. Lords of the ring. *J. Cell Biol.,* **150,** F13-F19.

272. Vanik,D.L., Surewicz,K.A., and Surewicz,W.K. (2004). Molecular basis of barriers for interspecies transmissibility of mammalian prions. *Mol. Cell,* **14,** 139-145.

273. Vaughan,C.K., Gohlke,U., Sobott,G., Good,V.M., Ali,M.M., Prodromou,C., Robinson,C.V., Saibil,H., and Pearl,L.H. (2007). Structure of an Hsp90-Cdc37-Cdk4 complex. *Mol. Cell,* **23,** 697-707.

274. von Ahsen,O., Lim,J.H., Caspers,P., Martin,F., Schonfeld,H.J., Rassow,J., and Pfanner,N. (2000). Cyclophilin-promoted folding of mouse dihydrofolate reductase does not include the slow conversion of the late-folding intermediate to the active enzyme. *J. Mol. Biol.,* **297,** 809-818.

275. Walker,J.E., Saraste,M., Runswick,M.J., and Gay,N.J. (1982). Distantly related sequences in the alpha- and beta-subunits of ATP synthase, myosin, kinases and other ATP-requiring enzymes and a common nucleotide binding fold. *EMBO J.,* **1,** 945-951.

276. Walter,S. (2002). Structure and function of the GroE chaperone. *Cell Mol. Life Sci.,* **59,** 1589-1597.

277. Wandinger,S.K., Suhre,M.H., Wegele,H., and Buchner,J. (2006). The phosphatase Ppt1 is a dedicated regulator of the molecular chaperone Hsp90. *EMBO J.,* **25,** 367-376.

278. Wang,X.J. and Etzkorn,F.A. (2006). Peptidyl-prolyl isomerase inhibitors. *Biopolymers,* **84,** 125-146.

279. Warth,R., Briand,P.A., and Picard,D. (1997). Functional analysis of the yeast 40 kDa cyclophilin Cyp40 and its role for viability and steroid receptor regulation. *Biol. Chem.,* **378,** 381-391.

280. Watanabe,Y.H., Motohashi,K., and Yoshida,M. (2002). Roles of the two ATP binding sites of ClpB from *Thermus thermophilus*. *J. Biol. Chem.,* **277,** 5804-5809.

281. Watanabe,Y.H., Takano,M., and Yoshida,M. (2005). ATP-binding to NBD1 of the ClpB chaperone induces motion of the long coiled-coil, stabilizes the hexamer and activates NBD2. *J. Biol. Chem.*.

282. Weber-Ban,E.U., Reid,B.G., Miranker,A.D., and Horwich,A.L. (1999). Global unfolding of a substrate protein by the Hsp100 chaperone ClpA. *Nature,* **401,** 90-93.

283. Wegele,H., Haslbeck,M., Reinstein,J., and Buchner,J. (2003). Sti1 is a novel activator of the Ssa proteins. *J. Biol. Chem.,* **278,** 25970-25976.

284. Wegrzyn,R.D., Bapat,K., Newnam,G.P., Zink,A.D., and Chernoff,Y.O. (2001). Mechanism of prion loss after Hsp104 inactivation in yeast. *Mol. Cell Biol.,* **21,** 4656-4669.

285. Weibezahn,J., Schlieker,C., Bukau,B., and Mogk,A. (2003). Characterization of a trap mutant of the AAA+ chaperone ClpB. *J. Biol. Chem.,* **278,** 32608-32617.

286. Weibezahn,J., Tessarz,P., Schlieker,C., Zahn,R., Maglica,Z., Lee,S., Zentgraf,H., Weber-Ban,E.U., Dougan,D.A., Tsai,F.T., Mogk,A., and Bukau,B. (2004). Thermotolerance requires refolding of aggregated proteins by substrate translocation through the central pore of ClpB. *Cell,* **119,** 653-665.

287. Whitesell,L., Mimnaugh,E.G., De Costa,B., Myers,C.E., and Neckers,L.M. (1994). Inhibition of heat shock protein HSP90-pp60v-src heteroprotein complex formation by benzoquinone ansamycins: essential role for stress proteins in oncogenic transformation. *Proc. Natl. Acad. Sci. U. S. A,* **91,** 8324-8328.

288. Wickner,R.B. (1994). [URE3] as an altered URE2 protein: evidence for a prion analog in *Saccharomyces cerevisiae*. *Science,* **264,** 566-569.

289. Woo,K.M., Kim,K.I., Goldberg,A.L., Ha,D.B., and Chung,C.H. (1992). The heat-shock protein ClpB in *Escherichia coli* is a protein-activated ATPase. *J. Biol. Chem.,* **267,** 20429-20434.

290. Wu,C. (1995). Heat shock transcription factors: structure and regulation. *Annu. Rev. Cell Dev. Biol.,* **11,** 441-469.

291. Wu,Y. and Sha,B. (2006). Crystal structure of yeast mitochondrial outer membrane translocon member Tom70p. *Nat. Struct. Mol. Biol.,* **13,** 589-593.

292. Xu,Y. and Lindquist,S. (1993). Heat-shock protein hsp90 governs the activity of pp60v-src kinase. *Proc. Natl. Acad. Sci. U. S. A,* **90,** 7074-7078.

293. Xu,Z., Horwich,A.L., and Sigler,P.B. (1997). The crystal structure of the asymmetric GroEL-GroES-$(ADP)_7$ chaperonin complex. *Nature,* **388,** 741-750.

294. Yamamoto,A., Mizukami,Y., and Sakurai,H. (2005). Identification of a novel class of target genes and a novel type of binding sequence of heat shock transcription factor in *Saccharomyces cerevisiae*. *J. Biol. Chem.,* **280,** 11911-11919.

295. Yanisch-Perron,C., Vieira,J., and Messing,J. (1985). Improved M13 phage cloning vectors and host strains: nucleotide sequences of the M13mp18 and pUC19 vectors. *Gene,* **33,** 103-119.

296. Young,B.P., Craven,R.A., Reid,P.J., Willer,M., and Stirling,C.J. (2001). Sec63p and Kar2p are required for the translocation of SRP-dependent precursors into the yeast endoplasmic reticulum in vivo. *EMBO J.,* **20,** 262-271.

297. Young,J.C., Agashe,V.R., Siegers,K., and Hartl,F.U. (2004). Pathways of chaperone-mediated protein folding in the cytosol. *Nat. Rev. Mol. Cell Biol.,* **5,** 781-791.

298. Young,J.C., Hoogenraad,N.J., and Hartl,F.U. (2003). Molecular chaperones Hsp90 and Hsp70 deliver preproteins to the mitochondrial import receptor Tom70. *Cell,* **112,** 41-50.

399. Zenthon,J.F., Ness,F., Cox,B., and Tuite,M.F. (2006). The [*PSI*+] prion of *Saccharomyces cerevisiae* can be propagated by an Hsp104 orthologue from *Candida albicans*. *Eukaryot. Cell,* **5,** 217-225.

300. Zhao,R., Davey,M., Hsu,Y.C., Kaplanek,P., Tong,A., Parsons,A.B., Krogan,N., Cagney,G., Mai,D., Greenblatt,J., Boone,C., Emili,A., and Houry,W.A. (2005). Navigating the chaperone network: an integrative map of physical and genetic interactions mediated by the hsp90 chaperone. *Cell,* **120,** 715-727.

301. Zhao,R. and Houry,W.A. (2005). Hsp90: a chaperone for protein folding and gene regulation. *Biochem. Cell Biol.,* **83,** 703-710.

302. Zietkiewicz,S., Krzewska,J., and Liberek,K. (2004). Successive and synergistic action of the Hsp70 and Hsp100 chaperones in protein disaggregation. *J. Biol. Chem.,* **279,** 44376-44383.

303. Zolkiewski,M. (1999). ClpB cooperates with DnaK, DnaJ, and GrpE in suppressing protein aggregation. A novel multi-chaperone system from *Escherichia coli*. *J. Biol. Chem.,* **274,** 28083-28086.

304. Zolkiewski,M. (2006). A camel passes through the eye of a needle: protein unfolding activity of Clp ATPases. *Mol. Microbiol.,* **61,** 1094-1100.

APPENDIX

A.1 Multiple sequence alignment of Hsp100/ClpB proteins

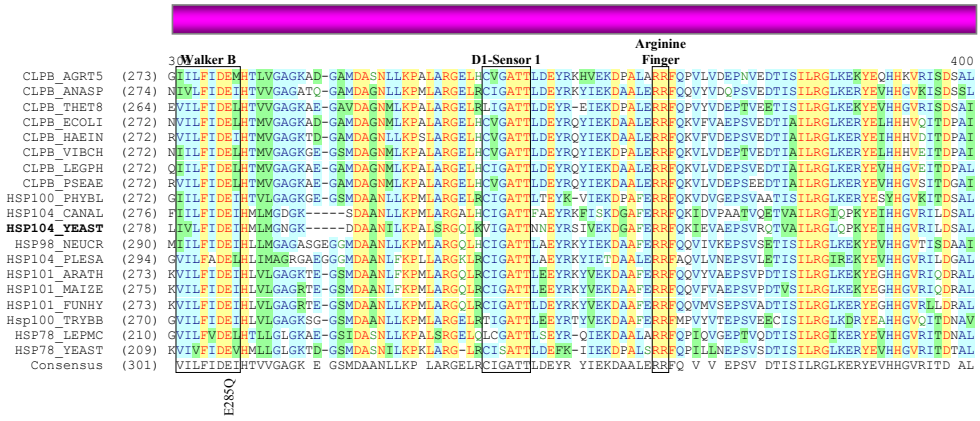
Arginine Finger
Walker B
D1-Sensor 1
E285Q


Middle Domain

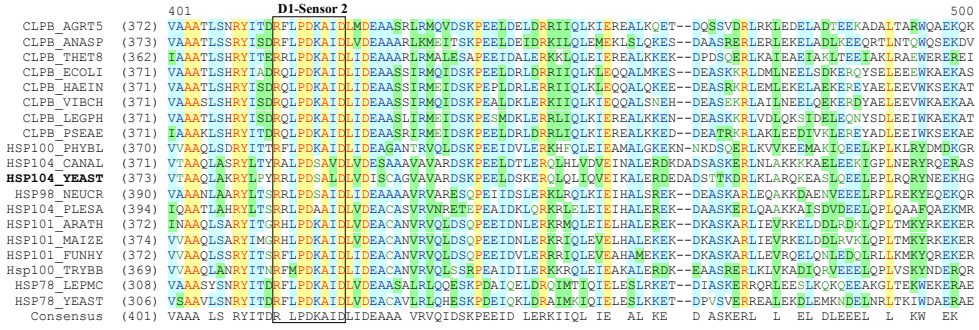
D1-Sensor 2

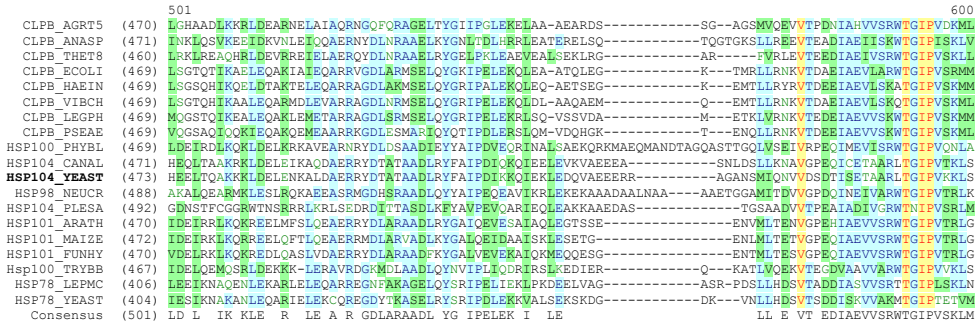

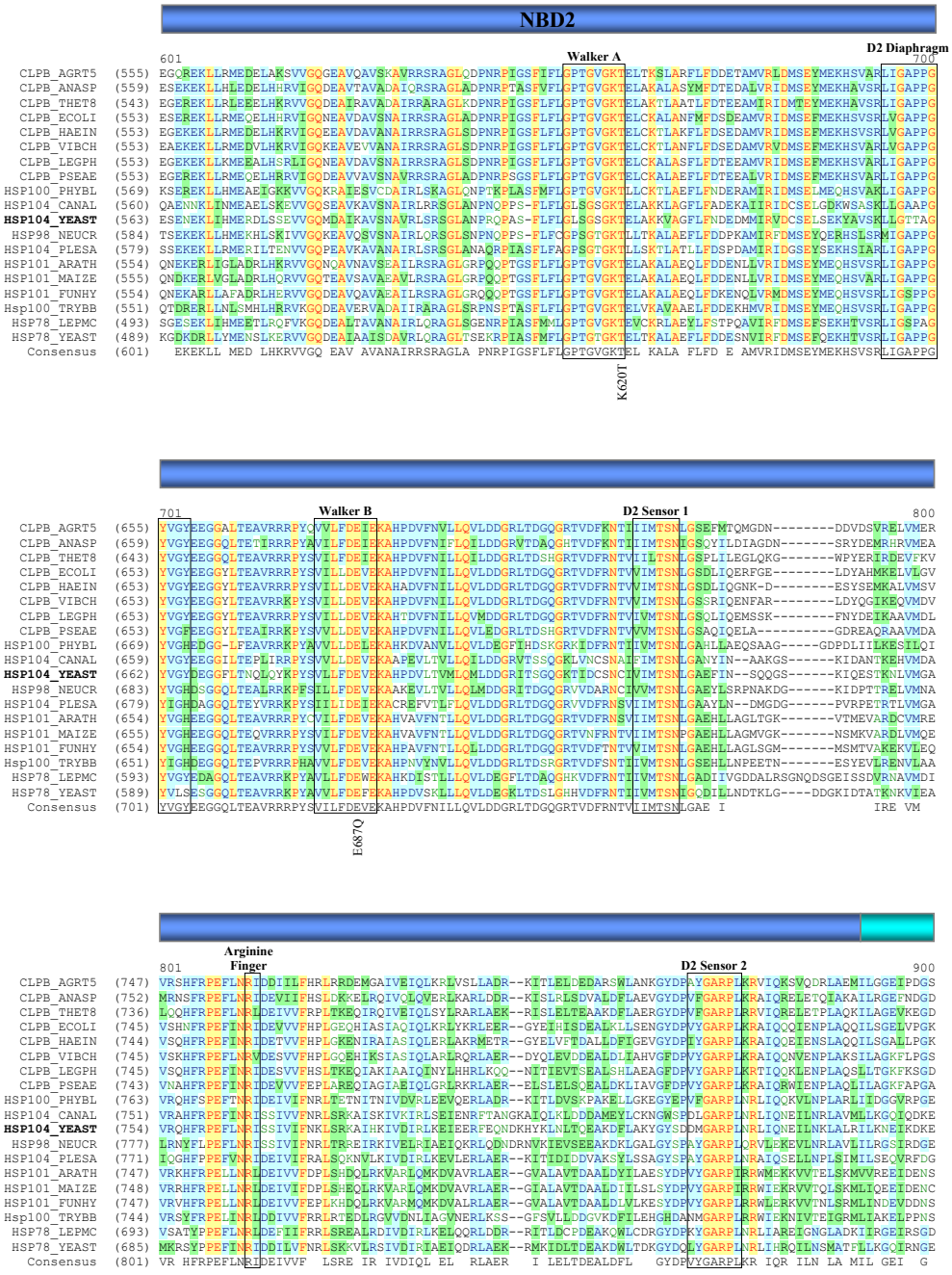
NBD2
Walker A
D2 Diaphragm
K620T
Walker B
D2 Sensor 1
E687Q
Arginine Finger
D2 Sensor 2
CLPB_AGRT5
CLPB_ANASP
CLPB_THET8
CLPB_ECOLI
CLPB_HAEIN
CLPB_VIBCH
CLPB_LEGPH
CLPB_PSEAE
HSP100_PHYBL
HSP104_CANAL
HSP104_YEAST
HSP98_NEUCR
HSP104_PLESA
HSP101_ARATH
HSP101_MAIZE
HSP101_FUNHY
Hsp100_TRYBB
HSP78_LEPMC
HSP78_YEAST
Consensus

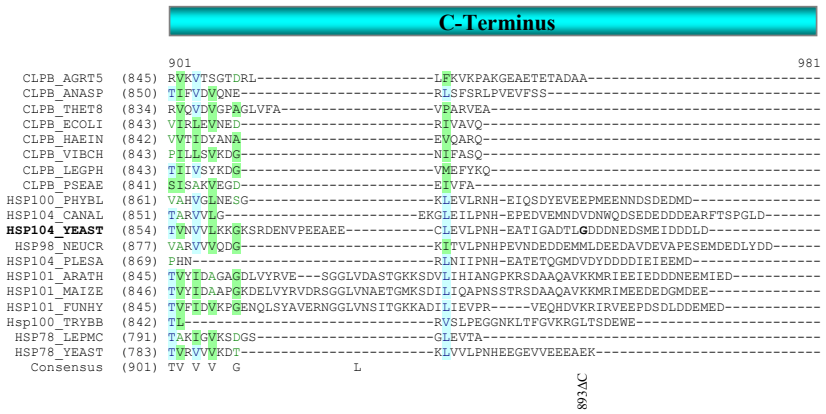

Identical residues are indicated by red on a yellow background, conserved residues are indicated by a blue background, a block of similar residues is indicated by a green background, and weakly similar residues are indicated by green letters. The alignment was performed using the program Vector NTI. The domain organization and the location of sequence motifs of Hsp100/ClpB proteins are predicted by a comparison to the known crystal structures of ClpA (Guo *et al.*, 2002) and ClpB (Lee *et al.*, 2003), and regarding a hydrophobicity plot (see Fig. 4.2). Point mutations performed in this work are given below the alignment blocks, if indicated.

Following representative members of the Hsp100/ClpB protein family were included into the multiple sequence alignment:

CLPB AGRT5: Q7CU92 - *Agrobacterium tumefaciens*
CLPB ANASP: Q8YM56 - *Anabaena sp*. (strain PCC 7120)
CLPB THET8: Q9RA63 - *Thermus thermophilus*
CLPB ECOLI: P63284 - *Escherichia coli*.
CLPB HAEIN: Q4QM42 - *Haemophilus influenzae*
CLPB VIBCH: Q9KU18 - *Vibrio cholerae*
CLPB LEGPH: Q5ZUP3 - *Legionella pneumophila*
CLPB PSEAE: Q9HVN5 - *Pseudomonas aeruginosa*
HSP100 PHYBL: Q96TW3 - *Phycomyces blakesleeanus*
HSP104 CANAL: Q96W69 - *Candida albicans*
HSP104 YEAST: P31539 - *Saccharomyces cerevisiae* (baker's yeast)
HSP98 NEUCR: P31540 - *Neurospora crassa*
HSP100 PLESA: Q9UVM4 - *Pleurotus sajor-caju* (oyster mushroom)
HSP101 ARATH: P42730 - *Arabidopsis thaliana* (mouse-ear cress)
HSP101 MAIZE: Q6RYQ7 - *Zea mays* (maize)
HSP101 FUNHY: Q2VDS9 - *Funaria hygrometrica* (moss)
Hsp100 TRYBB: P31543| - *Trypanosoma brucei brucei* (pathogenic, causes sleeping sickness)
HSP78 LEPMC: Q873Z4 - *Leptosphaeria maculans* (mitochondrial homologue from blackleg fungus)
HSP78 YEAST: P33416 - *Saccharomyces cerevisiae* (mitochondrial homologue from baker's yeast)

A.2 Sedimentation equilibrium experiment of $Hsp104_{WT}$ shows a 611 kDa complex

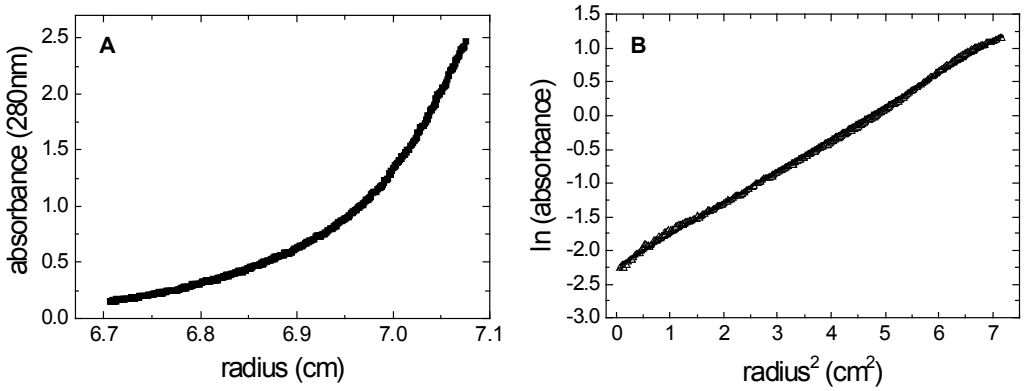

A sedimentation equilibrium experiment of $Hsp104_{WT}$ (15 µM) was carried in order to determine its apparent molecular weight in presence of 0.5 µM ATPγS at 20°C in standard assay buffer including protease inhibitor. (A) The equilibrium absorbance profile in the sample cell after 82 h at 3,700 rpm in an Optima XL-I analytical ultracentrifuge was used to (B) calculate the molecular weight based on the linear log(c) vs. r^2 plot by the ultrascan software. In this form of plot, a single species gives a straight line with a slope proportional to solution mass. The linear fit shows the slope predicted for a single species of 611 kDa.

A.3 Structure of Gdm^+ and similar compounds

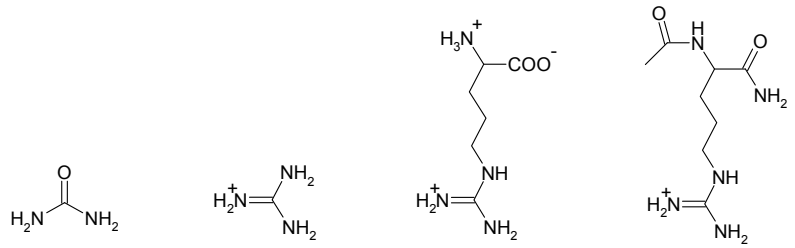

a b c d

Chemical structures of (a) urea, (b) guanidinium ion, (c) arginine ion, and (d) N-acetylarginine amide ion (NAAA). The structures refer to the ionic state, which is found in water at pH 7.5.

A.4 Truncation of the C-terminus of Hsp104 does not affect hexamerization

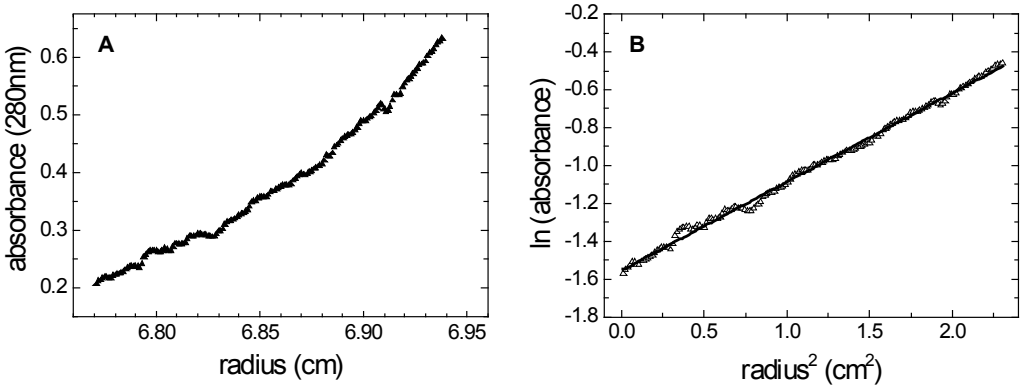

A sedimentation equilibrium experiment of $Hsp104_{893\Delta C}$ (15 µM) was carried in order to determine its apparent molecular weight in presence of 2.5 µM ATPγS at 20°C in standard assay buffer including protease inhibitor. (A) The equilibrium absorbance profile in the sample cell after 70 h at 3,700 rpm in an Optima XL-I analytical ultracentrifuge was used to calculate the molecular weight based on the linear log(conc.) vs. r^2 plot by the ultrascan software. In this form of plot, a single species gives a straight line with a slope proportional to solution mass. The linear fit shows the slope predicted for a single species of 602 kDa.

LIST OF PUBLICATIONS

[1] **Grimminger, V.**, Richter, K., Imhof, A., Buchner, J. & Walter, S. (2004): The prion curing agent guanidinium chloride specifically inhibits ATP hydrolysis by Hsp104. ***J. Biol. Chem.*** 79: 7378-7383.

[2] Boesl, B.*, **Grimminger, V.***, & Walter S. (2005): Substrate binding to the molecular chaperone Hsp104 and its regulation by nucleotides. ***J. Biol. Chem.*** 280: 38170-38176. (* authors contributed equally)

[3] Boesl, B., **Grimminger, V.** & Walter S. (2006): The Molecular Chaperone Hsp104 - A Molecular Machine for Protein Disaggregation. ***J. Struc. Biol.*** 156: 139-148.

[4] Schmid, A., Dittmann, S., **Grimminger, V.**, Walter, S., Heesemann, J., & Wilharm, G. (2006): *Yersinia enterocolitica* type III secretion chaperone SycD: recombinant expression, purification and characterization of a homodimer. ***Protein Expr. Purif.*** 49: 176-182.

[5] Debela, M., Magdolen, V., **Grimminger, V.**, Sommerhoff, C., Messerschmidt, A., Huber, R., Friedrich, R., Bode, W. & Goettig, P. (2006): Crystal Structures of Human Tissue Kallikrein 4: Activity Modulation by a Specific Zinc Binding Site. ***J. Mol. Biol.*** 362: 1094-1107.

[6] Schaupp, A., Marcinowski, M., **Grimminger, V.**, Boesl, B. & Walter, S. (2007): Processing of Proteins by the Molecular Chaperone Hsp104. ***J. Biol. Chem.*** submitted manuscript.

[7] **Grimminger, V.**, Tuite, M. & Walter, S.: The Yeast Cyclophilin Cpr6 is a Cochaperone of Hsp104. Manuscript in preparation.

The current study was carried out under the supervision of Dr. Stefan Walter in the laboratory of Prof. Dr. Johannes Buchner, Chair in Biotechnology, Department of Chemistry, Technische Universität München. My PhD-student position as well as the visit of several international conferences was funded by the "Sonderforschungsbereich 594 – Molecular Machines in Protein Folding and Protein Transport" of the German Research Foundation (Deutsche Forschungsgemeinschaft). Further, I was student member in the "Elite Network of Bavaria" graduate student program "Protein dynamics in health and disease", which financed several scientific courses as well as scientific equipment for my thesis.

I want to thank Prof. Dr. Johannes Buchner for providing a productive and stimulating working atmosphere as well as excellent scientific equipment.

My supervisor, Dr. Stefan Walter, has always provided me with help and advice during this thesis work. I highly appreciate that he permitted me the freedom to direct my own research course while guiding me with his comments and challenging discussions and I wish to thank him for all his efforts.

I spent three months of my thesis work in the in the laboratory of Prof. Dr. Mick Tuite, Director of Research in the Department of Biosciences of the University of Kent, Canterbury, United Kingdom. In his laboratory I had the opportunity to benefit from his expertise, and I acquired the necessary techniques to study the interaction of Cpr6 and Hsp104 *in vivo*. I wish to thank Prof. Dr. Mick Tuite for giving me the chance to work in his laboratory and for supporting me in many ways during my stay in England. I enjoyed very much being a guest in his group and the *in vivo* data obtained in Canterbury complement the *in vitro* data of my thesis work in Munich very well. I want to thank all my lab mates in Canterbury for their warm welcome. In particular, I wish to thank Dr. Brian Cox, Dr. Lee Byrne, Dr. Lyne Josse, and Gloria Merrit for helpful discussions and scientific instructions.

In this respect I would like Prof. Dr. Fritz Kreißl who – as a representative of the Bavarian Research Foundation (Bayerische Forschungsstiftung) – has favorably considered my request for this short-term fellowship and in doing so made my visit in Canterbury possible.

I would like to thank Prof. Dr. Wolfram Bode, Abteilung Strukturforschung, Max-Planck-Institut Biochemie, Martinsried, Germany, for his expert opinion on the structure of the Hsp104 hexamer, as well as for the interesting cooperation regarding human kallikreins which has led to a scientific publication. His support further contributed to the fact that I was offered a FEBS-fellowship.

I wish to express my gratitude to my cooperation partners, especially Dr. Axel Imhof, Adolf-Butenandt-Institut, Ludwig-Maximilians-Universität München, Germany, for giving me the opportunity to perform static light scattering experiments in his laboratory and Dr. Gottfried

Wilharm, Max von Pettenkofer Institut, Munich, Germany, for collaborating on a project on SycD of *Yersinia enterocolitica* which also has led to a scientific publication.

Simone Hess and the group of Dr. Thomas Scheibel provided me with mouse DHFR and Sup35NM-GFP constructs for which I am grateful.

Dr. Klaus Richter was always available for inspiring scientific discussions. Klaus initially provided me with some TPR-domain containing cochaperones to test whether or not they have any influence on Hsp104.

The technical assistence that my former master student Anne Röthig and my former bachelor student Moritz Marcinowski as well as all "Mitarbeit am Arbeitplatz" students, especially Ferdinand von Meyenn, have provided were of great value for the success of this study.

I thank Frau S. Hilber for her always friendly support with all aspects of office work and Frau S. Quedzuweit for her skillful assistance with protein purification.

Dr. Stefan Walter, Dr. Ulf Marquardt, Dr. Emma Simpson, Dr. Jeannette Winter, Christian Ackerschott, Matthias Feige, Simone Hess, Moritz Marcinowski, and Andreas Schaupp deserve appreciation for their helpful comments on the manuscript of this thesis.

I would like to thank all my lab mates in Munich for their helpfulness and consideration allowing an open productive working atmosphere, which made laboratory work not only interesting but also fun.

It was the unconditional support and endless faith of my family that allowed me to complete this work, and I would like to express my gratitude for all their support.

Finally, I would like to thank Dr. Ulf Marquardt for helpful discussions, his countless words of encouragement and his care during the week-ends during the final phase of preparation of this thesis.

Hiermit erkläre ich, dass ich die vorliegende Arbeit selbständig verfasst und keine anderen als die hier angegebenen Quellen und Hilfsmittel verwendet habe. Die Arbeit wurde noch keiner Prüfungskommission vorgelegt.

München, März 2007